THE EFFECT OF HEMICELLULOSES AND CYCLIC HUMIDITY ON THE CREEP OF SINGLE FIBERS

A Thesis Submitted by

Kelly M. Sedlachek

A.B. 1989, Ripon College

M.S. 1991, Institute of Paper Science and Technology

in partial fulfillment of the requirements
of the Institute of Paper Science and Technology
for the degree of Doctor of Philosophy,
Atlanta, Georgia

August, 1995

SUMMARY

Natural wood fibers consist of polymers based on cellulose and hemicellulose. These polymers are sensitive to conditions of changing moisture content. In paper and wood products this sensitivity leads to gradual stress-induced changes in dimensions of material composed of these fibers. Recent work on the lifetime of corrugated containers suggests that the extent of hydroexpansion of the components of the container, the linerboard and corrugating medium, are related to the amount of creep strain developed in cartons under load especially under conditions of changing humidity. The response of the wood pulp fiber to cyclic humidity conditions is also important in the dimensional stability of other products such as copy paper and decorative laminates.

Most of the paper-related literature addresses the effect of humidity on paper sheets. The question of the relative contribution of fibers and fiber-to-fiber bonds to the creep response of paper cannot be addressed with this data. Since there is very limited data concerning the creep behavior of single fibers, this thesis addresses that topic. More specifically, it considers the question of whether hemicellulose components significantly affect the tensile creep behavior of single pulp fibers under both constant and cyclic humidity conditions. If hemicellulose components are significant in tensile creep response, then modification of the hemicellulose component of the fibers is a possibility to modify creep response.

The behavior of loblolly pine holocellulose fibers and otherwise similar fibers in which the arabinoxylan and mannan had been removed by a mild caustic extraction have been studied. Fiber creep was first measured under an axial load at constant humidity levels. In a second set of experiments, the relative humidity was cycled. Although differences were found between the two pulp types, the differences were generally small compared to the differences between fibers. The first creep response of single fibers fits the Eyring model for polymers, but the permanent set of the fibers is a large component of the observed first creep strain. Only a small part of the permanent set can be explained by classical polymer theory that is linear in time and stress. Most of

the permanent set occurs in the loading step and may be due to a reorganization of the cell wall material on a scale much larger than the unit cell.

Experiments under cyclic humidity conditions were designed to address two questions: (1) Is the strain rate under cyclic humidity conditions different than the strain rate under constant humidity conditions? (2) Is the total strain under cyclic humidity conditions larger than the total strain under constant humidity conditions? The creep of single fibers was measured under axial load and two initial conditions. Fibers were conditioned at 50% RH, then loaded and cycled between 50% and 90% RH. The second set of conditions started with the fiber conditioned at 90% RH. The response of the fiber to cyclic humidity conditions was indicative of a superposition of states at constant humidity. The strain rate at any time under cyclic humidity conditions was equivalent to the strain rate under constant humidity conditions. The total strain rate under cyclic humidity conditions will be higher than the lower constant humidity state. When the fiber is conditioned at 50% RH the total strain exceeds the strain of the 90% RH state after several cycles. This excess strain can be explained by the strain developed in the first creep cycle at 50% RH. When the fiber is conditioned at 90% RH there is very little difference in strain between constant and cyclic humidity conditions.

Results show that creep strain is strongly influenced by the strain developed in the initial loading and first humidity cycle. Results also show that this strain is responsible for most of the permanent set of the fiber. These results point to a neglected area of research. It is necessary to measure and explain the instantaneous strain of single fibers before their behavior under either constant or cyclic humidity conditions can be fully quantified. Paper strained at a constant load and humidity is known to have a large component of permanent set. It is suspected that the total strain of paper studied under cyclic humidity conditions is dominated by the strain developed in the first humidity cycle. Until the origin of this component of the creep strain is subjected to theoretical interpretation it is unlikely that we can develop a predictive theory for the dimensional stability of paper products or the lifetime of corrugated containers.

TABLE OF CONTENTS

INTRODUCTION

Pulp fibers can be extracted from almost any vascular plant found in nature. However, wood is by far the most abundant source of papermaking fibers and is virtually the only source utilized in North America. Except for seed hairs, vegetable fibers in their native state are embedded in a matrix of nonfibrous material (mostly lignin but also containing hemicelluloses, resins, and gums).[1] In plant fibers, cellulose is the component that determines the character of the delignified fiber and permits its use in papermaking. During chemical treatment of wood to produce pulp, the various hemicelluloses, unlike cellulose, are easily degraded and dissolved, so that their percentage is usually less in the pulp than in the original wood. The term "holocellulose" is used to describe the total carbohydrate (cellulose and hemicellulose) content of fibers.

Cellulosic fibers exhibit a number of properties which fulfill the requirements of papermaking. Their hydrophilic nature plays an important role, since the papermaking process occurs in an aqueous medium. The fibers readily absorb water and are easily dispersed in a water suspension. When wet fibers are brought together during the sheet forming operation, bonding is promoted by the polar attraction of the water molecules for each other and for the hydroxyl groups covering the cellulose surface. As the water is evaporated, the hydroxyl groups of cellulose surfaces ultimately link together by means of hydrogen bonds. The hydrophilic nature of cellulosic fibers, though it allows hydrogen bonding to form a sheet of paper, is also disadvantageous for the structural integrity and dimensional stability of many paper products. Cellulosic fibers interact with water and swell, thereby changing their dimensions. This phenomenon affects the end-use performance of many paper products.

Another behavior exhibited by cellulosic fibers that affects product performance is viscoelasticity. One manifestation of this is the time dependence of their mechanical properties. Several time-dependent phenomena may be discerned, including creep, or deformation under

constant stress, creep recovery, or decay of deformation upon removal of load, and creep relaxation, or decay of stress at constant deformation. When a fiber is stretched under constant load, the extension is found to increase rapidly at first and more slowly later; when the load is removed, the extension decreases or the fiber contracts, again more rapidly at first. In some synthetic fibers under the proper conditions, the recovery after stretching proceeds until the initial length is attained; in natural cellulose fibers there remains, even after prolonged times of retraction, a residual extension or permanent set. These time-dependent phenomena affect dimensional stability and other performance characteristics of paper products.

The change in relative humidity of the surrounding atmosphere dictates water absorption by, or desorption from, cellulose fibers. This phenomenon is known to have a dramatic effect on the mechanical properties of fibers and, consequently, the performance characteristics of paper products such as corrugated containers, printing and writing papers, and laminates. The dependence of creep characteristics upon change in relative humidity can cause significant deterioration in the load-bearing capability of corrugated containers stored in a warehouse. (See Figure 1). At constant 80% RH, a box will fail in 72 days. When relative humidity is cycled between 30 and 80% RH, every 12 hours, box will fail in four days. A decrease in deflection was reported for each absorption (30–80% RH) cycle and an increase for each desorption (80–30% RH) cycle. This is a consequence of the fact that the stress-induced hygroexpansion is greater than the combined effects of elastic and creep response in the time interval studied.[3,4] Cycling of relative humidity leads to an accelerated decay in load-bearing capability. If this phenomenon were better understood, then corrective action could be taken, leading to an increased profitability for the corrugated container industry.

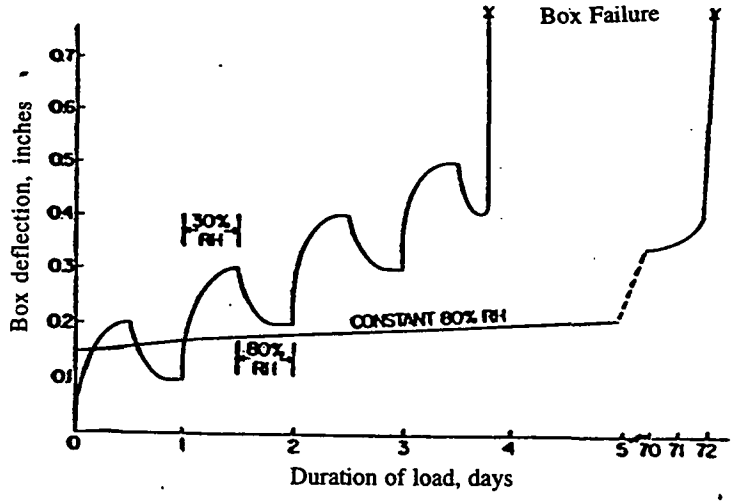

Figure 1: Box deflection versus duration of load. [2]

The creep response of paper is a composite of the creep response of its component fibers and that of the interfiber bonds. There is, consequently, a need to independently study the fibers which make up the bonded network.

Investigation of the tensile creep behavior of individual pulp fibers has usually been limited to environments where the relative humidity is maintained constant. Brezinski[5] examined the effects of various constant relative humidities on tensile creep of paper handsheets. He concluded that the structural changes occurred at the molecular level and were not just the uncurling or slipping of whole fibers in the web. In a study of individual pulp fibers, Hill[6] found that tensile creep increased fiber strength and modulus of elasticity. He concluded that fiber creep resulted in a possible decrease in fibril angle, indicating that there was movement of crystalline regions within the fibrils or, more likely, of the fibrils within the fibers. Little is known about the tensile creep response of individual pulp fibers in a changing relative humidity environment.

Since natural cellulose fibers belong to a class of polymers based on cellulose and hemicellulose, they are sensitive to conditions of changing moisture content. This sensitivity leads to changes in dimensions of their components. There is consequently a need for

fundamental understanding of the role of individual components in the creep response of pulp fibers.

This thesis addresses the question of whether hemicellulose components affect the tensile creep behavior of single fibers at either constant relative humidity or under cyclic humidity conditions. If hemicellulose components are important in tensile creep response, then modifying them is a possibility to reduce creep response.

The relative importance of interfiber and intrafiber phenomena as factors contributing to the tensile creep response of paper has not been resolved, due to the difficulty of independently controlling either of these factors in a sheet of paper. The study of individual fibers is a logical approach to gaining a better understanding of the time-dependence of strain and to obtaining information which will further our knowledge of the viscoelastic nature of paper. This, in turn, will provide the means to minimize dimensional instability as demands on the performance of paper and paper board products increase.

LITERATURE REVIEW

COMPONENTS OF CELLULOSIC FIBERS

Molecular Structure

The cellulose fiber is a complex composite structure. Its major polymeric components are cellulose, hemicellulose, and lignin. Of these, the lignin is almost completely removed in chemical pulping and bleaching processes, as are the miscellaneous materials such as pectinaceous and resinous components. Cellulose, the major component, consists of long linear chains of glucose anhydride units linked together by beta-1,4 glycosidic bonds. The hemicelluloses are generally combinations of sugars: mannose, xylose, arabinose, galactose, and glucose. The most common hemicellulose polymer chains are 4-O-methylglucuronoarabino-xylan (softwoods; no arabinose in hardwoods) and glucomannan. The hemicellulose polymer chains also have internal linkages of some type of glycosidic bond.

Cellulose exists in the fiber wall in both crystalline and amorphous forms. Crystallization is favored by the linearity of the molecule; the tendency of the hydroxyl groups to form hydrogen bonds; and the geometric arrangement of the atoms within the glucose unit, which allows a closely packed structure. Hemicelluloses are generally more amorphous in nature; as a result of their branching they tend to form a less-ordered structure than the glucose units.[7] The aggregation and orientation of these chain molecules in the cell wall relative to other cell constituents has been the subject of debate.

Natural cellulosic fibers usually have a cellulose I crystal lattice structure. Meyer and co-workers postulated the generally accepted monoclinic unit cell (Figure 2). The unit cell has dimensions of a = 8.35 Å, b = 10.3 Å, c = 7.9 Å, and $\beta = 84°$. The planes of the anhydroglucose units lie in the ab plane, and the axes of the cellobiose units are parallel to the b axis.

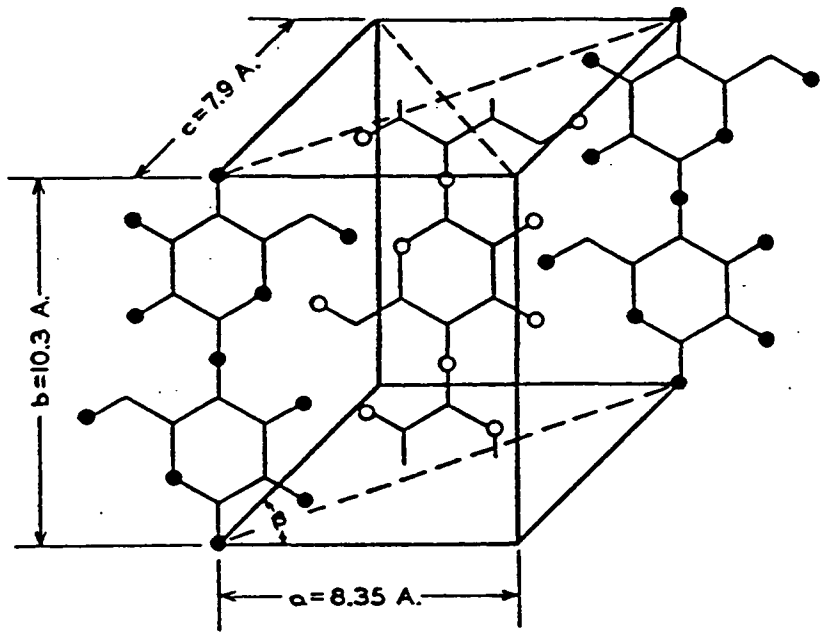

Figure 2: Unit cell of cellulose I.[7]

Three types of forces are present in the cellulose unit cell. Along the b axis the glucose units are held together by the beta-1,4-glucosidic primary valence bonds. The formation of hydrogen bonds between oxygen atoms of adjacent molecules is suggested by the 2.5 Å. separation of the glucose rings along the a axis and the types of atoms present. Along the c axis the nearest distance between atomic centers is 3.1 Å, which indicates van der Waals forces are holding the lattice together. These bonds determine the strength of the structural polysaccharide framework in the fiber cell wall. The framework is the primary load-bearing strength providing component of the cell wall.

The cellulose unit cells form molecular chains of polysaccharides which in turn are able to form fibrillar units. The formation of well-ordered fibrils is a known property of the cellulose molecules. The smallest fibrillar units which were detected as constant elements 30–35 Å in diameter in various lower and higher plants are called "elementary fibrils." These elementary fibrils are densely packed into higher units 120 Å in diameter. There must be interfaces between the elementary fibrils; otherwise they could not be separated in such a uniform manner by

chemical treatment. Heyn[8] showed that, in the natural swelling state of the wood cell wall, the elementary fibrils are visible even without chemical treatment. It is assumed that the interfaces between the elementary fibrils are formed by less-ordered cellulose chains and by hemicellulose chains. From the fibril-forming properties of isolated hemicelluloses, it is concluded that these molecules are oriented in the direction of the cellulose fibrils within the cell wall.

The next higher-level system is represented by the microfibrils which are built up of 120 Å fibrils. The microfibril unit does not seem to be as stable as the two lower systems, since the microfibrils are easily split off into 120 Å units by alkali treatment. The interfaces between these units are assumed to consist mainly of hemicelluloses. The microfibrils in turn are surrounded by hemicelluloses and lignin. Figure 3 shows a cross-sectional view of the model.

The elementary fibrils represented by framed square fields are bordered by narrow interfaces containing a few hemicellulose molecules within the 120 Å units. The main portion of the hemicelluloses is deposited around the 120 Å fibrils within as well as without the microfibril unit. It is assumed that the movement of water within the cell wall takes place mainly in the interfaces. At the surface of the microfibrils, the hemicelluloses are in intimate contact with the lignin; thus, in these places chemical bonds between lignin and hemicelluloses exist.

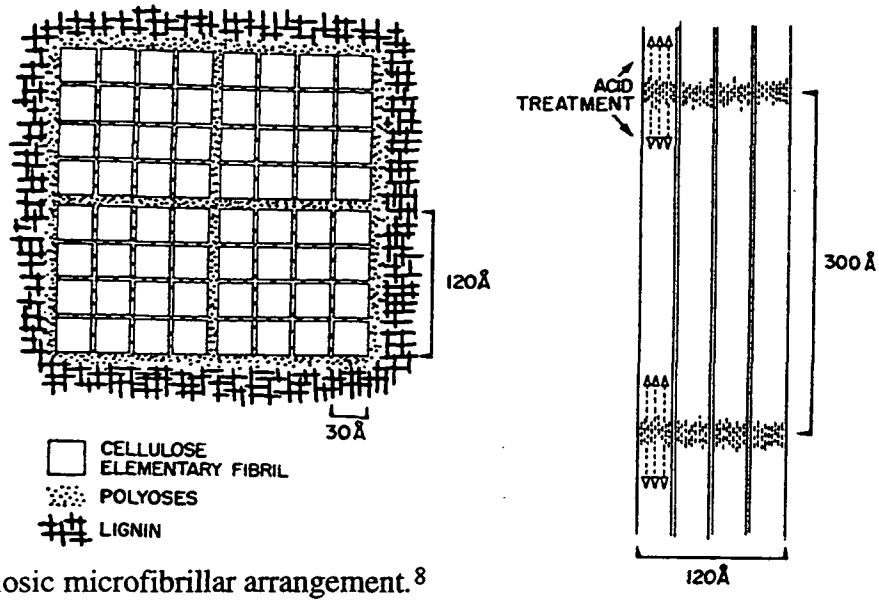

Figure 3: Cellulosic microfibrillar arrangement.[8]

The supermolecular arrangement of the polymer chains within the fibrillar and subfibrillar structure of the wall consisting of microfibrils which in turn are composed of elementary fibrils has been the subject of many theories. From a variety of x-ray data it is known that the cellulose chains are packed partially or wholly into crystallite regions called micelles or crystallites. Two principal extended-chain polymer theories attempt to explain the crystalline structure of the cellulose fiber in light of the chemical and physical discoveries.

The fringed micelle theory states that the micelles or crystalline regions alternate with the less-ordered regions, and within broad limits, there is no connection between the length of the crystalline regions and the molecular chain length. There are no sharply defined crystalline limits, but rather there are gradual transitions from regions of high lateral order to regions of low lateral order. The fringed micelle theory is supported by crystalline interference in x-ray diffraction test results, together with amorphous rings or background scattering attributable to a large portion of amorphous component. Similarly, other filamentous materials, such as silk, viscose rayon, and nylon can be accounted for by the fringed micelle theory.

The second theory, proposed by Hearle,[9, 10] is the fringed fibril theory of cellulose crystallinity. He suggests abandoning the assumption, implicit in the fringed micelle theory, that there are discrete crystallites present in the structure. Instead, the crystalline regions are regarded as continuous "fringed fibrils," composed of molecules diverging from the essentially crystalline fibril core at different positions along the fibril's length. Hearle assumes that branching of the fibrils is possible and that some distortion of the crystal lattice may occur.

Figure 3 shows a longitudinal view of a 120 Å fibril with additional consideration of the results of hydrolytic and thermal decomposition. In this longitudinal view, the 120 Å unit is composed of four elementary fibrils. The chain-length measurement of cellulose from thermally treated wood leads to the conclusion that there are amorphous regions located at 300 Å from each other. In the model the amorphous regions are outlined by dashed lines. These amorphous regions are visible when using an electron microscope. Heyn[8, 11] observed a beaded appearance

of the elementary fibrils after freeze-drying the samples. The elementary fibrils are viewed as smooth stretched strings in an untreated state. Hemicelluloses may appear as the nodules in Heyn's freeze-drying treatment and may tie the elementary fibrils together into larger fibrils that were shown by Preston.[12] Hemicelluloses may also bind elementary fibrils together into a larger fibril.

Loosely arranged hemicellulose regions should presumably give separated fibrils a high flexibility. Muhlethaler[13] demonstrated the elementary fibrils to be very stiff, so much that they cannot be bent except in a large radius. It is, therefore, assumed that the sensitivity of certain regions of the elementary fibrils is not caused by disarrangement of the whole system at that point. Deviations of a few molecules from the complete order, causing a lattice defect and/or the presence of molecular chain ends, is believed to be a sufficiently good reason for a sensitive region. A slight reduction of the lattice order in the sensitive regions of regenerated cellulose is assumed to occur by Kiessig[14] from the results of x-ray low-angle investigations. Ruck[15] also concluded from results of mercerizing studies on cellulose that the molecular chains in the accessible regions show only slight deviations from the lattice order. Thompson[16] advocates galactoglucomannan as crystallizing. These hemicelluloses may be present in the sensitive regions as these regions of the cellulose fibrils are attacked during chemical treatments such as partial acid hydrolysis. These regions are highly accessible to staining materials, and these accessible regions evidently grow towards the less accessible regions depending on reaction conditions. The influence of a chemical attack on the sensitive regions is indicated by dashed arrows in Figure 3.

The second theory would explain the presence of microscopic fibrils and the division between crystalline and noncrystalline regions. The main difference between the two theories is that in the fringed fibril theory, the amorphous regions lie along the periphery of the fibril; but in the fringed micelle theory, the amorphous and crystalline regions alternate along the fibrillar axis. This difference could be important when interpreting fiber response to axial stress.

The possibility of chain folding in fibers has led to a third plausible theory of fiber structure. Holland[17] and Tonnesen and Ellefsen[18] have discussed the folding of the cellulose molecule upon itself in the crystalline regions. Manley[19] obtained data to support the chain folding hypothesis. In his model, the basic structural element of the plant cell wall is a filament 35 Å wide which consists of a ribbon wound as a tight helix. The molecules assume a folded configuration, and the microfibrils exist in ordered arrangement of the cell wall. This work was done with single crystals of a cellulose derivative. Dolmetsch[20] noted that when cellulose is formed "freely" in the substrate, it can follow its "own laws of crystallization," but when formed in cellular tissues, its freedom is spatially limited. Therefore, the internal structure that may occur in a single crystal may not occur in a cellulosic fiber. None of the proposals for folded chains can be reconciled with the x-ray and polarization optical evidence that the chains are aligned in the direction of the microfibrillar axes. Regardless of the chain alignment problem, the folded chain proposals do not account for observed physical and mechanical behavior of cellulosic walls, which are characterized by low extensibility, high strength, and lack of the glass transition behavior typical of synthetic polymers.

Another characteristic which could be expected of folded chains in tension is a very inelastic deformation behavior, especially at high stress levels,[21,22] because the hinges between folded-chain microcrystals would tend to unkink. The strain behavior of wood and/or natural cellulosic fibers in tension is quite elastic up to very high stress levels.

Murphey[23] and Jentzen[24] have shown that when the wood cell wall is strained in tension, there is an increase in crystallinity. This can occur only if the chains are initially extended. In such a case, tension will straighten out slight deviations in chain alignment. By contrast, if polymer chains are folded to start with, a tensile stress will unfold them, reducing crystallinity.[25]

Microscopic Structure

The length and diameter of wood fibers vary greatly with species, even within the individual tree. The average length of loblolly pine fibers is 4 mm. The average diameter is between 30–45 microns, and the average cell wall thickness is 5.2 microns.[17,7] The fiber cross section is roughly elliptical and has a hollow center which forms the fiber lumen.

Morphologically, the fiber consists of a layered structure (Figure 4). In most fibers there are five distinct layers: (1) the intercellular substance or middle lamella, (2) the primary wall or P layer, (3) the outer layer of the secondary wall or S_1 layer, (4) the central layer of the secondary wall or the S_2 layer, and (5) the inner layer of the secondary wall or tertiary wall, referred to as the S_3 layer. Except for the middle lamella, each of these layers is composed of a fibrillar structure which in turn can be broken down into finer fibrils. Frey-Wyssling[26] classifies the elements based on their cross-sectional dimensions as macrofibrils, microfibrils, and elementary fibrils. Their sizes, respectively, are 4000 by 4000 Å, 250 by 250 Å, and 30 by 100 Å. These dimensions were determined for the elements in ramie and would be expected to vary somewhat in other fibrils.

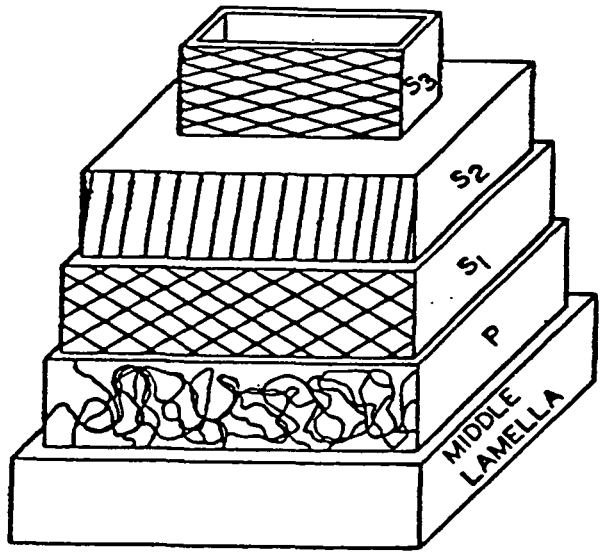

Figure 4: Layer structure of fiber.[7]

The fibrils of all layers except the primary wall are wound helically around the fiber axis. The fibrils in the primary wall are randomly oriented in a loosely woven texture except at the corners where they are longitudinal.[27] The S_1 layer has at least two counter-rotating symmetrical helixes arranged at an angle of 55 to 75° to the fiber axis in softwood tracheids.[28] The fibrils of the S_2 layer are closely parallel, run in a steep helix, and form an angle of 10 to 20° to the fiber axis.[27] This layer forms the bulk of the fiber cross section. The S_3 layer has a crossed helical structure[25] as does the S_1 layer; however, the helix angles are between 65 and 90°. The contact between S_1 and S_2 and between S_2 and S_3 is usually very loose.[28]

Springwood and summerwood differ in their cell wall thickness, the size of the lumen, the diameter of the fiber, the fiber length, and specific gravity.[7] The springwood fibers have a thinner wall but a large lumen and diameter. The average specific gravity increases from springwood to summerwood within the annual ring. This increase can be attributed to an increase in the cell wall thickness of the fibers.[29] Significant within-tree variations exist between the springwood and the summerwood tracheids of each annual ring. Table 1 illustrates some of these differences. The amount of the S_2 layer determines the difference in summerwood and springwood cell wall thickness. For a softwood springwood tracheid[30] the P layer composes about 10% of the total wall, S_1 about 8%, S_2 about 78%, and S_3 about 4%.

Table 1: Within-tree variations that occur between loblolly pine springwood and summerwood tracheids.[29]

Variable	Springwood	Summerwood
Fiber length (mm)	4.25 ± 0.07	4.80 ± 0.06
Cell wall thickness (μm)	3.40 ± 0.70	8.20 ± 1.50
Specific gravity	0.25–0.34	0.63–0.85

Meier[31] found that about 60 to 65% of the carbohydrate material in the S_2 layer, 50 to 60% in the S_1 layer, and 35 to 40% in the P layer was cellulose. The hemicelluloses were in the

reverse order. The location of the hemicelluloses most likely has an important bearing on the fiber properties. Meier felt that the hemicelluloses may lie between the cellulosic fibrils either as an amorphous or as a crystalline granular material, or they may form their own microfibrils which may or may not have crystalline regions. Most workers, however, feel that the hemicelluloses are located around the outside of the microfibrils,[32, 33] although there is some speculation[33, 34] that some hemicelluloses may be located within the microfibrils.

LOCATION OF HEMICELLULOSES IN THE CELLULOSE STRUCTURE

Studies have been performed to discern the distribution of the hemicelluloses in the microstructure of the wood pulp fiber. Meier[31] indirectly located the hemicelluloses in the cell-wall layers by studying pine fibers in different stages of maturation. He assumed that when a layer of polysaccharides is laid down in the growing cell wall, the layer remains unchanged as successive layers are placed over it. Since the middle lamella and primary wall are formed first, and the other walls are added later, analysis of fibers in different stages of maturation will yield an estimate of sugar concentration in the different cell layers (Table 2). No information was obtained as to the microlocation of the xylans and glucomannans in the P, S_1, S_2, and S_3 layers.

Table 2: Sugar content in cell layers of Pinewood. [31]

Sugar	M + P %	S_1 %	S_2 Outer Part %	S_2 Inner Part + S_3 %
Galactan	20.1	5.2	1.6	3.2
Cellulose	35.5	61.5	66.5	47.5
Glucomannan	7.7	16.9	24.6	27.2
Arabinan	29.4	0.6	0.0	2.4
Glucurono-arabinoxylan	7.3	15.7	7.4	19.4

Nearly all of the experimental work on the location of hemicellulose fractions in the fiber's internal network is based on extraction data. The principal basis for using the data of this

work is the assumption that the relative differences in ease of extraction of the various hemicellulose components are caused by their different locations in the fiber network.

Beyers[35] directly determined the distribution of hemicelluloses within the tracheid cell wall. Radioactive hemicellulose precursors were supplied to living three- and four-year-old pine trees. The cells metabolized the precursors and incorporated them into the cell wall as radioactive hemicelluloses. Electron microscope autoradiography revealed that the arabinose labeled tracheids contained higher concentrations of radioactivity in the P and S_1 layers of the cell wall than in the S_2 layer. The mannose labeled tracheids contained their highest concentration of radioactivity in the S_2 layer and much lower concentrations in the inner and outer cell wall layers. Autoradiography results indicated that the hemicelluloses are not evenly distributed across the cell wall.

Autoradiography and extraction work[35-43] have supported the hypothesis that the arabinans and galactans are located mainly in the exterior layers of the fiber. The xylans are in the interior of the fiber, probably between the fibrils. The mannans, principally in the form of glucomannan, appear mainly to be associated intimately with the cellulose fibrils.

Loblolly pine chips were pulped using a peracetic acid-sodium borohydride combination. The retention of sugars is shown in Table 3. Most of the arabinans and galactans are easily removed in dilute caustic (Tables 3 and 4) while removal of the xylans requires stronger caustic solutions. Removal of glucomannans requires even stronger concentrations of caustic, with the addition of complexing agents like boric acid. Timell[44] felt that the borate forms a complex with the 2,3-cis-hydroxyl groups of the mannose residues, thus rendering the polymer more acidic and therefore more soluble in alkali.

Following the peracetic acid-sodium borohydride pulping the loblolly pine fibers were extracted with alkaline reagents to gradually remove various sugars. The extraction sequence is shown in Table 4. Different polysaccharides were removed during three distinct stages of the

extraction sequence.[36] In the first stage, which comprises extraction with DMSO, hot water and very dilute alkali, the galactan was removed preferentially. This is easily understood, since most of the galactan-containing polysaccharides are known to be located in the outside cell wall layers.[35-43]

In the second stage, which comprised extractions with 0.4N and 1.5N KOH, almost all of the xylan-based polysaccharides were removed. In the third stage, which comprised extraction with KOH of increasing concentration, in the presence of borate, the glucomannan was removed preferentially.

Table 3: Retention of sugars in wood after pulping.[37]

	Yield %	Glucan %	Galactan %	Mannan %	Arabinan %	Xylan %
Loblolly summerwood	71.7	100	72	93	50	99

Table 4: Extraction of loblolly pine summerwood.[37]

	Yield %	Glucan %	Galactan %	Mannan %	Arabinan %	Xylan %
Wood	100	46.9[a]	1.6	11.0	0.7	6.4
Holo (peracetic)	71.7	47.3	1.2	10.2	0.4	6.3
DMSO	70.7	47.7	1.1	9.2	0.1	6.2
Hot water	68.5	47.0	0.7	9.4	0.0	5.9
0.1N KOH	64.5	46.3	0.0	9.2	–	5.8
0.4N KOH	62.8	46.1	–	8.9	–	4.8
1.5N KOH	57.3	46.5	–	9.0	–	0.9
1.5N KOH + 0.75 H_3BO_3	52.8	44.7	–	7.4	–	0.8
3.6N KOH + 0.75 H_3BO_3	51.7	44.2	–	6.0	–	0.5

[a] Percentages based on oven-dry wood.

Nelson[42] followed the width of an appropriate x-ray diffraction peak during extraction of slash pine chlorite holocellulose with alkali. The drop in peak width was proportional to removal of mannan but showed no relation to removal of xylan. These results indicated that at least part of the mannans are located in close association with the cellulose, since its removal results in a higher degree of order. Nelson also felt this agreed with the data on differences in ease of alkali extractions of xylans and glucomannans, both sets of data indicating that the glucomannans are located more deeply inside the framework of the cellulose fibrils than the xylan. The xylan may be located on the outside of the fibrils and between them. The conclusion from the cited literature is that the data and the fiber-wall sugar analysis strongly support the hypothesis that the hemicelluloses are located in the microstructure of the fiber.

If the above explanation is to be accepted, then the hemicellulose content of a fiber is important for its internal strength as well as its ability to bond to other fibers in a paper sheet. One of the major factors determining sheet characteristics is the carbohydrate composition of the pulp fiber, not only of its surface layer but also of the interior of the fiber.

CREEP OF SINGLE FIBERS

Delayed Deformation

Cellulose fibers, being viscoelastic materials, exhibit both instantaneous elastic deformation and delayed, time-dependent deformation when subjected to an externally applied load. Creep, which is the delayed, time-dependent deformation, can be divided into two components: primary creep and secondary creep or permanent set, which is nonrecoverable. Tertiary creep or accelerated permanent set is not considered in the creep experiments reviewed for this thesis. For a thorough treatment of the creep behavior of fibers, the reader is referred to Leaderman.[45]

Primary Creep

Primary creep is the time-dependent recoverable portion of the delayed deformation. This response of viscoelastic materials is thought to be due primarily to configurational changes in molecular structure produced by the applied load. Alfrey[46] discusses the mechanisms of such molecular movement. The packing of molecules in the amorphous regions of high polymers is less than optimum; therefore, the solid may be considered to contain void spaces through these regions. When the amorphous regions are subjected to stress, the molecules tend to align themselves in the direction of the stress by moving into new positions. This movement may occur when there is a void space available to be occupied and when sufficient energy is supplied to overcome the forces which previously defined the molecular structure. These movements in fibers may require the breaking of secondary bonds which may be re-formed in new positions. Upon removal of the external stress, the stored energy is released and the molecules tend to

return to their normal, more random, positions. Theoretical treatment of configurational response is complicated by the presence of crystalline regions and strong secondary bonding, but this mechanism should be active in the stressed amorphous material of pulp fibers.

Leaderman[45] has suggested that the configurational changes may be explained in terms of the fringe theory of structure of amorphous and crystalline fibers. He proposed this theory for nylon filaments and suggested that the straightening of the molecular chains reaches a point where crystallite growth at the expense of the amorphous material is possible. The nylon filament was "stiffer" after removal of load following long-duration creep than compared to the stiffness on the original load application. This effect was noted by recovery curves which were lower in total deformation at earlier times and steeper in slope than the preceding creep curves. Leaderman attributed this behavior to reductions in the percentage of amorphous material during the creep test because of crystallization, which reduced the amount of configurational elastic recovery at early times. The creep deformation was entirely recoverable at a 1:1 ratio of recovery time to creep time.

Nylon, like cellulose, has long crystalline chains arranged in parallel fashion. In passing from one crystalline region to the next, the chain is organized in a more random manner. A region of the cellulose fiber similarly is occupied by other molecular chains or amorphous regions. Assume these flexible chains in nylon fringe regions are highly kinked due to thermal agitation. Secondary bonds hold the chains together in the crystallite regions. Similar bonds hold chains together in the amorphous regions. Leaderman interprets the primary creep phenomenon under small loads as due to the rearrangement of secondary bonds in the amorphous regions. When a large constant load is applied to a nylon fiber, a large reversible extension occurs, which he attributes to the straightening of the chains in the amorphous regions. The branched chains at the ends of the crystalline region are therefore brought closer together. Under these conditions of extension the crystallites grow along their length during the creep test under constant load. The proportion of the amorphous material gradually decreases, and the newly

formed secondary bonds are between the now parallel chains which augment the crystallite region. When the load is removed, the nylon fiber is "stiffer," since the amount of amorphous region material has been reduced. Thermal agitation of molecular chains in the amorphous regions breaks the new bonds in the augmented portions of the crystallites, and creep recovery takes place while the fiber gradually reverts back to its initial state.

In Leaderman's explanation of creep and creep recovery of nylon under large loads he has assumed that gradual increase in the degree of crystallinity takes place in the fiber while under load and that new secondary bonds are formed. Following load removal decrystallization takes place accompanied by a gradual disappearance of these bonds.

The same effects have been observed for viscose rayon and for acetate rayon. X-ray studies that revealed increased crystallinity, or at least better molecular packing, occurred in cotton and ramie yarns dried under tension. However, Jentzen,[24] employing similar methods, did not observe such behavior in his holocellulose fibers.

Secondary Creep

Secondary creep is that portion of the total sample deformation which is nonrecoverable at the test conditions after removal of the load. A portion of the configurational elastic response may not be recoverable at the test conditions but may be recovered if the polymer is swollen by raising the moisture content. Permanent deformations are caused by viscous flow, irreversible crystallization, and molecular chain rupture.[47]

Configurational deformations are susceptible to being "frozen in" or to attaining metastable equilibrium states in those polymers in which secondary bonding per unit length of the molecule is high (such as cellulose and hemicelluloses). It is necessary to rupture these relatively weak secondary bonds to allow configurational changes in the amorphous regions of the fiber. Once broken, these bonds may form new bonds with previously unbonded atoms; they may unite with other broken bonds, or they may remain broken. The formation of new bonds

can lead to secondary creep when the load is released if there is not enough energy stored in the system to break the new bonds and return the bonding group to its original position. The breaking and reforming of bonds and molecular configuration changes are equilibrium processes. All such processes require a finite time to attain equilibrium. The time required to reach new equilibrium states is one of the factors which produce creep. If metastable equilibrium states are reached, permanent deformations will result. The rate and amount of creep recovery will depend on the stability of the new bonds and on the stored energy of the system.

The term "viscous flow" is used to describe the stress behavior of polymeric materials. "Viscous flow" is normally applied only to truly permanent deformations involving the transfer of entire molecules in amorphous polymers. It is generally agreed that the flow of entire molecules is not possible in crystalline polymers such as cellulose. Molecules are so firmly bonded in the crystalline regions that relative movement of entire molecules is prohibited by these juncture points. This can be related to the fringe theory of structure. Molecules are much longer than the length of a crystallite and are considered to pass through many crystallites and regions of amorphous structure. True viscous flow, therefore, is limited to polymers in which entire molecules exist in an amorphous continuum.

Crystal growth might occur as configurational changes bring the molecules into very close proximity and alignment. The evidence for this phenomenon is indirect and inconclusive. Such growth would necessitate the formulation of a very high secondary bond density in the crystal structure and should resist a reversal.

A final important response mechanism of pulp fibers when subjected to an external stress is the rupture of primary valence bonds. Rupture of a primary valence bond produces free radicals at the newly formed chain ends which will likely react with a water molecule. The re-formation of these bonds is not likely since the stress on the molecule would serve to separate the new chain ends and prevent the coupling reaction. The occurrence of a region of stress-concentration sufficient to rupture valence bonds may possibly initiate failure of the entire fiber.

Creep Curve

Creep data are recorded as deformations observed at various times after application of a constant load to the specimen. The load is applied rapidly. Data is obtained within a limited time interval. Testing is terminated before breaking of the fiber or cessation of creep, limiting creep to primary and secondary creep. Data is represented as a creep curve which is usually a plot of deformation versus log-time, where time is measured from the instant the load is fully applied.

The stages of deformation are pictured in Figure 5 as a creep curve. Total creep deformation is the delayed deformations. In order to calculate the delayed deformation, the elastic modulus must be known so that the initial extension may be removed from the total deformation. The elastic modulus is determined by using the initial slope exhibited by the specimen in a load-deformation test. At low loads and short times the creep effects are small, and the initial slope of the test is a measure of the elastic modulus.

Upon removal of the load, there is an immediate elastic recovery. This elastic recovery is followed by the recoverable deformation, termed "primary creep," and the nonrecoverable deformation, termed "secondary creep" or "permanent set." The immediate elastic behavior must be known before determination of the two delayed deformations. The deformations which occur during creep may change the elastic modulus of the material in such a way that a new modulus must be determined or the creep recovery data must be extrapolated to zero recovery time in order to determine the immediate elastic contraction.

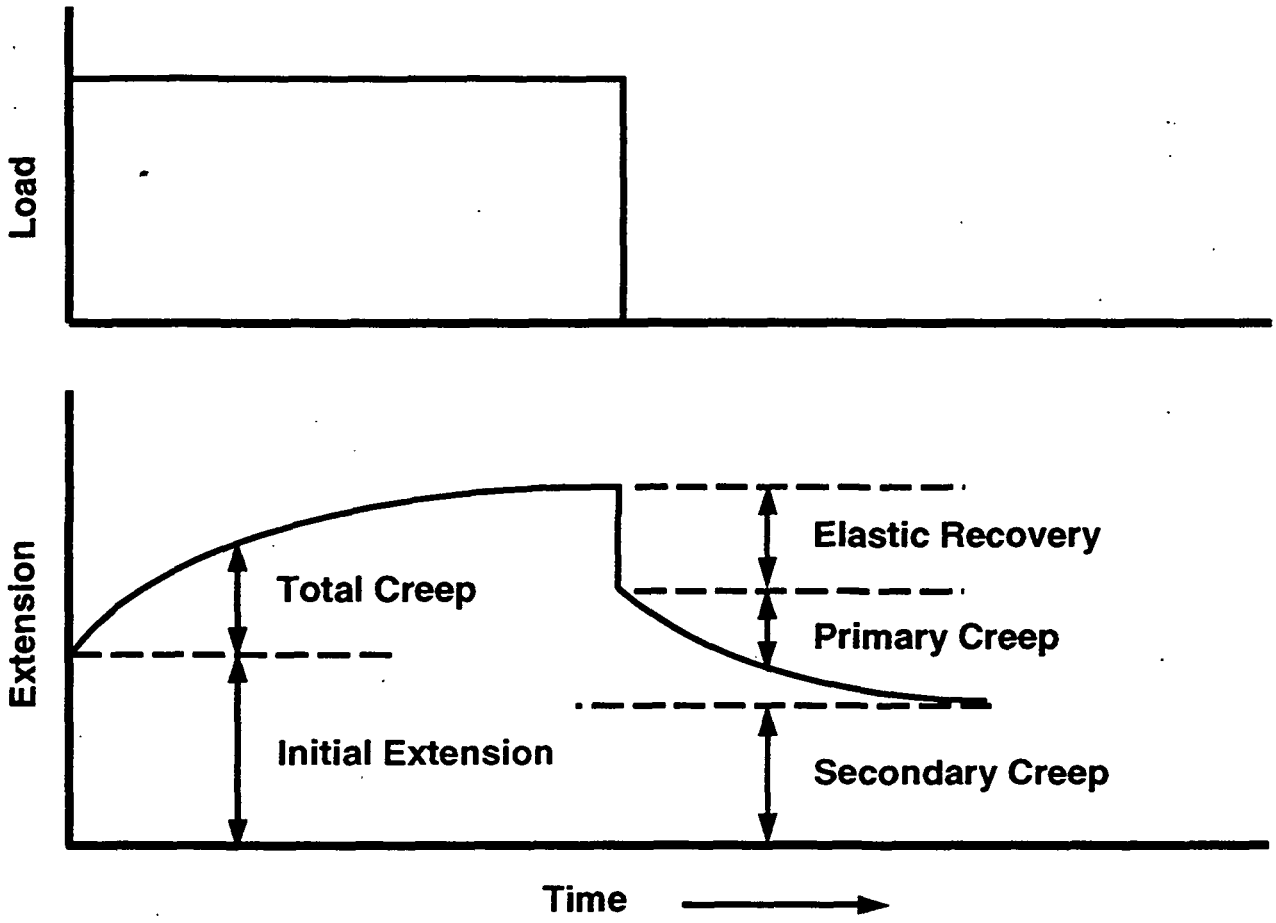

Figure 5: Load-time and extension-time representations.

Fiber Creep

In the creep test, a load is applied rather rapidly to a specimen then held constant, and the deformation is recorded as a function of time. Leaderman,[45] Halsey,[48] and Holland[49] have investigated the creep behavior of viscose rayon. Since rayon possesses the fundamental structure of cellulose, a similar behavior of the two types of fibers is to be expected. Leaderman tested mechanically conditioned viscose rayon at 65% RH and 21°C at four stress levels: 1.54 x 10^8, 2.35 x 10^8, 3.82 x 10^8, and 4.70 x 10^8 dynes/cm^2. Figure 6 represents the four creep curves plotted as percent extension vs. time. The fiber was first mechanically conditioned by loading for 24 hours with the highest load to be used, followed by 24 hours recovery. This procedure brought the fiber into an elastic state, eliminating some of the development of further permanent set. Stresses are expressed in units of dynes/cm^2, obtained by dividing the load in dynes by the

original area of cross section of the fiber in cm^2, in order to make comparisons of data for fibers of different cross-sectional area.

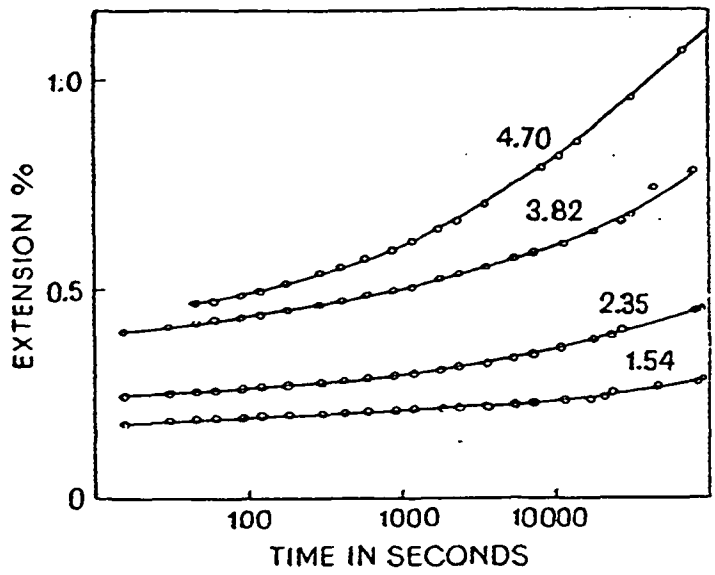

Figure 6: Total extension curve for mechanically conditioned viscose rayon.[45]

On the semilog plot, the curves are concave upward and represent the primary and secondary creep. Since the curves are nearly horizontal at short times, the instantaneous extension can be estimated by extrapolating back at short times. This is not very accurate for investigating the relationship between the load and magnitude of the delayed extension. Leaderman adopted the following procedure: from the total extension at any instant the value of the total extension corresponding to a time of one minute is subtracted, so that a relative delayed extension is obtained which avoids errors due to extrapolation and to any shock on the fiber which may be produced by applying the load.

In Table 5, values of instantaneous extension and delayed extension are given for viscose rayon, acetate rayon, silk, and nylon fibers as a percentage of the total extension for a constant load of 3×10^8 dynes/cm^2 acting for 20 hours. Under these conditions, ordinary viscose rayon I

has a delayed extension equal to about half the total extension, the same as nylon II. The viscose II was the same origin as the viscose I but had been stretched wet about 40% and dried in tension. Stretching viscose I approximately 40% to produce viscose II has the effect of increasing the Young's modulus and increasing the amount of instantaneous extension to about 70% of the total extension. Its creep behavior is then similar to that of silk and cellulose acetate which also show about 70% instantaneous extension. The nylon II sample has a higher modulus than nylon I, probably due to greater applied stretch during manufacture, and its percentage of instantaneous extension is higher, simulating the case of the stretched viscose rayon.

Table 5: Creep data for cellulosic fibers. Constant load of 3 $x10^8$ dynes/cm^2 acting for 20 hours at 65% RH.[45]

Fiber type	Total extension(%)	Instantaneous extension(%)	Delayed extension(%)
Viscose I	0.57	51	49
Viscose II	0.30	71	29
Acetate	0.76	70	30
Silk	0.34	69	31
Nylon I	2.16	40	60
Nylon II	1.26	50	50

Meyer and Lotmar[50] calculated a theoretical cellulose fiber modulus based on molecular forces deduced from Raman spectra. Only an upper limit to the modulus can be calculated because only data applying to the crystalline part of the cellulose were used. Computing a total compliance of a glucose residue, taking into account stretching of the valence bonds and opening of the valence angles, a theoretical modulus of 12 $x10^{11}$ dynes/cm^2 is computed. Meredith[51] found a dynamic Young's modulus of 9 $x10^8$ dynes/cm^2 for ramie fibers dried under tension. Jentzen[24] studying holocellulose longleaf pine found a Young's modulus based on the cross-sectional area for summerwood fibers of 10.3 $x10^{11}$ dynes/cm^2 dried under tension. Spiegelberg,[43] using the same fiber sample as Jentzen, calculated 9.7 $x10^{11}$ dynes/cm^2 for fibers dried under tension. Data of both Spiegelberg and Jentzen indicate that the theoretical modulus can be closely approached by holocellulose fibers dried under tension. The theoretical modulus

will be higher because it is assumed to be 100% crystalline, highly oriented, and dry. Data reported by Spiegelberg and Jentzen were collected at 50% RH.

Influence of Hemicellulose Content on Single Fiber Creep

No data concerning the relationship between creep and hemicellulose content in single fibers has been found. However, the tensile strength of individual fibers has been related to the hemicellulose content of the fiber.[52] Leopold and McIntosh used a peracetic acid holocellulose from loblolly pine chips. The delignified fibers were extracted with a series of KOH, KOH + borate, and NaOH treatments. The degree of polymerization of the extracted residue continually decreased upon application of stronger extractants, although the change was not extensive (10–15% overall). One would expect the degree of polymerization to increase upon extraction of the holocellulose loblolly pine fibers because of the removal of lower D.P. materials, unless the cellulose itself was being degraded, which evidently happened in this case. Cellulose degradation can be attributed to the 24-hour extraction procedure at room temperature and a subsequent 7-hour extraction with fresh reagent.

The tensile strength of the individual fibers was determined by gluing fibers between two paper tabs. The axial tensile load was applied through Jeweler's chains attached to the tabs. The applied load was obtained by running water into a beaker which was attached to one chain. When the fiber broke, the beaker was weighed to determine the breaking load. Tensile testing of approximately 20 fibers chosen at random from one sample was sufficient to set limits on the mean tensile strength and area of the summerwood fibers of ±10% at the 95% confidence level and approximately ±15% on data for springwood fibers. The cross-sectional area was measured by embedding the fibers in cellulose acetate, microtoming them, and taking a picture of the cross section.

Fiber tensile strength (gm/fiber) was proportional to xylan content (Figure 7). No correlation for mannan content and fiber strength was noted (Figure 8).

Several criticisms of the above work can be made. The fibers were obtained from the tenth to twelfth growth rings of the tree, and juvenile fibers are not uniform from fiber to fiber in this range.[53] Fifty percent of the fiber breaks occurred at this point (compared to roughly 20% for work done on the I.P.C. Fiber-Load Elongation Apparatus).[24] No significant difference was noticed between the overall values for fibers broken at the glue line and those broken elsewhere; therefore, the results were used.

The same mechanical test was performed on loblolly-pine kraft fibers pulped to different yields and then holopulped with peracetic acid.[52] A correlation was found between mannan content and fiber strength (g/fiber) for the kraft fibers. The following criticisms of the work can be made: (1) The fiber population was not very homogeneous because extreme variation in cross-sectional area was noted. (2) Peracetic acid was used as needed, immersing each fiber group for different times without recording the amount or length of treatment time used. (3) Strength versus yields were plotted and showed a general decrease in strength with decreasing yield for summerwood fibers. From this, Leopold[52] claimed that he had determined a correlation with mannan content, although this correlation was not apparent. A graph substantiating this correlation was not presented.

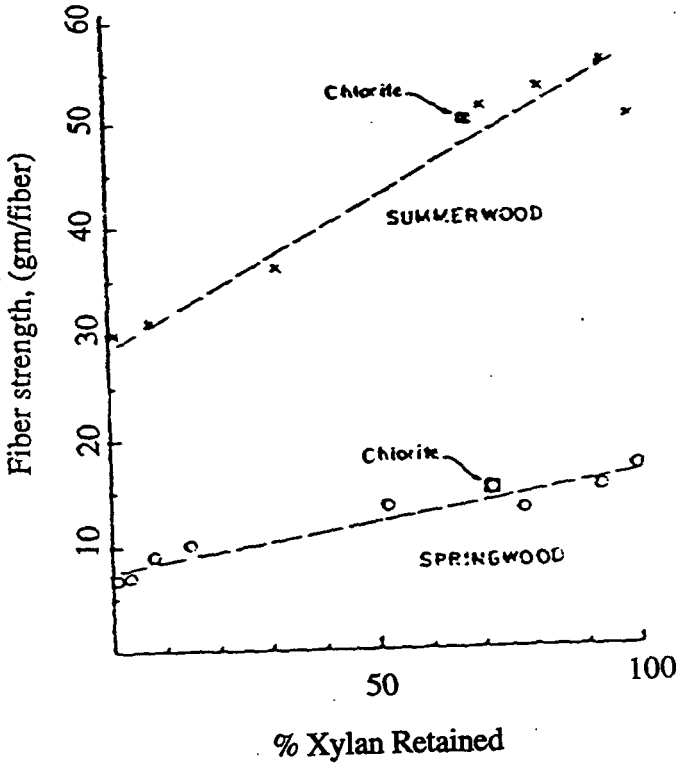

Figure 7: Correlation between xylan and fiber strength.[52]

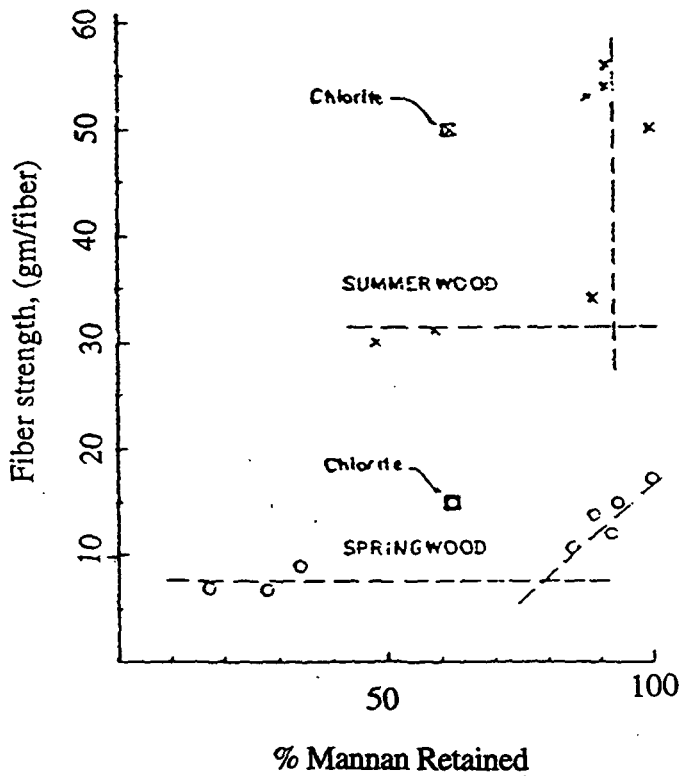

Figure 8: Correlation between mannan on fiber strength. [52]

Spiegelberg[43] extracted longleaf pine holocellulose fibers and plotted percent sugar retained versus tensile breaking stress of the fibers (Figure 9 and 10). The shape of the curves resembles Leopold and McIntosh's work[52] and indicates that the strength of the fibers is dependent on xylan and glucomannan content. The strength of the fibers correlates linearly with the xylan content of the fibers, with the exception of the last extraction point. Here a slight drop in strength occurs with essentially no change in xylan content. Analyzing the glucomannan-strength curve, removal of the sugars in the first two extractions lowers the strength of the fiber. However, the third extraction, which removes only glucomannan, does not appreciably reduce the strength. Since the data show that removal of the mannans and xylans in the first and second steps reduces the strength but removal of the glucomannan alone in the third extraction step does not appreciably reduce the fiber strength, one can surmise that either the xylan principally affects the strength or that the mannans removed in the first and second extraction are different from the mannans removed in the third extraction, as regards location in the internal fiber structure and relationship to the cellulose fibrils. The easily extractable polysaccharides (exclusive of the pectic materials and the galactans and arabinans) appear to affect the strength of the fibers much more than those extracted with great difficulty. This suggests that the polysaccharides located outside the crystalline cellulose network, possibly xylans in combination with glucomannan or galactoglucomannan, affect fiber strength. This supports the evidence presented that the hemicellulose contribution to fiber strength is in the manner with which they allow the cellulose fibrils to adjust internally to an externally applied load. This conclusion will also impact on holocellulose single fiber creep. If holocellulose fibers are selectively extracted and the hemicelluloses are removed, the extracted holocellulose fiber undergoing creep should allow less extension at a given time when compared with unextracted holocellulose fibers undergoing creep.

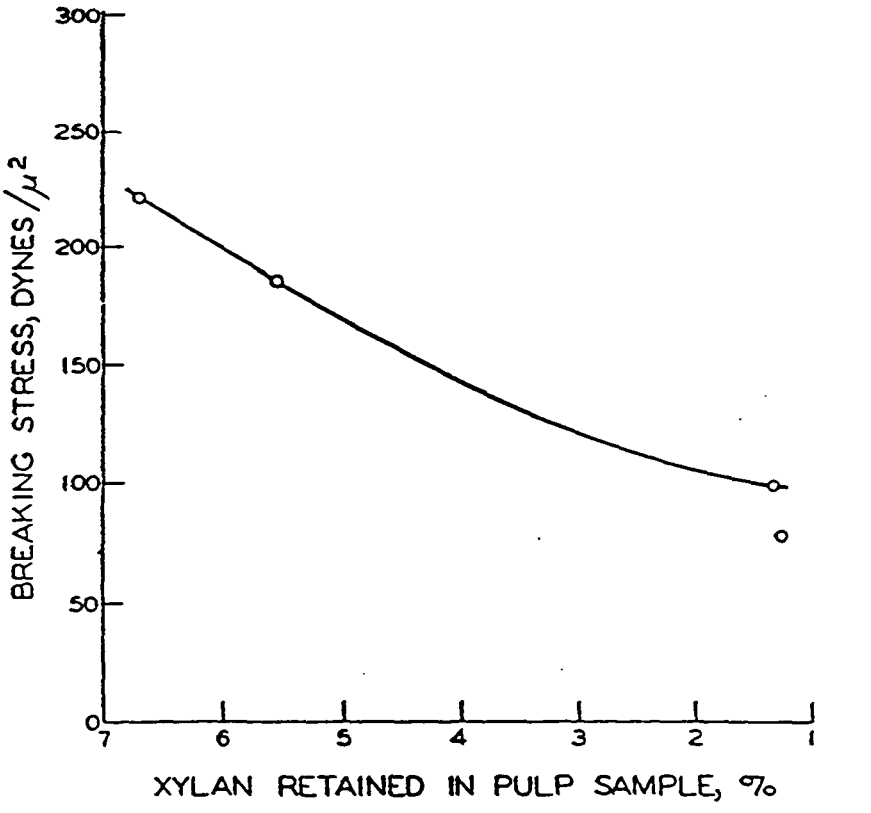

Figure 9: Correlation between xylan and fiber strength. [43]

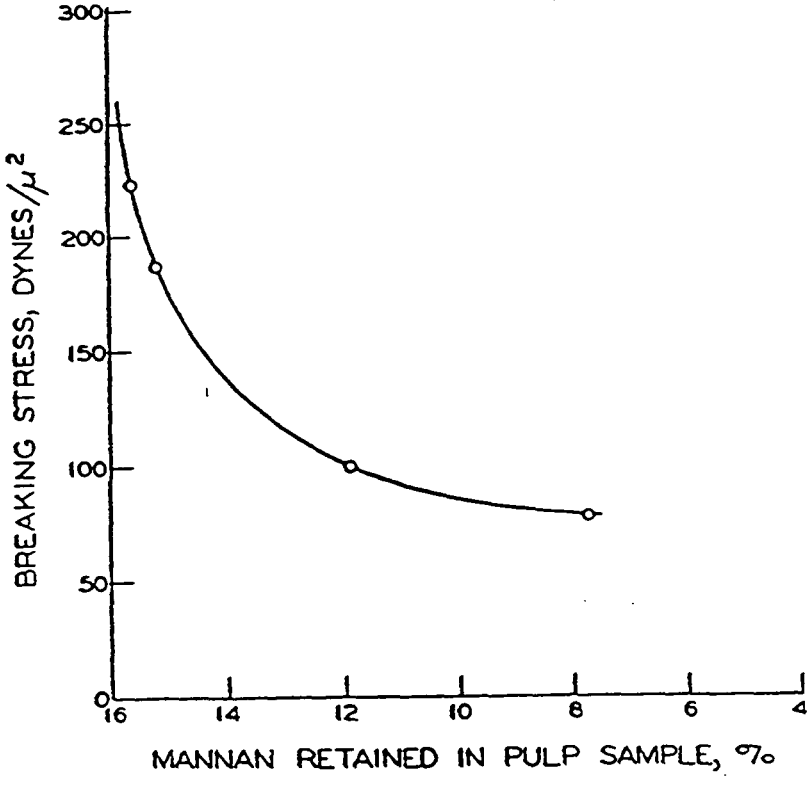

Figure 10: Correlation between mannan and fiber strength. [43]

Influence of Moisture on Fiber Creep

Wood fibers are hydrophilic. They attract water, and they swell when water is adsorbed. Since cellulosic fibers show a preferred orientation in the direction of the fiber axis and the crystallites are much longer than they are wide, the same thickness of noncrystalline fiber-water phase surrounding a crystalline region will produce greater swelling lateral to the fiber direction than longitudinally. For example, on wetting bone-dry viscose rayon, fibers will increase in length 4% while they increase in diameter 26%. Similarly, cotton fibers under the same conditions increase 1.2% in length and increase 15% in diameter. [51] Changes in mechanical properties will certainly occur because of water adsorption and dimensional changes.

Fibers undergo a hysteresis effect when subjected to relative humidity changes. The hysteresis in the relation between the regain of a cotton fiber (regain = mass of adsorbed water in specimen/mass of dry specimen *100%) and the relative humidity are shown in Figure 11. Curve A, the absorption isotherm, is a plot of equilibrium regains at successively higher humidities of an initially bone-dry specimen. Curve B, the desorption isotherm, is a plot of an initially wet specimen at successively lower humidities. Fibers will have a different regain and moisture content when dried from a wet state to a certain relative humidity than if wetted from a dry state to the same ambient humidity. This effect is important to note when observing fiber properties. Similarly, the amount of water held within a cellulose fiber at a given relative humidity is greater for fibers that have previously been in equilibrium with higher humidities than it is for the same fibers at lower humidities.

It is more accurate to specify a fiber property at a given moisture content than at a given relative humidity. Unfortunately, not all past researchers have believed in this. Many have reported results are in terms of relative humidity. While reading this section it is important to keep in mind that the wood fiber is a composite material as previously described. It will be seen later that this perspective is essential in understanding why fibers act as they do when subject to environmental change.

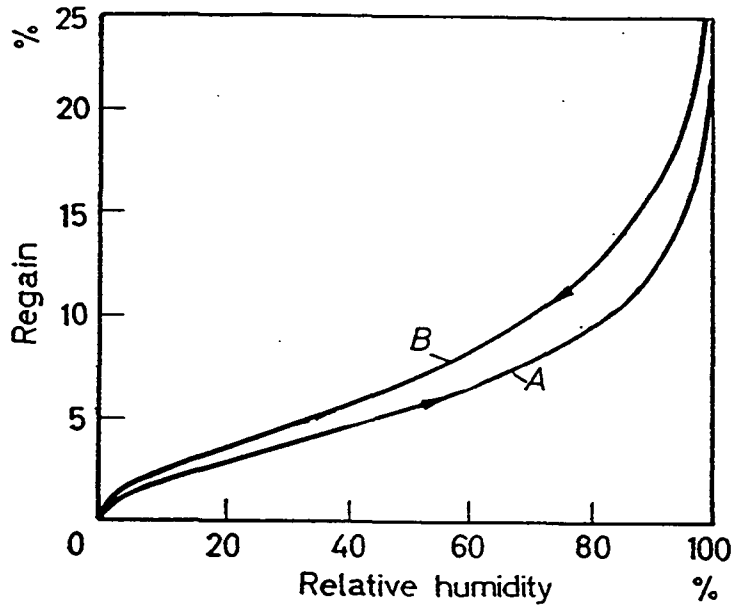

Figure 11: Absorption (A) and desorption (B) curves of regain vs. relative humidity. [54]

Fiber Component Behavior

The importance of viewing a wood fiber as a composite material has already been stated. Different components of the wood fiber adsorb water at different rates. The crystalline cellulose is hydrophilic but not much is accessible to water penetration. Hemicelluloses are quite hydrophilic and amorphous, capable of adsorbing large amounts of water. Lignin is also amorphous but relatively hydrophobic. Figure 12 compares water adsorption rates of lignin and hemicellulose as a function of relative humidity.[55, 56]

Relative differences in water adsorption capacity manifest themselves in the change of various components mechanical properties with changes in moisture content of the components. Cousins isolated hemicellulose and lignin fractions from *Pinus radiata*. He tested their elastic moduli as a function of moisture content by a "ball indention" method. The modulus of the hemicellulose decreased by nearly three orders of magnitude (from 8 GPa to 10 MPa) in going from a dry to a saturated state.[55] In contrast, the elastic modulus of periodate lignin only decreased from 6.7 GPa to 3.1 GPa over the same environmental change (only about half-order of magnitude). [55] One key to this difference in behavior is seen in Figure 12. Near saturation

(100% RH) periodate lignin has about 17% moisture content. The hemicelluloses have moisture contents approaching 60–80%.[55] It is questionable how applicable these results are to the exact behavior of the compounds when they are components within the composite fiber structure. However, the general relationships are of use in understanding how the fiber behaves as a whole.

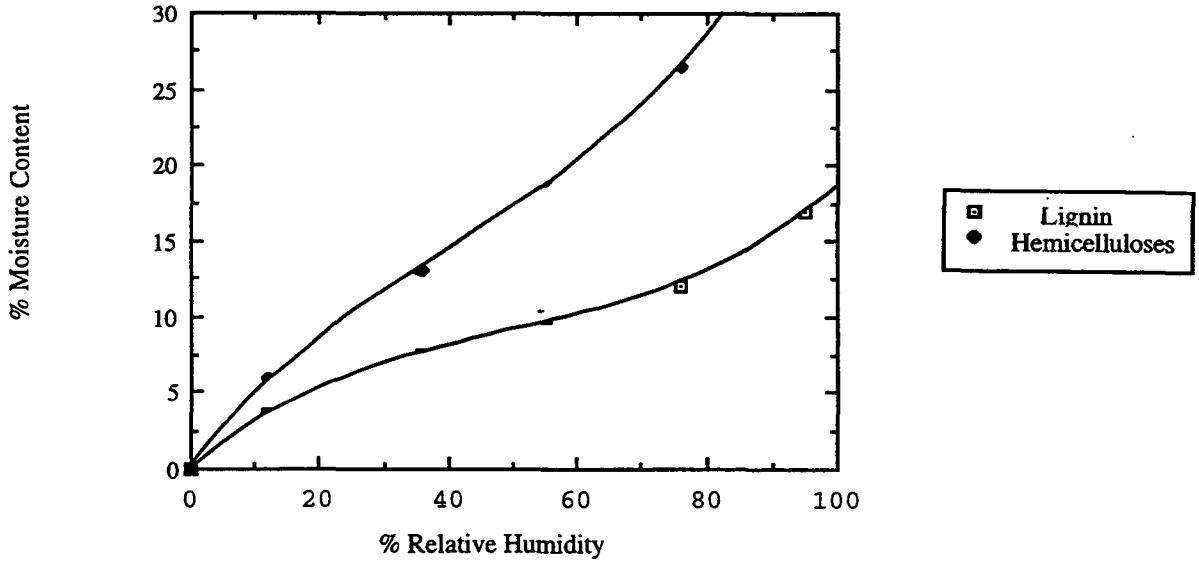

Figure 12: Sorption of water by hemicelluloses and lignin.[55, 56]

In the highly crystalline cellulose structure, another phenomenon occurs. It is known that as cellulose absorbs moisture it becomes less rigid and the number of strength reducing defects within the microfibrils decreases. This is thought to occur because the addition of some water to the microfibrils lubricates them, allowing slippage by one another to redistribute stress more evenly. If water is not present, the fibrils become more brittle and prone to defect. This cellulose moisture theory predicts a reduction in stiffness (elastic modulus) with an increase in the cellulose moisture content. As the moisture content increases, fibrils slip by one another, and consequently more elongation under a given load and a lower elastic modulus result.[57]

Hardacker[58] agrees with the cellulose moisture theory. In crystalline fibers, the added moisture permits greater mobility of the fibers past one another. This movement can readjust and redistribute stress within the fiber. It reduces or eliminates weak spots, thus strengthening the overall fiber. This goes along with the "weak-link" theory, which states that a fiber is like a linked chain and will break at its weakest link. Making the weak links stronger will strengthen the overall fiber. [58]

Effect of Moisture Content Changes on Single Fiber Creep

It is generally accepted that water does not readily enter the crystalline region of fibers but rather breaks hydrogen bonds in the less-ordered amorphous regions. The sorption of water, therefore, reduces the number of secondary bonds between the carbohydrate molecules and breaks bonds in the less ordered, amorphous regions between the fibrils. This bond breakage provides less resistance to deformation and allows greater extensions. Water and the accompanying bond breakage also allow the stress to be more evenly distributed, and this explains the higher wet tensile strength of natural cellulose fibers. [43]

Since cellulose acetate possesses the fundamental structure of cellulose, a similar behavior of the two types of fibers is to be expected. Steinberger[59] made a series of single fiber tensile creep measurements using cellulose acetate. He tested fibers at a constant load equivalent to a nominal stress of 6.5×10^8 dynes/cm^2 covering a range of relative humidities from 0 to 100%. The effect of increasing the relative humidity in steps of 10% is shown for cellulose acetate in Figure 13. From 0 to 40% RH, the amount of creep is small, but above this relative humidity it rises rapidly. The curves for 71% RH and 80% RH are composite curves based on the values for more than one fiber.

The striking feature about these curves is that each looks as though it might be part of a common sigmoidal curve or master creep curve that is shifted along the log-time axis to shorter times as the relative humidity is raised. Moreover, the group of curves bears a strong

resemblance to those of Hill's[6] which will be discussed later, where the relative humidity was held constant and the load varied, instead of the load being held constant and the relative humidity varied.

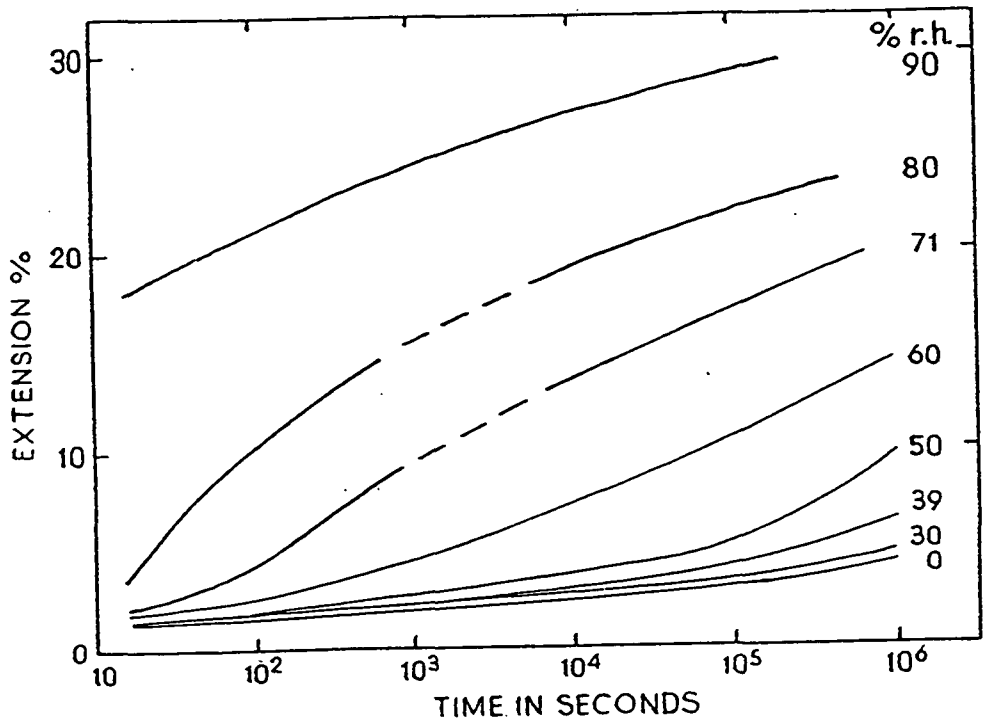

Figure 13: The effect of relative humidity on the creep of cellulose acetate fibers.[55]

The tensile creep of cellulose acetate and viscose rayon was also studied by Pinte and Henno[60] under constant loads from 1.2 to 9.4 x 10^8 dynes/cm^2 at relative humidities from 30 to 65%. The extensions after creep for 24 hours for cellulose acetate and viscose rayon are shown in Table 6. In general, increase in relative humidity has a smaller effect on the extension at 24 hours for cellulose acetate than for viscose rayon.

Table 6: Extension of cellulose acetate and rayon after 24 hours under constant load at 18°C.[60]

Constant load grams	Stress 10^8 dynes/cm^2	Extension (%) at 30% RH	40% RH	55% RH	65% RH
		Viscose Rayon			
10	1.34	0.25	0.38	0.40	0.50
20	2.68	0.70	0.72	0.74	1.0
30	4.02	1.1	1.2	1.6	3.8
40	5.36	1.4	2.4	3.4	6.7
50	6.70	2.4	4.9	5.8	9.3
60	8.04	3.6	7.5	8.5	11.0
70	9.38	5.0	9.7	11.0	13.0
		Cellulose Acetate			
10	1.17	0.2	0.3	0.35	0.4
20	2.34	0.6	0.64	0.8	0.8
30	3.51	1.0	1.1	1.2	1.4
40	4.68	1.4	1.5	2.1	4.5
50	5.85	1.9	2.7	3.5	7.4
60	7.02	3.5	3.8	5.8	9.7
70	8.19	6.0	6.4	9.6	13.5

Table 7 gives values of stress proportional to the strain reached after 24 hours under constant load. This strain is reversible, consisting of instantaneous extension and primary creep. As the relative humidity increases, the stress corresponding to the "elastic limit" decreases appreciably for viscose rayon but not so for cellulose acetate. The amount of extension that is recoverable is about twice as great at 30% RH compared with 65% RH for viscose rayon but only one third greater for acetate. The magnitude at the elastic limit is less than 2%. It seems intuitively obvious that wet fibers under prolonged stress will elongate further than dry fibers under similar stress conditions.

Table 7: Stress and extension after 24 hours, below which recovery is perfect, at 18°C. [60]

Relative humidity	Viscose rayon		Cellulose acetate	
	Stress		Stress	
%	10^8 dynes/cm^2	Extension %	10^8 dynes/cm^2	Extension %
30	5.4	1.4	5.8	1.9
40	4.0	1.2	5.2	1.8
55	3.1	1.0	4.1	1.6
65	2.1	0.7	3.7	1.4

PAPER CREEP

Hemicellulose content and relative humidity may affect the tensile creep of paper and single fibers in an analogous manner. No data concerning the relationship between creep and hemicellulose content in paper was found. However, the tensile strength of individual fibers has been related to the hemicellulose content of the fiber in a preceding section.

Brezinski[5] tested the relative humidity effect on the tensile creep of commercial softwood alpha pulp handsheets at various relative humidities. The moisture content at the various relative humidities is listed in Table 8. Prior to testing, the handsheets were air dried to equilibrium at 50% RH and 73°F with essentially zero shrinkage in the plane of the sheet. The creep tests were run at various stresses for a 24-hour interval followed by 24-hour recovery tests. The total 24-hour creep deformations are plotted versus initial stress at 23.5, 50, 60, 73.5, 83, and 90% RH (Figure 14). The effect of increasing relative humidity is a speeding up of the creep response at constant initial stress.

Table 8: Handsheet moisture content vs. relative humidity in creep tests at 73°F.

	Handsheet moisture content, % (oven-dry basis)	
Relative humidity	Absorption series	Desorption from 97.8% RH
23.5	4.6	4.7
50	7.4	8.0
63	8.5	10.4
73.5	10.4	12.6
83	14.0	16.1
94	21	
97.8	24	

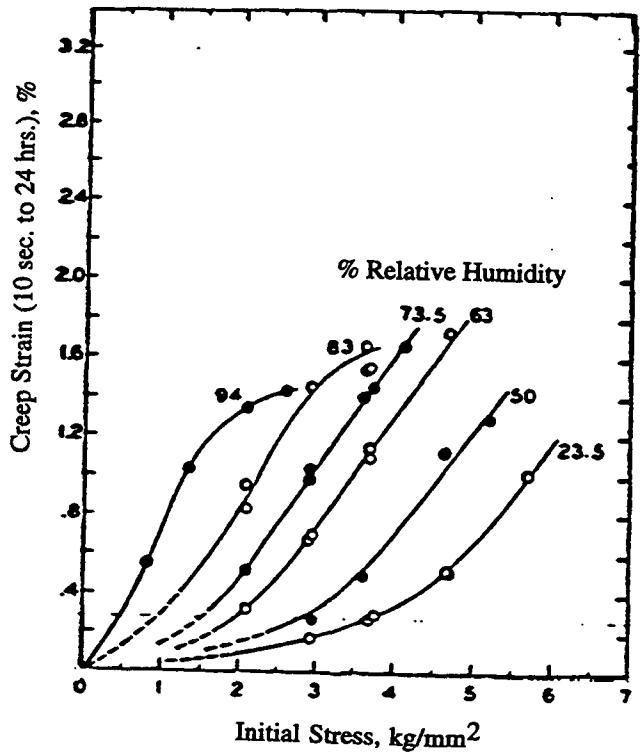

Figure 14: Total creep deformation versus initial stress at various relative humidities in 24-hr tests.[5]

Changes in recoverability of total creep deformations with relative humidity depend on the extent of deformation. Minimums in the percentage of recovery occurred between 70 and 80% RH when the total 24-hour recovery deformations exceeded 0.6% and the percentage of recovery increased rapidly from 60 to 50% RH. The latter change correlated with sharp breaks in curves relating total 24-hour creep deformations to relative humidity at constant initial stress. The breaks in response are shown by double logarithmic plots of the initial stress required to reach specified total 24-hour creep deformations versus 100 minus the relative humidity in percent (Figure 15).

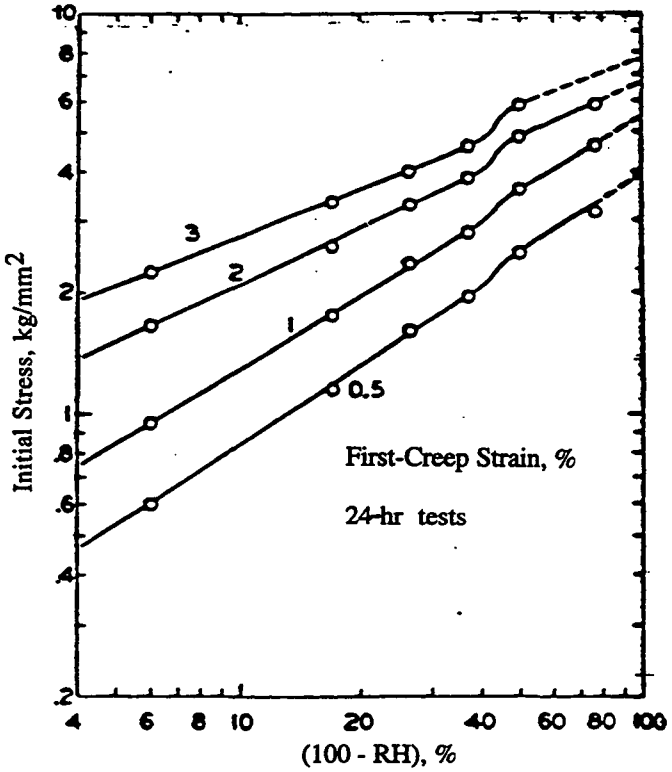

Figure 15: Initial stress required to reach specified total creep deformations in 24 hours versus (100 - RH).[5]

The sharp rise in initial stress does not occur in similar plots for total recovery deformation and is attributable to the nonrecoverable component of the creep deformation. Similar breaks in response between 60 and 70% RH in load deformation response versus relative humidity are reported for machine-made papers. The breaks in response are toward a reduced percentage of nonrecoverable deformation at lower relative humidities. A reduced percentage of nonrecoverable deformation can be considered as "partial mechanical conditioning." In this case mechanical conditioning is effective at relative humidities below those of the mechanical conditioning test, but the effect is destroyed progressively as the relative humidity is increased to higher values. For these specimens, the "partial mechanical conditioning" effect might occur as a result of structural changes during drying.[5]

A mechanism of deformation which is unaffected by changes in specimen moisture content would involve changes in the crystalline structure. Earlier deformation may be due to changes in molecular configuration in the amorphous areas of the fiber.

Byrd[61] studied the tensile creep response to moisture content in southern pine bleached kraft handsheets. He compared the creep response at constant 90% RH conditions with the creep response obtained when the relative humidity was cycled between 90% and 35%. The handsheets were cycled between 35 and 90% RH several times to relieve drying stresses prior to equilibration at 50% RH. Two series of creep measurements were made: (a) sheets loaded at a given stress level were exposed to cyclic relative humidity conditions [relative humidity alternated between 90 and 35%] for 10 cycles, and (b) sheets loaded at the same stress level and exposed to a constant environment of 90% RH for a time equivalent to 10 cycles. Cyclic creep tests were started at 90% RH; however, the length of conditioning at 90% RH prior to testing was uclear. All creep tests were carried out at 23°C. At any applied load, the permanent deformation after 24 hours of creep, the creep rate (Table 9), and the total deformation at times above about 1000 minutes (Figure 16) were greater in the cyclic tests than in the constant 90% RH tests.

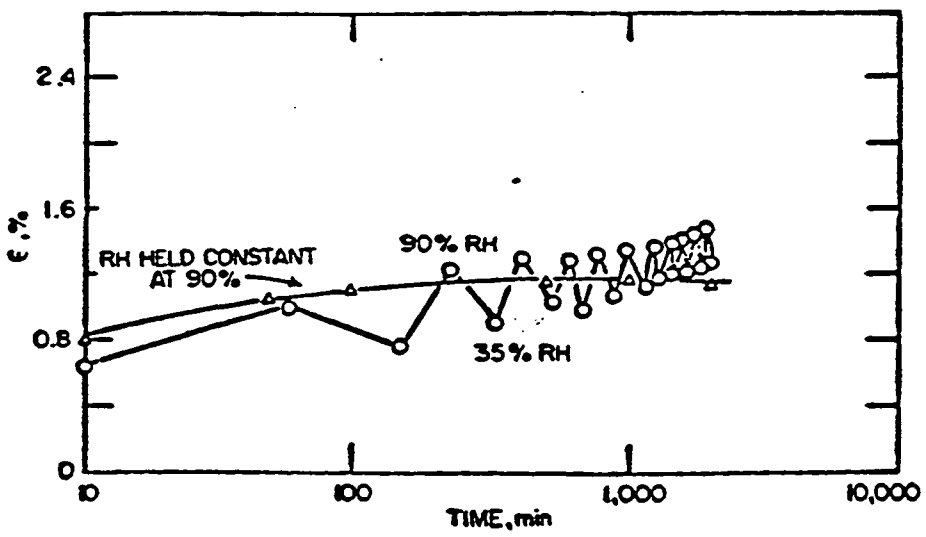

Figure 16: Typical creep response of paper in cyclic and constant RH environments at 70% of maximum tensile stress. [61]

The fact that the creep in paper during relative humidity cycling exceeds the creep obtained at the high relative humidity employed cycling was attributed to fiber-fiber bond rupture during each drying cycle of the cyclic test. The creep rates were calculated from the differential forms of the regression equations describing creep response during constant relative humidity creep and the deformations in equilibrium at 90% RH (absorption) during cyclic relative humidity creep. The creep rates are compared in Table 9. The creep deformation as well as the creep rate is increased by cycling the relative humidity in handsheets.

Table 9: Comparison of creep and cyclic relative humidity creep properties.[61]

Stress level, % of max.	Creep deformation after 5,000 min, %	Permanent set after 24 hr, %	Creep rates after 500 min of creep, %/day
		Constant (90%) RH	
40	0.71	0.20	0.0644
55	1.18	0.57	0.0834
70	1.52	0.67	0.103
		Cyclic (90–35%) RH	
40	1.12	0.43	0.276
55	1.50	0.88	0.336
70	2.36	1.21	0.510

The increase in creep rate exhibited by handsheets undergoing cyclic relative humidity changes leads to a shorter life expectancy for paper products exposed to variable relative humidities. A handsheet at 80% of maximum stress was exposed to a cyclic relative humidity environment (90–35% RH). The specimen creeped to failure in 16 days. Under the same tensile stress, a handsheet exposed to a constant 90% RH environment creeped to failure in 64 days. Rupture-life of wood is also reduced at all stress levels by exposure to a variable relative humidity environment.[62]

Greater creep under cyclic moisture conditions has led to the term "accelerated creep" when describing this phenomenon. Accelerated creep occurs on both sorption and desorption. In order to see this most clearly, the dimensional changes caused by swelling or shrinkage must be

accounted for. For example, the measured compressive creep accompanying sorption is equal to the actual creep minus the dimensional changes caused by the swelling of the sample. If this swelling is appreciable compared to the actual compressive deformation, the measured creep might decrease even though the actual creep is increasing.

The greater the magnitude of change in relative humidity the larger is the accelerated creep. With a larger humidity change, a higher moisture content is reached than if the paper is exposed to several smaller humidity steps. The sorption of water also occurs relatively more rapidly if the change in humidity is large. According to Salmen,[63] with more non-bonded water present with a larger moisture gradient, stresses may be released to a greater extent than if the moisture increase occurs in small intervals. With a constant moisture gradient through the sample, no accelerated creep effects are observable. In this case, water molecules associated with the hydroxyl groups of the wood polymers may be more stationary, only those having a lower bonding energy moving through the sample without the interacting with the more bonded water. This could leave the wood polymers unaffected or at least not give them any greater freedom of movement, since no exchange of water molecules would occur. With water as the interacting medium, it is highly probable that accelerated creep is related to an increased mobility of the molecules.[63]

The removal of the load after accelerated creep causes immediate and delayed recovery of dimensions, similar in magnitude to those which would occur after a normal creep test, where moisture has been held constant. However, a far greater recovery, consisting of the bulk of the creep caused by the mechanosorptive effect, can be realized if sample moisture is cycled in the unloaded state.[64] It appears that some portion of the sample "remembers" its original shape.

In addition to increased creep, moisture cycling under load can lead to failure at low loads. In these cases, the creep at failure is far greater than breaking strains obtained under equilibrium moisture conditions. Also, tensile stiffness, measured by the initial slope of a stress-

strain curve, decreases during accelerated creep, gradually dropping by 20–30% prior to failure.[65]

Many problems involve the dimensional changes in paper products by uncontrolled relative humidity environments, but so far their causes have not been deduced by studying the response of paper to creep. Creep in paper is the result of two types of phenomena: the individual fiber creep and fiber-fiber bond creep. There is need to independently study the fibers which make up the bonded network. There is need for fundamental understanding of the role of amorphous hemicellulose components in the creep response of pulp fibers. Little is known about the tensile creep response of individual pulp fibers in a changing relative humidity environment.

SUMMARY

Spiegelberg[42] indicates that hemicelluloses exert a strong influence on the strength and the internal stress redistribution of a fiber. Work by Jentzen[24] and others[7] indicates that an internal stress redistribution occurs in fibers when they are dried under an external load. Evidence on whether hemicelluloses influence creep behavior of pulp fibers has not been experimentally obtained.

Hemicelluloses are quite hydrophilic and amorphous, capable of adsorbing large amounts of water.[55,56] The adsorption and desorption of water affects the mechanical properties of fibers. Experimental results now available are not adequate to define single fiber creep response in relation to hemicellulose content as a function of relative humidity.

No completely satisfactory explanation describing all of the characteristics of accelerated paper creep and single fiber creep is presently available. Experimental results now available are not adequate to define whether single fiber cyclic creep response in relation to hemicellulose content as a function of relative humidity is indeed accelerated creep.

THEORETICAL ANALYSIS OF DATA

INTRODUCTION

Creep and creep recovery tests gauge the dimensional stability of a material, and because the tests can be of long duration, such tests are of practical importance. Creep measurements are of interest to chemists and engineers in any application where the polymer must sustain loads for long periods. Creep and creep recovery data can be analyzed statistically. However, a more fundamental approach is desired, and several theories exist to explain the creep and creep recovery phenomena. One well established theory is that of Eyring.[51] Eyring's molecular model represents the rheological behavior of fibers by applying the kinetic theory of rate processes to the relative movement of flow units in the fiber.[51] The Eyring approach can be represented in a more traditional manner as a combination of spring and dashpot elements. Eyring analyzed creep curves on the basis of a three-element model consisting of two Hookean springs and a nonlinear dashpot. The theory can be used to compute both the elastic and viscous contributions to strain. Hill,[6] Haslach,[66] and Byrd[61] have successfully used empirical constitutive equations to analyze the standard stress strain relationship or creep phenomenon. The empirical constitutive constants that are obtained are not detailed in terms of molecular structure. Eyring's model offers a view of correlating these properties with molecular constants such as the volume of the cellulosic flow unit and the activation energy for flow. A model in which the kinetic theory of rate processes[48] has been applied to relative movement of the long chain molecules in fibers has been established. However, fibers exhibit permanent set or irrecoverable deformation when released from their strained position, and Eyring's model does not account for this.

Primary creep and creep recovery are time-dependent phenomena. For example, the longer the time after unloading, the greater the fraction of creep recovered. If a fiber is subjected to a number of loadings and unloadings, complex creep phenomena may result. These are reduced to a simple scheme by the superposition principle proposed by Boltzmann.[51] A time-

temperature superposition principle describes the effect of temperature on the time scale of response.[67] Time is the major factor in determining the mechanical properties of a polymer.

The purpose of this chapter is first to familiarize the reader with the general kinetic theory of rate processes. Second, the kinetic approach to polymer creep is compared to the mechanical models used to represent creep. Third, the role permanent set plays in the shaping of the creep and creep recovery response is explored. Finally, as a result of the time-dependence of the primary creep and creep recovery phenomena, the superposition of load and temperature will be discussed as a premise for the superposition of moisture in cyclic creep data analysis.

KINETIC THEORY OF RATE PROCESSES

Cellulose chains, as previously described, may be arranged in an orderly manner to produce crystallites. Alternatively, the cellulose chains may be disordered where they are attached to each other by secondary bonds at relatively few points, and the application of strain will cause these molecules to slip throughout the structure from one equilibrium position to another. Secondary bonds may be hydrogen bonds or Van der Waals forces.[7] Strain may cause these chain molecules to slip, especially if they are only loosely held at the crystalline areas.

When a load is applied to a fiber thus creating a shearing stress, there will be a general displacement in the direction of the load, and the energy dissipated in the process will constitute an internal friction or viscosity. In order to examine the role of creep in fundamental terms, Eyring and his coworkers[48,49,51] extended the theory of chemical reaction rates to describe the phenomena of viscosity and viscoelasticity in fibers.

According to the kinetic theory of matter, all atoms and molecules or, in this case, flow units are in motion. In a fiber, each flow unit can be depicted as sitting at the bottom of a potential energy well (Figure 17). At equilibrium, a flow unit in its well appears satisfied where it is. But, because it is in constant motion, it can occasionally surmount the energy barrier and obtain a new position of minimum energy (Figure 17). In a solid this jumping of the energy

barrier is less frequent than in a liquid, and on the average there are just as many jumps forward as there are backward. So there is no net movement of the flow unit.

The statistical thermodynamic theory of reaction rates[68] tells us that the number of jumps per unit time in the forward direction, n+, is given by

$$n+ = (kT/h)\exp(-\Delta F/RT) \qquad (1)$$

where $k =$ Boltzmann's constant, 1.38×10^{-23} J/°K

$T =$ temperature, °K

$h =$ Planck's constant, 6.626×10^{-34} Jsec

$R =$ the gas constant, 1.987 cal/mol°K

$\Delta F =$ free energy of activation (cal. per mole) for the flow process, or the height of the potential energy barrier.

The number of jumps per unit time in the opposite direction

$$n- = (kT/h)\exp(-\Delta F/RT) \qquad (2)$$

is identical, so on the average, there are just as many jumps forward as there are backward. No net motion occurs.

A fiber as modeled according to Eyring's theory consists of basic structural elements that are crystalline in nature (Figure 18). At equilibrium, the crystallite structures are free to undergo thermal vibration; the flow unit pictured just above A will be supposed to move backward n times per second and forward an equal number of times. All movement takes place at empty or void places in the structure as indicated at A and B in Figure 18. Flow units cannot move into a space occupied by another unit. Voids are assumed to occur at intervals of λ_1. In order to move, the flow unit will have to overcome a symmetrical potential energy barrier at a distance, $\lambda/2$.

On the average the cellulosic flow unit does not have sufficient energy to overcome the barrier called the free energy of activation for the flow process, ΔF, until it acquires additional strain energy due to the applied load. If the force per square centimeter of surface is f, then the effective force acting to displace a single flow unit is $f\lambda_2\lambda_3$, where $\lambda_2\lambda_3$ is the effective cross-sectional area of the flow unit normal to the direction of flow. The applied load contributes the work, $f(\lambda_2\lambda_3\lambda/2)$, toward surmounting the energy barrier. The work towards surmounting the energy barrier is equivalent to a symmetric distortion of the potential energy barrier (Figure 17). The driving force for this movement is a final state that is lower in potential energy than the initial state, so net movement takes place from the initial to the final state. The distance the flow unit is displaced from the initial to the final states is λ.

The situation changes when, superimposed upon this symmetrical energy barrier, an external load is applied to the fiber. The tendency of the flow unit to jump the barrier in one direction is different from the tendency to jump the barrier in the reverse direction.

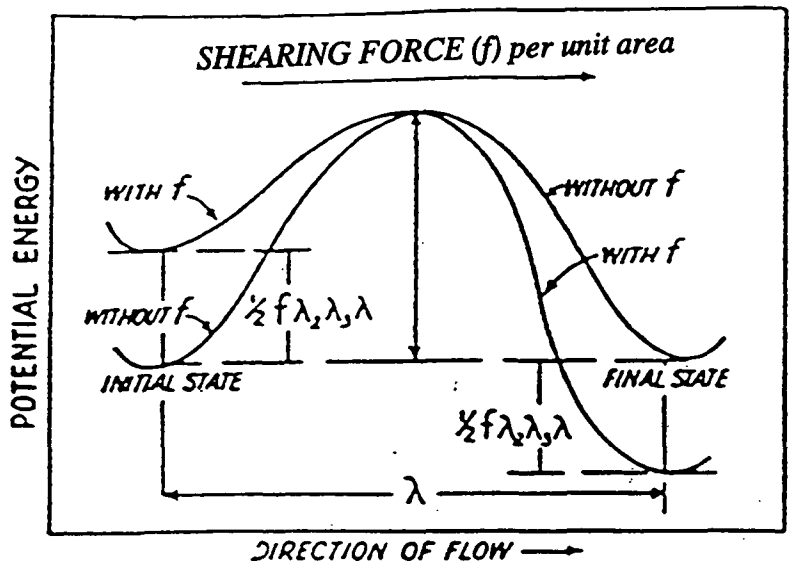

Figure 17: Potential energy diagram of a flowing molecular segment as it passes from one equilibrium position to another.[51]

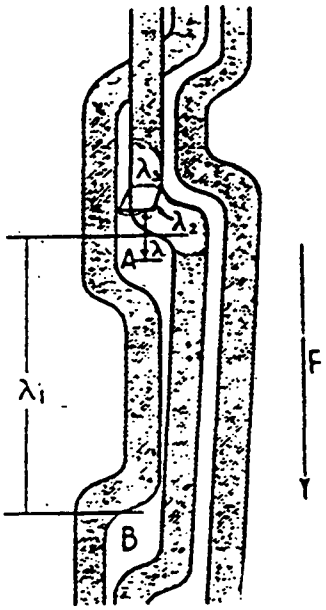

Figure 18: Cellulosic fiber model containing a cellulosic flow element and voids.[51]

For this unsymmetric energy barrier the flow unit moves in the forward direction $(kT/h)\exp(-\Delta F/RT)\exp(f\lambda_2\lambda_3\lambda/2kT)$ times per second and in the reverse direction $(kT/h)\exp(-\Delta F/RT)\exp(-f\lambda_2\lambda_3\lambda/2kT)$ times per second. The forward velocity of the cellulosic flow unit is the net number of times the flow unit moves forward times the distance it jumps,

$$\lambda(kT/h)\exp(-\Delta F/RT)[\exp(f\lambda_2\lambda_3\lambda/2kT) - \exp(-f\lambda_2\lambda_3\lambda/2kT)] \qquad (3)$$

The resulting rate of strain is obtained by dividing this velocity by the distance λ_1 between points of flow in the direction of flow and substituting the expression of the hyperbolic sine into Eq. (3).

Then $$de/dt = (\lambda/\lambda_1)(kT/h)\exp(-\Delta F/RT)[\exp(f\lambda_2\lambda_3\lambda/2kT) - \exp(-f\lambda_2\lambda_3\lambda/2kT)] \qquad (4)$$

$$\sinh x = (e^x - e^{-x})/2 \qquad (5)$$

So the relative change in length of fiber per second due to flow is

$$de/dt = 2(\lambda/\lambda_1)(kT/h)\exp(-\Delta F/RT)\sinh(f\lambda_2\lambda_3\lambda/2kT). \qquad (6)$$

The volume of the flowing cellulosic unit is $V_m = \lambda_1\lambda_2\lambda_3$. This is assumed to be the dimensions of the cellulose unit cell, (10.3 x 8.35 x 7.9) $Å^3$. The volume of the void left by the cellulosic flow unit is $V_f = \lambda_2\lambda_3\lambda$. The rate of flow can be described as

$$de/dt = 2(V_f/V_m)(kT/h)\exp(-\Delta F/RT)\sinh(fV_f/2kT). \quad (7)$$

The resulting rate of strain from Eq. (7) can be expressed as

$$de/dt = 2(\lambda/\lambda_1)(kT/h)\exp(-\Delta F/RT)\sinh(f\lambda/2NkT) \quad (8)$$

and N is the number of cellulosic flow units per unit area of cross section on which the stress is acting. Rewriting Eq. (8) in terms of two constants, χ and α, the rate of strain is

$$de/dt = \chi\sinh(\alpha f) \quad (9)$$

where

$$\chi = 2(\lambda/\lambda_1)(kT/h)\exp(-\Delta F/RT) \quad (10)$$

and

$$\alpha = \lambda/2NkT. \quad (11)$$

Eq. (9) represents a nonlinear relation between stress and strain rate; the rate of strain increases more than in direct proportion to the applied load. The behavior is represented by a hyperbolic sine law of viscous flow. The parameters, χ and α, in Eq. (9) can describe cellulosic fiber behavior. In the limit of α approaching zero, $\sinh x = x$, and the flow rate reduces to

$$de/dt = \chi\alpha f = f/\eta, \quad (12)$$

the traditional linear relationship, so the behavior of the viscous process is Newtonian. The rate of strain caused by a stress is proportional to the stress. Newtonian behavior can occur when the λ is very small or N, the number of cellulosic flow units per unit area of cross section, is very large. Eq. (12) is also written as a function of viscosity, η. The product of Eyring's viscous parameters, χ and α, is equivalent to the inverse of viscosity.

As α increases in value, the expansion of sinh x gives the exponential character to flow because when $x >> 1$, $\sinh x = 1/2e^x$. The rate of strain will be non-Newtonian and represented by the following relationship

$$de/dt = \chi e^{\alpha f}/2. \qquad (13)$$

It is shown that, depending on the size of α, the viscous behavior will be Newtonian or exponential. Both behaviors are explained and connected by a hyperbolic sine law. According to Eyring,[51] if $\alpha f < 1$, the behavior will be Newtonian. For values of $\alpha f > 3$, the behavior will be exponential.

Eyring analyzed fiber creep on the basis of a three-element model (Figure 19) consisting of two Hookean springs and a non-Newtonian dashpot. The dashpot behavior is represented by a hyperbolic sine law of viscous flow, Eq. (9), where the rate of strain has a nonlinear relation with stress. Eyring[51] proposed that the dashpot represents the flow of the cellulosic chain units.

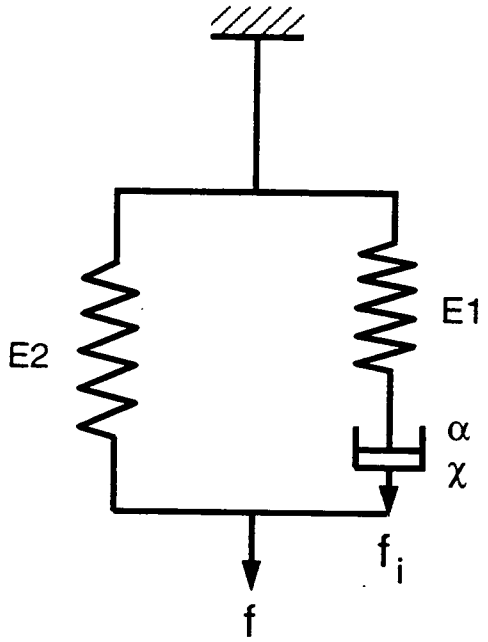

Figure 19: Three-element model used to describe the behavior of fibers.

In addition to the movement of flow units there is an initial extension corresponding to the elastic deformation of the structure. This can be represented by a spring, E1, in series with a

dashpot and a second spring, E2, in parallel in the three-element model (Figure 19). Both springs in the three-element model are Hookean. The modulus, E1, and the internal stress, f_i, corresponding to the right-hand spring can be expressed as follows

$$de/dt = (1/E1)(df_i/dt) + \chi \sinh(\alpha f_i). \tag{14}$$

Eyring[51] proposed that E1 represents the modulus of the linear chain molecules and E2 represents the modulus of the molecular network. Consequently, modulus, E2, and stress, f, correspondingly to the left-hand spring can be expressed as follows

$$e = (f - f_i)/E2 \tag{15}$$

or

$$f_i = f - eE2. \tag{16}$$

The expression for the total strain is given in Eq. (15). Rearranging Eq. (15), the expression for the internal stress is given in Eq. (16). Using Eq. (16) to eliminate the internal stress from Eq. (14), the following differential expression results

$$d/dt[(E1 + E2)e - f] = E_1 \chi \sinh\alpha(f - eE2) \tag{17}$$

which gives the relation between external stress, f, the external strain, e, and time, t, in terms of the constants, E1, E2, χ, and α, for Erying's model including the non-Newtonian dashpot. For creep at constant stress, fc, where f = fc and the rate of stress, df/dt = 0, Eq. (17) can be integrated and rewritten as follows,

$$e = e_\infty[1 - (1/\alpha fc)\ln \coth 1/2(A't + B')] \tag{18}$$

where

$$A' = \alpha\chi fc(1 - e_0/e_\infty)/e_\infty \tag{19}$$

$$B' = \ln \coth 1/2\alpha fc(1 - e_0/e_\infty). \tag{20}$$

The two constants, A' and B', involve the four unknown quantities $e_0 = f/(E1 + E2)$, $e_\infty = f/E2$, α, and χ. Single pulp fiber creep curve data can be analyzed in this manner.

Other researchers[6, 9] have analyzed creep curve data where the creep deformation is proportional to the logarithm of time. Logarithmic creep is described by Eq. (21),

$$e = a + b\ln(t) \tag{21}$$

where e = the total strain; immediate elastic and time-dependent

t = the time from the instant of application of stress

a and b = constants.

The Eyring model can be expressed as a function of logarithmic time when the applied load is small and the time is less than 100,000 seconds. The hyperbolic cotangent term in Eq. (18) can be expanded and truncated at the first term such that coth x = 1/x, and then Eq. (18) reduces to a function of logarithmic time,

$$e = e_o + (e_\infty/\alpha fc)\ln[1 + (A'/B')t]. \tag{22}$$

The Eyring equation can approximate the lnt as described by Eq. (21). The Eyring[51] theory encompasses constitutive and mechanical models normally used in the analysis of creep.

In primary creep, the various parameters assigned to the springs and dashpot for Eyring's theory of fiber creep have physical significance of the molecular fiber structure to which the configuration response can be attributed. However, to simulate some of the peculiar rheological properties of fibers, various other mechanical models have been devised. They too consist of spring elements to provide the elastic effects and dashpot elements to provide for the slow creep or recovery behavior. It is interesting to compare the model used by Eyring to that of an alternative three-element model when both are under Newtonian flow conditions.

MECHANICAL MODEL COMPARISON

Mechanical models are often used to simulate creep response. If the springs are Hookean and the viscous flow is Newtonian, it is possible to describe mathematically the behavior of the

models under stress. A Maxwell unit consists of a Hookean spring in series with a Newtonian viscous element. The Eyring theory which represents a Maxwell unit in parallel with a spring is illustrated in Figure 19. For the Maxwell unit in Figure 19 the relation between stress and strain is

$$de/dt = (1/E1)df_i/dt + f_i/\eta \tag{23}$$

where the internal stress is $f_i = f - E2e$. Eq. (23) can be rewritten by eliminating the internal stresses and multiplying through by E1 as follows

$$(E1)de/dt = df/dt - (E2)de/dt + (E1/\eta)(f - eE2). \tag{24}$$

Rearranging,

$$d/dt[(E1 + E2)e - f] = (E1/\eta)(f - eE2) \tag{25}$$

or $$de/dt = -eE1E2/((E1 + E2)(\eta)) + E1f/((E1 + E2)(\eta)) + df/dt \tag{26}$$

the three-element model (Figure 19) represented in Eq. (25) is in a similar form to that of Eyring's model represented by Eq. (17) which gives the relation between external stress, f, external strain, e, and time, t, in terms of the constants, E1, E2, and η, including a Newtonian dashpot. For creep at constant stress, fc, where f = fc and the rate of stress, df/dt = 0, Eq. (26) can be integrated and rewritten as follows,

$$e = fc/(E1 + E2)[1 + E1/E2(1 - e^{-tE1E2/(E1 + E2)\eta})] \tag{27}$$

or $$e = fc/(E1 + E2)[1 + E1/E2(1 - e^{-t/\tau})] \tag{28}$$

where the relaxation time is $\tau = \eta(E1 + E2)/E1E2$.

CREEP RECOVERY

Theoretically creep and creep recovery data should be mirror images of each other.

Leaderman[45] found creep and creep recovery could be represented by an identical form

$$e = e_o + \theta(fc)\psi(t) \qquad (29)$$

where e = extension after time t

e_o = instantaneous extension

$\theta(fc)$ = a function of stress

$\psi(t)$ = a function of time

so the changes in length during creep and creep recovery must follow the same curve and be inverses of each other.

Figure 20 illustrates the theoretical creep and creep recovery behavior of a sample using the Eyring parameters from Eq. (18). The Eyring parameters used in the creep and creep recovery example in Figure 20 are listed in Table 10. If a load is applied to a sample, there is an immediate extension at time zero equal to the elastic extension. As the load is held constant, the sample extends with increasing time. The hypothetical creep curves illustrated in Figure 20 show the load applied for 24 and 48 hours before the load is removed for creep recovery.

Upon removal of the load, an immediate decrease in extension called the elastic recovery, (fc/(E1+ E2), is observed. The sample continues to decay in extension with increasing time while under no load until the sample fully recovers to its initial form.

Figure 20: Creep and Creep Recovery (Mirror Images)

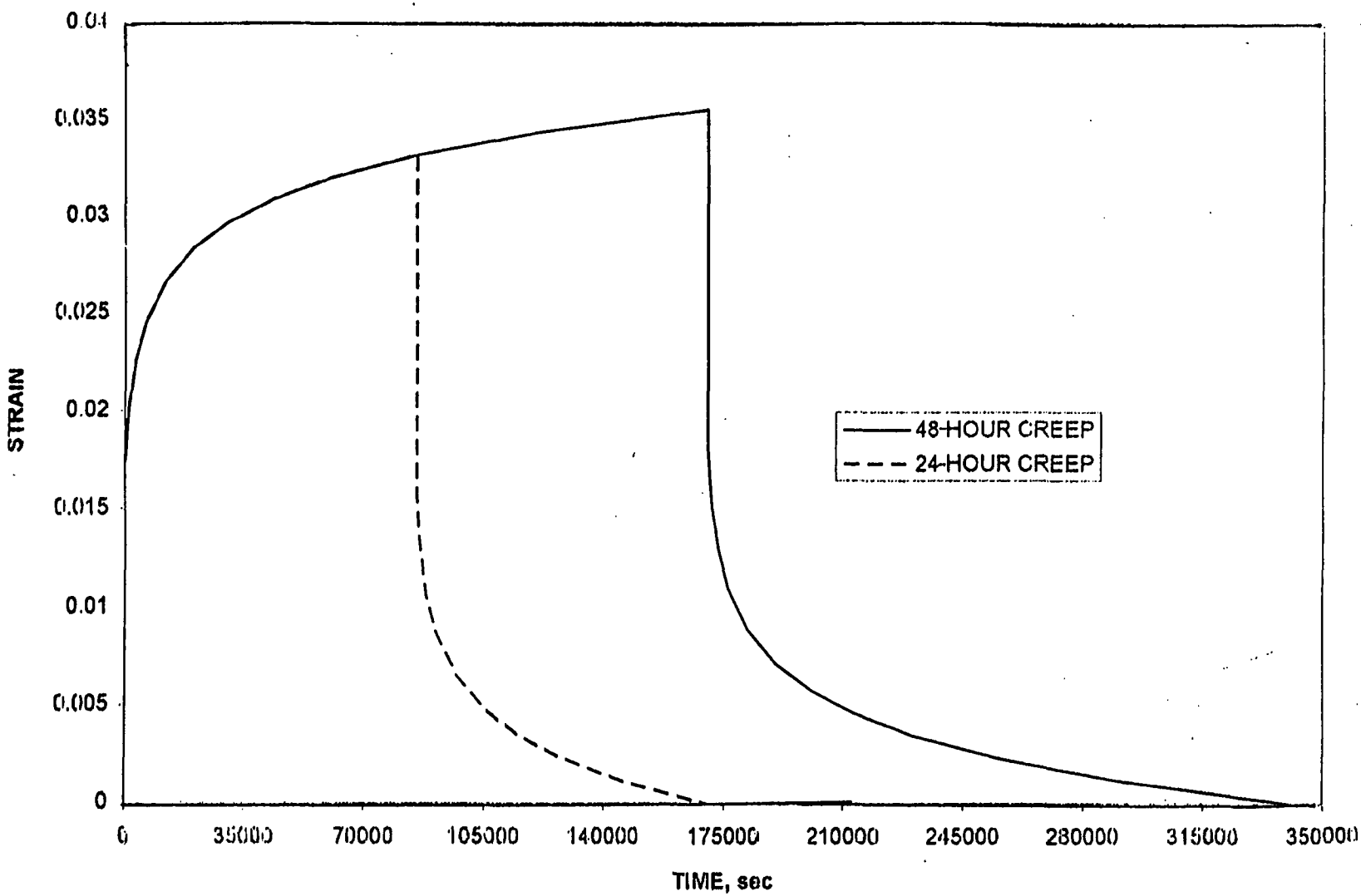

Table 10: Creep and creep recovery parameters.

fc	α	χ	E1	E2
3.79	2.01	1.81	4.81	1.68

Units: Stress 10^9 dynes/cm^2, Alpha 10^{-8} cm^2/dynes, Chi 10^{-14} sec^{-1}, Moduli 10^{11} dynes/cm^2

Theoretically creep and creep recovery data collected for single fibers should be mirror images of each other if the delayed extension is small compared with the instantaneous extension; however, they are not.

PERMANENT SET

If fibers are maintained at constant stress and allowed to creep, they may exhibit a permanent set or irrecoverable deformation when the stress is released. The mechanical model in Figure 19 does not sufficiently describe the creep and creep recovery behavior of single fibers exhibiting permanent set. A modified mechanical model is presented in Figure 21. The four-element model can be used to describe creep.

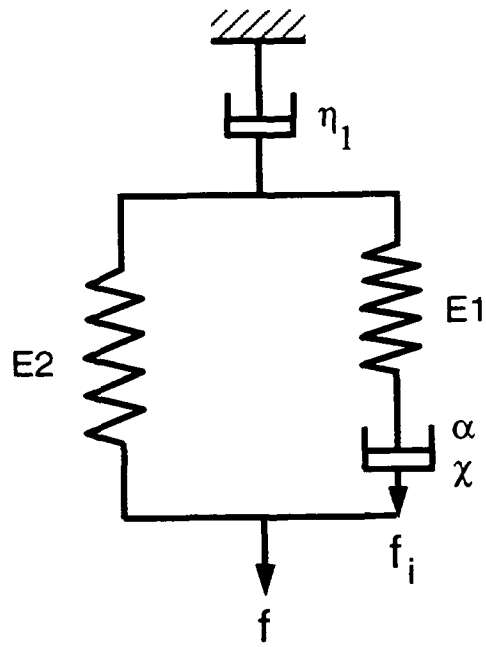

Figure 21: Four-element model used to describe the behavior of fibers.

When a constant load is applied, the elongation comes from the single spring with the modulus, E1, as well as the elongation from the spring, E2, and the dashpot, η, in parallel, and the dashpot with the viscosity, η_1. The total elongation of the four-element model is the sum of the individual elongations of the parts, thus Eq. (30):

$$e = f/(E1 + E2)[1 + E1/E2(1 - e^{-E1E2t/(E1 + E2)\eta}] + (f/\eta 1)t. \quad (30)$$

In a recovery test after the load is removed at time, t_1, the creep is all recoverable except for the flow that occurred in the dashpot with viscosity, η_1. The Eyring equation must be modified to compensate for permanent set or the second dashpot in the four-element model, so

$$e = e_\infty[1 - (1/\alpha f)\ln \coth 1/2(A't + B')] + (f/\eta_1)t. \quad (31)$$

The hypothetical creep and creep recovery of a single loblolly pine fiber is presented in Figure 22. The creep experiments last 24 and 48 hours, and then the load is removed for the creep recovery experiments. The instant the load is removed there is a reduction in the elongation of the model equal to f/(E1 + E2). The fiber continues to decay in extension with increasing time but does not fully recover to its initial form. The fiber assumes a nonzero non-recoverable value of extension. The nonrecoverable extension or permanent set in Figure 22 is defined as $(f/\eta_1)t'$ where t' = 24 hours and $(f/\eta_1)''$ where t'' = 48 hours. Figure 22 illustrates the creep and creep recovery of a four-element model with the viscosity of the second dashpot, η_1 = 2.0×10^{17} dynes sec/cm^2.

In classical polymer theory a line called the Permanent Set Line (PSL) is constructed.[68] The PSL is comprised of the intersection point of each creep recovery curve at their unloading times, t' = 24 hours and t'' = 48 hours. The PSL is comprised of intersection points for each creep recovery curve and should go through the origin. A theoretical PSL is generated in Figure 22 with a slope, $f/\eta_1 = 1.895 \times 10^{-8}$ sec^{-1}. If the PSL is a linear function of time as the classical theory predicts, then the Eyring equation can be modified as described by

Figure 22: Creep and creep recovery with permanent set.

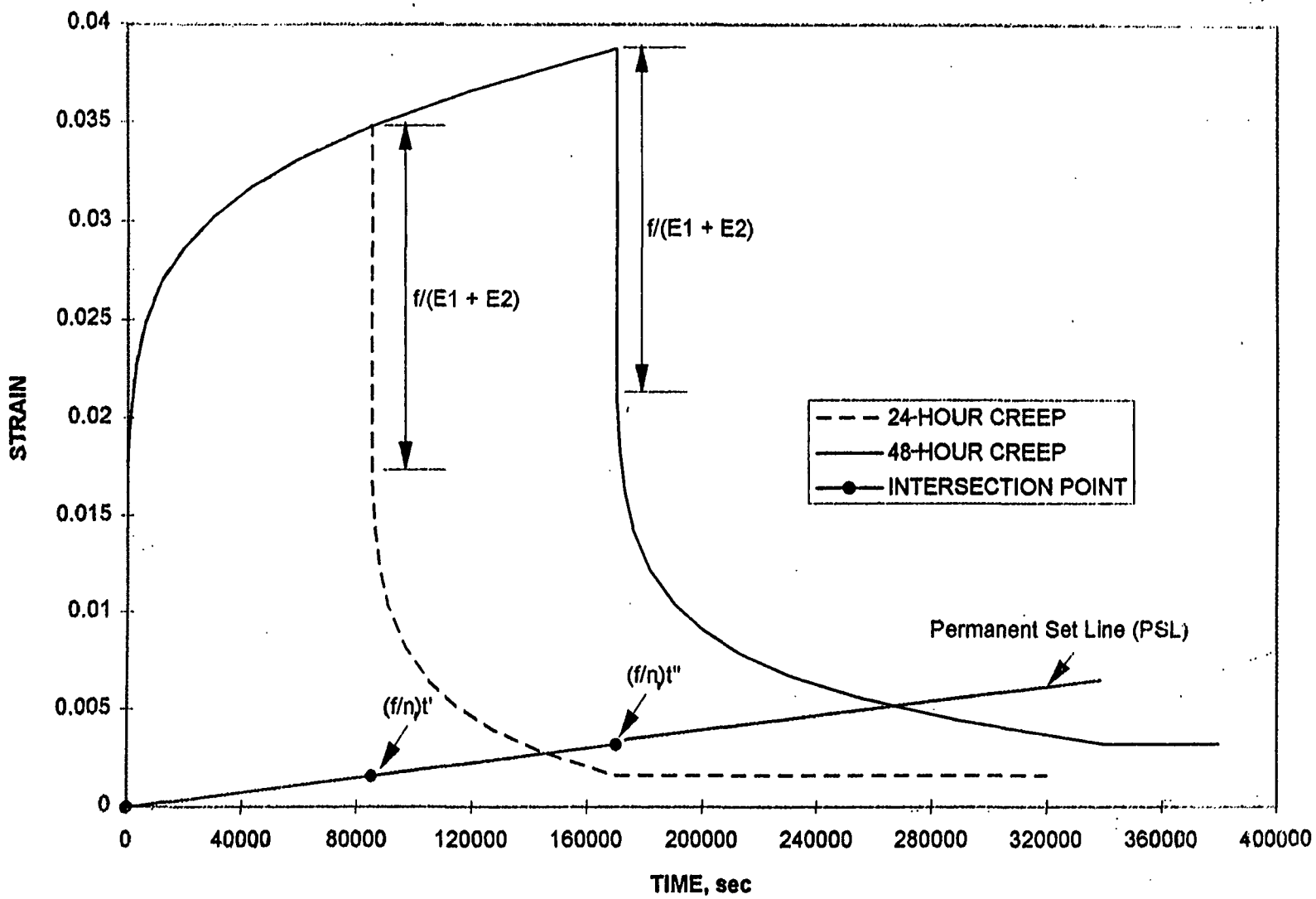

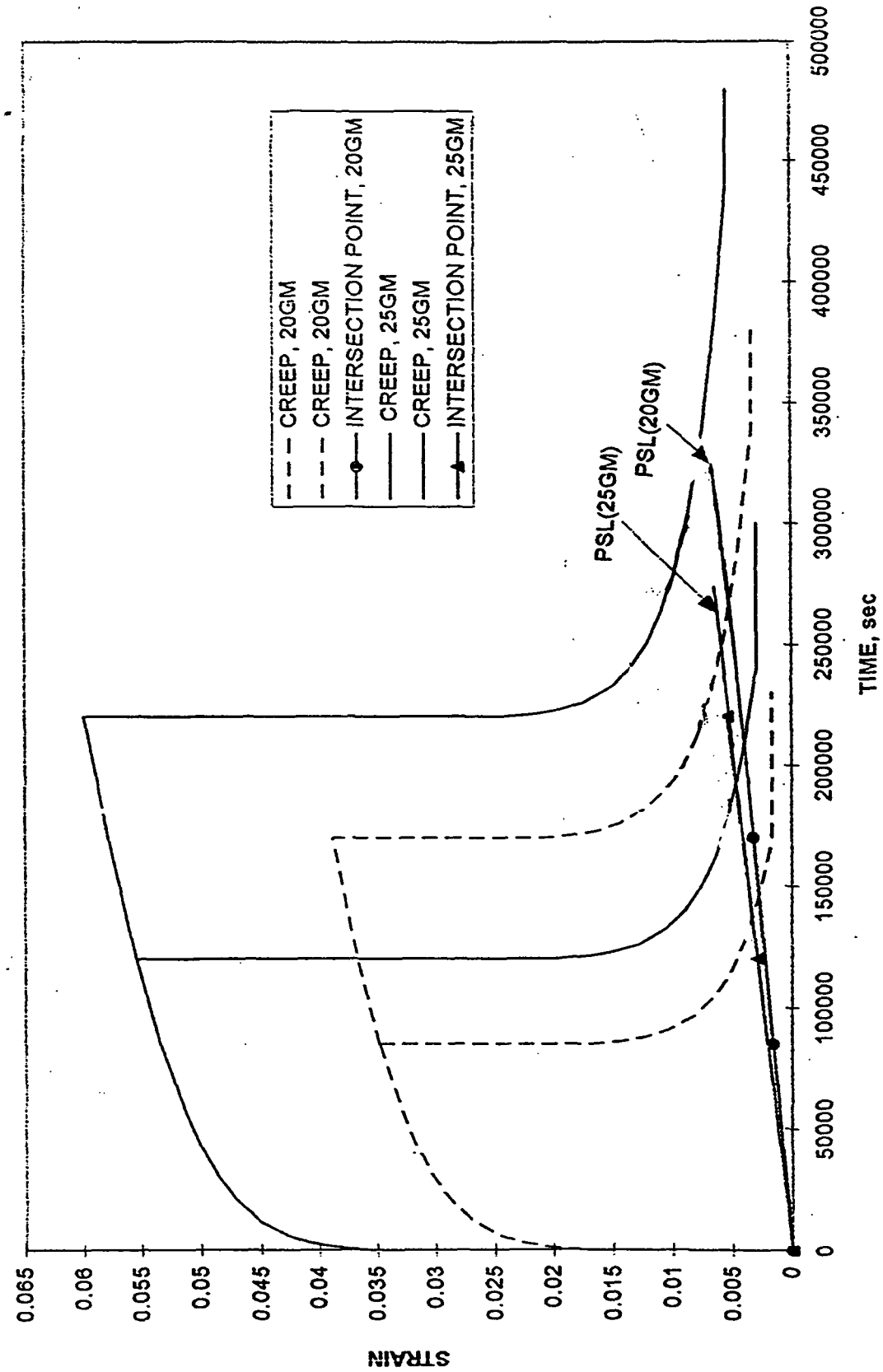

Figure 23: PSL variation with stress.

Eq. (31). However, if the PSL is not a linear function of time, the necessary Eyring modification would be an alternative form.

It is also interesting to note how the PSL varies with stress. The creep and creep recovery of a fiber at 3.79 x 10^9 dynes/cm^2 (20 grams) and a fiber at 4.89 x 10^9 dynes/cm^2 (25 grams) is presented in Figure 23. The cross-sectional area of the fiber loaded to 20 grams is 5.2 x 10^{-6} cm^2. The cross-sectional area of the fiber loaded to 25 grams is 5.0 x 10^{-6} cm^2. The hypothetical creep experiments lasted 24 and 48 hours, and then the load was removed for the creep recovery experiments. A PSL is generated for each stress at the corresponding intersection points. The slope of the PSL for the 4.89 x 10^9 dynes/cm^2 stress (25-gram load) is 29% higher than the slope of the 3.79 x 10^9 dynes/cm^2 (20-gram load). Clearly, if using a modified Eyring analysis and simultaneously fitting for parameters at several different stresses, the relationship between permanent set and stresses needs to be addressed.

SUPERPOSITION PRINCIPLE

The Boltzmann superposition principle describes the response of a material to different loading histories in the absence of secondary creep and nonrecoverable deformations. The superposition principle proposed by Boltzmann states that the deformation at any time of the material exhibiting primary creep is due not only to the load acting at that instant but also to the entire previous loading history. The material exhibits a memory effect; however, the response of a material to a given load is independent of the response of the material to any load that is already on the material. The effect of the different loading states is additive.[51] For the observed deformation at any time during a creep test, the deformations caused by the different loading states are summed up to that point in time. Removing a load is the application of a negative load. The creep function for a negative load is the same as that for a positive load.

For the case of creep, if there are several loading stresses, $fc_0, fc_1, fc_2, \ldots\ldots, fc_{i-1}$, applied at times, $0, t_1, t_2, \ldots\ldots, t_{i-1}$, the Boltzmann superposition principle may be expressed by

$$de/dt = J(t)fc_0 + J(t- t_1)(fc_1 - fc_0) + ... + J(t- t_i)(fc_i - fc_{i-1}). \qquad (32)$$

The creep at time t depends on the compliance function, J(t), which is characteristic of a material at a given temperature and a given initial stress, fc_0. At a later time, t_1, the load is changed to a value of fc_1. At still later times, t_i, the load may be increased or decreased to fc_i, but for each additional stress, a different time scale has to be employed in $J(t - t_i)$, the time over, the load was applied. Also, while de/dt for any load is given by the product, J(t)fc, the stress of concern is the incremental added stress or $(fc_i - fc_0)$.

Figure 24 illustrates the Boltzmann superposition for a material that obeys the Eyring model. The load is doubled after 600 seconds. Doubling the load after 600 seconds gives a total creep that is the superposition of the original creep curve shifted by 600 seconds on top of the extension of the original curve.

Factors other than load are important in describing the mechanical behavior of viscoelastic polymers. One such variable is temperature. Temperature can be applied to a superposition principle. The WLF (Williams, Landel, and Ferry) equation of time-temperature superposition principle describes the effect of different temperature states on the time scale of the response.[67] Leaderman[45] analyzed creep curves at different temperatures by displacing horizontal shifts along a logarithmic time scale to give a single creep curve covering a long range of time. Williams, Landel, and Ferry showed the reference temperature to the superimposed curves was related to T_g.

Assuming the stress relaxation of a hypothetical material with a given reference temperature, T_g, experimental stress relaxation data at a series of different temperature states is collected over a period of time from one minute to 10^4 minutes. Experimental data such as logarithm of stress relaxation modulus are plotted versus logarithm of time for a series of temperatures to form a family of curves. The stress relaxation modulus, $E_r(t)$, is multiplied by a

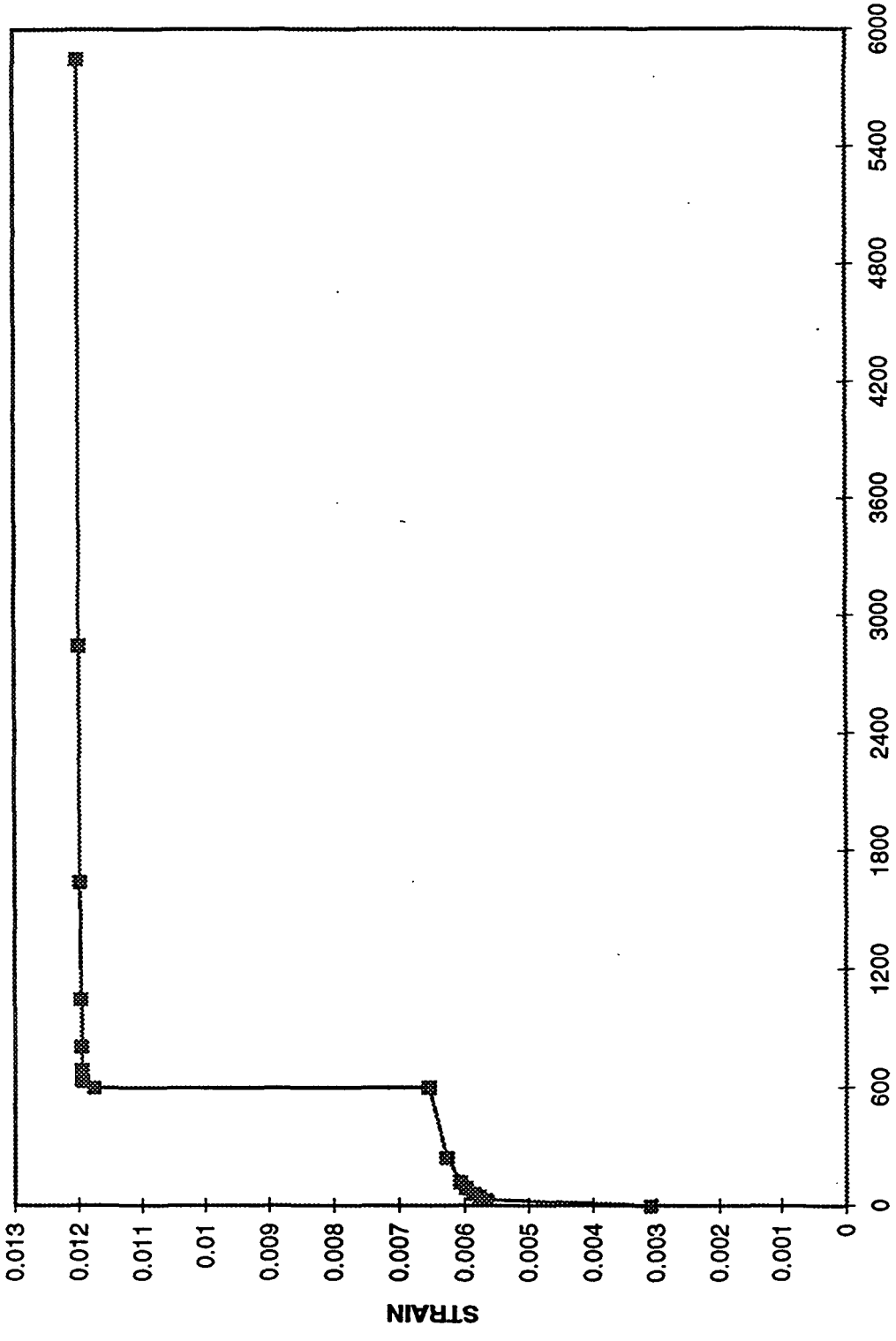

Figure 24: Boltzmann superposition of load.

temperature correction factor, f(T), and the corrected modulus curves are displaced along the logarithmic time scale until they superimpose. Curves at temperature states above the reference temperature, T_g, are shifted to the right, and those below the reference are shifted to the left. The generated master curve or superimposed curve covers 18 decades of time compared to the original data covering four decades.[69] Superimposed master curves give the expected response at other times at that state; in the WLF case the intrinsic variable displaced is temperature instead of load. The ability to displace intrinsic variables in different states will be employed in the analysis of cyclic relative humidity creep data for single pulp fibers where the intrinsic variable is moisture.

ANALYSIS OF HILL'S DATA

CREEP

In the creep test, a load is applied rather rapidly to a specimen, then held constant, and the deformation is recorded as a function of time. A study of single-fiber creep properties of longleaf pine holocellulose fibers was conducted by Hill.[6] The pine holocellulose fibers were obtained from a single chip. This chip was from the summerwood portion of either the 27th or the 28th growth ring of a 49 year old tree to decrease the fiber-to-fiber variability. All fibers were tested at 50% RH. A single-creep curve describes the relationship between deformation and time at a single initial stress. Hill tested fibers at four different initial stresses (1.85, 2.83, 3.79, and 4.89 x 10^9 dynes/cm^2) for a duration of 12, 24, and 48 hours in order to investigate the effects of stress on creep response. Loads (10, 15, 20, and 25 grams) were chosen to limit fiber breakage at the higher stresses and to increase the delayed deformation at the lower stresses. Creep tests made on materials which have not been previously subjected to external loading are commonly termed first creep tests. Average first-creep curves at each applied load and test duration are plotted in Figure 25 as the average strain vs. the logarithm of time in seconds. Average deformation is the mean deformation at various times for all individual fiber tests at a given load and is presented as average strain. Approximately 50 individual fibers were tested for the conditions of initial stress and time except for the 48-hour tests in which ten fibers were tested.

Two types of creep response are represented by the creep curves. The initial creep associated with the behavior of lower initial stresses or shorter times often fits a power function as shown in Eq. (33),

$$e = (B)t^a + C \tag{33}$$

where

e = the total strain; immediate elastic and time-dependent

t = the time from the instant of application of load

B and a = constants

C = immediate elastic strain at t = 0.

At longer times under load or at higher stresses, one notes a departure in the creep response from the power function extending through a transitional region to a form where the creep deformation is proportional to the logarithm of time. This is exemplified by the 25-gm load curve and the last two decades of log-time at 20 gm. Logarithmic creep is described by Eq. (21) in the previous chapter.

An increase in initial stress affects the fiber creep response. First there is an increase of the amount of delayed deformation for both the initial creep response and the logarithmic creep response. Second logarithmic creep response occurs at earlier times as the initial stress is increased. The various first-creep curves of Figure 25 show the nonlinear effect of increasing stress on the time-dependent response. The constant, b, representing the slope of the logarithmic creep response curves was proportional to the initial stress. Brezinski[5] found a similar relationship for softwood alpha pulp handsheets. It would appear that intrafiber mechanisms were controlling at least the limiting creep behavior of the handsheets. Since the individual fibers studied were not the same as those which made up Brezinski's handsheets, a valid comparison was not possible.

Hill's average single fiber data can be used to verify the use of Eyring's model, Eq. (18), in analyzing single pulp fiber creep behavior and compare single fiber creep behavior to other cellulosic fiber behavior. Eq. (18), as previously discussed, is capable of describing the creep and creep recovery for cellulosic fibers such as cellulose acetate and viscose rayon up to extensions of approximately 5%. Eyring's equation, which gives a relationship between the external stress, f, the external strain, e, and time, t, in terms of the constants, E1, E2, χ, and α, was used for Hill's average single-fiber data. Eq. (18) can be fit to Hill's average single fiber first-creep 10-, 15-, 20-, and 25-gm load data for α, χ, E1, and E2 using Statistical Analysis Systems (SAS).

Figure 25: Hill's average first-creep data. (Data from reference 6)

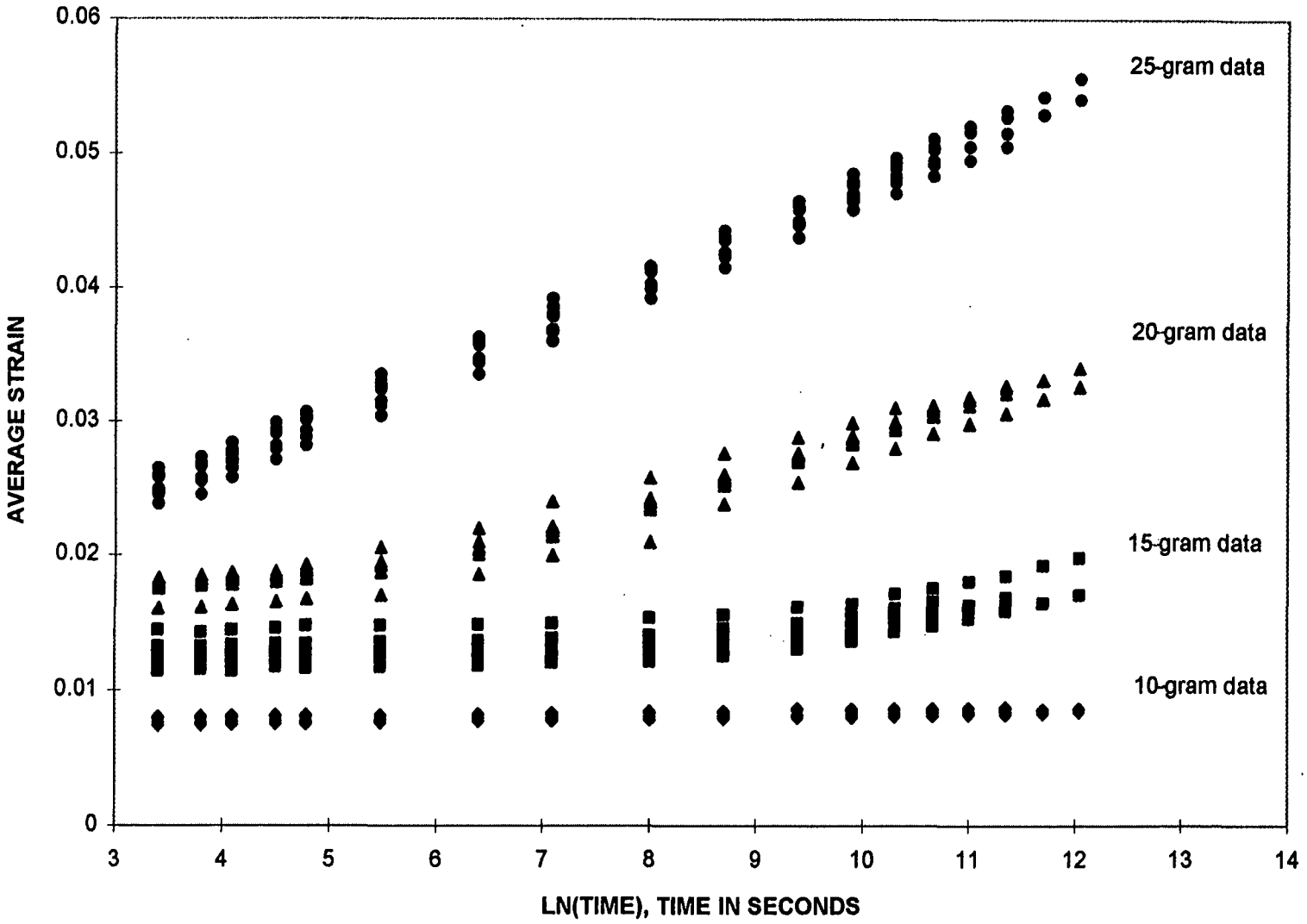

Figure 26: Theoretical Eyring fit of Hill's average first-creep data. (Data from reference 6)

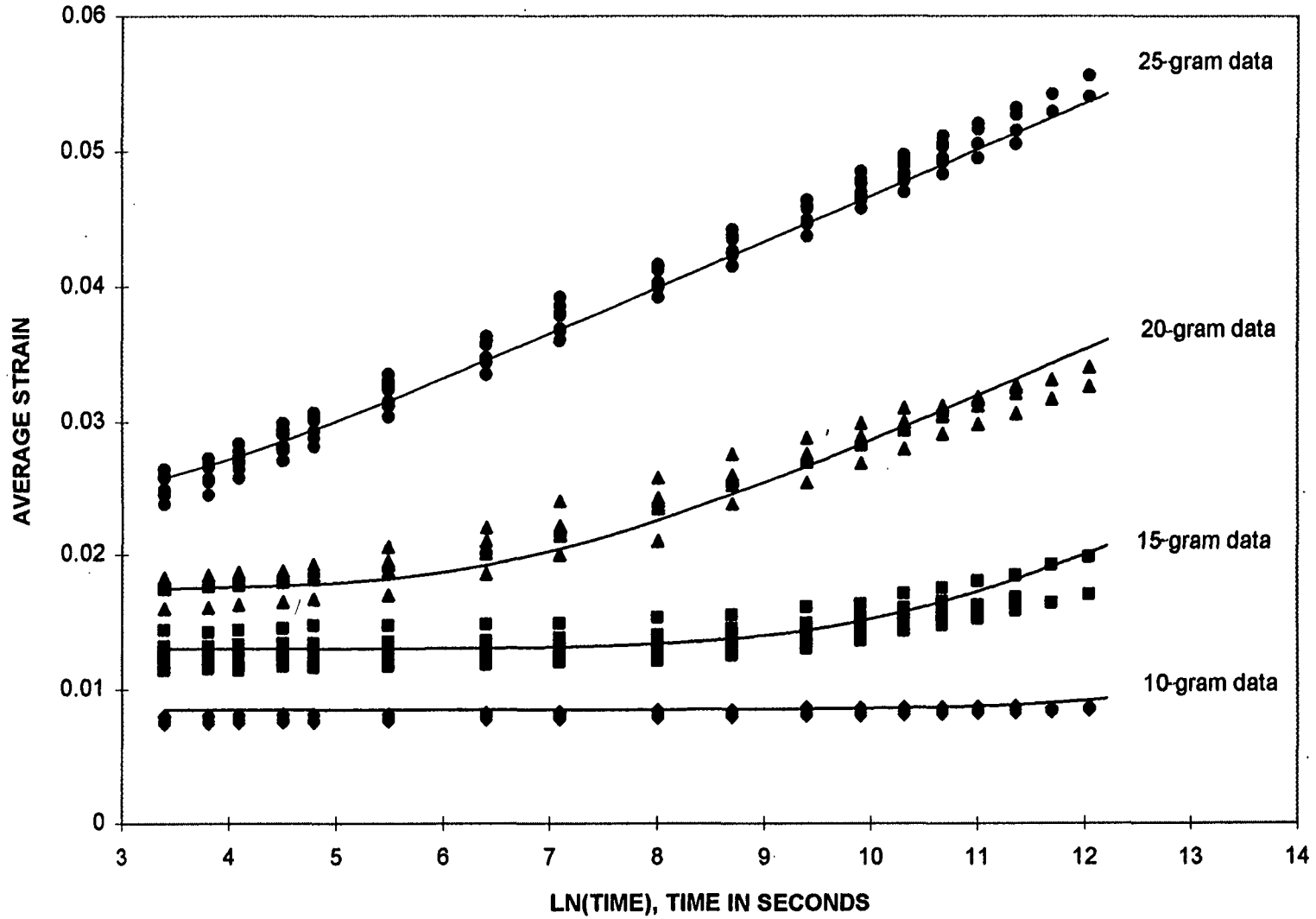

SAS[70] fit the Eyring model by least-squares regression using a Gauss-Newton iterative method which regresses the residuals onto the partial derivatives of the model with respect to the parameters, E1, E2, α, and χ, until the estimates converge. The fitted parameters are listed in Table 12.

Table 12: Nonlinear SAS fitting of Hill's average creep data.[6]

α	χ	E1	E2
4.85	1.93	1575	605

Units: Alpha x 10^{-9} cm^2/dynes, Chi x 10^{-11} sec^{-1}, Moduli x 10^8 dynes/cm^2

Parameters, E1, E2, α, and χ, all have errors an order of a magnitude less than their fitted values. Using the fitted parameter estimates, Eq. (18) is plotted in Figure 26. This fitting may not be a unique solution, but the predicted plot compares well with Hill's average experimental data points; therefore, the proposed Eyring mechanism fits single-pulp-fiber creep data.

Reaction-rate theory calculations can be applied to Hill's average first-creep data for single fibers. Therefore, single-pulp fibers behave similarly to other cellulosic polymers such as cellulose actetate and viscose rayon. According to Eyring,[51] single-fiber pulp behavior can be compared to other polymers in terms of four parameters: ΔF, the activation energy of the flow process; V_f, the volume of the cellulosic flow unit; E1, the modulus representing the linear chain molecules; and E2, the modulus representing the molecular network.

Solving Eq. (10) in terms of $-\Delta F$ and assuming $\lambda/\lambda_1 = 1/2$, a value for ΔF can be calculated using $\chi = 1.93 \times 10^{-11}$ sec^{-1} from the nonlinear SAS fitting of Hill's data

$$-\Delta F = RT[\ln(\lambda/\lambda_1) - \ln \chi + \ln(2kT/h)] \qquad (34)$$

where k = Boltzmann's constant, 1.38×10^{-23} J/°K

T = temperature, 298°K

h = Planck's constant, 6.626×10^{-34} Jsec

R = the gas constant, 1.987 cal./mol°K.

The assumption, $\lambda/\lambda_1 = 1/2$, is justified since λ/λ_1 can change over a fairly wide range without having an effect on the calculated activation energy.[48,71,72] Substituting the constants and χ for the SAS nonlinear fit into Eq. (34),

$\Delta F = 32{,}000$ cal./mole. (Hill First-Creep Data)

Values generated using NLIN SAS[70] were similar in magnitude to values calculated for the other fiber types listed in Table 13. Since the free energy of activation for longleaf pine is similar in magnitude to other H-bonded cellulosic fibers regardless of the method used to calculate the values, the indication exists that the mechanism of the flow process is similar in the various fibers despite the differences in chemical properties. The activation energy for the flow process may be indicative of the mechanism for H-bond breakage which does not vary for these fibers.

The creep behavior of cellulosic fibers can be described by a second parameter, V_f, the volume of the flow unit which is a function of the fitted viscous parameter, $\alpha = 4.85 \times 10^{-9}$ cm^2/dynes , by means of Eq. (35),

$$V_f = 2\alpha kT /10^{-7} \qquad (35)$$

where k = Boltzmann's constant, 1.38×10^{-23} J/°K

T = temperature, 298°K

10^{-7} = conversion factor for dynes to J/cm.

Hill's fitted creep data for the volume of the flow unit is comparable with other cellulosic fiber types. The volume of the flow unit is of the same order of magnitude as the volume of a unit cell of cellulose I crystalline structure (10.3 * 8.35 * 7.9), 679 $Å^3$.

Table 13: Comparison of cellulosic fiber types.[48,49]

Fiber Type	ΔF	V_f	E1	E2
Cotton	22.5	610	300	300[1]
Viscose Rayon A	23.5	320	2000	6000
Viscose Rayon B	24.7	1330	1095	1095[1]
Viscose Continuous Filament	25.4	133	1390	1390[1]
Cellulose Acetate	26.3	1180	560	560[1]
Longleaf Pine (NLIN Hill fit)	32.0	400	1570	605

Units: Free energy kcal/mole, Flow volume $Å^3$, Moduli x 10^8 dynes/cm^2

[1] Halsey assumed E1 = E2.

The third comparative parameter, E1, represents the elastic component of the linear chain molecules.[51] The Eyring model does not account for orientation; therefore, one cannot predict the fibril angle. Fibril angle refers to the S_2 orientation in the fiber cell wall. The microfibrillar orientation of the S_2 has been correlated to the modulus of the cellulosic material.[73,74,75] A smaller fibril angle, determined by the angle the S_2 makes with the fiber axis, will result in greater stiffness and resistance to fiber creep in response to axial stress.

Mark[73] calculated a theoretical elastic modulus in the polymer chain direction for the structural crystalline framework, E1, as 1.3430 x 10^{12} dynes/cm^2. Since the microfibrils are not perfectly aligned with the fiber axis, the stress in the cellulose lattice has a lateral component, and the stress in the fiber direction is a resultant of lateral and longitudinal microfibrillar stresses. The longitudinal stress is sustained disproportionately by well-aligned microfibrils.

Lastly, modulus E2 characterizing the elastic properties of the molecular network can be compared with other E2 values for various cellulosic fibers.[51] The modulus values are again characteristic of cellulosic polymers as well as the theoretical value calculated by Mark[73] equal to 2.00 x 10^{10} dynes/cm^2. The matrix elastic constant calculated by Mark includes the solid-solution voids as well as the chemical constituents.

CREEP RECOVERY

Creep recovery tests determined that approximately 85% of the initial creep behavior was recoverable, but only 40% of the logarithmic creep behavior was recoverable as the majority of creep resulted in permanent set. The modulus of elasticity increased with both initial stress and time under stress and approached a limiting value as logarithmic creep began. The limiting value represented a change of 70% in this property. The amount of this change recovered following first-creep recovery decreased as the initial creep stress and time under stress were increased. Hill's creep and creep recovery results indirectly imply that structural changes occur within fibers resulting from tensile stress. The mechanical properties of the fiber are dependent on the internal structure of the fiber and change as the structure reacts to an applied load. For example, the modulus of elasticity is sensitive to structural changes and is dependent on prerupture behavior of the fiber. Hill directly supported his premise that structural change in the fibers had occurred due to tensile stress, by collecting x-ray diffraction data to study both the crystallinity and fibrillar orientation of the fibers. No significant change in crystallinity occurred for creep or creep recovery tests. If crystallization processes occurred, techniques available were not sensitive enough to discern very small changes in fiber crystallinity. However, these data did show a small increase in fibrillar orientation occurs as a result of applied load. After creep recovery, there was no significant difference in orientation after creep. This evidence serves to substantiate that structural changes occurred within the fibers as inferred from viscoelastic and mechanical behavior of the fibers.

After reviewing and understanding Hill's single-fiber data, it is acknowledged that Hill's data, which is comprised of creep and creep-recovery data from separate experiments at several different stresses, offers an excellent opportunity to verify the use of Erying's model for single pulp fiber behavior in terms of creep and creep recovery. Insight can further be gained by reanalyzing the creep recovery data in terms of permanent set as a function of various stresses.

This will allow single-fiber PSL behavior to be compared with that of classical polymer behavior presented in the previous chapter.

The average creep and creep recovery data is plotted for Hill's 10-, 15-, 20-, and 25-gm loads in Figures 27–30. Hill's creep experiments lasted 12, 24, and 48 hours, and then the stress was removed for the creep recovery experiments. Using Eq. (21) and allowing SAS to fit Hill's single fiber creep recovery 15-, 20-, and 25-gm load data, fitted values for α, χ, E1, and E2 are listed in Table 14. Parameters, α, χ, E1, and E2, listed in Table 14 all have errors an order of magnitude less than their fitted values. Eq. (18) is plotted using the fitted parameter estimates from Table 14. Each of the three load levels fit contained creep recovery tests at 12, 24, and 48 hours. The stresses corresponding to each load and creep-recovery-time combination were used to fit the actual data. The predicted plots generated from the average stresses at loads of 10, 15, 20, and 25 gms compare well with the Hill's actual experimental data points (Figure 31). The 10-gm load which does not fit predicts higher than the experimental data. The 10-gm data was not used in the fitting of the data because it caused biasing of the average curves.

Table 14: Nonlinear SAS fitting of Hill's average creep recovery data.[6]

α	χ	E1	E2
1.89	6.38	4810	2000

Units: Alpha x 10^{-8} cm^2/dynes, Chi x 10^{-11} sec^{-1}, Moduli x 10^8 dynes/cm^2

Figure 27: Hill's average creep and creep recovery at 10-gm load. (Data from reference 6)

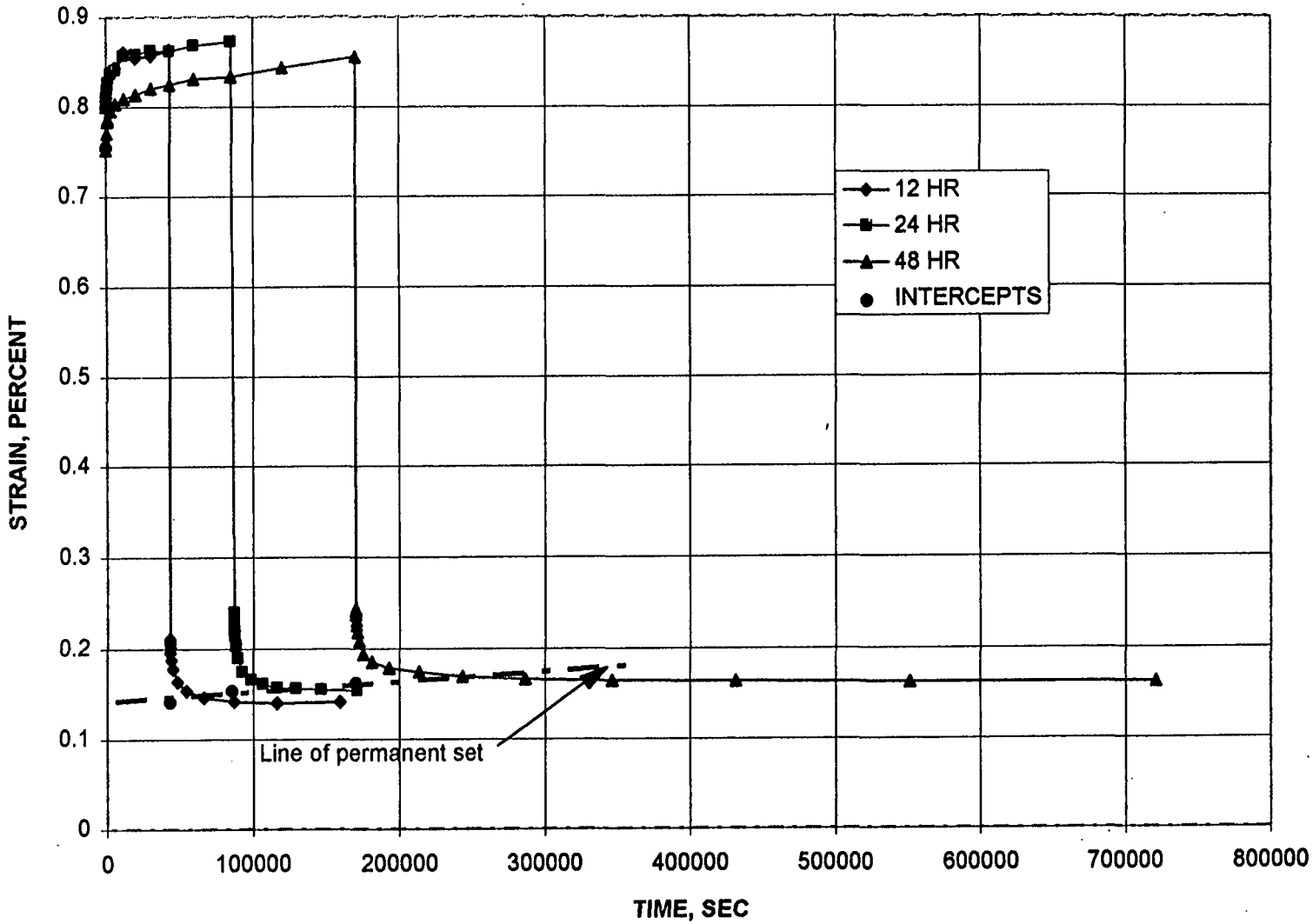

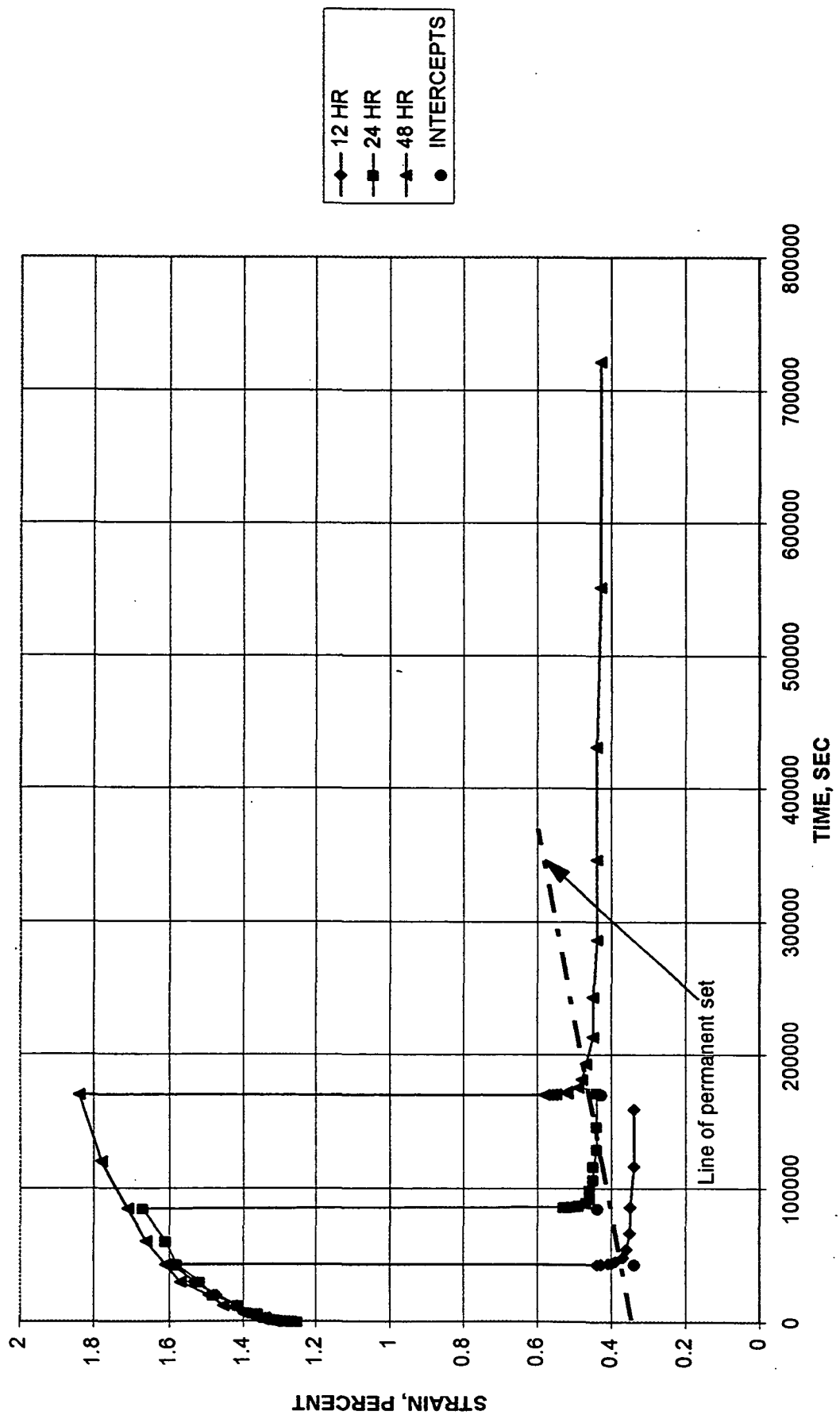

Figure 28: Hill's creep and creep recovery at 15-gm load. (Data from reference 6)

Figure 29: Hill's creep and creep recovery at 20-gm load. (Data from reference 6)

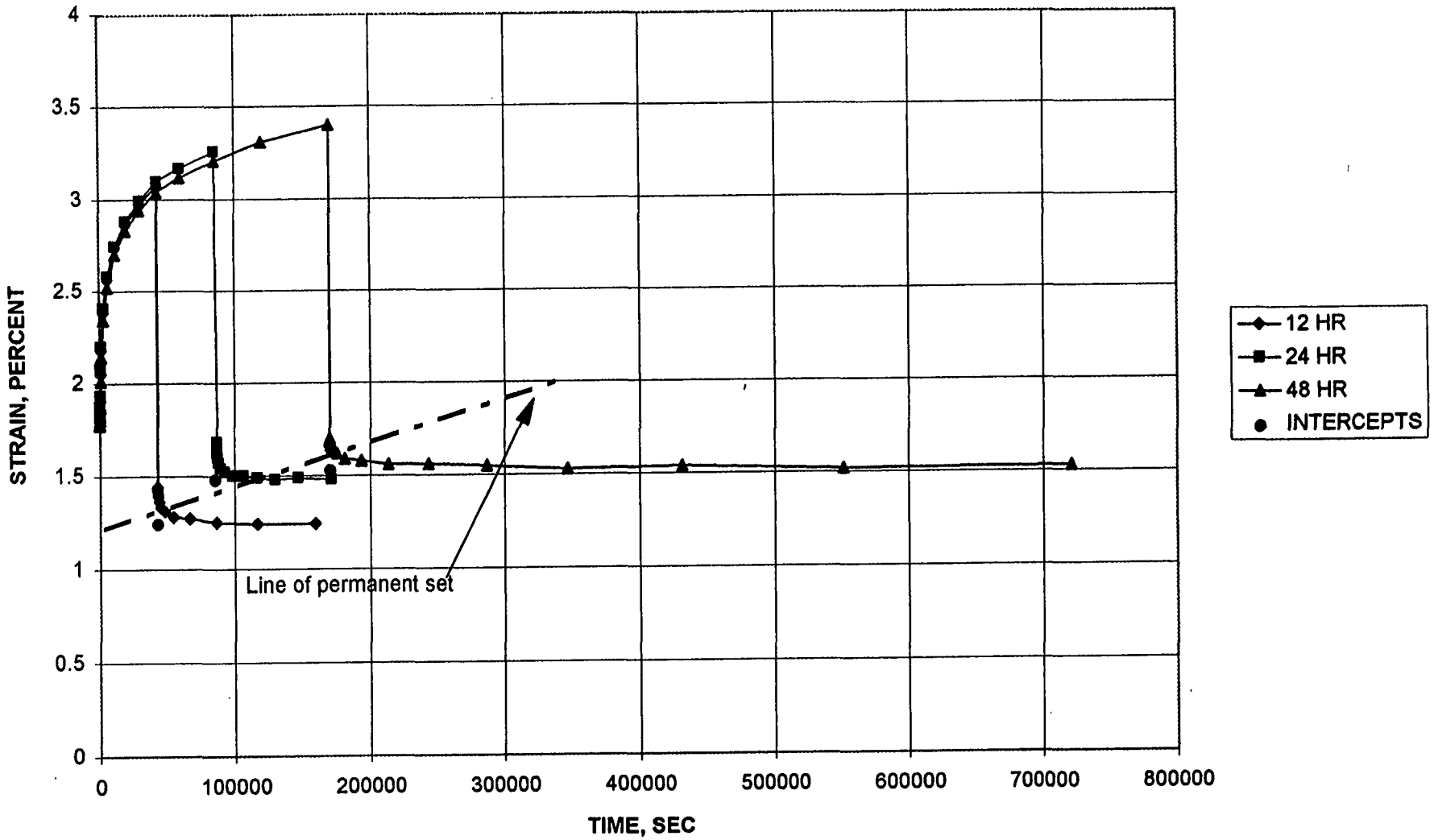

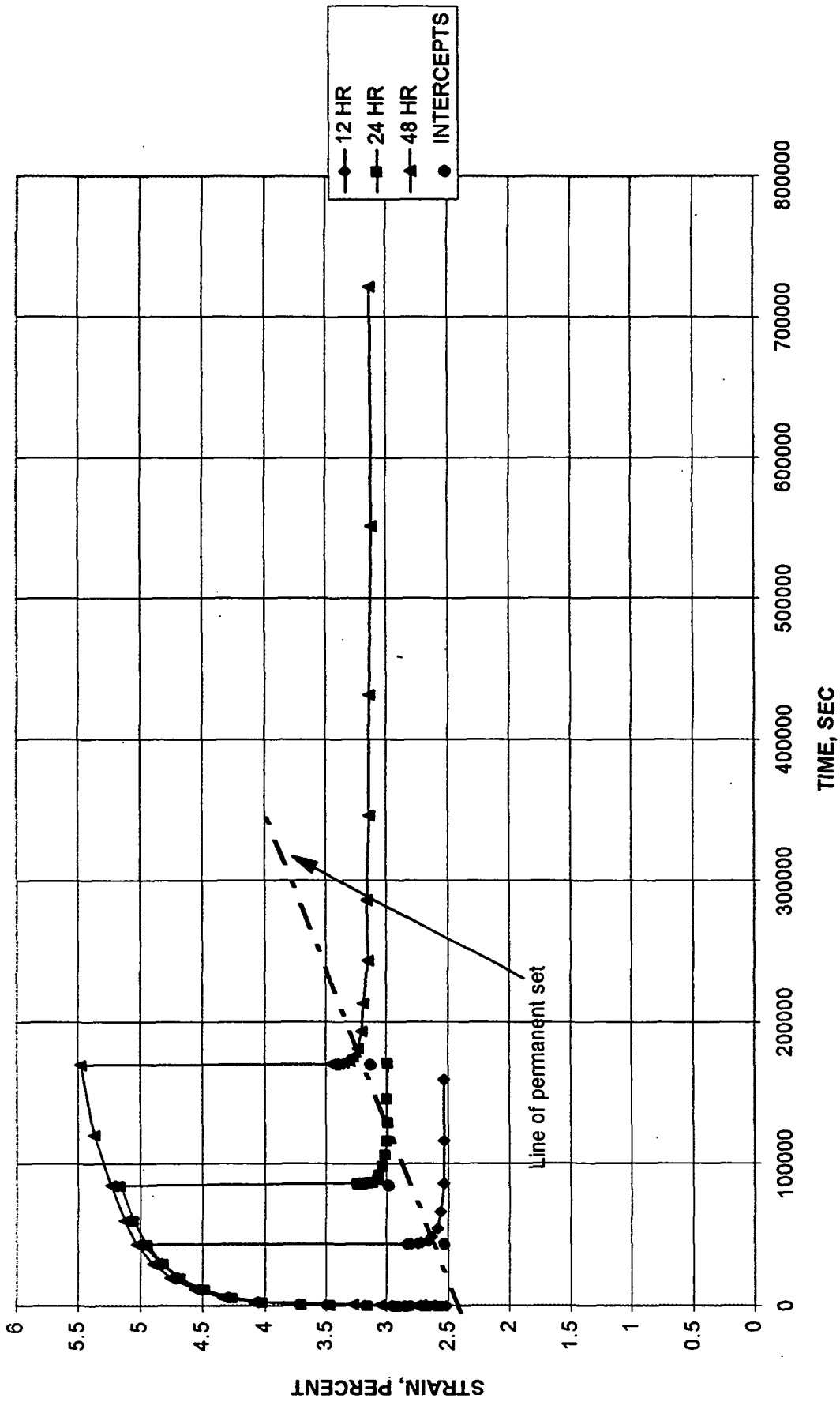

Figure 30: Hill's creep and creep recovery at 25-gm load. (Data from reference 6)

Figure 31: Theoretical Erying model fit to Hill's creep recovery data. (Data from reference 6)

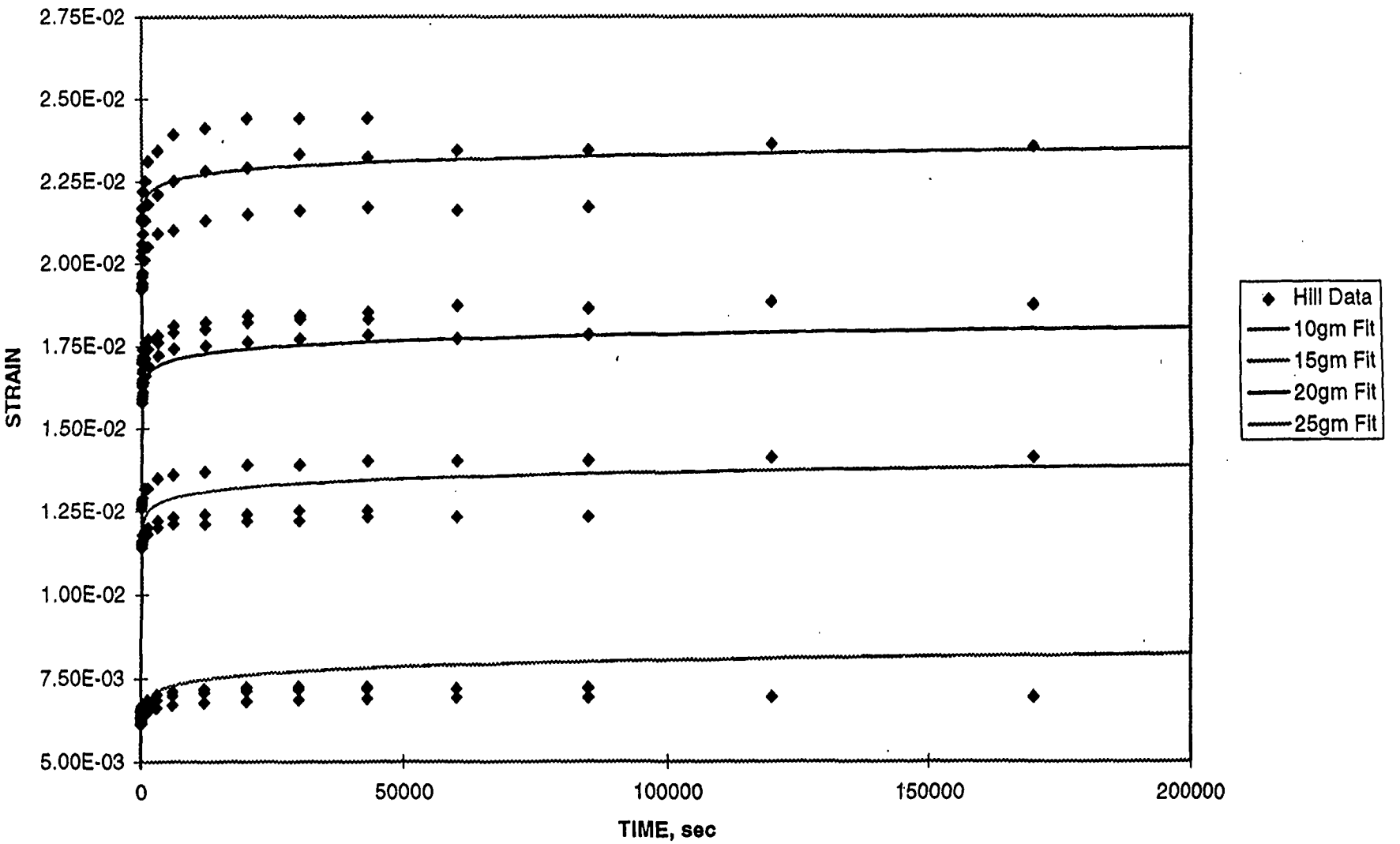

Table 15: Nonlinear SAS fitting of Hill's average creep recovery data compared to average creep data.[6]

Test Mode	ΔF	V_f	E1	E2
Creep	32.0	400	1570	605
Creep Recovery	31.3	1550	4810	2000

Units: Free energy kcal./mole, Flow volume $Å^3$, Moduli x 10^8 dynes/cm^2

Values generated using NLIN SAS fit were compared to values calculated for the creep data as listed in Table 15. Hill's fitted creep recovery and creep values for the free energy of activation for the flow process are essentially the same regardless of the test mode; therefore, the mechanism of the flow process is similar despite the difference in test mode. The activation energy for the flow process may be indicative of the mechanism for H-bond breakage.

The volume of the flow unit increases in the creep recovery mode. This implies that the fiber after undergoing creep and creep recovery is more structurally ordered as compared to the fiber that undergoes creep. Structural reorganization may include pulling out micro compressions and kinks. Hill could not find direct evidence of increased crystallinity due to creep recovery, but fitting to the Eyring model indirectly suggests increased crystallinity by the increased volume of the flow element. This further suggests that primary creep has reordered or reorganized the structure, but available experimental measurements are not sensitive enough to recognize the changes apparent in the modeled parameters. Holland,[49] Halsey, and Eyring also found that the average flow unit volume was appreciably larger than the constant for the corresponding creep experiments.

The modulus values, E1 and E2, are higher for the creep recovery data. The fiber appears to be a different material after it is allowed to undergo creep and creep recovery; therefore, it has different elastic and viscous constants associated with it. Hill's work does not support an increase in modulus for creep recovery as compared to creep. Hill[6] reported an increase in fiber modulus after creep and creep recovery for the 10- and 20-gram loads when compared to the unstressed fiber. However, the fiber modulus reported after first creep appeared higher than the

modulus reported after creep recovery. This increased fiber modulus reported after creep can be explained by Hill's probable increase in fibril angle after creep. The fibril angle after creep recovery was not significantly different from the fibril angle of the unstressed fiber. Hill proposed that the increase in fibril angle observed after creep may have been caused by experimental technique.

Spiegelberg[43] supported the idea that configurational mechanisms in the amorphous regions of the fiber should govern the behavior of the microfibrils which support and transmit the applied load throughout the fiber. The fibril structure of the fiber may govern the observed mechanical properties of the fibers with significant additional effects due to the amorphous regions. Considering this, there are several explanations for an observable increase in modulus due to creep and creep recovery conditions.

The first explanation is related to the effects of nonrecoverable increases in crystallinity. The fringed micelle theory suggests that an increase in crystallinity would occur within the fibrils at the expense of the amorphous matrix. This would result in a more completely crystalline load-supporting element and hence a larger elastic modulus of the fibrils. The fringed fibril theory suggests that an increase in crystallinity increases the stress supporting cross sectional area of the fibrils since amorphous regions are surrounding an essentially crystalline fibrillar core. There would be no change in the fibril structure considering this theory. Changes in crystallinity may be either reversible or partially reversible. High secondary-bond density of crystalline cellulose would indicate only partial reversibility. Hill[6] found no change in crystallinity following creep and creep recovery.

The second explanation leading to a time-dependent increase in elastic modulus as creep progresses is that a larger portion of the microfibrils share in supporting the external stress. Amorphous material separating fibrils may deform and allow slippage of these stiff and highly crystalline elements. This would effectively increase the stress distribution in the fiber; thus, the modulus would appear to increase as internal stress redistribution occurs.

Fitting Hill's creep and creep recovery data to the Eyring model shows that the creep and creep-recovery curves are not mirror images of each other. In fact, the creep-recovery curve has modulus values at least three times that of the creep curve. Reorganization within the fiber may have taken place; however, the techniques available to provide direct evidence of this are not sensitive enough to see a difference in crystallinity. Probable increases in fibril angle do not offer sufficient direct evidence to substantiate reorganization. An alternative method to provide direct evidence of structural reorganization is necessary to substantiate the difference in Eyring parameters between creep and creep recovery.

PSL Analysis

Erying's model for single pulp fiber behavior has been used to re-evaluate Hill's data in terms of creep and creep recovery. Further insight can be gained by reanalyzing the creep recovery data in terms of permanent set as a function of various stresses. This will allow single fiber PSL behavior to be compared with that of classical polymer behavior presented in the previous chapter.

Hill's creep experiments lasted 12, 24, and 48 hours, and then the stress was removed for the creep recovery experiments. The creep and creep recovery experiments in Figures 27–30 show that the instant the stress was removed there was an immediate reduction in elongation followed by a continued decay of extension with increasing time. But the fibers did not fully recover to their initial forms. They assumed a nonzero nonrecoverable value of extension. There is a substantial amount of nonrecoverable extension or permanent set; therefore, a modified version of the Eyring theory is necessary to describe this system.

A PSL is comprised of the intersection points of creep-recovery curves at their unloading times and is shown for each stress in Figures 27–30. The intersection points lie on a straight line, but the PSL does not go through the origin. Since a PSL exists, the total permanent set has a

component that follows classical theory that is a linear function of time and some slope. These slopes are listed in Table 16. The 15-, 20-, and 25-gram data all have good least-squares fits. The least-squares fit for the 10-gram data is poorer. The four slopes (Table 16) are different and expected to be so. The slopes increase with increasing load level.

Table 16: Least-squares fit of Hill's PSL creep recovery data.[6]

Load	Average Stress	PSL Slope	PSL Intercept	R^2
10	1.86	0.0766	0.001421	0.6233
15	2.98	1.39	0.003368	0.9976
20	3.82	2.18	0.01191	0.7320
25	4.91	4.75	0.02423	0.9747

Units: Load grams, Average Stress x 10^9 dynes/cm^2, Slope x 10^{-8} sec^{-1}

It is interesting to explore the mathematical structure of the PSL. First, how do the PSL slopes vary as a function of stress? If the PSL slopes are a linear function of stress, then the classical theory can be applied and should have the form, f/η_1, as previously described. The PSL slopes are plotted against the corresponding stresses in Figure 32. The PSL slope is not a linear function of stress; therefore, the second dashpot in the four-element model (Figure 21) is not Newtonian in behavior. The behavior does not follow the classical linear dashpot, so it is imperative to explore the type of nonlinear dashpot in order to explain Hill's data.

The behavior in Figure 32 appears to follow that of a general exponential function of the form

$$y = a_S * e^{b_S fc} \tag{36}$$

where a_S and b_S are constant for the PSL slopes and fc is average stress. Taking the natural log of Eq. (36),

$$\ln y = \ln a_S + b_S * fc \tag{37}$$

Eq. (37) was plotted in Figure 33 in order to extract values for the constants, a_s and b_s. The least-squares fit is shown in Table 17.

Table 17: Least-squares fit of Eq. (37).[6]

Load	Average Stress	a_s	b_s	R^2
10	1.86	1.25×10^{-10}	1.3×10^{-9}	0.8666
15	2.98			
20	3.82			
25	4.91			

Units: Load grams, Average Stress x 10^9 dynes/cm^2

Since the general power function in Eq. (36) gives a reasonable explanation for the nonlinearity of the PSL slope with stress, the Eyring model, Eq. (18), can be represented by $\Psi(t)$ and modified to include the first component of permanent set. This component of permanent set is linear in time and nonlinear in stress.

$$e = \Psi(t) + t * a_s * e^{b_s s^{fc}} \tag{38}$$

The non-Newtonian dashpot controlling the first component of the permanent set supports the choice of a modified approach like Eyring's where Newtonian as well as exponential behavior is possible. The Eyring theory encompasses constitutive and mechanical models normally used in the analysis of creep.

Since the PSL does not intersect the origin in Figures 27–30, but instead intersects the y axis, a second component of the total permanent set can be defined as the PSL intercept. The PSL is developed in the loading step and contributes to the total strain. This second component

Figure 32: PSL slope vs. stress.

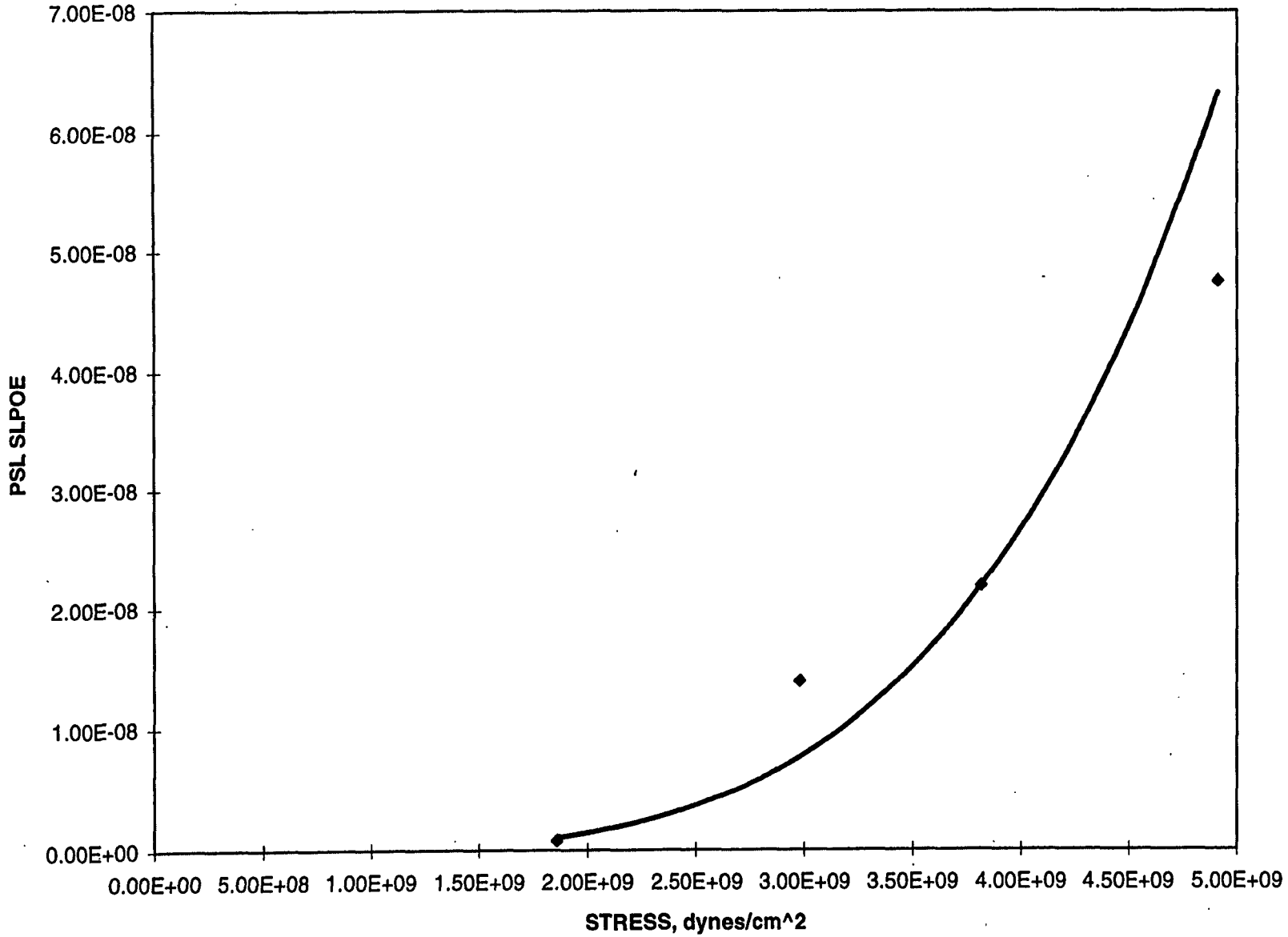

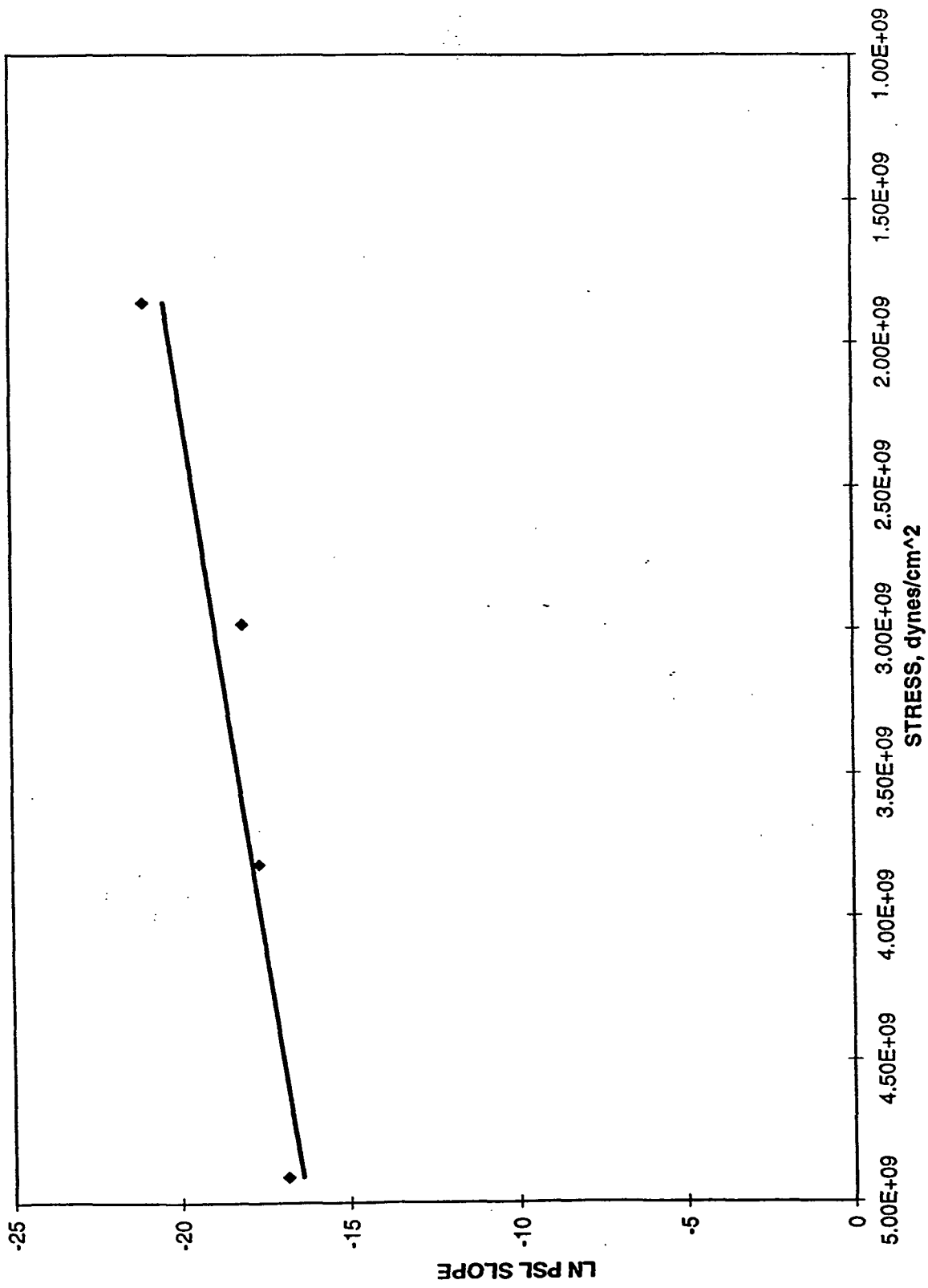

Figure 33: Ln PSL slope vs. stress.

Figure 34: PSL intercept vs. stress.

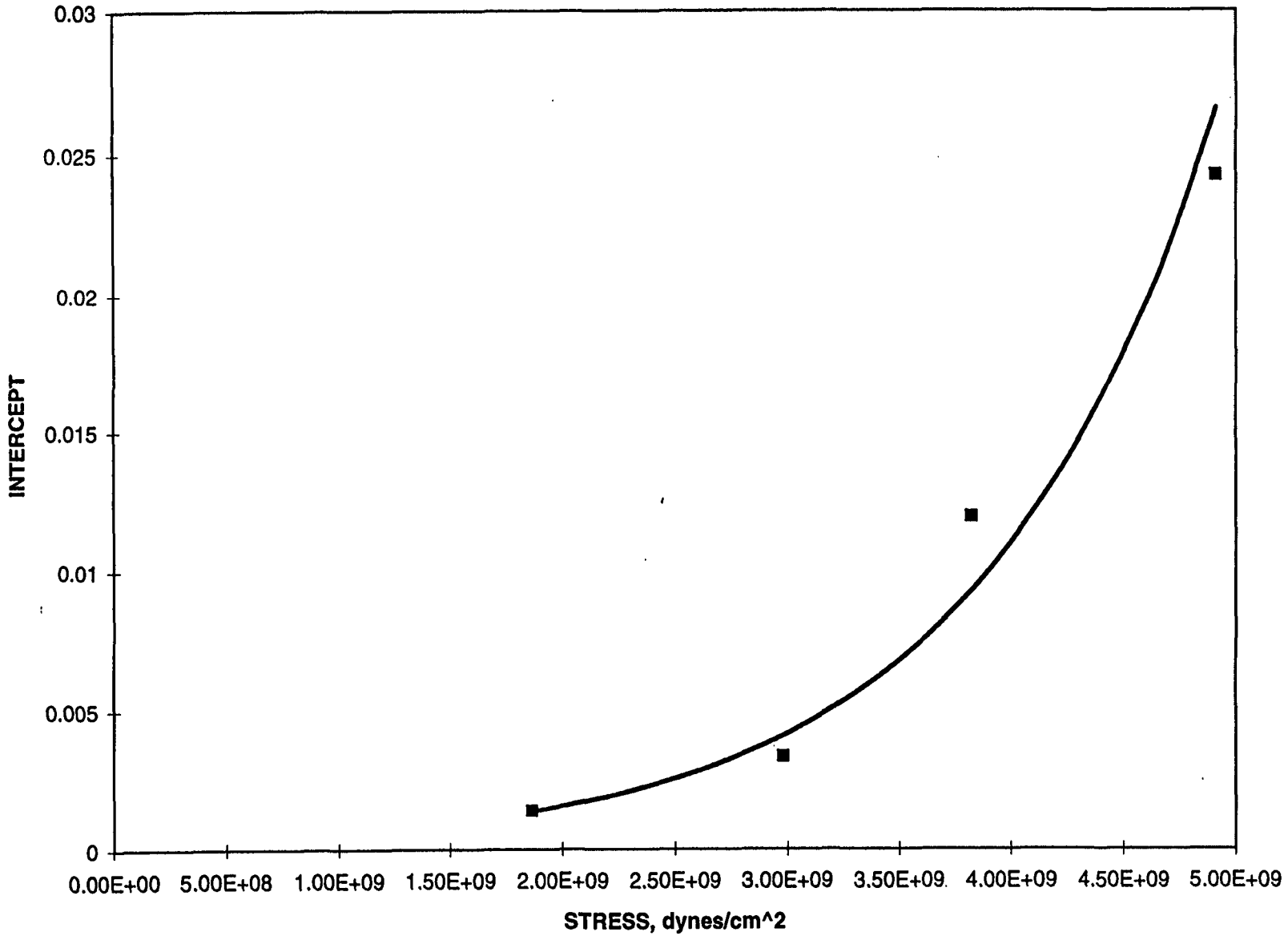

Figure 35: Ln PSL intercept vs. stress.

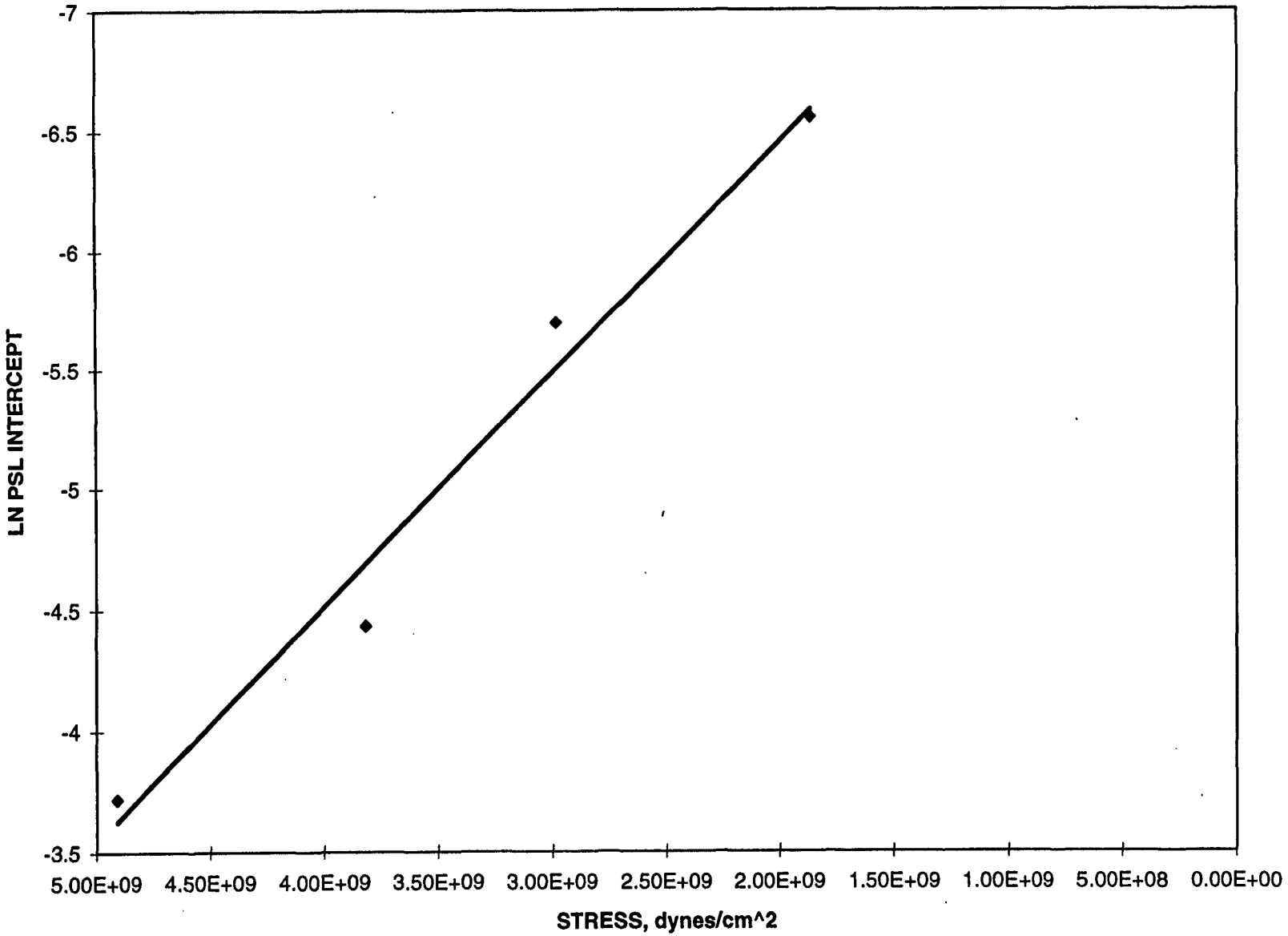

of the total permanent set is included in the modulus values, E1 and E2, of the Eyring fit. Modulus values are higher in creep recovery data. There is an element of permanent set represented in modulus values for the first creep tests which is accounted for in the creep recovery tests. Strain in the first creep data at time, t = 0, has a large component of permanent set; therefore, major structural and dimensional changes in the fiber may occur that are not accomplished by elastic or viscous flow but are fully plastic.

In continuing to explore the mathematical structure of the PSL, the PSL-intercept component of the total permanent set needs further explanation. How do the PSL intercepts vary as a function of stress? Since classical theory describes the intercept as zero, it would be preferable if the intercept were a constant with respect to stress. A second option may be that the second component of permanent set is linear with stress; however, this is not the case. The PSL intercept is neither constant nor linear with respect to stress as shown in Figure (34). The PSL intercepts are a nonlinear function of stress. The nonlinear relationship appears to be exponential in form as in Eq. (39)

$$y = a_i * e^{b_i fc} \tag{39}$$

$$\ln y = \ln a_s + b_s * fc \tag{40}$$

where a_i and b_i are constants for the PSL intercepts and fc is average stress. The natural-log form of Eq. (39) was plotted in Figure 35. The values for the constants are listed in Table 18.

Table 18: Least-squares fit of Eq. (40).[6]

Load	Average Stress	a_i	b_i	R^2
10	1.86	2.26×10^{-4}	9.71×10^{-10}	0.9766
15	2.98			
20	3.82			
25	4.91			

Units: Load grams, Average Stress x 10^9 dynes/cm^2

The least-squares fit is very good and indicates that the second component of permanent set, the PSL intercept, follows this general nonlinear behavior as a function of stress. The Eyring model can be further modified to account for the total permanent set in Eq. (41)

$$e = \Psi(t) + t * a_s * e^{b_s \sigma_{fc}} + a_i * e^{b_i \sigma_{fc}}. \qquad (41)$$

The permanent set is comprised of two components in Eq. (41). The first component, the PSL slope, is classical in the sense that it is linear in time and follows the behavior of an ordinary nonlinear dashpot as a function of stress. The second component, the PSL intercept, is a constant that is nonlinear with stress. There is a large component of strain which cannot be accounted for in either classical theories of creep or permanent set. Possible explanations for this strain may include fracture in the border pits at low stresses. A fracture mode would induce a large strain and would eventually be accounted for by permanent set. A second alternative could be the straightening of crimps or kinks and microcompressions. These too would contribute a portion of strain at low stresses upon loading single fibers. The strain component may be a combination of both suggestions; however, this component may be embedded in the high fiber to fiber variability for single fiber testing. This behavior tends to dominate the total strain of single fiber cyclic humidity data.

A complex process is occurring in the loading step that is nonlinear in load for the PSL intercept. This process significantly contributes to the total permanent set of the system. Little is known about this component except that it occurs in the loading step within the first 20 seconds and is nonlinear with stress. Eq. (40) is not sufficient to do any real predictive work. More information is needed at conditions at time, $t = 0$, in order to quantify creep response in terms of extension and permanent set. Then it would be possible to separate the permanent set of the fibers from the first creep response. Hill's data is used to get an idea of how permanent set in single fibers develops. These analyses strongly imply the understanding of permanent set is important in the creep behavior of single fibers. A substantial amount of permanent set (40%) is incorporated into Hill's creep and creep recovery curves.

ANALYSIS OF BYRD'S DATA

Byrd[61] studied the tensile creep response to moisture content in both paper and single fibers of southern pine bleached kraft pulp. The handsheets were cycled between 35 and 90% RH several times to relieve drying stresses prior to equilibration at 50% RH. Single fibers were withdrawn from these handsheets and attached to an aluminum frame with an epoxy resin. The span was measured to obtain an original length and a total weight of 3.76 grams; approximately 45% of maximum fiber stress (determined at 90% RH) was applied. The deformation was continuously recorded with a strip-chart recorder, and duplicate creep tests were run under constant and cyclic relative humidity conditions. The method by which single fibers were withdrawn from the handsheets is not discussed but is none the less important as a state of preconditioning prior to creep testing. The method of attaining single fibers impacts on the defects in the fiber cell wall as well as on the stress strain history of the fibers. Single fibers withdrawn from handsheets that have been pressed and dried would not be expected to exhibit the same mechanical behavior as never-dried fibers.

Two series of creep measurements were made: (a) specimens loaded at the stress level were exposed to cyclic relative humidity conditions [relative humidity alternated between 90 and 35%] for 10 cycles, and (b) specimens loaded at the same stress level were exposed to a constant environment of 90% RH for a time equivalent to 10 cycles. Cyclic creep tests were started at 90% RH; however, it is unclear what the length of conditioning at 90% RH was prior to testing.

Preliminary experiments showed that 20 minutes were required to change the relative humidity from 35 to 90% (adsorption), while about 60 minutes were required to go from 90% to 35% (desorption). The average time required for a complete cycle (90 to 35 to 90% relative humidity) was about 80 minutes. Ten relative humidity cycles required about 5000 minutes because the relative humidity was kept constant at 35% when the cyclic relative humidity creep tests were left unattended. All creep tests were carried out at 23°C. Considering the length of

time necessary for the humidity chamber to cycle from 35% to 90% and 90% to 35% relative humidity, the fibers were tested under transient conditions.

Byrd's tensile creep response to cyclic relative humidity in single fibers of southern pine bleached kraft pulp is shown as Figure 36. The upper curve is not surprising. Under 45% maximum tensile load at 90% RH for seven days, a single fiber elongated almost 14%. Hill's 0.1% elongation of single southern pine fibers during 50% constant relative humidity creep was less than Byrd's elongation at 90% RH at a comparable stress level. What is astonishing is the lower curve. Under the same tensile stress, but exposed to cyclic humidity variations between 35 and 90% RH, similar single fibers actually contracted 2% over a three-day period. Byrd[61] suggests this behavior results from drying stresses which are not released during the rewetting portion of the relative humidity cycles.

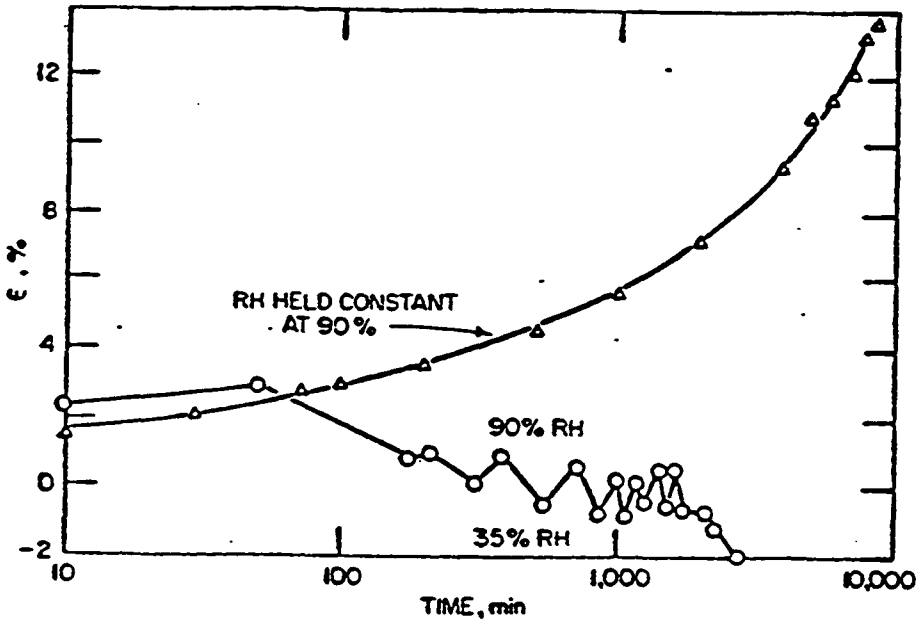

Figure 36: Creep curves of single southern pine pulp fibers at 45% of maximum tensile stress.[61]

As previously discussed, creep-curve data can be analyzed by various methods including constitutive, theoretical, and mechanical models. Byrd chose a constitutive method to analyze his data. Byrd's regression equations were fitted directly to the data points for creep of paper at 35, 50, and 90% RH. The equations at 35 and 50% RH are linear in ln time, whereas the equation at 90% RH is quadratic in ln time. Similarly, Hill's single fiber data is linear in ln time at 50% RH. Byrd's single-fiber data at 90% RH is plotted in Figure 37 and fitted with the regression form of Eq. (21). The single fiber data at 90% RH is plotted in Figure 38 and fitted with the regression equation of the form

$$e = a + b(\ln t) + c(\ln t)^2 \qquad (42)$$

where the symbols are described in Eq. (21). The regression analysis used time in units of seconds and is given in Table 19. The simple correlation coefficient, r, is a measure of how well the regression equations describe the data. Critical values of r at 13 degrees of freedom, df, are listed. The linear relationship does not fit well for the single fibers at 90% RH; however, the quadratic expression fits the data very well at 90% RH, as evidenced by the high correlation coefficient.

Table 19: Regression analysis for single fibers at 90% RH.

Model	r[a]	f[b]	df
ln(t)	0.894157	101.38	1
$(\ln t)^2 + \ln(t)$	0.985058	362.59	2

[a] r (critical) at the 0.01 significance level is 4.75.
[b] f (1, 13) = 4.67 and f (2, 13) = 3.81

Creep of paper and single fibers at 50% RH is linear in ln time; however creep of single fibers at 90% RH is nonlinear in ln time and a quadratic relationship is required to fit the data at 90% RH. It is unlikely the ln(t) model will fit single-fiber data at both 50 and 90% RH as seen with

Figure 37: Creep response of single fibers at 90% RH fitted with linear response.[61]

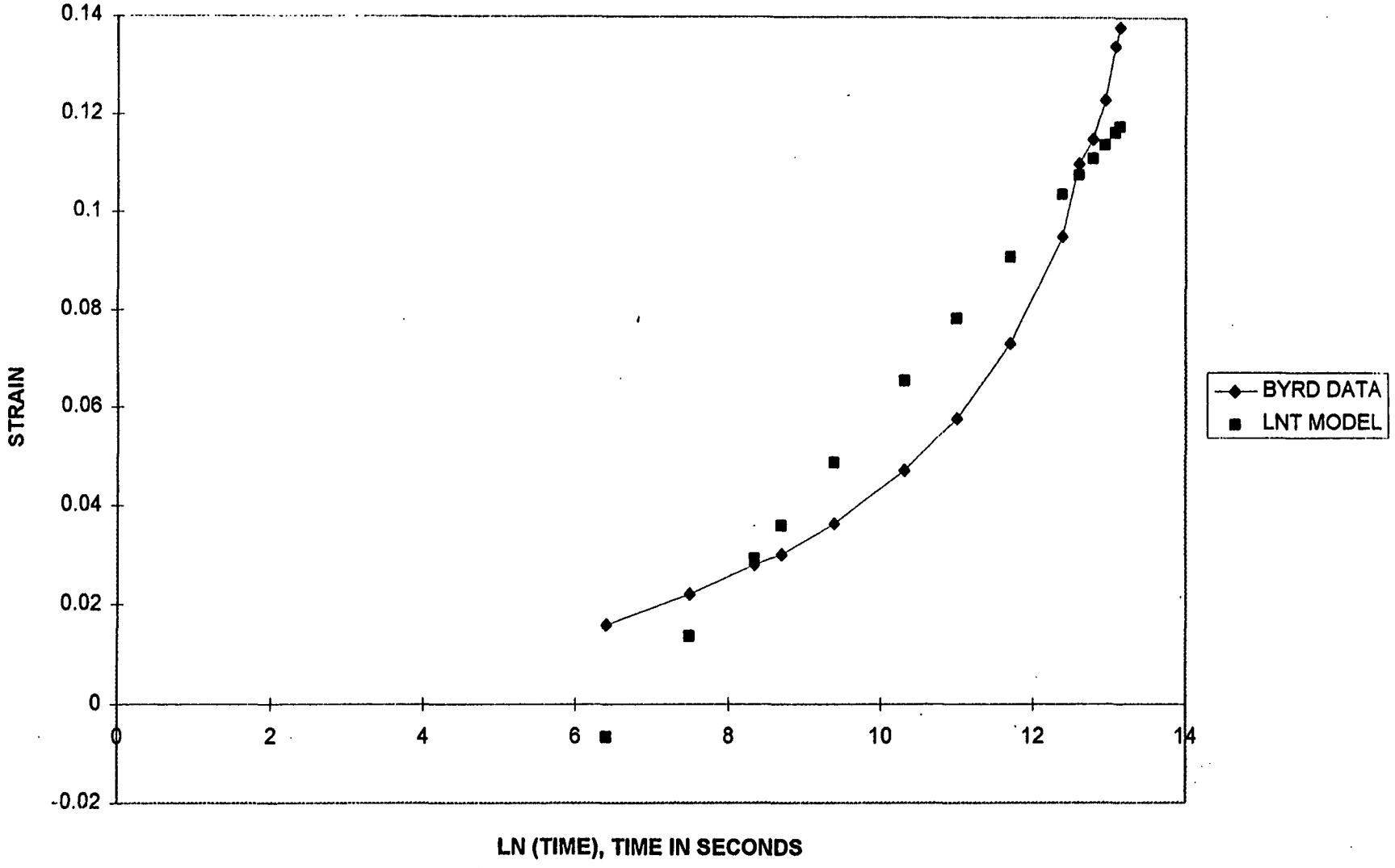

Figure 38: Creep response of single fibers at 90% RH fitted with quadratic response.[61]

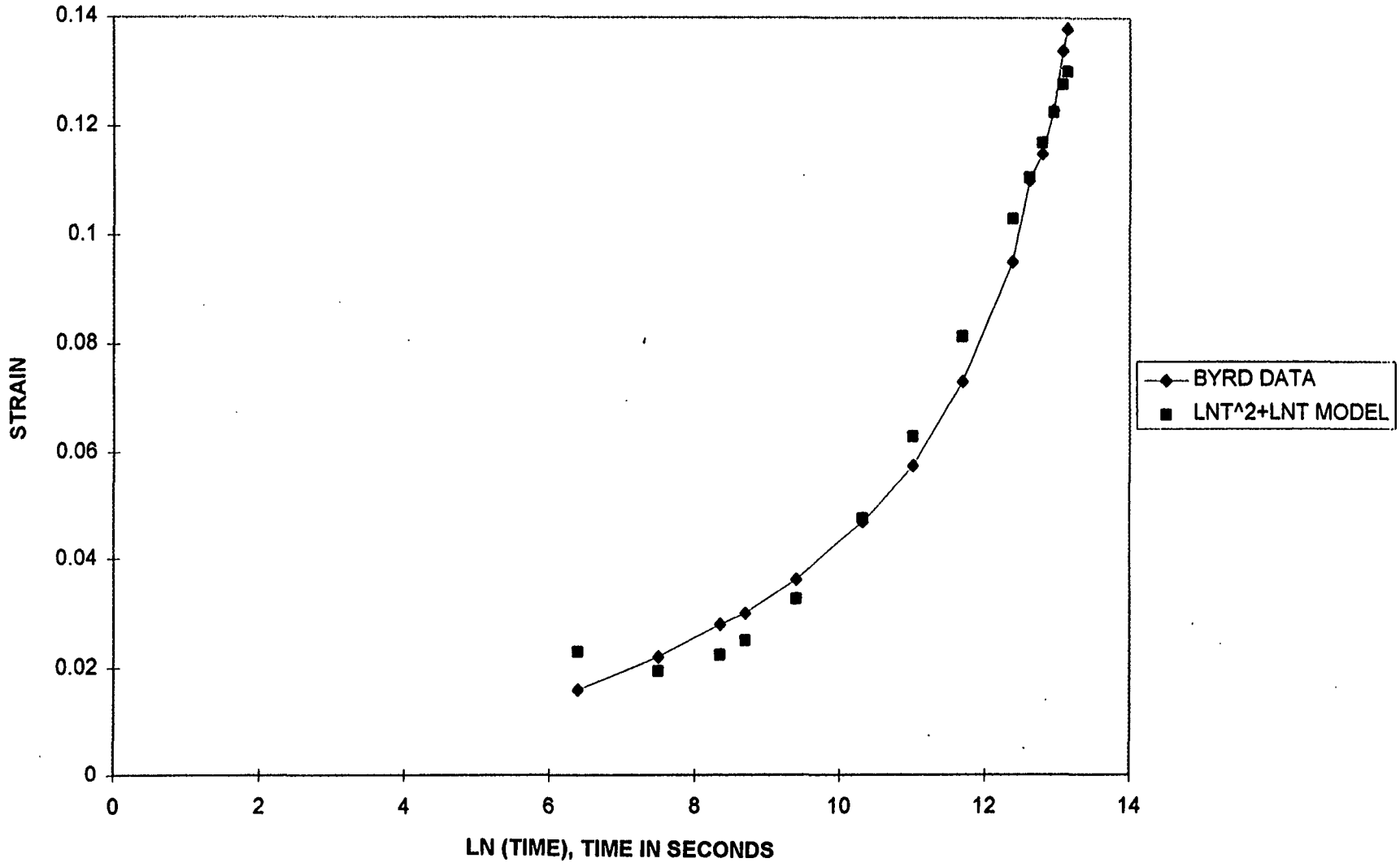

the data analysis of Byrd's single fibers at 90% RH; therefore, the Erying model is a more general way to describe the data. The Eyring model can be expressed as a function of logarithmic time as previously described. The reader is referred to the Theoretical Analysis of Data section for comparison of the Eyring model to other typical creep-data analyses.

EYRING ANALYSIS OF BYRD SINGLE FIBER DATA

Byrd's single-fiber creep data was reanalyzed using a form of the Eyring equation. The first creep response of single fibers fits the Eyring model, but as previously noted, the permanent set of the fibers is a large component of the observed first-creep strain in Hill's data. Therefore, the modified Eyring equation represented by Eq. (38) is used to fit Byrd's single-fiber data at 90% RH. Parameters, E1 and E2, are listed in Table 20 as well as calculated values for ΔF and V_f. Eq. (31) is plotted using the fitted parameter estimates from Table 20. The predicted plot compares well with the Byrd's actual experimental data points (Figure 39). It appears the modified Eyring model fits the single fiber creep data at 90% RH.

Table 20: Modified Eyring equation parameters for Byrd's and Hill's creep data.[61, 6]

Creep Data	RH	ΔF	V_f	E1	E2
Byrd	90	29.9	430	940	99
Hill	50	32.0	400	1570	605

Units: Relative humidity %, Free energy kcal/mole, Flow volume $Å^3$, Moduli x 10^8 dynes/cm^2

Even though Byrd and Hill's creep parameters listed in Table 20 are from different fibers and different experimental setups, it is interesting to note how these parameters change with humidity. The free energy of activation for the flow process and the volume of the flow unit are on the same order of magnitude and appear not to be affected by the difference in relative humidity. Early work by Eyring[51] and others[48,49] shows that free energy is not very sensitive to moisture content.

Figure 39: Modified Erying model fit to Byrd's single-fiber creep data 90% RH.[61]

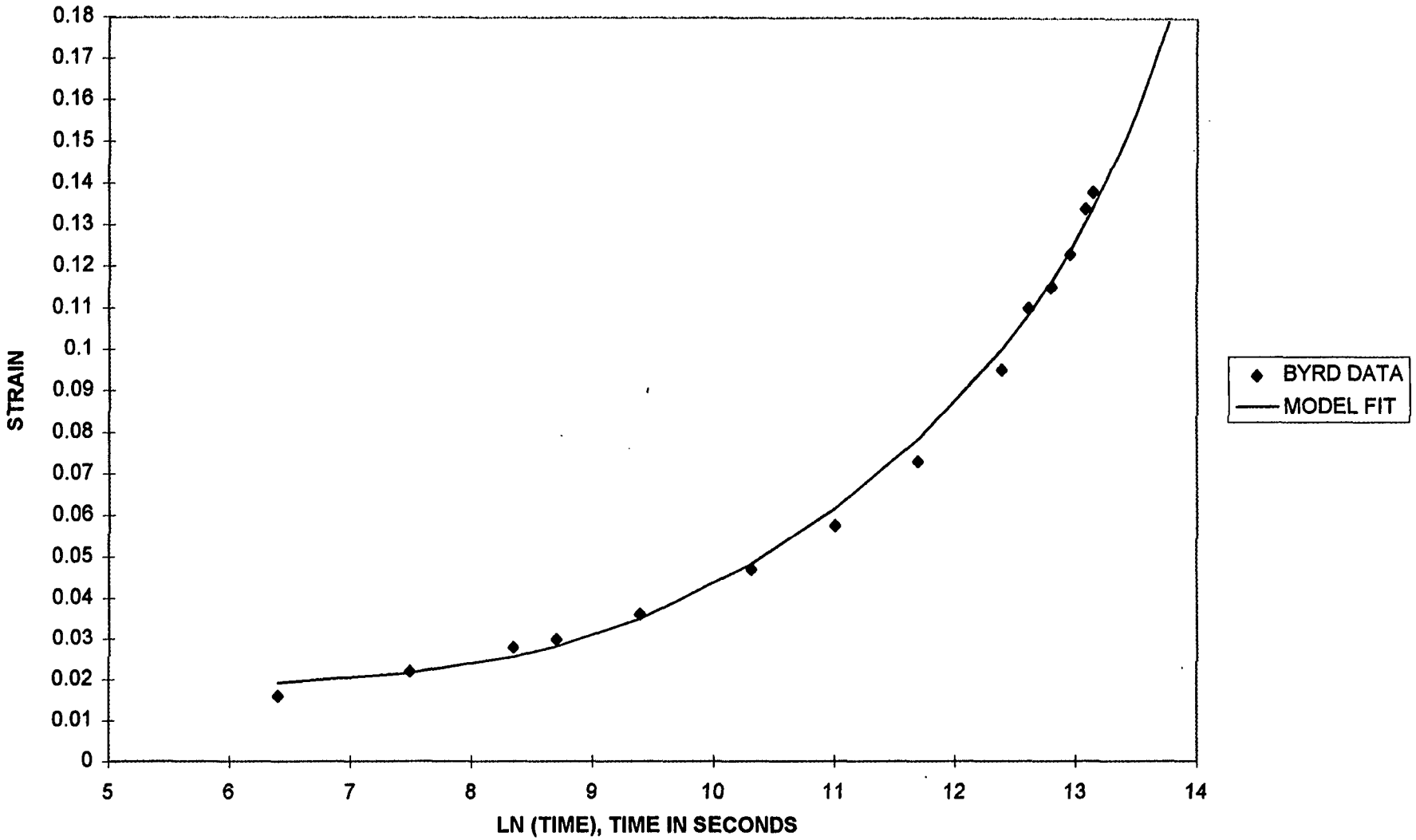

The modulus values for the different fibers, E1 and E2, are 40 and 84% lower for the 90% humidity creep data as compared to the Hill[6] 50%-humidity-creep data. From the analysis of Hill's creep-recovery data there is a large component of strain which cannot be accounted for in either classical theories of creep or permanent set which is incorporated in the modulus values. More information is needed at conditions at time t = 0 in order to know how much creep response is due to extension and how much is due to permanent set. However, since the classical theory for permanent set was used in fitting the 90% humidity fiber data, a PSL slope can be calculated and compared with the PSL slope values from Hill's reanalysis in Figure 32. (See Table 21.)

Table 21: PSL Slope for Byrd's and Hill's creep data.[61, 6]

Creep Data	Load	Average Stress	PSL Slope
Byrd	3.76	18.6	7.44
Hill	10	18.6	0.0766
	15	29.8	1.39
	20	38.2	2.18
	25	49.1	4.75

Units: Load grams, Average Stress x 10^8 dynes/cm^2, PSL slope x 10^{-8} sec^{-1}

The slope term listed in Table 21 is 100 times higher for the 90% humidity creep data analysis at a similar average stress level than for the 50% humidity creep data analysis; therefore, the nonrecoverable creep term may play a greater role at higher humidities. Again it is difficult to draw firm conclusions using two different fiber sources.

The modified Eyring model is used to analyze single-fiber-creep and creep-recovery data. This model is sufficiently sophisticated to analyze data at various humidities as well as various stresses. However, the model does not take into account the large component of strain which cannot be accounted for in either classical theories of creep or permanent set. This large component of permanent set will be incorporated in fitted modulus values.

THESIS OBJECTIVE

The objective of this thesis research was to determine, in a systematic manner, whether hemicelluloses influence tensile creep behavior of individual pulp fibers under both constant and cyclic humidity conditions. In the course of this research, the following hypotheses were tested to achieve the stated objective:

1. Tensile creep behavior of individual pulp fibers as a function of relative humidity is dependent on hemicellulose content.

2. The hemicellulose component of fibers undergoing tensile creep facilitates cellulose microfibril slippage.

3. Tensile creep behavior of individual pulp fibers under cyclic humidity conditions is dependent on hemicellulose content.

Such a characterization may provide an increased understanding of the extent to which hemicellulose components are significant in tensile creep of single fibers at various relative humidities. Consequently, if hemicellulose components are significant in tensile creep response, then modification of the hemicellulose component of the fibers is a possibility to reduce creep response.

EXPERIMENTAL APPROACH

To achieve the above objective, hemicelluloses were extracted from holocellulose fibers. These fibers were subjected to systematic axial tensile creep experiments under constant humidity conditions of 50 and 90% and conditions of humidity cycling between 50 and 90%, 50-90% RH, and 90-50% RH. The independent variables were hemicellulose content and relative humidity, while the dependent variables were parameters characterizing the creep phenomenon. The experimental approach, including aspects of fiber preparation, characterization, and axial creep measurement, is considered here.

FIBER PREPARATION

Loblolly pine (*Pinus taeda L.*) was selected as the wood species to be used in this research for two reasons: (1) it has relatively long fibers, simplifying handling procedures, and (2) it has relatively wide growth rings, making separation of the springwood and summerwood easier. A loblolly pine tree was procured from the Union Camp Corporation Woodlands Division, Savannah, Georgia.

Fiber samples originated from a 25-year-old plantation-raised loblolly pine. The 18th summerwood growth ring was hand-chipped and holopulped,[76,77] thereby being reduced to fibers. The process used to convert the wood chips to holocellulose fibers used a mixture of sodium chlorite and acetic acid. Upon completion of the procedure, the holopulped sample contained 0.18% ± 0.01% Klason lignin. A fiber sample was dyed with Congo red and characterized in terms of summerwood and springwood content by the Research Services Division at the Institute of Paper Science and Technology. The cell wall thickness of 1,150 randomly selected holocellulose fibers was measured using 100x magnification on a Zeiss Axioskop. The fiber sample consisted of 80.9% summerwood and 19.1% springwood. The reported precision of the characterization was ± 5%. Hemicelluloses were selectively removed[37] from approximately half the holopulped fiber sample by aqueous alkaline extractions. Detailed

fiber preparation procedures including holopulping and hemicellulose extraction procedures, are given in Appendix 1.

FIBER PROPERTIES

The two fiber types, holocellulose and extracted holocellulose, were characterized according to carbohydrate composition, fiber width, and lumen diameter. Carbohydrate composition of the holocellulose and extracted holocellulose fiber types were analyzed by Econotech Services Limited, Annacis Island, New Westminster, B.C., using capillary gas chromatography.[78] Pulp samples were hydrolyzed with sulfuric acid and neutralized; then the sugars were reduced to the alditols with sodium borohydride. The alditols were acetylated with acetic anhydride and sulfuric acid, and the additol acetates were extracted with methylene chloride and injected into the gas chromatograph. Carbohydrate results are listed in Table 22.

Table 22: Carbohydrate composition.

	Sugar, % o.d. sample weight				
Fiber Type	Arabinan	Xylan	Mannan	Galactan	Glucan
Holocellulose	0.6	5.6	16.8	0.5	76.3
Extracted Holocellulose	<0.1	<0.1	3.8	<0.1	96.2

The extracted holocellulose fiber sample differs from the holocellulose fiber sample in sugar content. The arabinan, xylan, and galactan have been essentially removed from the extracted holocellulose fiber. Approximately 77.4% of the mannan was removed by the extraction procedure. Mannan is most closely associated with glucose, and its complete removal would result in degradation of the cellulose.[37, 79]

In order to obtain information on the extent of degradation of the cellulose caused by the alkali extraction, viscosities were determined in 0.5% cupriethylenediamine solution for pulp samples during various stages of the extraction procedure according to TAPPI method T-230 om-89.[80] The data are listed and compared to the viscosity of the unextracted holocellulose in Table 23.

Table 23: Viscosities of extracted holocellulose fibers.

Sample	Viscosity (cP)	Std. dev.	Number of observations
Unextracted holocellulose	19.3	0.2	5
Extracted with 1.5N KOH	23.7	0.2	4
Extracted with KOH + H_3BO_3	25.8	0.3	4
Extracted with 6.0N NaOH	18.1	0.5	4

The increase in viscosity of the holocellulose when extracted with 0.1N KOH is probably due to the removal of the short-chain hemicelluloses in this extractive step. The increase for the subsequent extraction is smaller due to the increased chain length of the hemicelluloses removed. Similar carbohydrate results due to hemicellulose extraction have been reported by Spiegelberg and others.[43, 37] Upon extraction with the sodium hydroxide, the viscosity decreased, signifying the possibility of cellulosic chain cleavage reactions taking place. The viscosities of the unextracted holocellulose and the sodium hydroxide extracted holocellulose sample were statistically different at the 95% confidence level.

Cellulose integrity was estimated by calculating the cellulose yield from the glucan content. Two assumptions were used in the estimation: (1) hemicelluloses contributed nothing to viscosity, and (2) holocellulose integrity was completely intact. The cellulose yield for the extraction procedure was approximately 75%, so a loss of 25% of the cellulose integrity was estimated. The cellulose may have been degraded by oxygen in the water used to make the sodium hydroxide solution.[81] Gentile[82] prevented oxygen degradation of the cellulose by removing the oxygen from water by distilling and boiling the water prior to solution preparation. In the current study, the reaction vessel was purged and blanketed with nitrogen; however, oxygen may have been contained in the pulp samples as well as in the sodium hydroxide solution. Secondly, in washing the pulp after the sodium hydroxide extraction step, any air drawn through the fiber mat may have contributed to the decrease in viscosity of the pulp.

Cellulose degradation was not evident in the tensile strength data collected. Tensile strength measurements of the holocellulose and extracted holocellulose fibers were determined at 50% RH. There was no significant difference between the tensile strength of the holocellulose and extracted holocellulose fibers. The single-fiber load to failure curves are plotted as load versus elongation for the holocellulose (five fibers) in Figure 11A and for the extracted holocellulose (seven fibers) in Figure 12A in Appendix 2.

The two fiber types, holocellulose and extracted holocellulose, were also characterized in terms of fiber width and lumen diameter. (See Table 24.) The width and lumen diameter of 100 randomly selected holocellulose and 100 randomly selected extracted holocellulose fibers were measured using 400x magnification on a Zeiss Axioskop with the aid of OPTIMAS image analysis software.[83] The reader is referred to Appendix 1 for a comprehensive listing of the individual fiber measurements.

Table 24: Characterization of fiber width and lumen diameter.

Fiber Type	Fiber Width(μm)	Lumen Diameter(μm)	Cell Wall Thickness(μm)
Holocellulose	29.3 ± (5.6)	13.2 ± (4.6)	8.0 ± (2.5)
Extracted Holocellulose	30.7 ± (5.4)	11.6 ± (3.6)	9.5 ± (2.6)

Typical loblolly pine fiber widths range from 35-45 μm.[84,85] The fiber width remained essentially constant from pulp to pulp. However, the difference in lumen diameter was statistically significant at the 95% confidence level. As a result of the lumen diameters' being significantly different, the average measurements listed in Table 24 were used to determine the cross-sectional area for the holocellulose fiber sample as 537 μm^2, and the cross-sectional area for the extracted holocellulose fiber sample as 633 μm^2. When applying a 20-gm tensile load to the single fibers, the engineering stress was calculated to be 36.8 x 10^8 dynes/cm^2 for a holocellulose fiber and 31.2 x 10^8 dynes/cm^2 for an extracted holocellulose fiber. Engineering

stress is obtained by dividing the load in dynes by the initial cross-sectional area of the fiber at 50% RH in cm^2.

MOISTURE CONTENT

The moisture content of each fiber type was determined at 50% RH using a modified TAPPI T210 cm-85 procedure.[86] Approximately 5 mg of single fibers conditioned at 50% RH were dried to a constant weight using a 102°C oven. At 50% RH the holocellulose fibers contained 10.4% moisture whereas the extracted holocellulose fibers contained 8.7%. Since the holocellulose fiber contained more hemicelluloses than the extracted fiber, it was expected that the holocellulose fiber would have a greater moisture content at a given relative humidity.[87]

The determination of the moisture pickup of single fibers when the sample is cycled from 50-90% RH and from 90-50% RH was necessary to establish the time necessary for single fibers at 50 and 90% RH to come to equilibrium. Samples of single fibers weighing approximately 5 mg were placed in a stainless steel wire basket that was attached to a microbalance. The basket was positioned in a double-walled relative humidity chamber. The relative humidity chamber design is pictured in Figure 15A of Appendix 2. The humidity was monitored to within ± 2.5% RH at a given set point. Holocellulose and extracted holocellulose fiber samples were conditioned at 50% RH and then cycled from 50% to 90% RH every three hours in the relative humidity chamber. Additional fiber samples were conditioned at 90% RH and cycled from 90% to 50% RH every three hours. Average air flow rate for 50% and 90% RH was 5.3 and 4.2 l/min. The moisture pickup of the fibers and the basket at 50 and 90% RH was automatically recorded from the microbalance. The moisture pickup from the basket was subtracted from the reported moisture regain values. The change in moisture content, MC, information is highlighted in Table 25. The percent average change in moisture content of both fiber types and relative humidities was significantly different at the 95% confidence level.

Table 25: Moisture regain.

	% Avg. Change MC from 50-90% RH	% Avg. Change MC from 90-50% RH
Holocellulose	6.28	7.04
Extracted Holocellulose	5.52	5.89

Holocellulose and extracted holocellulose fibers essentially came to equilibrium at 50 and 90% RH instantaneously. Since the single fiber samples reached equilibrium instantaneously, a cycle time of 10 minutes was used to change relative humidity conditions during creep testing. The percent average change in moisture content from 50-90% RH was also used to calculate the moisture content of single fibers conditioned at 90% RH. The average moisture content of the 90% RH samples was calculated by adding the percent average change in moisture content from 50-90% RH in Table 25 to the measured average moisture contents at 50% RH for each fiber type. The measured moisture contents at 50% RH and the calculated moisture contents at 90% RH are listed in Table 26.

Table 26: Moisture content.

Fiber Type	% MC at 50% RH	% MC at 90% RH
Holocellulose	10.4	16.6
Extracted Holocellulose	8.7	14.3

At 90% RH, holocellulose fibers contained 16.6% moisture and the extracted holocellulose fibers contained 14.3%. The moisture contents of single holocellulose fibers were significantly higher than the single extracted holocellulose fibers at the 95% confidence level. The reader is referred to Appendix 3 for additional information concerning moisture regain.

CREEP MEASUREMENT

Prior to creep testing, an epoxy resin, EPOXI-PATCH 907 BLUE, was used to mount single fibers on a set of pins. The epoxy, formerly called EPON 907 as used by Hill,[6] was purchased from the

Dexter Adhesives and Structural Materials Division of the Dexter Corporation. The epoxy was mixed using a 10:6 ratio by weight of resin to hardener component. Hill[6] confirmed that there was no bulk flow in the 10:6 mixture of epoxy; therefore, there should be no error in the measured fiber strain data due to creep in the epoxy. This was reconfirmed by determining the creep response of a paper clip and comparing the results to the creep response of a paper clip mounted on a set of pins with the 10:6 mixture of epoxy. The paper clip mounted to the pins was tested in a 50% as well as a 90% relative humidity testing chamber. The procedure developed to mount a single fiber is in Appendix 2. The epoxy was used for approximately 10 minutes after mixing, and it was possible to mount 10-15 fibers in this 10-minute time period. Mounted fibers were conditioned in a 73°F and 50% RH laboratory for at least 24 hours prior to testing.

Creep and creep recovery were measured under conditions of constant 50% and 90% RH. Single fibers were also conditioned at 50% RH and loaded to 20 grams. After 10 minutes, the humidity was cycled to 90% RH. The humidity was cycled every 10 minutes between 50% and 90% RH for a duration of 100 minutes (Figure 40). Approximately 15 seconds were required to change the relative humidity from 50 to 90% RH or from 90 to 50% RH. Fibers were also conditioned at 90% RH, loaded to 20 grams, and then cycled between 90 and 50% RH.

The various relative humidities were reached by mixing dry house air with filtered house air saturated with moisture, by passing it as a stream of fine bubbles through a five-foot column of water. The water column was designed to facilitate cleaning of the column and the screen at the bottom of the column. Settling of biological sediment on the inside of the tank and in the screen pores can decrease the ability to attain 90% RH. The design allows access to the full diameter of the tank at the top and bottom. The screen is removable and can be pressure-washed to remove any blockages in the pores. The relative humidity range was 3-100% RH. Probe accuracy was ±2.5% RH at a given set-point. All equipment was located in a 50% RH and 73°F laboratory (Figure 41).

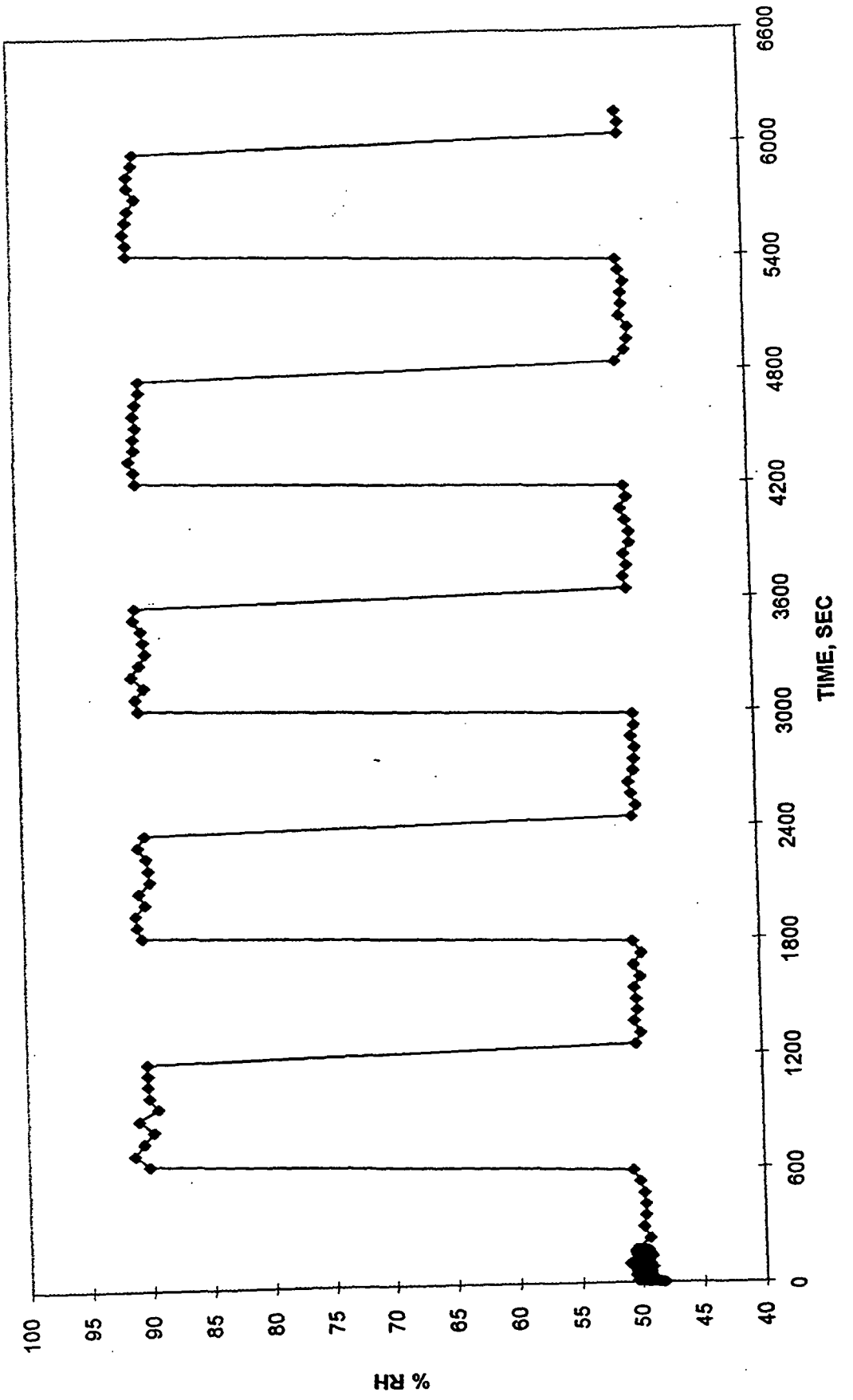

Figure 40: Relative humidity control.

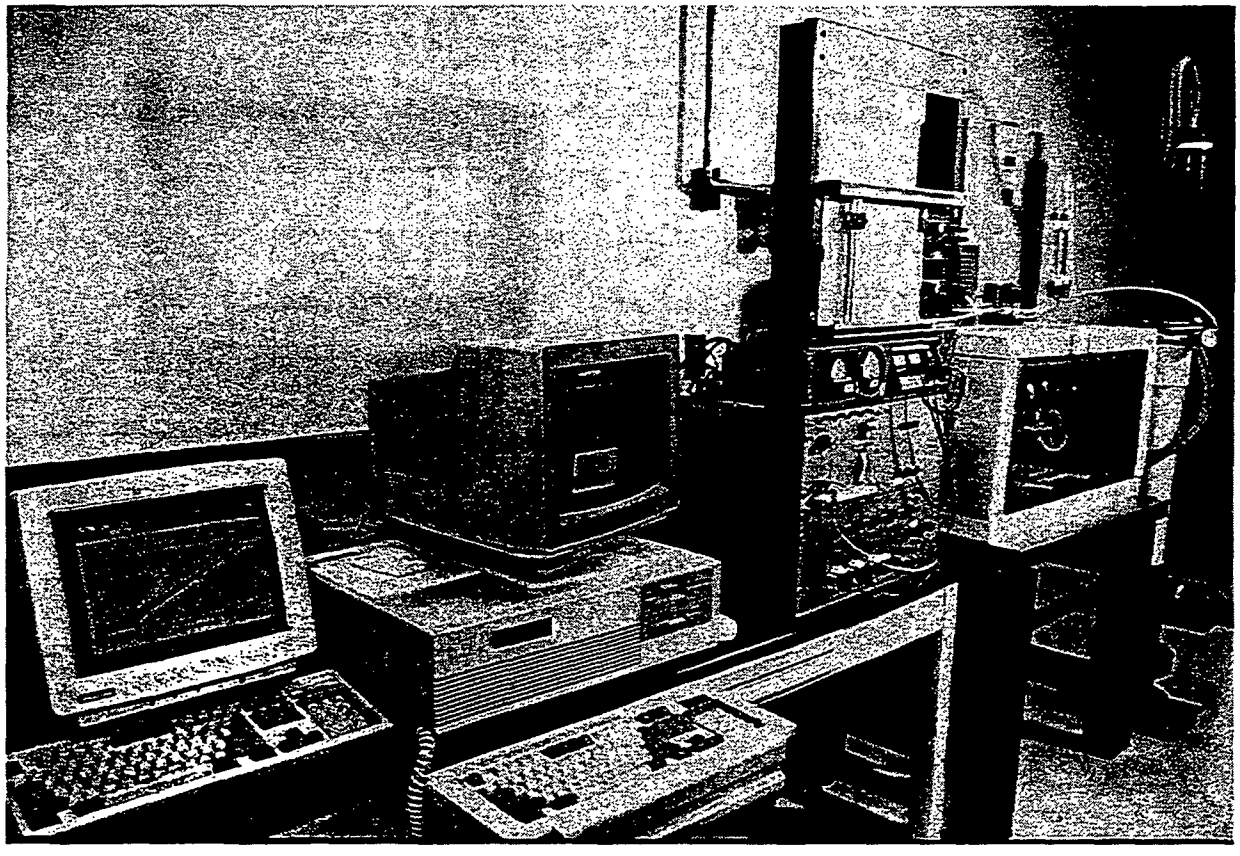

Figure 41: Overview of laboratory.

A relative humidity chamber was designed to completely enclose the jaws of the single-fiber creep apparatus and fiber test specimen. The relative humidity chamber and jaws are pictured in Figure 3A in Appendix 2. The chamber also allowed shorter cycling times during testing. The humidity chamber has a removable front cover which allows the insertion of the fiber into the fiber holders. The front cover is perforated to allow continued fresh air flow into the chamber. The relative humidity and temperature sensor was located inside the relative humidity chamber opposite the air inlet. A strain sensor was located on the active load cell arm. This sensor had a 0.5-mm full scale range and a 0.50μm sensitivity.

The Fiber Load Elongation apparatus (Figure 42) used by Hardacker[88] was used for the creep determinations. The operation of the instrument was as follows: the fiber pin holders were held between clamps, F, the right-hand one of which was positioned by the microscope focusing mechanism, G, and fixed rigidly in place with clamp, H. The left-hand clamp was attached to the sensing member of an electronic balance cell, A, which was supported from flex members, C. When the cell was moved to the left by differential screw, E, and servo motor, D, a tensile load was applied to the specimen. The magnitude of the load was sensed by the electronic balance cell. Specimen deformation allowed movement of the left-hand clamp, which was sensed by a capacitive displacement transducer, I.

A versatile feature of the apparatus was achieved by driving the servo motor to minimize the error between a reference voltage and the signal from the load transducer. A variable slope, reversible, linear ramp generator supplied the reference voltage. The ramp set the time pattern of loading and/or unloading while one of the transducer signals interacted with this to produce a constant rate of loading to be maintained with respect to time. The apparatus was positioned on a 63-511 Micro-g Series 630500 high-performance vibration isolation table. A more complete review of the apparatus, procedures, and calibration techniques is in Appendix 2.

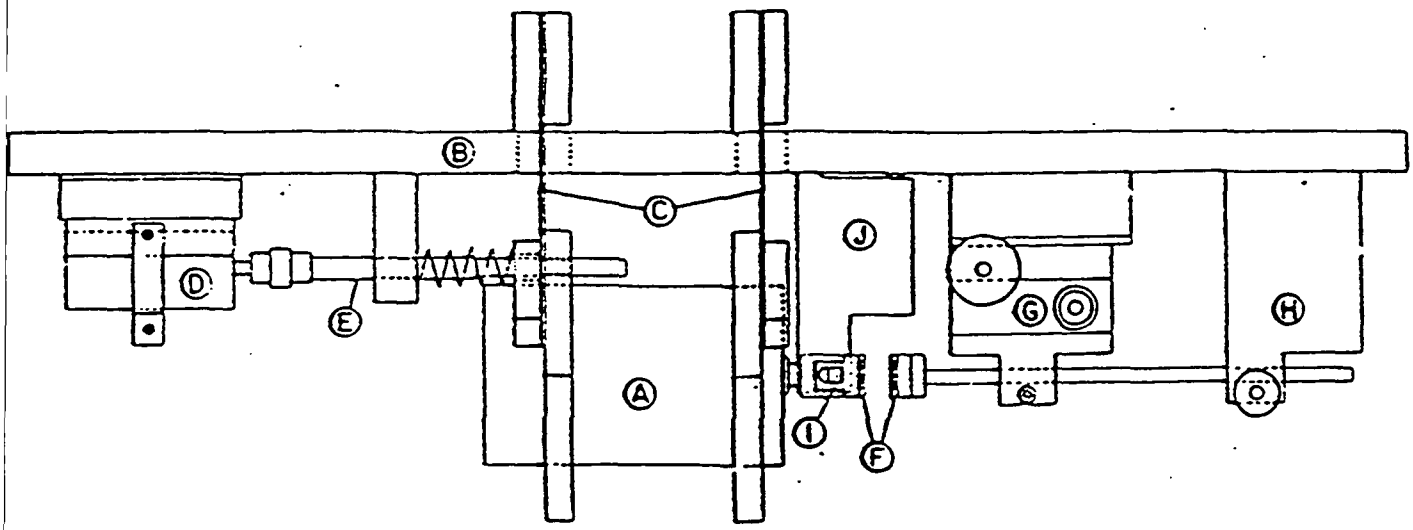

Figure 42: Scale drawing of apparatus. A: electronic weighing cell. B: mounting plate. C: flexure hinges D: DC servo motor. E: differential screw F: pin holder clamps. G: microscope focusing mechanism. H: pillar clamp. I: capacitive displacement transducer. J: support pillar for displacement transducer.

RESULTS AND DISCUSSION

The Results and Discussion consists of two sections. The first section is comprised of all constant humidity data and is presented in two parts. Part 1 presents the actual single-fiber-creep data at constant humidity levels. The creep data is analyzed statistically using the Eyring model. Part 2 focuses on the creep-recovery data for single fiber creep. The hypothesis that tensile creep behavior of individual pulp fibers as a function of relative humidity is dependent on hemicellulose content will be developed throughout this section as will the second hypothesis that the hemicellulose contribution to fibers undergoing tensile creep facilitates cellulose microfibril slippage.

The second section contains cyclic humidity creep data and addresses the third hypothesis, that tensile creep behavior of individual pulp fibers under cyclic humidity conditions is dependent on hemicellulose content.

SINGLE FIBER CREEP AT CONSTANT HUMIDITY

Two series of creep measurements were made at constant humidity conditions: (a) single holocellulose and extracted holocellulose fibers loaded to 20 grams were exposed to a constant environment of 50% RH, and (b) single holocellulose and extracted holocellulose fibers loaded to 20 grams were exposed to a constant environment of 90% RH. While creep tests were run for 24 hours, for the sake of simplicity the plots shown are for six hours, which was representative of the behavior of the total system. The fibers stressed at 90% RH were conditioned by holding the fiber at the test humidity for 30 minutes prior to testing. Average strain was determined at selected times for an individual fiber test upon reaching a 20-gm load and comprises the method used for combining raw data into a creep curve.

This averaging procedure created the same time scale for each single fiber tested. Single fibers were loaded at 1.0 gram per second. Strain data were collected every 0.2 seconds for the first 180

seconds and then every 60 seconds for the duration of the test. Process control programs are in Appendix 2. Data was compiled using the following averaging process for each fiber:

1. Upon reaching a load of 20 grams, the time scale was adjusted accordingly and strain data was reported as time zero (t = 0).
2. Using the adjusted time scale, an averaged creep curve for each single fiber was constructed. Strain at t = 30 sec was compiled by averaging strain from $t_{0\ sec}$ to $t_{60\ sec}$.
3. Strain at t = 60 sec was compiled by averaging strain from $t_{30\ sec}$ to $t_{90\ sec}$.
4. Strain at t = 90 sec was compiled by averaging strain from $t_{60\ sec}$ to $t_{120\ sec}$.
5. Strain at t = 150 sec was compiled by averaging strain from $t_{120\ sec}$ to $t_{180\ sec}$.
6. Strain at t = 180 sec was equal to $t_{180\ sec}$.
7. Strain at t = 240 sec was equal to $t_{240\ sec}$.
8. Strain at t = 300 sec was equal to $t_{300\ sec}$.
9. This process was continued for the remainder of the strain data.

Strain is plotted as a fraction of the initial fiber test span versus time in seconds for extracted holocellulose fibers at 50% RH (Figure 43). Single extracted holocellulose fibers were also stressed at 90% RH (Figure 44). The fibers stressed at 90% RH were conditioned by holding the fiber at the test humidity for 30 minutes prior to testing.

Previous workers[6, 61] have used plots of the strain versus the logarithm of time to analyze creep data. In Figure 45, the 50% RH plot of the extracted single fibers is linear as observed by Hill for longleaf pine fibers. The 90% RH plot (Figure 46) exhibits some curvature, as previously reported in Figure 39 of the Byrd Analysis section.

Similarly, single holocellulose fibers were stressed at 50 and 90% RH. The fibers stressed at 90% RH were conditioned for 30 minutes prior to testing. Average strain was determined at selected times for all individual fiber tests upon reaching a 20-gm load and is plotted as a fraction of the initial fiber test span versus time in seconds for the holocellulose fibers at 50 and 90% RH in Figures 47 and 48. The single holocellulose fibers at 50% RH

Figure 43: Creep of single extracted holocellulose fibers at 50% RH.

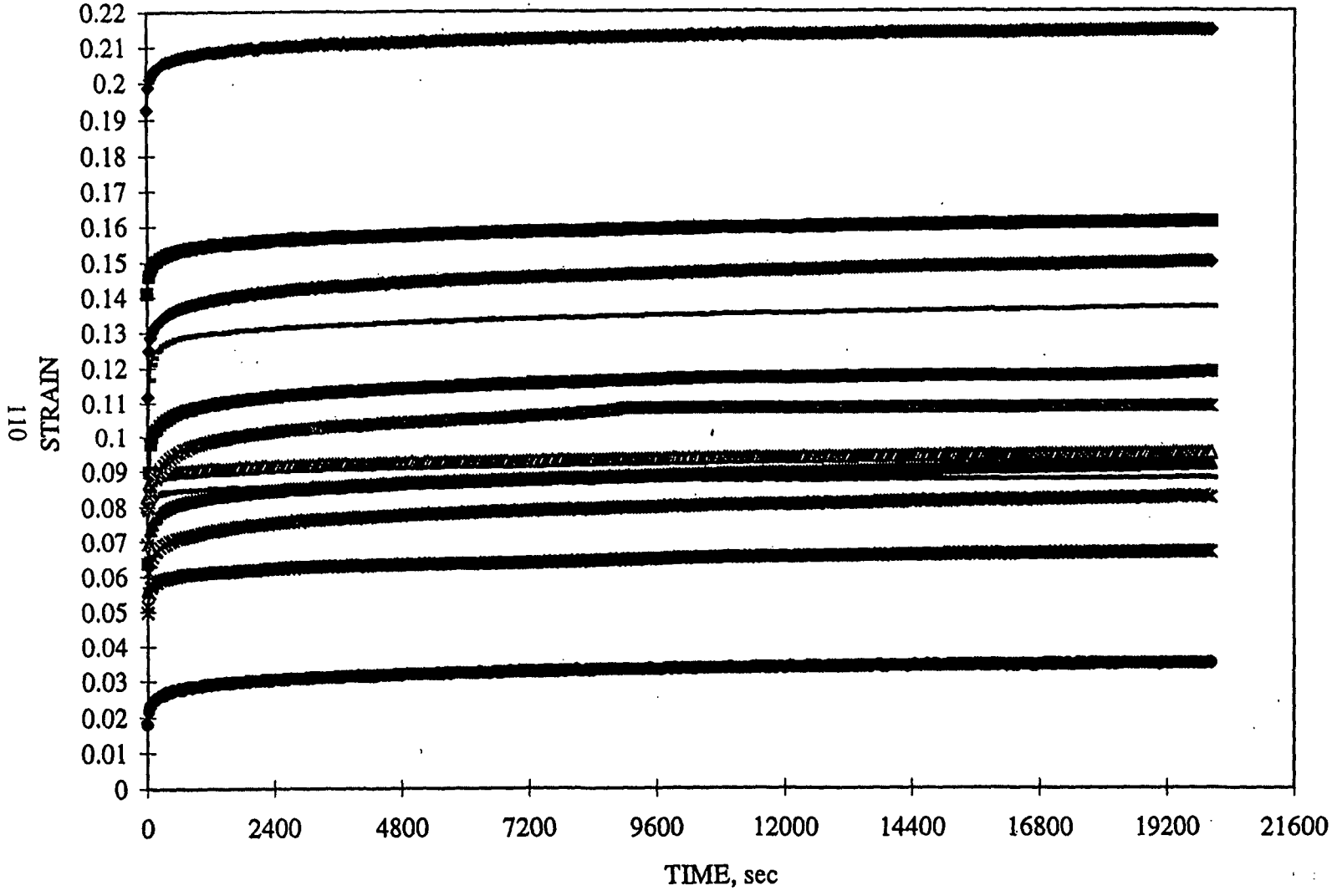

Figure 44: Creep of single extracted holocellulose fibers at 90% RH.

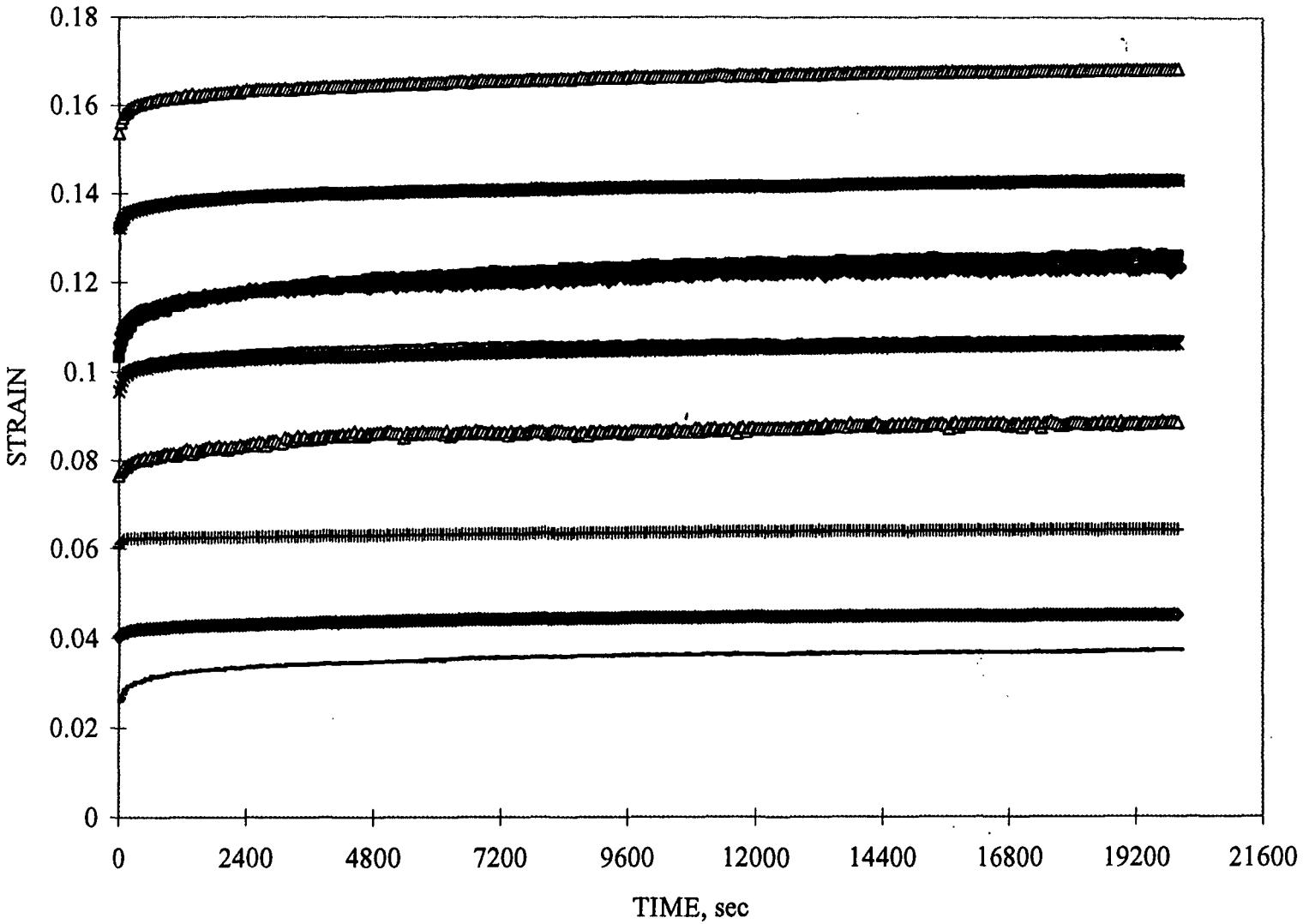

Figure 45: Creep of single extracted holocellulose fibers at 50% RH as a function of ln time.

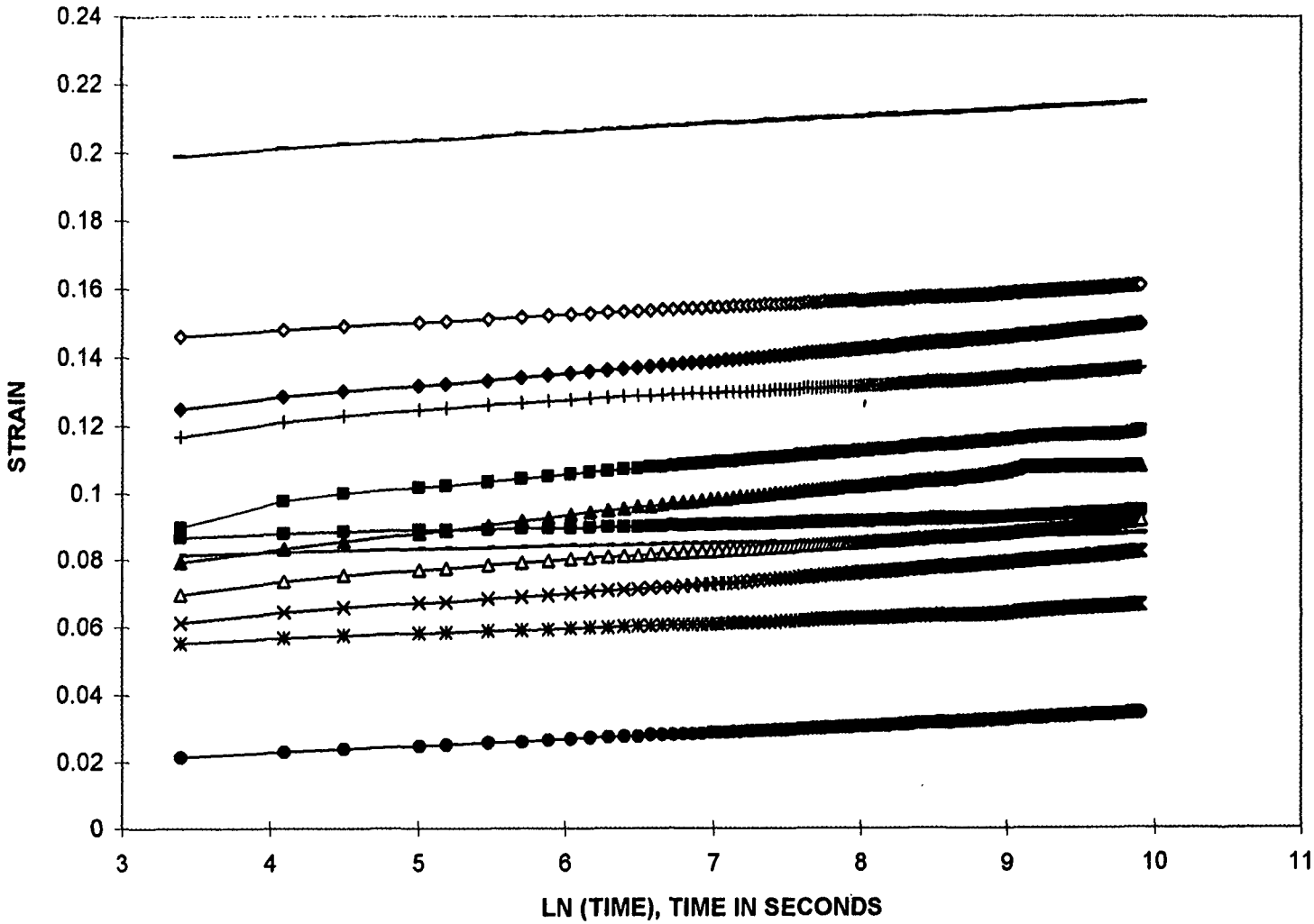

Figure 46: Creep of single extracted holocellulose fibers at 90% RH as a function of ln time.

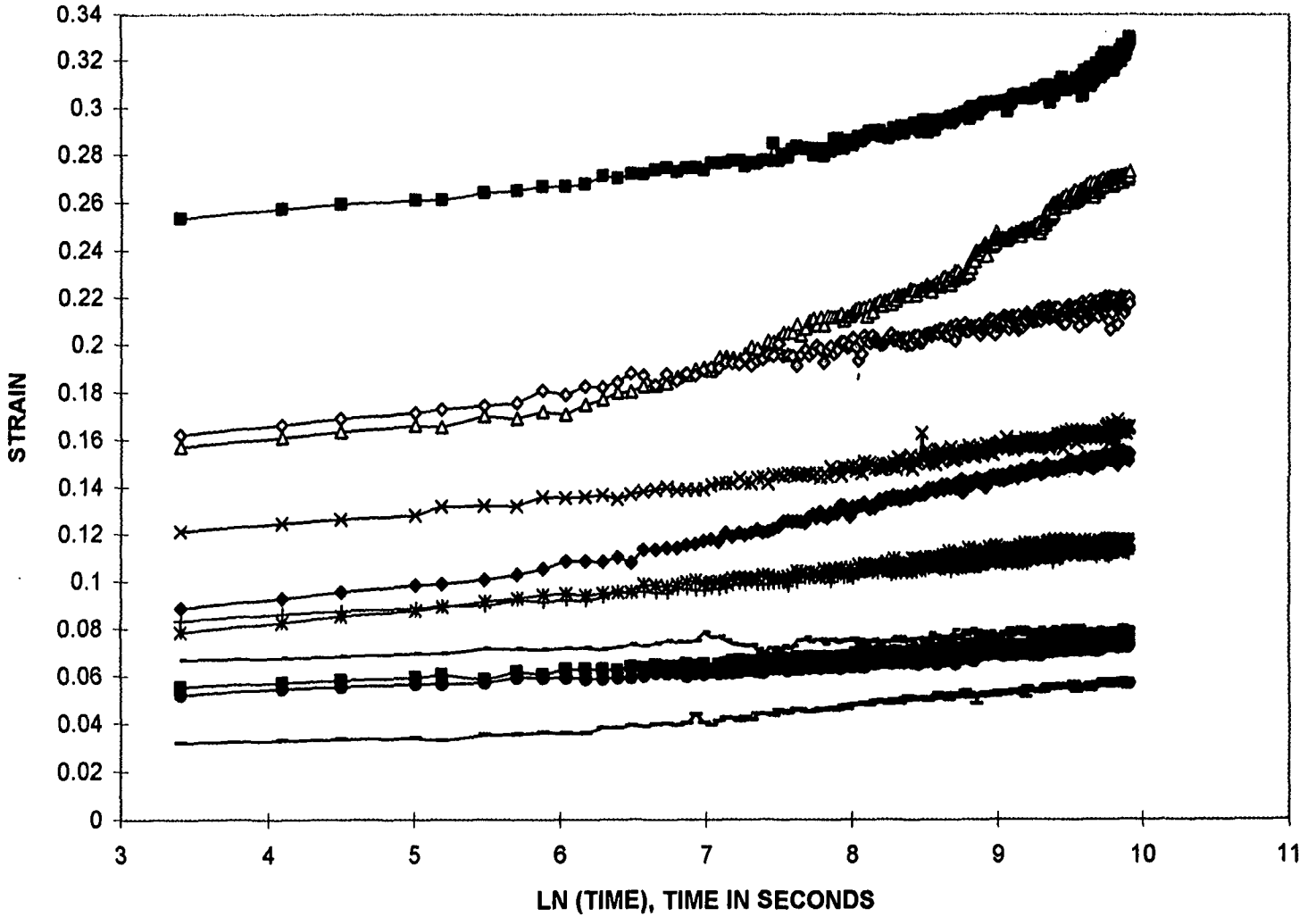

Figure 47: Creep of single holocellulose fibers at 50% RH.

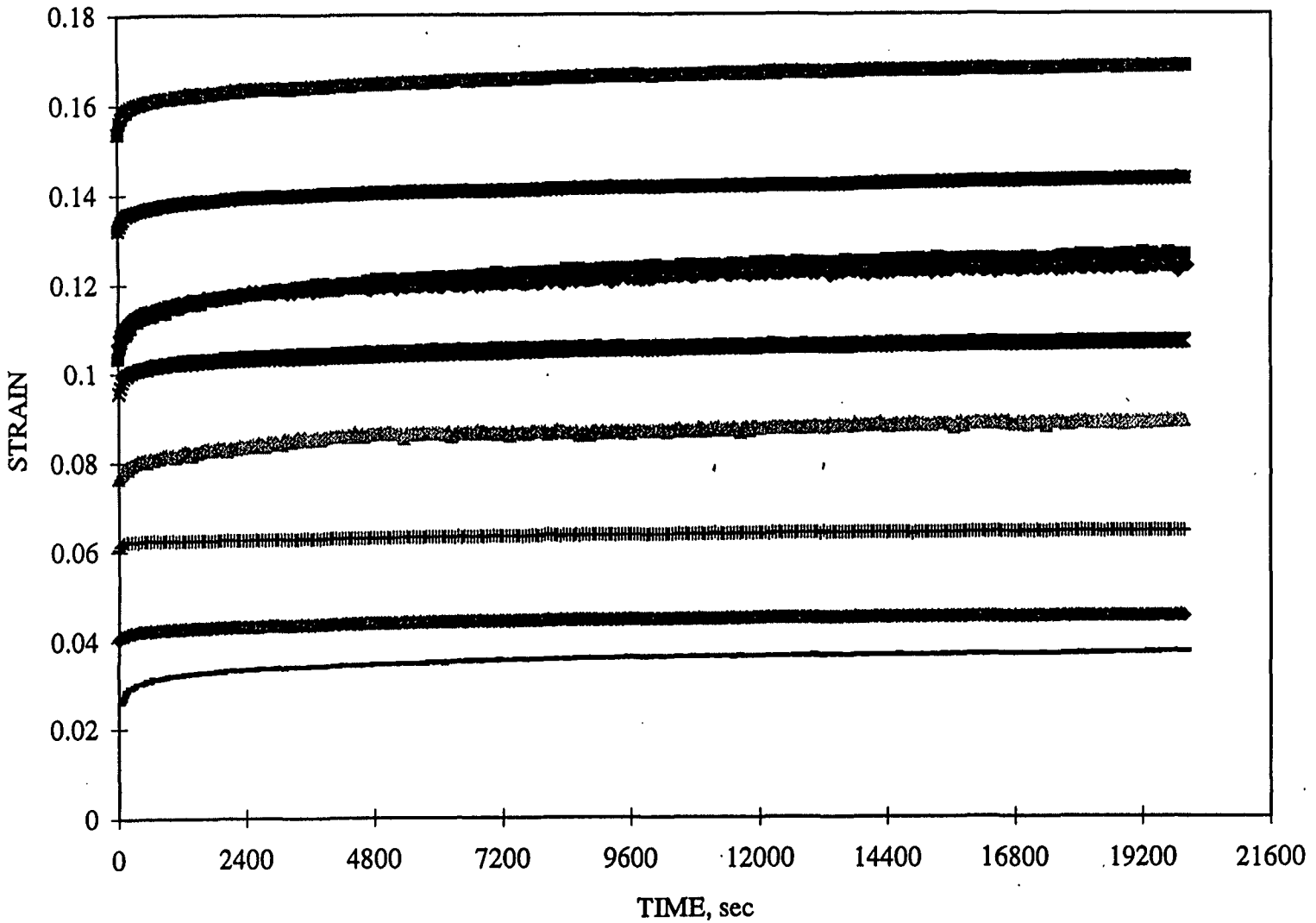

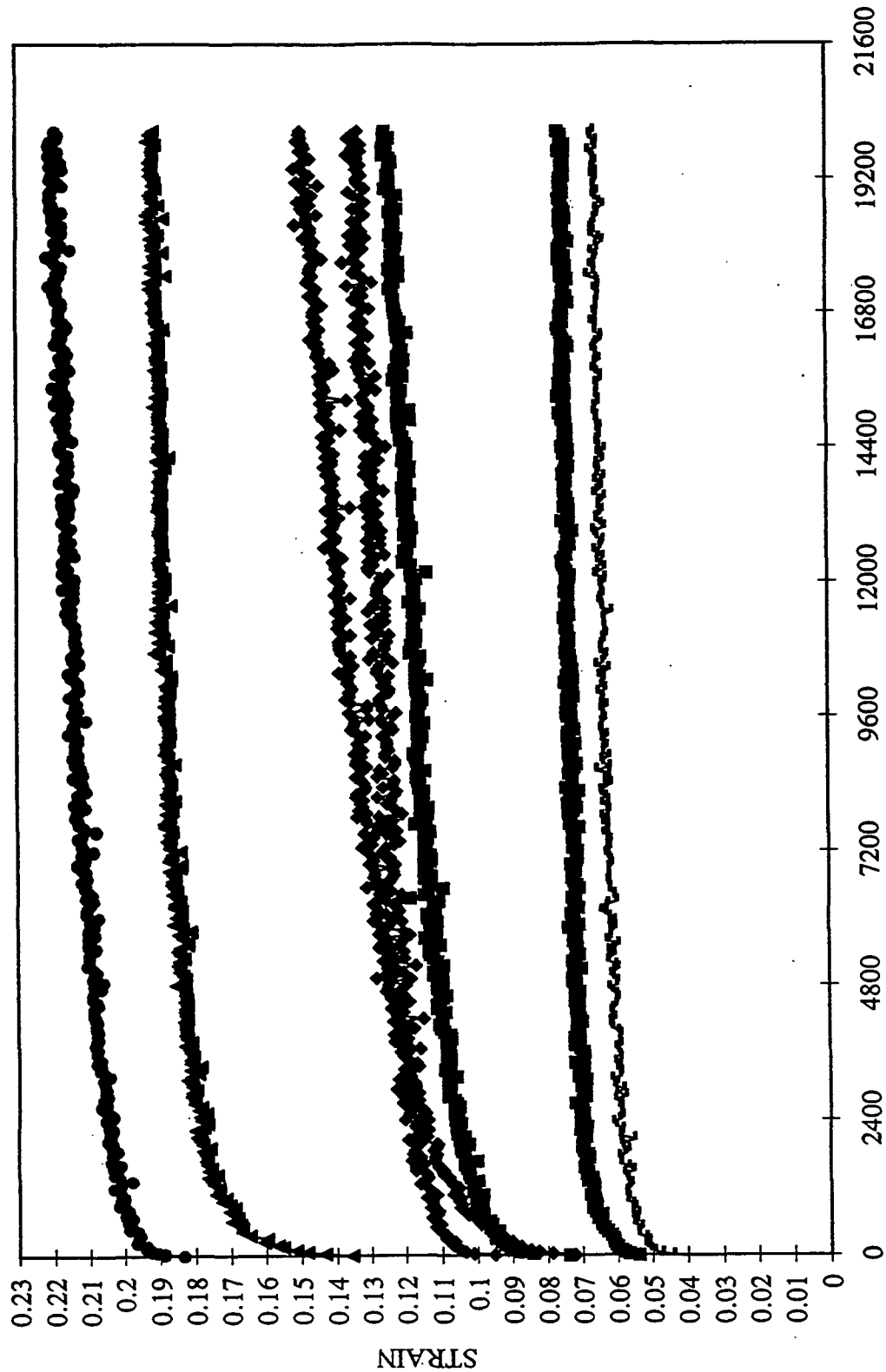

Figure 48: Creep of single holocellulose fibers at 90% RH.

exhibited the same linear behavior as the extracted fibers as a function of logarithmic time. Both fiber types at 90% RH exhibited curvature as a function of logarithmic time.

Statistical Analysis

The purpose of the statistical analyses is first to describe the range of strain test values exhibited by each fiber type and relative humidity combination. The range of test values can be ascribed primarily to two broad sources of variation: interfiber variation and experimental error. Secondly, the significance of two factors in the creep experiments, the relative humidity (50% or 90%) and the fiber type (holocellulose or extracted holocellulose), was determined relative to the Eyring parameters. This secondary analysis is necessary in order to address the first thesis hypothesis, that the tensile creep behavior of individual pulp fibers as a function of relative humidity is dependent on hemicellulose content. In addressing this hypothesis, the method of multiple regression analysis was employed to determine the statistical significance of the relative humidity and the fiber type with respect to the creep results. Analyses using this statistical method are presented and discussed.

Interfiber Variation

Possible sources of interfiber variation include differences in the physical structure of the fibers, nonuniform mechanical action on the fibers, and the overall mounting angle of the fibers on the pins. Analysis of the interfiber variation within each relative humidity and fiber type combination used the following model,

$$y = b_o + b_1 x_1 + b_{11}(x_1)^2 \qquad (43)$$

where y = strain

b_o = intercept

b_1, b_{11} = coefficients

$x_1 = \ln(t)$, time is in seconds.

Analysis of the interfiber variation for all fibers used the following model,

$$y = b_o + b_1x_1 + b_{11}(x_1)^2 + b_2x_2 + b_3x_3 \quad (44)$$

where y = strain

b_o = intercept

b_1, b_{11}, b_2, b_3 = coefficients

x_1 = ln(t), time is in seconds

x_2 = relative humidity

x_3 = fiber type.

A general linear model (GLM) regression was run for the models.[70] The following model,

$$y = b_o + b_1x_1 \quad (45)$$

where y = strain

b_o = intercept

b_1 = coefficient

x_1 = ln(t), time is in seconds

did not fit single fiber data at both 50 and 90% RH as seen with the data analysis of Byrd's single fibers at 90% RH; therefore, the quadratic model was employed. As previously described, the creep of Hill's single fibers at 50% RH was linear in ln time. However creep of single fibers at 90% RH was nonlinear in ln time, and a quadratic relationship was required to fit Byrd's data at 90% RH. One can also regress ln(t) for the Eyring model, not to discover physical parameters but to use ln(t) as a statistic to explore the use of strain. The Eyring model can be expressed as a function of logarithmic time as previously described. The reader is referred to the Theoretical Analysis of Data section for a comparison of the Eyring model to other typical creep-data analyses.

The interfiber variation in strain is quite large and ranges from 41–56% within each fiber type and relative humidity combination listed in Table 27. For this experiment, 7–12 fibers were tested at each creep condition, giving approximately the same interfiber variation Hill reported when testing 50 fibers.[6] The interfiber strain variation expressed as coefficient of variation for the total single fiber population was 47.63%.

Table 27: Interfiber variation in strain.

Level of RH	Type	Number of fibers tested	% Coefficient of variation
50	Extracted	12	43.75
50	Holocellulose	10	41.06
90	Extracted	11	55.66
90	Holocellulose	7	42.40
Both	All	40	47.63

Jentzen[24] tested single holopulped summerwood longleaf pine fibers at various loading levels and found 28–40% interfiber strain variability. He tested 39–109 fibers for each loading level. Spiegelberg[43] similarly holopulped[76, 77] and selectively extracted longleaf summerwood pine chips from the 27th or 28th growth ring. He measured the yield point strain of 20–33 single holocellulose and extracted fibers at 50% RH. Interfiber variation for the yield point strain of the holocellulose fibers varied from 18–49%, whereas the extracted fibers varied from 22–67%. Considering the number of fibers tested, the interfiber variation in strain reported for the holocellulose and extracted loblolly pine fibers is certainly within the ranges reported by Jentzen and Spiegelberg for holocellulose and extracted pine fibers. Spiegelberg and Jentzen used a different fiber separation technique as well as different tensile testing equipment from that used for the loblolly pine fibers tested for this thesis; therefore, the interfiber variability may be from an alternate source.

Esser[89] conducted single fiber tensile tests using different mounting pin sets to which individual fibers were glued with Epoxy-Patch 907 Blue, the same epoxy and mounting procedure used on single fiber loblolly pine creep tests. Esser tested 42 individual black spruce

fibers. He reported the interfiber variation for percent strain in black spruce as being 41%. Considering fewer loblolly pine fibers were tested, the variability in strain is comparable to that of the black spruce even though the overall mounting angle of the fibers on the test pins and the mechanical action on the fibers prior to loading may have been different. Sources of interfiber variation other than overall mounting angle of the fibers on the pins and nonuniform mechanical conditioning prior to testing may account for the intervariation in the single fiber tests.

Brown, Mann, and Pierce[90] have tested the influence of humidity on the strain of various types of cotton. The percent strain at 66% relative humidity for various types of cotton had an interfiber variation of 38–54% when 34–46 single fibers were tested. The mean interfiber variation for the five cotton types was 45%. The weight average interfiber strain variation was 47.63% expressed as coefficient of variation for strain over the total single loblolly pine fiber population. Regardless of the type of cellulose fiber, the typical single interfiber variation for strain seems to fall within a similar range which may describe the variability in physical structure of fibers.

Possible differences in the physical structure of the fibers can be caused by fluctuations of cross-sectional area, pit patterns, fibril angle, and cell wall thickness. Dissimilarities in the minute structure of the cell wall can lead to the concentration of stress in a localized area,[75] premature failure, and apparent differences in the strain behavior of fibers. It should be pointed out that the stresses were computed assuming a uniform cross-sectional area along the length of the fiber. Since the dimensions were not uniform and the cross-sectional area at the zone of the test span may very well be the minimum cross-sectional of the fiber, it is highly probable that calculated stresses exceed those that the fibers actually possess.

Other potential sources of interfiber variability, including differences in the nonuniform mechanical action on the fibers during handling and separation procedures and the overall mounting angle of the fibers on the pin sets, can be eliminated to a certain degree because Hill,[6]

Spiegelberg,[43] Jentzen,[24] and others[89, 91, 92] have conducted single fiber tensile tests using various handling, separation, mounting, and testing techniques but still have a similar range of interfiber variation in strain measurement. Interfiber variation may be present in the single fiber tensile tests regardless of handling and testing techniques and may be attributed to the differences in physical structure of the fibers.

Measurement Error

A second source of variation in the strain data is measurement error. Experimental error could be comprised of the sensitivity of the strain sensor, the ability of the controller to maintain a load of 20 grams, and the ability of the relative humidity control to operate around a given set point. To quantify the experimental error, a regression model was run for each relative humidity and fiber type combination using the following model,

$$y = b_o + b_1x_1 + b_{11}(x_1)^2 + b_4x_4 \quad (46)$$

where y = strain

b_o = intercept

b_1, b_{11}, b_4 = coefficients

x_1 = ln(t), time is in seconds

x_4 = individual fiber tested.

Analysis of the experimental error for all fibers tested used the following model,

$$y = b_o + b_1x_1 + b_{11}(x_1)^2 + b_2x_2 + b_3x_3 + b_4x_4 \quad (47)$$

where y = strain

b_o = intercept

b_1, b_{11}, b_2, b_3, b_4 = coefficients

x_1 = ln(t), time is in seconds

x_2 = relative humidity

x_3 = fiber type

x_4 = individual fiber tested.

Intrafiber variation in strain is indicated in Table 28.

Table 28: Intrafiber variation in strain.

Level of RH	Type	Number of fibers tested	% Coefficient of variation
50	Extracted	12	1.24
50	Holocellulose	10	0.88
90	Extracted	11	3.40
90	Holocellulose	7	2.32
Both	All	40	2.97

The experimental error was approximately 2.97% for the strain measurement averaged over individual fibers. The first possible source of experimental error could be contributed to the sensitivity of the strain sensor. Considering the 0.5-μm sensitivity of the strain sensor, the strain sensor can contribute 0.05% error to a single strain measurement.

A second source of experimental error in strain could be the controller's influence on the applied load. Since two controllers were used in the creep experiments, one for the 50% RH experiments and a second one for the 90% RH experiments, the hypothesis that the two controllers had equivalent variances was tested. Using the pooled standard deviations for the 50 and 90% RH creep tests and applying an F-test at the 95% confidence level, the variances of the two controllers were not equivalent. As a result, the variance in load of each controller was estimated from 10 randomly chosen single fiber tests at each respective relative humidity. The first controller, for the 50% RH creep experiments, could contribute a variation in load of 0.003 gm around the mean applied load to the fibers tested whereas the second controller, for the 90% RH creep experiments, could contribute a variation in load of 0.724 gm around the mean applied load to the fibers tested. Possible experimental error in strain due to each controller could be estimated by converting load to stress and then taking the derivative of strain with respect to

stress. The first controller could contribute 0.008% strain to the experimental error in the strain compared to that of the second controller which could contribute approximately 2% strain. Therefore, opportunities for future improvement in the apparatus include replacement of the second controller and motor currently in the fiber load elongation apparatus.

A third component of the experimental error was due to a limitation in the ability of the relative humidity control to operate around a given set point. A 2.5% variance in relative humidity was estimated from 10 randomly chosen single fiber tests. Potential experimental error in strain contributed by the relative humidity controller can be estimated by taking the partial derivative of strain with respect to relative humidity at a time of 10,800 seconds. This enables one to estimate the contribution of experimental error to the measured strain. The nonlinear SAS parameter fittings of the loblolly pine single fiber creep data for each fiber type and relative humidity combination were used as the basis to calculate strain variation. The relative humidity varies 2.5% around the set point. This would cause an intrafiber variation in strain of about 1.9% in test samples.

Statistical Analysis for Creep Behavior

In order to address the first hypothesis, that the tensile creep behavior of individual pulp fibers as a function of relative humidity is dependent on hemicellulose content, the initial strain at t = 0 for each single fiber test was subtracted from each individual fiber's subsequent creep strains. Following this subtraction of the strain at t = 0, the individual fiber strain results were subjected to multiple regression analysis at a specific time interval of 10,800 seconds. The regression model used was

$$y = b_0 + b_1x_1 + b_2x_2 \qquad (48)$$

where y = strain at 10,800 seconds

b_0 = intercept

b_1, b_2 = coefficients

x_1 = fiber type; 0 for extracted fiber
1 for holocellulose fiber

x_2 = relative humidity; 0 for 50% RH
1 for 90% RH.

At a confidence level of 99%, fiber type and relative humidity revealed statistically significant results with respect to the tensile creep behavior of single fibers at a time of 10,800 seconds (Table 29). The effect of fiber type or hemicellulose content on the creep phenomenon is negative. The holocellulose fibers exhibit less creep strain than the extracted fibers at 10,800 seconds. The effect of the humidity level is positive; therefore, fibers exhibit greater creep strain at 90% RH as compared to 50% RH at 10,800 seconds. According to the regression analysis presented, the first hypothesis is accepted. The main effect variable, fiber type, is significant with respect to the creep phenomenon.

Table 29: Multiple regression analysis: effect of fiber type and relative humidity on creep strain at t = 10,800 seconds.

Independent Variable	**Parameter Estimate**	**Standard Error of Estimate**	**t-value**	**Confidence Level t is Significant**
b_o, Intercept	0.02609	0.00444	5.86	100
b_1, Fiber type	-0.01400	0.00552	-2.53	99
b_2, Humidity	-0.01837	0.00548	3.35	99

Root Mean Square Error = 0.5849

The single fiber creep data was fitted with the regression Eq. (42). The quadratic relationship was necessary to fit the extracted holocellulose at both humidity levels and the holocellulose at 90% RH. The coefficients of the regression analysis were used to calculate the rate of strain for individual fibers at specific time intervals, $\partial(\text{strain})/\partial(t) = b/t + (2c \times \ln(t))/t$. The single fiber strain rates at specified times of 1,800, 3,600, 10,800, and 21,600 seconds were fitted with the following regression model,

$$y = b_o + b_1x_1 + b_2x_2 \qquad (49)$$

where y = strain rate at a specified time in seconds

b_0 = intercept

b_1, b_2 = coefficients

x_1 = fiber type; 0 for extracted fiber
1 for holocellulose fiber

x_2 = relative humidity; 0 for 50% RH
1 for 90% RH.

The results (Tables 30–33) provide an answer to the second hypothesis, that the hemicellulose contribution to fibers undergoing tensile creep facilitates cellulose microfibril slippage. At a confidence level of 75%, fiber type revealed statistically significant results with respect to the tensile creep rate of single fibers at a time of 1,800 seconds (Table 30). The statistical significance of fiber type decreased as the selected time interval increased. At 21,600 seconds the fiber type was 62% significant with respect to the creep rate. The effect of fiber type or hemicellulose content on the rate of creep was negative for all time intervals selected. The extracted fibers exhibited a greater strain rate than the holocellulose fibers at the specified time intervals. The second hypothesis is not accepted. The main effect variable, fiber type, is significant with respect to strain rate based on the multiple regression analyses.

At a confidence level of 99%, relative humidity revealed statistically significant results with respect to the strain rate of single fibers all time intervals selected. The effect of the humidity level was positive; therefore, fibers exhibit a greater strain rate at 90% RH as compared to 50% RH at the specified time intervals.

Table 30: Multiple regression analysis: effect of fiber type and relative humidity on strain rate at t = 1,800 seconds.

Independent Variable	**Parameter Estimate**	**Standard Error of Estimate**	**t-value**	**Confidence Level t is Significant**
b_0, Intercept	15.47559	4.94318	3.13	99.7
b_1, Fiber type	-7.19029	6.13604	-1.17	75.1
b_2, Humidity	27.54286	6.09718	4.52	99.9

Root Mean Square Error = 19.1428

Table 31: Multiple regression analysis: effect of fiber type and relative humidity on strain rate at t = 3,600 seconds.

Independent Variable	Parameter Estimate	Standard Error of Estimate	t-value	Confidence Level t is Significant
b_0, Intercept	8.01371	2.99001	2.68	98.9
b_1, Fiber type	-3.96516	3.71154	-1.07	70.8
b_2, Humidity	15.82496	3.68804	4.29	99.9

Root Mean Square Error = 11.5788

Table 32: Multiple regression analysis: effect of fiber type and relative humidity on strain rate at t = 10,800 seconds.

Independent Variable	Parameter Estimate	Standard Error of Estimate	t-value	Confidence Level t is Significant
b_0, Intercept	2.82055	1.28598	2.19	96.5
b_1, Fiber type	-1.52001	1.59630	-0.95	65.3
b_2, Humidity	6.35612	1.58619	4.01	99.9

Root Mean Square Error = 4.9799

Table 33: Multiple regression analysis: effect of fiber type and relative humidity on strain rate at t = 21,600 seconds.

Independent Variable	Parameter Estimate	Standard Error of Estimate	t-value	Confidence Level t is Significant
b_0, Intercept	1.45517	0.73683	1.97	99.4
b_1, Fiber type	-0.81839	0.91463	-0.89	62.3
b_2, Humidity	3.51780	0.90884	3.87	99.9

Root Mean Square Error = 2.8534

The factors, relative humidity and fiber type, were significant with respect to the creep phenomenon. Since the effect of pulp type was significant with respect to the rate of strain, the pulp type will affect the Eyring parameters that determine the slope of the experimental data curves. In analyzing the influence of both factors, relative humidity and fiber type, on the behavior of single fiber creep, differences are expected in the Eyring parameters. The reader is referred to the Theoretical Analysis of Data chapter for a more complete discussion of the Eyring model.

Statistical Analysis for Creep Recovery

The interfiber variation in strain for all the creep recovery experiments was 35.12% (Table 34). Analysis of the interfiber variation for all fibers used the model described by Eq. (44). Analysis of the interfiber variation within each relative humidity and fiber type combination used the model described by Eq. (43).

Table 34: Creep recovery interfiber variation in strain.

Level of RH	Type	Number of fibers tested	% Coefficient of variation
50	Extracted	5	46.10
50	Holocellulose	5	41.90
90	Extracted	5	40.00
90	Holocellulose	5	20.40
Both	All	25	35.12

The intrafiber variation in strain was 2.60% for all the creep recovery experiments (Table 35). Analysis of the experimental error for all fibers tested used Eq. (47). Analysis of the experimental error for each relative humidity condition used Eq. (46). Intrafiber variation was not significantly different from the creep experiments.

Table 35: Creep recovery intrafiber variation in strain.

Level of RH	Type	Number of fibers tested	% Coefficient of variation
50	Extracted	5	2.84
50	Holocellulose	5	2.51
90	Extracted	5	2.12
90	Holocellulose	5	1.88
Both	All	25	2.60

In order to address the tensile creep recovery behavior of individual pulp fibers as a function of relative humidity and hemicellulose content, the individual fiber strain results at each humidity and fiber type were subjected to multiple regression at a specific time interval of 1,200 seconds. The regression model used was Eq. (48). At a confidence level of 71%, fiber type

revealed statistically significant results with respect to the tensile creep behavior of single fibers at a time of 1,200 seconds (Table 36). The effect of fiber type or hemicellulose content on the creep phenomenon is positive. The holocellulose fibers exhibit more creep strain than the extracted fibers at 1,200 seconds. Relative humidity was statistically significant with respect to creep behavior at 1,200 seconds at a confidence level of 99%. The effect of the humidity level is positive; therefore, fibers exhibit greater creep strain at 90% RH as compared to 50% RH at 1,200 seconds.

Table 36: Multiple regression analysis: effect of fiber type and relative humidity on creep recovery strain at t = 1,200 seconds.

Independent Variable	**Parameter Estimate**	**Standard Error of Estimate**	**t-value**	**Confidence Level t is Significant**
b_0, Intercept	0.02746	0.00613	4.47	99.9
b_1, Fiber type	0.00781	0.00708	1.10	71.5
b_2, Humidity	0.02180	0.00708	3.08	99.3

Root Mean Square Error = 0.1821

Previous workers[6, 61] have used statistical approaches when analyzing data. For example, Hill[6] tested approximately 6–50 fibers at each test condition and had an interfiber variation of anywhere from 23 to 54%. Mark[73] on the other hand argued against a statistical data analysis approach. He argued that the individuality of the molecular architecture dictates the molecular conformation, and this in turn dictates the pattern of stress distribution under load which ultimately determines every mechanical property of a wood fiber. For this thesis, a statistical analyses of data is presented as well as analyses of a theoretical approach by Eyring.[51]

Theoretical Eyring Analysis

Estimation of Eyring Parameters

Theoretical analysis of collected data was based on the Eyring theory of polymer creep as previously discussed. A nonlinear (NLIN) regression procedure[70] produced least-squares estimates of the parameters, E1, E2, α, and χ of the Eyring model, Eq. (18). For each set of data

analyzed using the nonlinear model, the following instructions were specified: (1) the names (E1, E2, α, and χ) and starting values of the parameters to be estimated, (2) the model [using a single dependent variable], (3) the partial derivatives of the model with respect to each parameter, and (4) the convergence criteria in terms of the change in the sum of squares. The NLIN procedure first examined the starting value specifications of the parameters. A grid of values was specified and NLIN evaluated the residual sum of squares at each combination of values to determine the best set of values to start the iterative algorithm. Then NLIN used the Gauss-Newton iterative method (Taylor series) to regress the residuals onto the partial derivatives of the Eyring model, Eq. (18), with respect to the parameters until the estimates converged. The iterations converged for CONVERGEOBJ = c if

$$(SSE^{i-1} - SSE^{i})/(SSE^{i} + 10^{-6}) < c \qquad (50)$$

where SSE^{i} is the sum of squares for the *i*th iteration. The value of c was 10^{-12}. The constant, c , should be a small positive number. The SAS programming for the Eyring model is in Appendix 5.

The DUD or secant iterative method was used instead of the Gauss-Newton method[70] for parameter estimates of the creep recovery data. The multivariate secant method is like the Gauss-Newton method, except that the derivatives are estimated from the history of iterations rather than supplied analytically. The method is also called the method of false position, or DUD for "Doesn't Use Derivatives."[93] If only one parameter is being estimated, the derivative for iteration i + 1 can be estimated from the two previous iterations. When k parameters are to be estimated, the method uses the last k + 1 iterations to estimate the derivatives.

Eyring's model of polymer creep, Eq. (18), was used to NLIN fit the average single-fiber extracted holocellulose curves in Figure 49. In Table 37, the modulus values for E1 and E2, the free energy of activation for the flow process, ΔF, and the volume of the flow element, V_f , are shown. Parameters, E1 and E2, are estimates from the NLIN SAS model. Parameters, ΔF and

V_f, are calculated values using Eq. (34) and Eq. (35), respectively. The Eyring equation appears to give a good fit for the experimental data at 50% RH. However, the Eyring fit appears to underestimate the experimental results at 90% RH. This was expected from the analysis of Hill and Byrd's data. Even though the Eyring model appears to fit the 50% RH creep data, there is a large component of nonrecoverable creep in pulp fibers as exemplified in the analysis of Hill's creep recovery data. The original creep equation proposed by Eyring does not account for this component of creep. Eyring[51] did not have much difficulty with nonrecoverable creep. Generally, his materials were subjected to considerable stress before his creep experiments were started.

Table 37: Parameters for average single-fiber-creep data (Figure 49).

Fiber Creep	RH	ΔF	V_f	E1	E2
Extracted	50	30.9	1390	135	232
Extracted	90	26.6	580	128	193

Units: Relative humidity %, Free energy kcal/mole, Flow volume $Å^3$, Moduli x 10^8 dynes/cm^2

A modified version of the Eyring equation in which a component of permanent set can be accounted for which is linear in time and stress was proposed as Eq. (31). The NLIN SAS program could use the modified model, Eq. (31), and fit parameter estimates for E1, E2, α, χ, and η_1. However, the modified Eyring equation, Eq. (31), is only a valid model if η_1 is linear. Considering the uncertainty in the theoretical model, it is difficult to assign physical interpretation to a single fiber using the fitted Eyring parameters. Therefore, the actual fitted values for the Eyring parameters cannot be physically significant with respect to single fiber creep. The Eyring model will be used to statistically determine the effect of fiber type and humidity on the tensile creep behavior of single fibers.

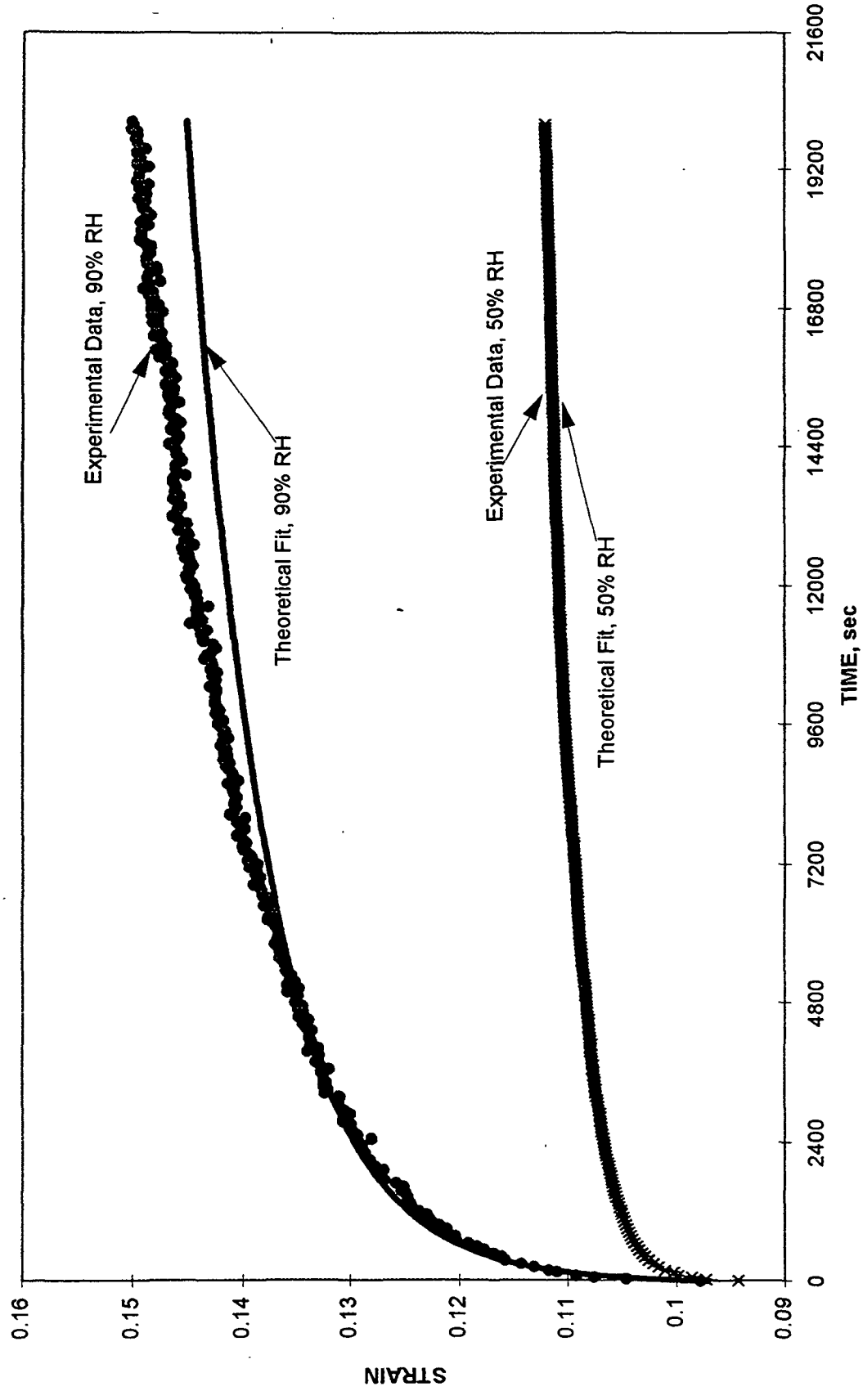

Figure 49: Creep of average single-fiber extracted holocellulose and theoretical fit at constant humidity.

Eyring's model for polymer creep, Eq. (18), was used to NLIN SAS fit the first 6,000 seconds of the single extracted holocellulose fiber creep data from Figures 43 and 44. The Eyring model appears to give an equally exceptional fit for the experimental data at 50 and 90% RH (Figures 50 and 51). Even though the Eyring model does not take into account the fibril angle and the permanent set, the fitted parameters (E1, E2, α, and χ) can be used to statistically determine the significance of increases and decreases in parameters with respect to humidity and fiber type. Similarly, Eyring's model, Eq. (18), was used to fit the first 6,000 seconds of the single holocellulose fiber creep data from Figures 47 and 48. The actual experimental holocellulose 50 and 90% RH creep data are compared to the theoretical fits in Figures 52 and 53. The fitted Eyring parameters for the extracted and holocellulose single fiber creep data for the first 6,000 seconds of creep are reported in Appendix 5. Multiple regression analysis for each of the four fitted parameters (E1, E2, α, and χ) determined statistical significance with respect to humidity and hemicellulose content or fiber type using the following model,

$$y = b_o + b_1 x_1 + b_2 x_2 \qquad (51)$$

where y = the fitted Eyring parameter

b_o = intercept

b_1, b_2 = coefficients

x_1 = fiber type; 0 for extracted fiber
1 for holocellulose fiber

x_2 = relative humidity; 0 for 50% RH
1 for 90% RH.

The multiple regression results are reported in Tables 38–41 for the dependent variables, E1, E2, α, and χ, fitted to the single fiber creep data. The data were statistically examined for outliers. None of the parameter fits could be rejected. The regression model, Eq. (51), was used for each dependent variable.

Figure 50: Creep of extracted holocellulose fibers and theoretical fit at 50% RH.

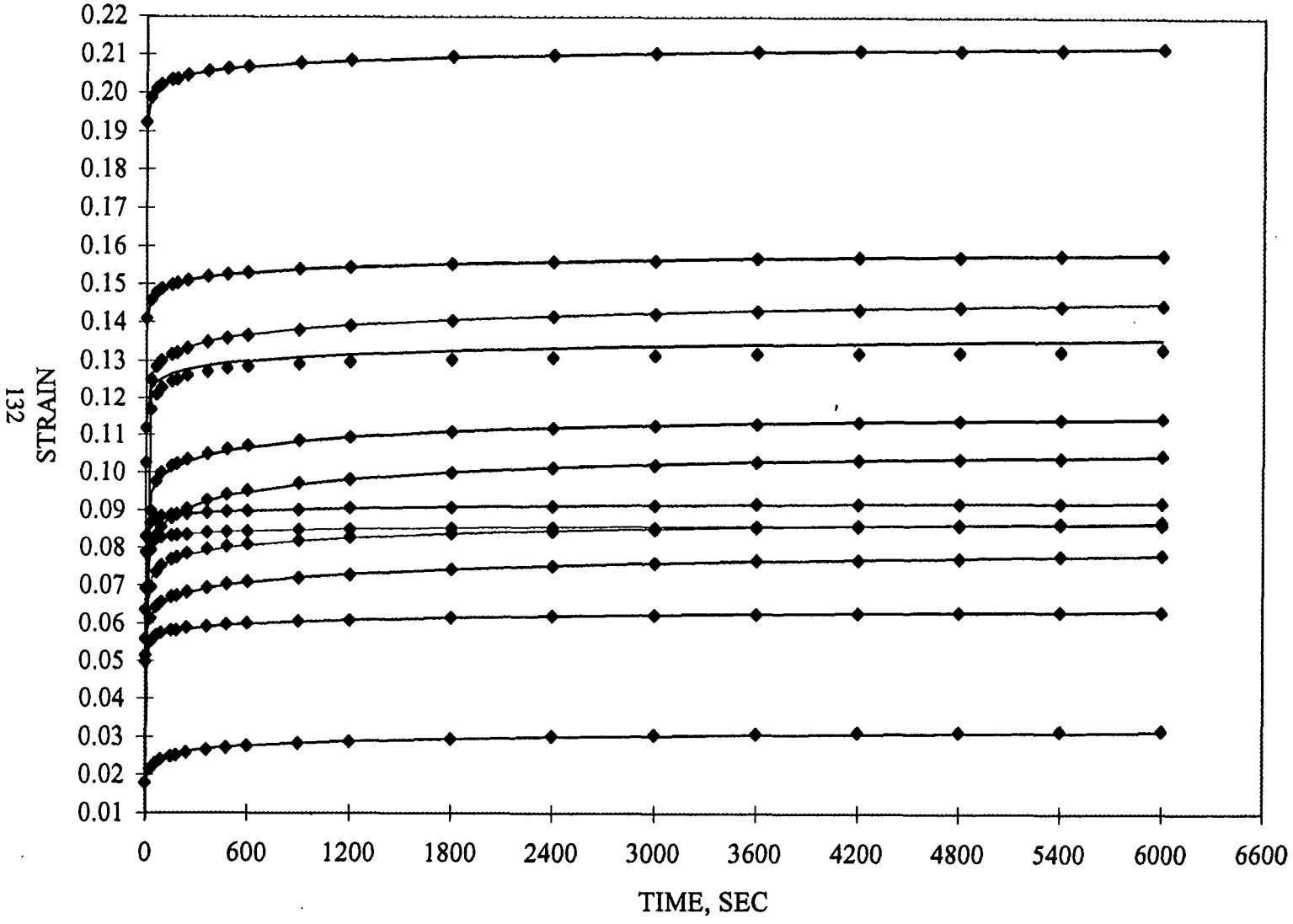

Figure 51: Creep of extracted holocellulose fibers and theoretical fit at 90% RH.

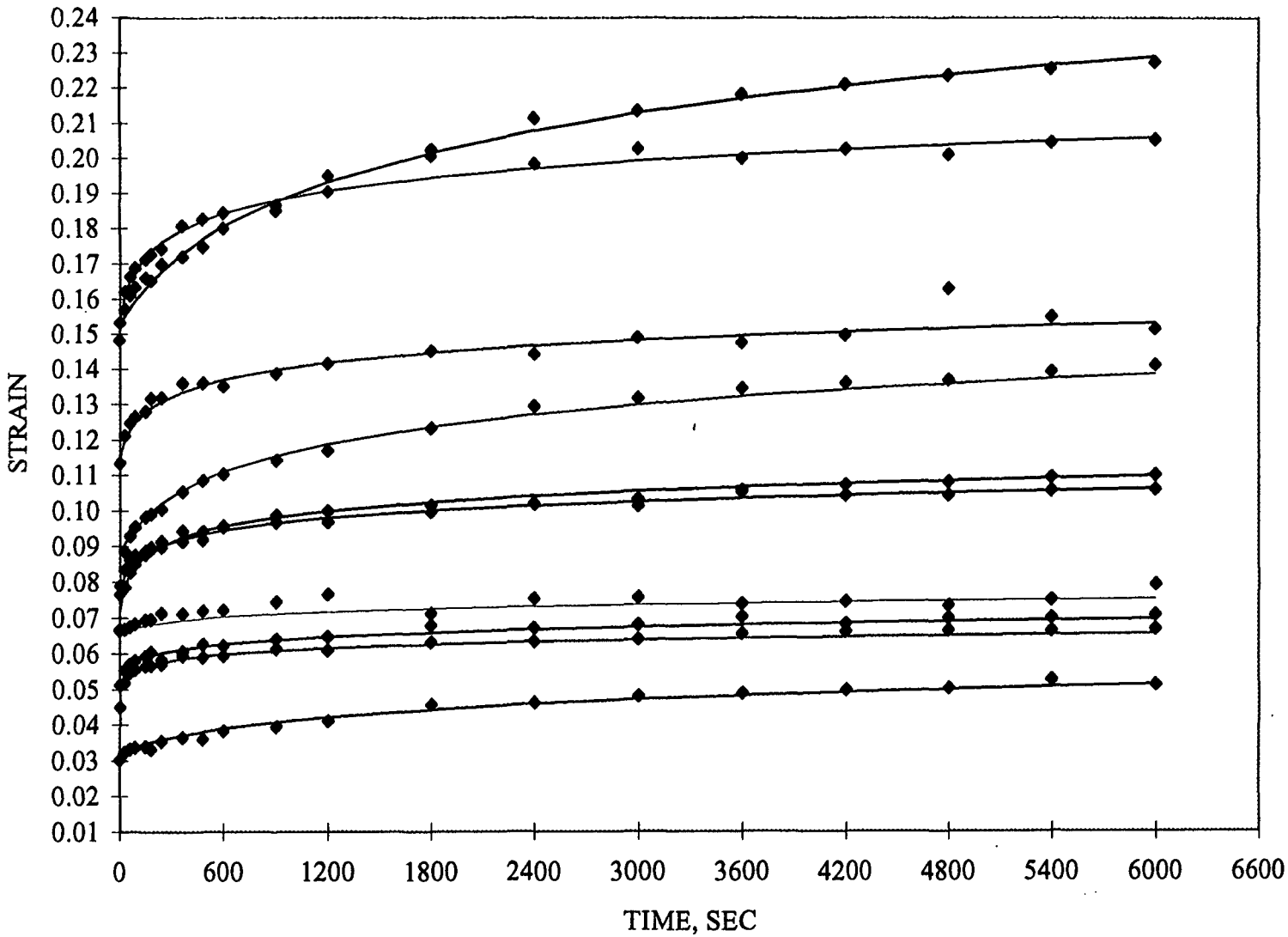

Figure 52: Creep of holocellulose fibers and theoretical fit at constant 50% RH.

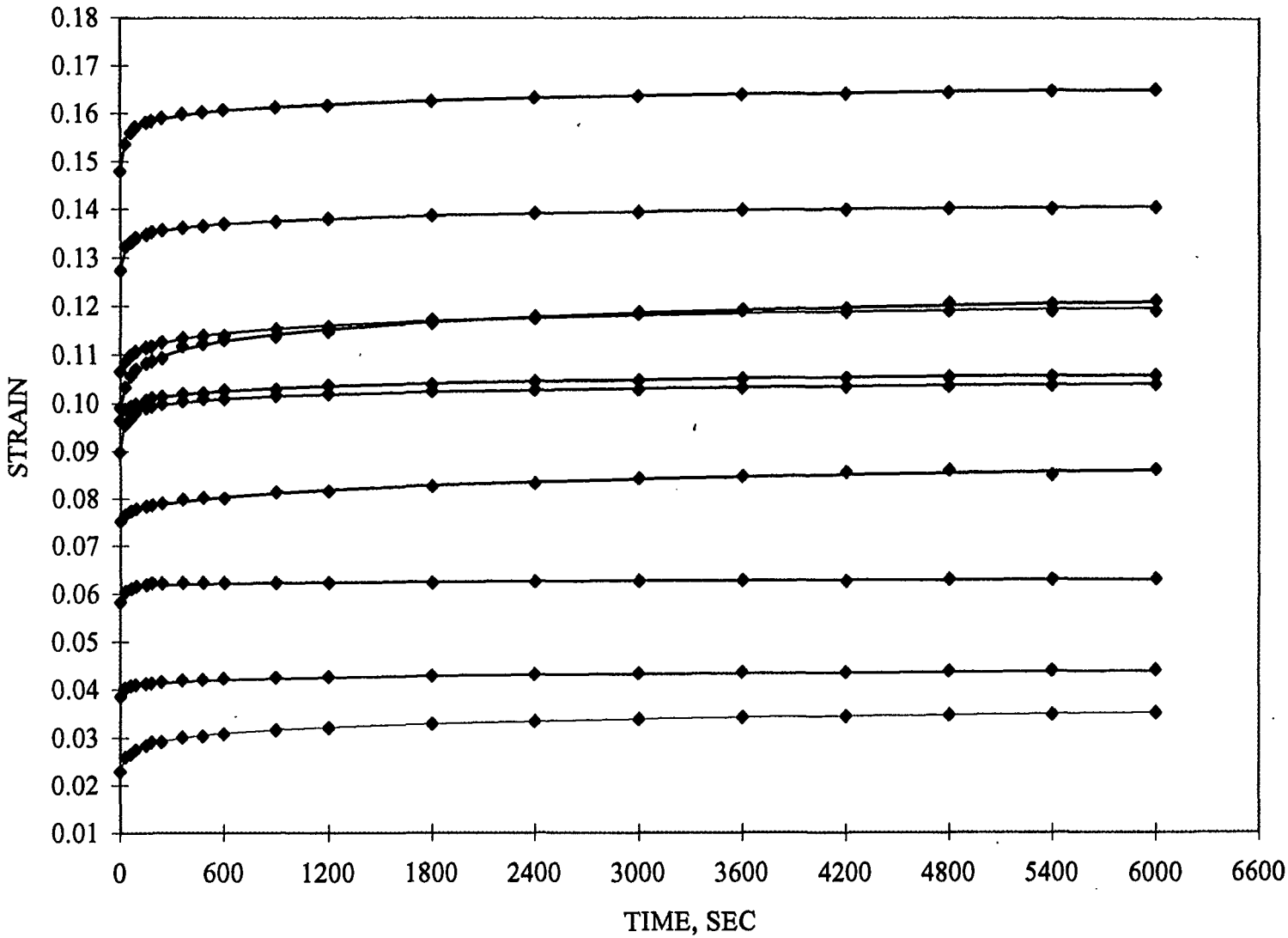

Figure 53: Creep of holocellulose fibers and theoretical fit at constant 90% RH.

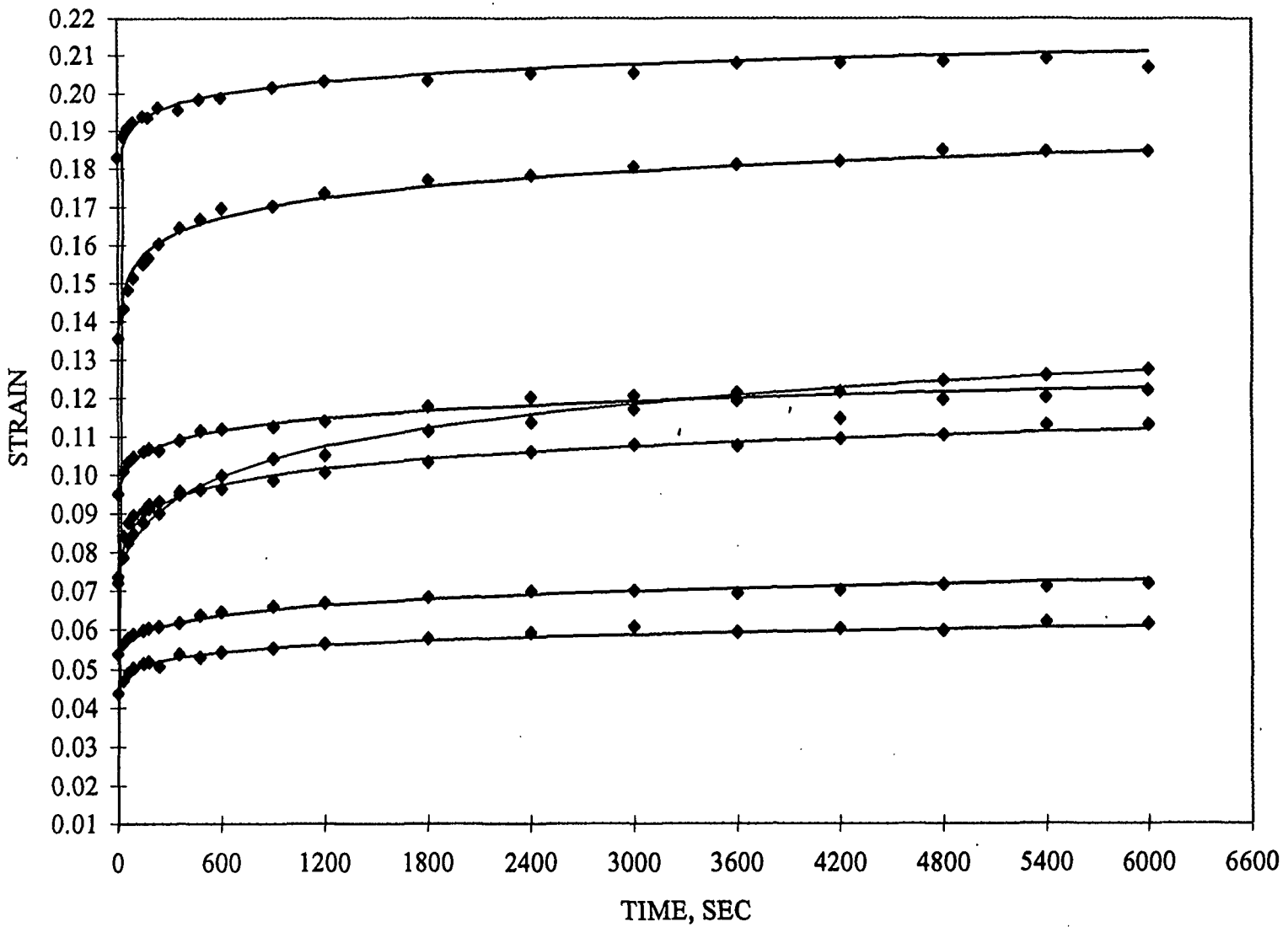

Table 38: Multiple regression analysis: effect of fiber type and relative humidity on y = the fitted Eyring parameter, E1 x 10^9 dynes/cm^2 .

Independent Variable	Parameter Estimate	Standard Error of Estimate	t-value	Confidence Level t is Significant
b_0, Intercept	19.7489	5.3498	3.69	99.9
b_1, Fiber type	0.6282	6.6408	0.09	7.5
b_2, Humidity	0.1939	6.5987	0.03	2.3

Root Mean Square Error = 20.7172

Table 39: Multiple regression analysis: effect of fiber type and relative humidity on y = the fitted Eyring parameter, E2 x 10^9 dynes/cm^2.

Independent Variable	Parameter Estimate	Standard Error of Estimate	t-value	Confidence Level t is Significant
b_0, Intercept	31.4692	4.1738	7.54	100.0
b_1, Fiber type	4.9976	5.1810	0.96	65.9
b_2, Humidity	-9.5338	5.1481	-1.85	92.8

Root Mean Square Error = 16.1630

Table 40: Multiple regression analysis: effect of fiber type and relative humidity on y = the fitted Eyring parameter, α x 10^{-9} cm^2/dynes.

Independent Variable	Parameter Estimate	Standard Error of Estimate	t-value	Confidence Level t is Significant
b_0, Intercept	20.0026	2.5453	7.86	100.0
b_1, Fiber type	2.1490	3.1595	0.68	49.9
b_2, Humidity	-11.8328	3.1395	-3.77	99.9

Root Mean Square Error = 9.8567

Table 41: Multiple regression analysis: effect of fiber type and relative humidity on y = the fitted Eyring parameter, χ x 10^{-8} sec^{-1}.

Independent Variable	Parameter Estimate	Standard Error of Estimate	t-value	Confidence Level t is Significant
b_0, Intercept	-14.0029	50.0439	-0.28	21.7
b_1, Fiber type	58.3819	57.7857	1.01	67.4
b_2, Humidity	65.1320	57.7857	1.13	72.5

Root Mean Square Error = 118.7813

The Eyring parameter estimates (Appendix 5) for each humidity and fiber type can be statistically evaluated. It is interesting to note how the parameters change with humidity. The parameter, E1, did not significantly change between 50 and 90% RH for the multiple regression results reported in Table 38. The parameter, E2, is significant at the 93% confidence level. This parameter is reduced when humidity is increased. The parameter, α, is directly proportional to the calculated Eyring parameter, V_f, and is significant at the 99% confidence level. Eyring termed V_f the volume of the flow unit, and this parameter decreases at the higher humidity. Statistically, humidity had no effect on χ. Early work by Eyring and others shows that free energy, a function of χ, is not very sensitive to moisture content.

The shape of the resulting creep curves is much the same at both humidities (Figures 50–53). However, decreases in E2 and α were statistically significant according to multiple regression analyses. The tensile creep behavior of the single fibers tested was a function of the humidity.

These results are supported by viscose rayon experiments where at higher humidities the spring constant decreased considerably.[49] The amount of time representing the transition from elastic to creep deformation became successively smaller as the humidity was decreased. This indicated that the dashpots of small relaxation times became frozen at low humidities. At low humidities a large amount of activation energy was required to make the flow units associated with these dashpots slip. According to Eyring's theory, one can conclude that at higher humidities, where the moisture content of the fibers is higher, the water molecules lubricate the slip of sections of flow units past each other by a separation of chains and a consequent decrease in the secondary valence forces which give rise to these energy barriers and associated activation energies.

In the absence of moisture, as with a vacuum-dried fiber, the dashpot stiffens so much that over moderate ranges of elongation the fiber is like a simple spring. At the other extreme, in liquid water the fiber absorbs enough water so that in terms of the three-element model the

dashpot becomes very loose and quite Newtonian. Throughout the middle range of humidities where the water content is not changing rapidly, the activation energy, a function of χ, changes very little with moisture content. Halsey and coworkers[49] observed that experimental error due to rayon interfiber variation is often greater than the variation caused by the moisture in this range.

The multiple regression analyses did not confirm an effect of hemicellulose content or fiber type on the Eyring parameters (E1, E2, α, and χ). According to the analysis described by Eq. (51), the first hypothesis, that the tensile creep behavior of individual pulp fibers as a function of relative humidity is dependent on hemicellulose content, is not accepted. These results contradict the multiple regression model Eq. (48) results where the first hypothesis was accepted. At a confidence level of 99%, fiber type and relative humidity revealed statistically significant results with respect to the tensile creep behavior of single fibers at a time of 10,800 seconds (Table 29). The effect of fiber type or hemicellulose content on the creep phenomenon was negative. The holocellulose fibers exhibit less creep strain than the extracted fibers at 10,800 seconds. The main effect variable, fiber type, was significant with respect to the creep phenomenon at a specific time interval. However, considering the effect of fiber type on the total creep behavior behavior, the first hypothesis is not accepted.

Creep Recovery of Single Fibers

The single fiber creep and creep recovery data is plotted for holocellulose and extracted holocellulose fibers in Figures 54–57. Single fibers were loaded to 20 grams at a rate of 1 gram per second. The single fibers were allowed to creep for 20 minutes, and then the load was released and held constant at 1 gram. Creep recovery data were collected for approximately 20 minutes. Using Eq. (18) and allowing SAS to fit the single fiber creep recovery data, fitted Eyring parameters were obtained and are listed in Appendix 5. SAS fits were done for each single fiber tested for the total 2,400 seconds of creep at each humidity level. The predicted plots using the fitted parameters compare well with the actual experimental data points (Figures 58–

61). A corresponding plot of experimental data and the theoretical Eyring fit are shown for each fiber type and relative humidity combination.

Multiple regression analysis model, Eq. (51), was used to determine the effect of humidity and fiber type for each of the four fitted parameters (E1, E2, α, and χ). The multiple regression results are reported in Tables 42–45 for the dependent variables, E1, E2, α, and χ, fitted to the single fiber creep recovery data. The data were statistically examined for outliers. None of the parameter fits could be rejected.

The holocellulose and extracted holocellulose creep recovery parameter, E2, is decreased at 90% RH. This trend is significant at the 99% confidence level in both fiber types. The parameters, E1, α, and χ, show no trend when humidity is increased. Differences between the creep recovery behavior for the fiber types can be summarized by the parameter α. The extracted holocellulose fiber type has a lower value of α than the holocellulose fiber type.

Figure 54: Single extracted holocellulose fiber creep and creep recovery 50% RH.

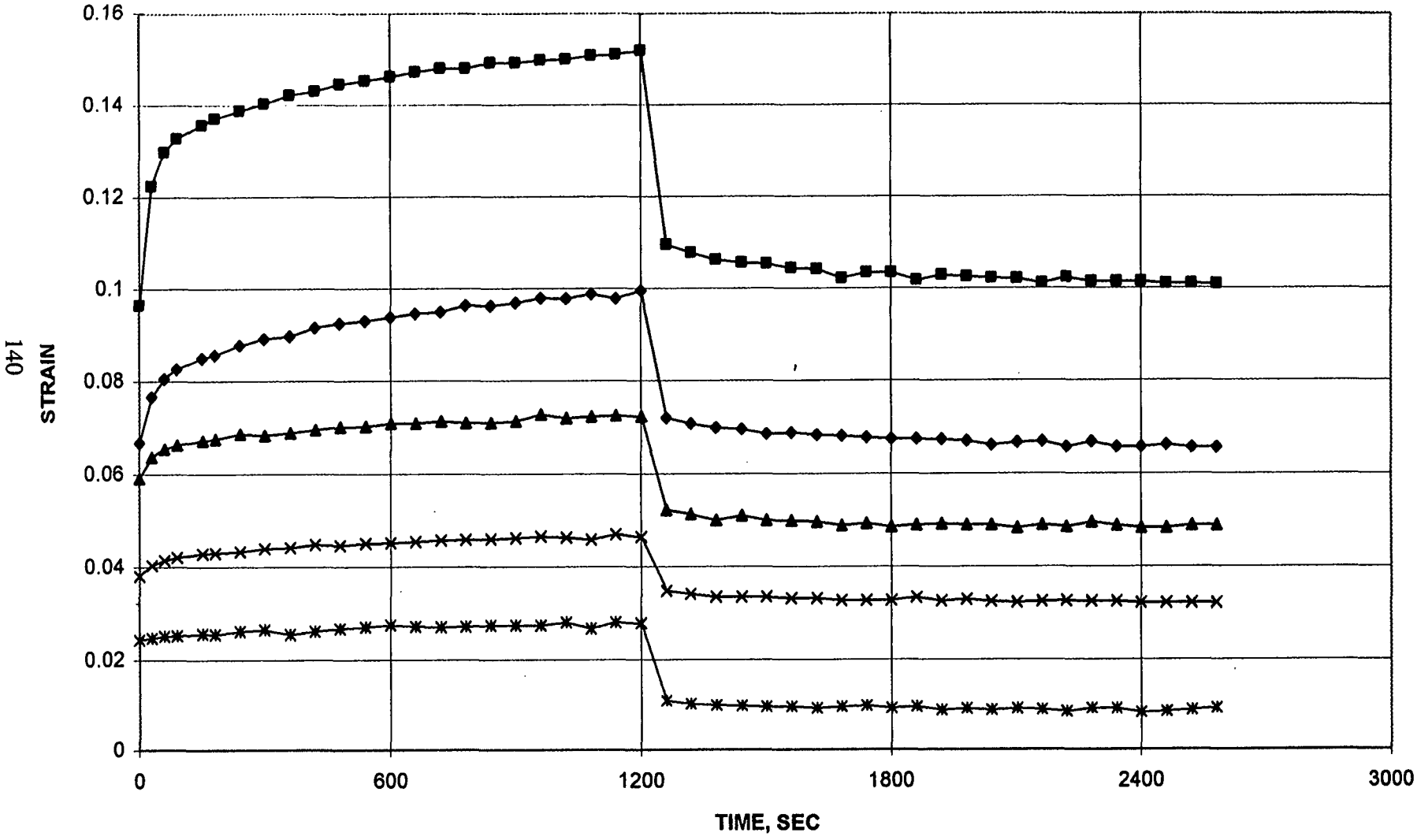

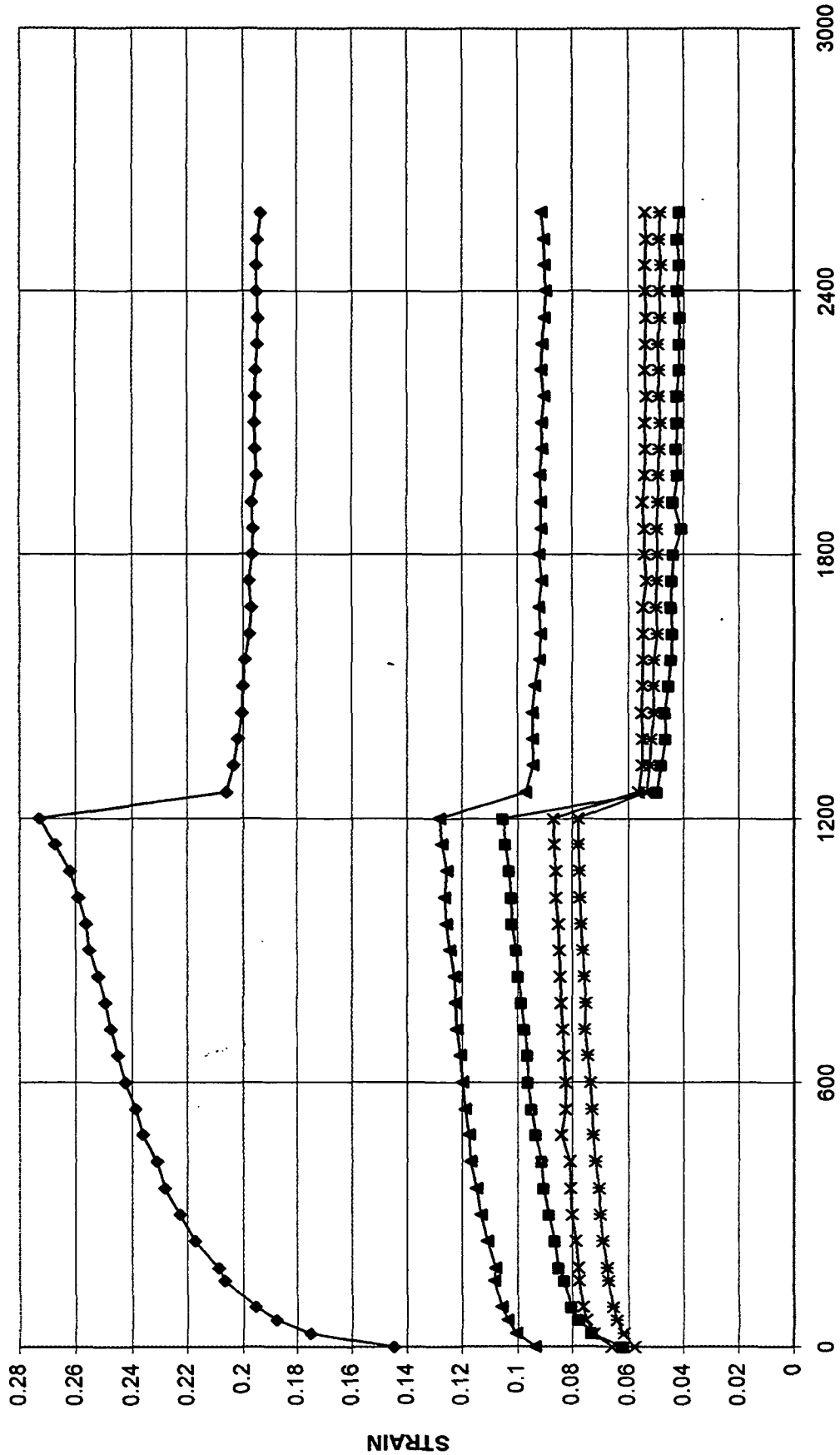

Figure 55: Single extracted holocellulose fiber creep and creep recovery 90% RH.

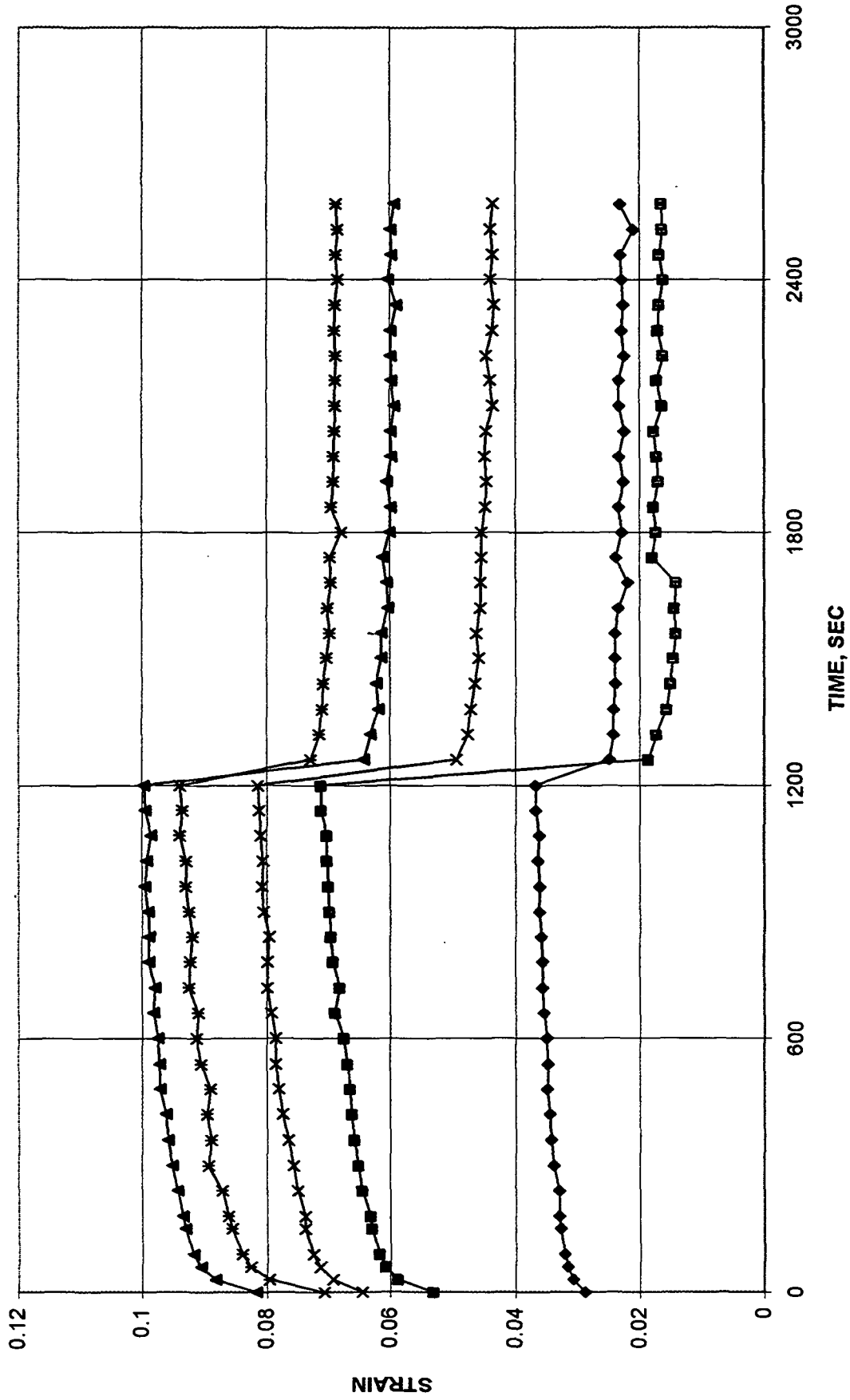

Figure 56: Single holocellulose fiber creep and creep recovery 50% RH.

Figure 57: Single holocellulose fiber creep and creep recovery 90% RH.

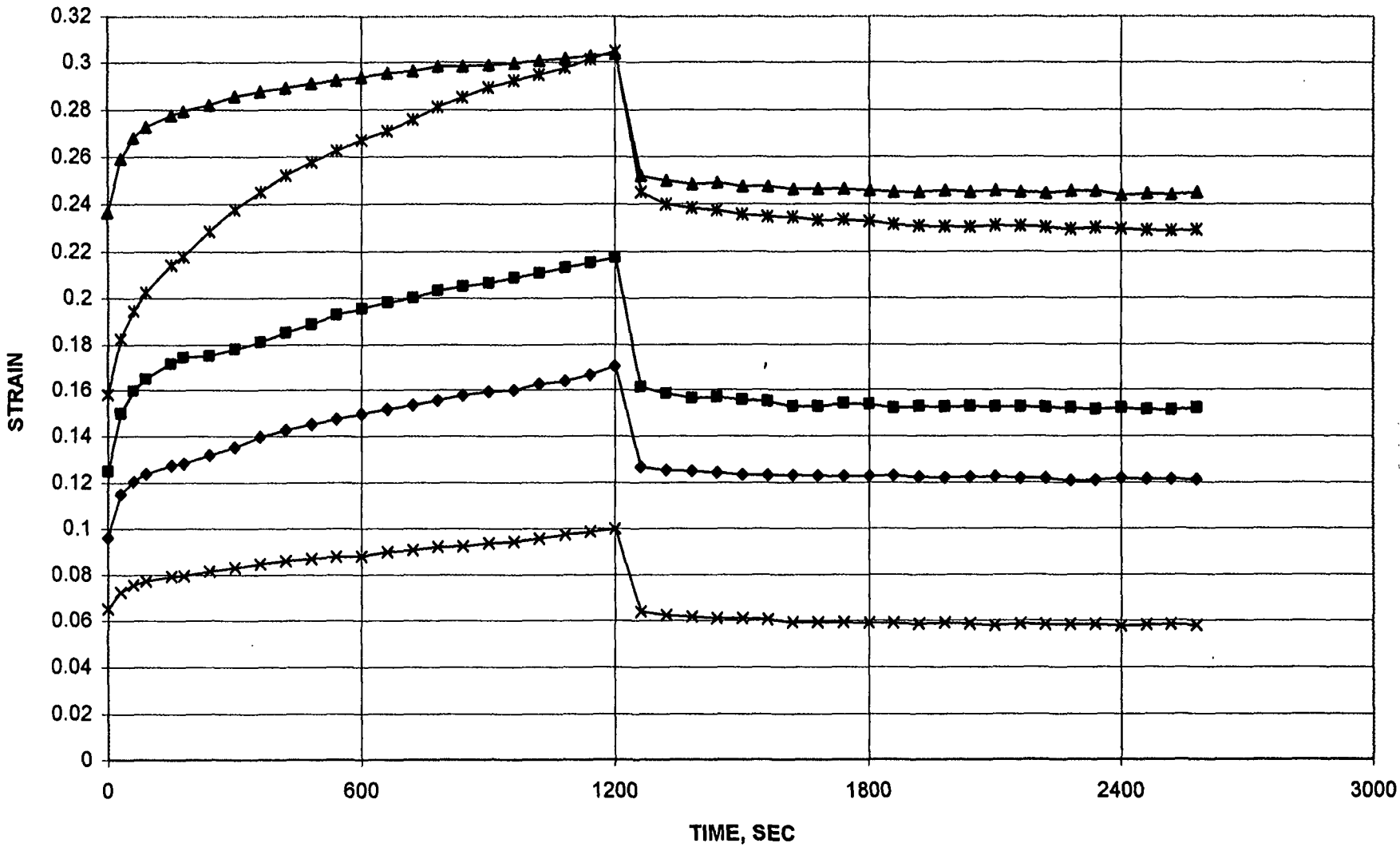

Table 42: Multiple regression analysis: effect of fiber type and relative humidity on y = the fitted Eyring parameter, E1 x 10^9 dynes/cm^2 (creep recovery).

Independent Variable	Parameter Estimate	Standard Error of Estimate	t-value	Confidence Level t is Significant
b_0, Intercept	120.3450	25.5238	4.72	99.9
b_1, Fiber type	20.0300	29.4723	0.68	49.4
b_2, Humidity	-8.1700	29.4723	-0.28	21.5

Root Mean Square Error = 65.9022

Table 43: Multiple regression analysis: effect of fiber type and relative humidity on y = the fitted Eyring parameter, E2 x 10^9 dynes/cm^2 (creep recovery).

Independent Variable	Parameter Estimate	Standard Error of Estimate	t-value	Confidence Level t is Significant
b_0, Intercept	115.0900	15.0495	7.65	100.0
b_1, Fiber type	-2.5999	17.3776	-1.15	11.7
b_2, Humidity	-52.7800	17.3776	-3.04	99.3

Root Mean Square Error = 38.8576

Table 44: Multiple regression analysis: effect of fiber type and relative humidity on y = the fitted Eyring parameter, α x 10^{-9} cm^2/dynes (creep recovery).

Independent Variable	Parameter Estimate	Standard Error of Estimate	t-value	Confidence Level t is Significant
b_0, Intercept	8.0985	1.2795	6.33	100.0
b_1, Fiber type	-2.8109	1.4774	-1.90	92.6
b_2, Humidity	1.9349	1.4774	1.31	79.2

Root Mean Square Error = 3.3038

Table 45: Multiple regression analysis: effect of fiber type and relative humidity on y = the fitted Eyring parameter, χ x 10^{-8} sec^{-1} (creep recovery).

Independent Variable	Parameter Estimate	Standard Error of Estimate	t-value	Confidence Level t is Significant
b_0, Intercept	85.5882	30.6731	2.79	99.2
b_1, Fiber type	-59.8284	38.0750	-1.57	87.5
b_2, Humidity	-59.6759	37.8338	-1.58	87.7

Root Mean Square Error = 129.2129

Figure 58: Creep recovery of extracted holocellulose and theoretical fit at 90% RH.

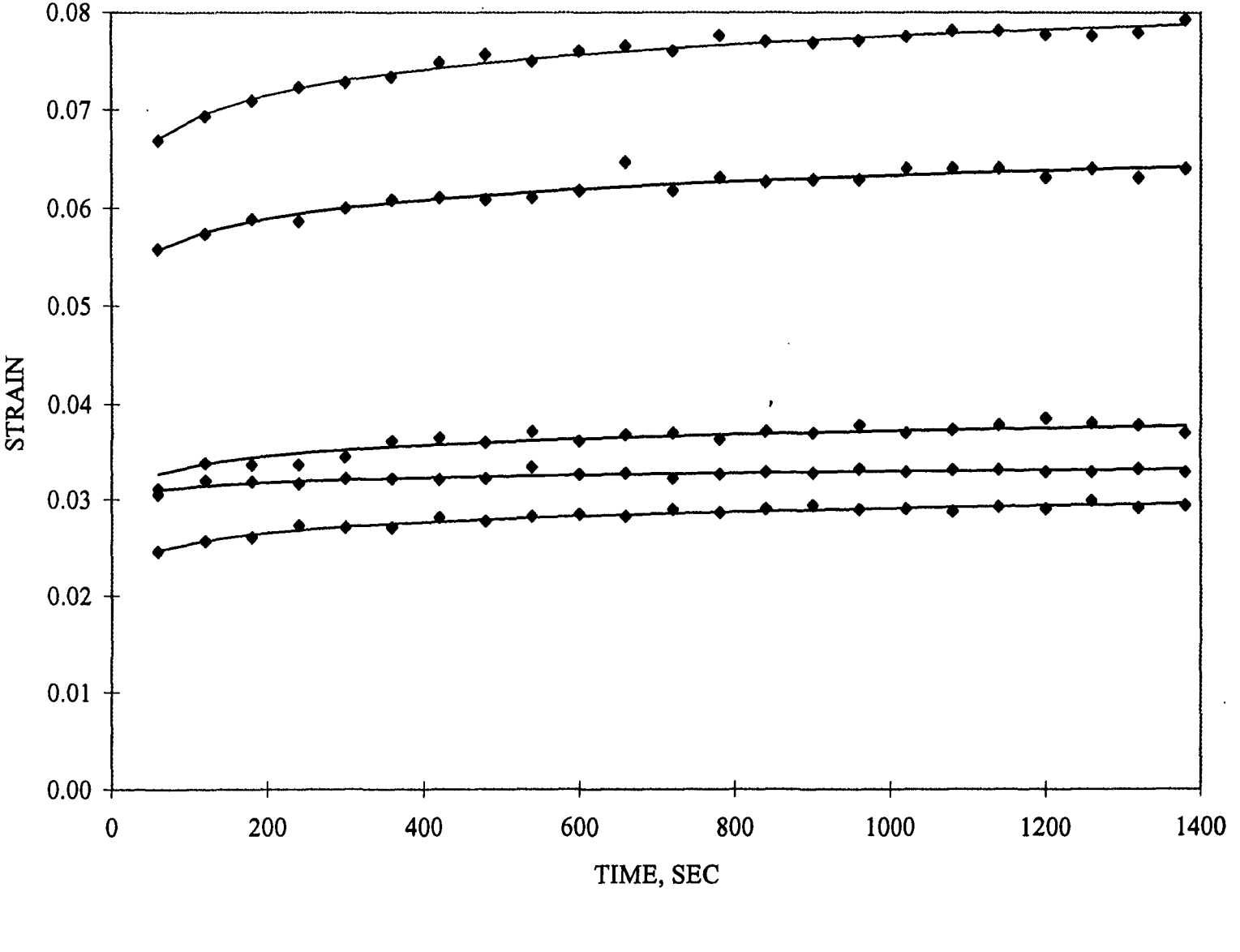

Figure 59: Creep recovery of extracted holocellulose and theoretical fit at 50% RH.

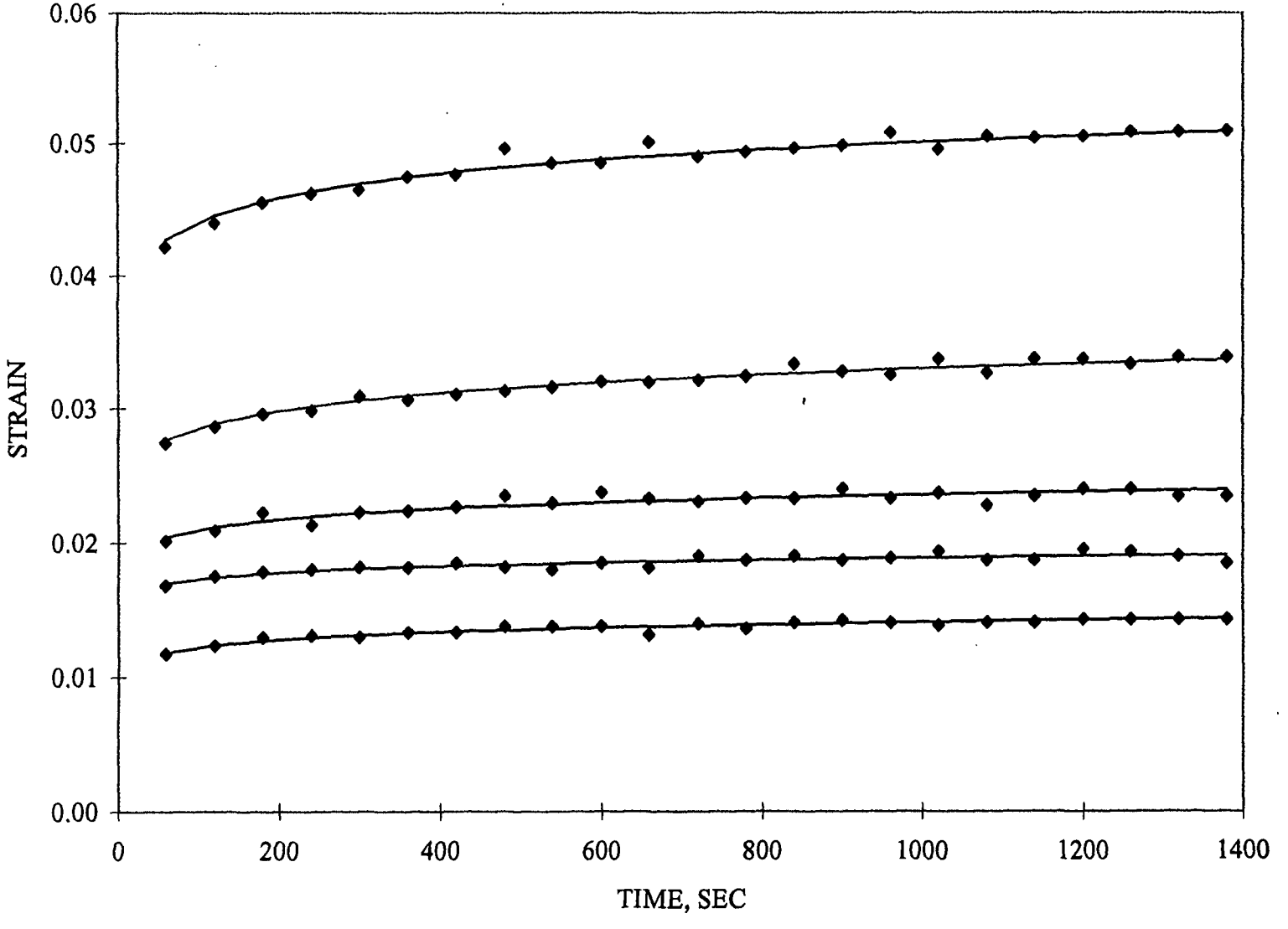

Figure 60: Creep recovery of holocellulose and theoretical fit at 90% RH.

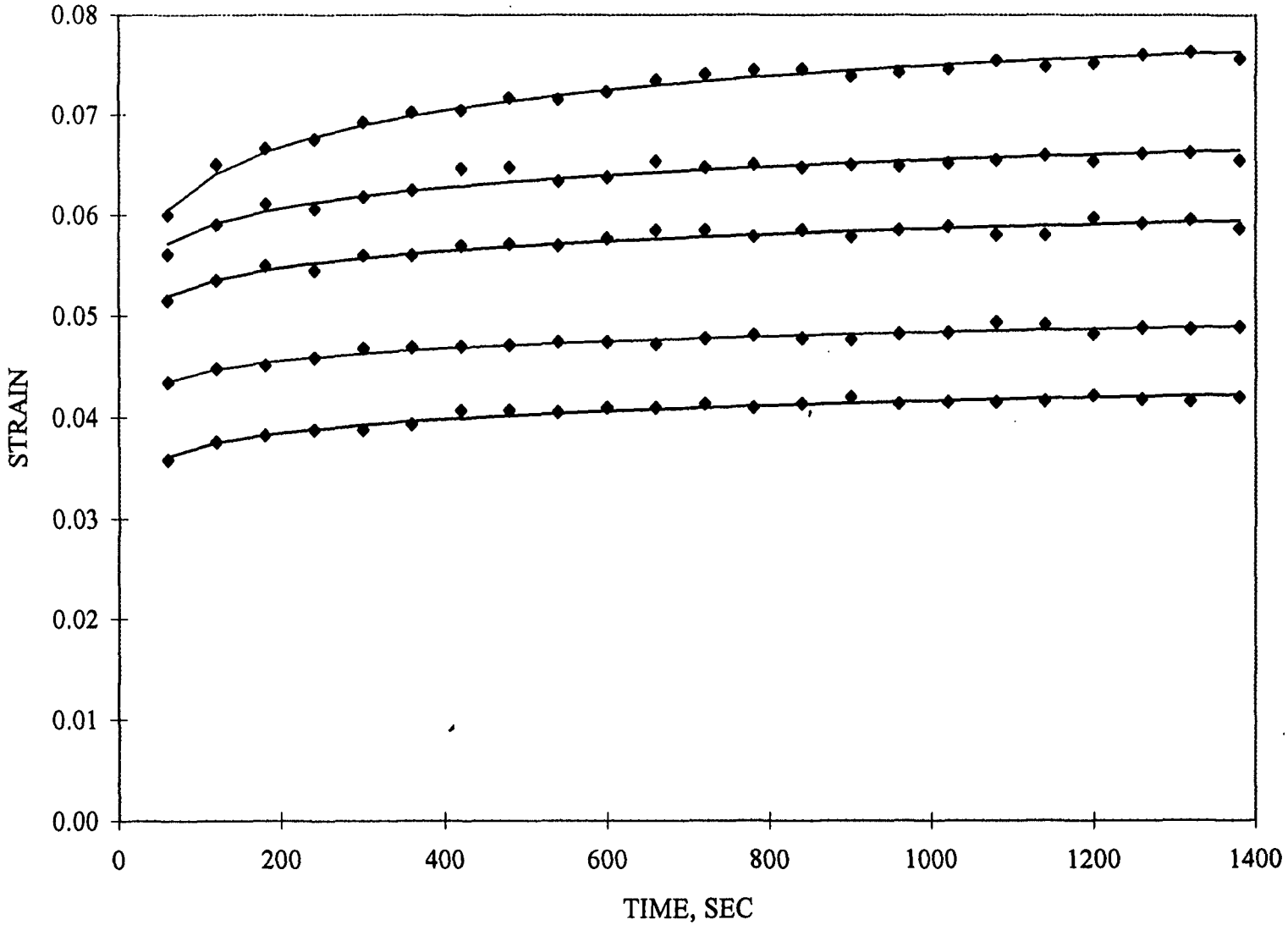

Figure 61: Creep recovery of holocellulose and theoretical fit at 50% RH.

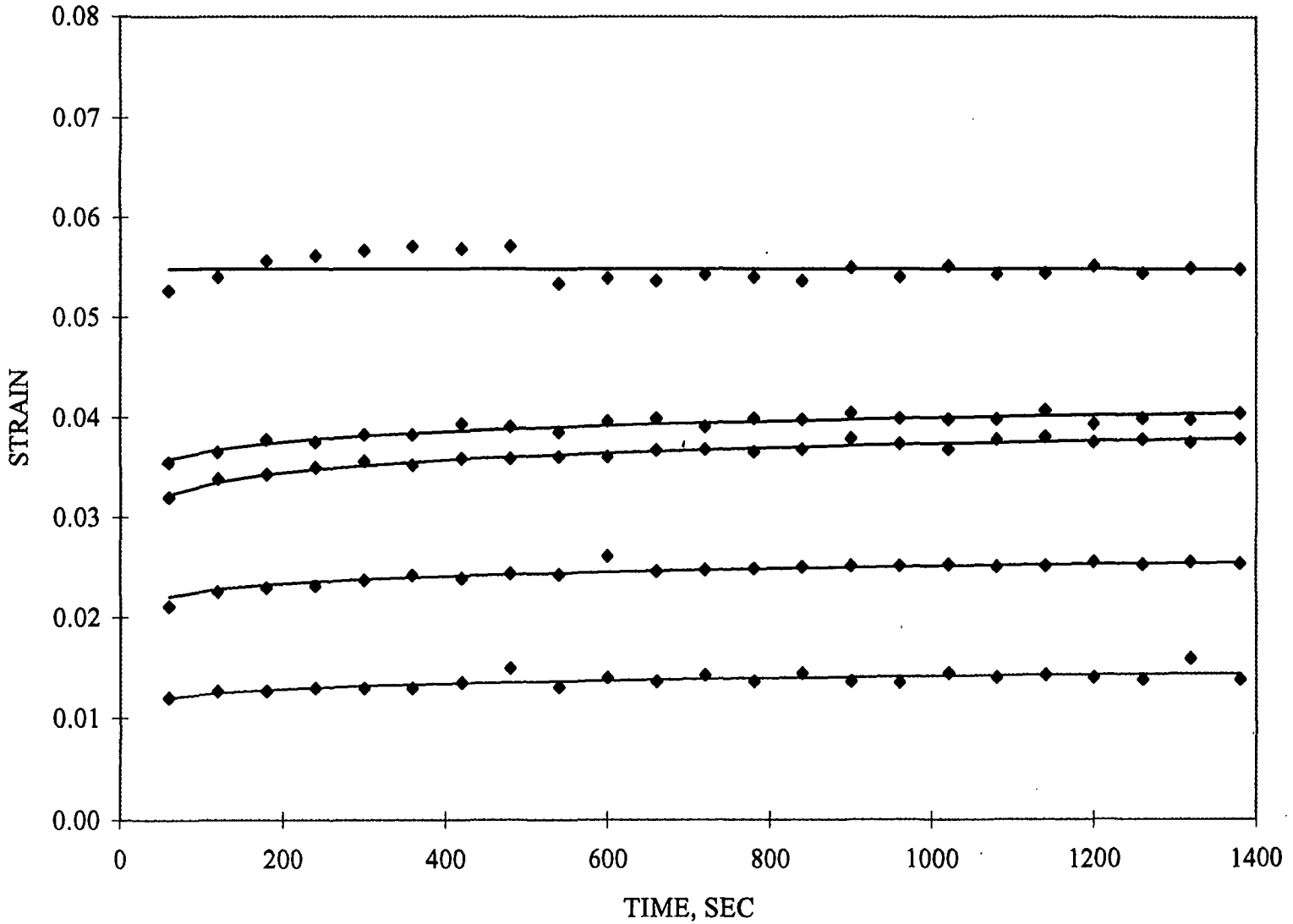

SINGLE-FIBER CYCLIC CREEP

For each fiber type, two series of creep measurements were made: (1) single fibers were conditioned at 50% RH, loaded to 20 grams, and exposed to cyclic relative humidity conditions [relative humidity alternated between 50 and 90%] for 10 cycles, and (2) single fibers were conditioned at 90% RH, loaded to 20 grams, and exposed to cyclic relative humidity conditions [relative humidity cycled between 90% and 50%] for 10 cycles. The fibers stressed at 90% RH were conditioned for 30 minutes at 90% RH prior to testing.

Preliminary experiments showed that single fibers came to equilibrium instantaneously when cycled from between 50 and 90% RH and 90 and 50% RH. Less than 15 seconds were required to change the relative humidity in the test chamber from 50 to 90% (adsorption), while the same time was required to go from 90% to 50% (desorption). All creep tests were carried out at 23°C. Considering the length of time necessary for the humidity chamber to cycle from 50% to 90% and 90% to 50% relative humidity, the fibers were tested under equilibrium conditions.

Average strain was determined at selected times for an individual fiber test upon reaching a 20-gm load. The same averaging procedure was used for combining all creep data at constant humidities. This procedure was previously described in the Single Fiber Creep at Constant Humidity section. Following the initial single fiber curve averaging process, each single fiber that was cycled within an identical humidity scheme was combined and averaged. This second averaging process formed a cyclic humidity creep response for a given humidity cycling. These average creep responses are plotted as strain versus time in seconds. Strain is presented as a fraction of the initial fiber test span.

The tensile creep response to cyclic relative humidity in single extracted holocellulose fibers is shown as Figure 62. Single extracted holocellulose fibers were conditioned at 50% RH and loaded to 20 grams. After 10 minutes, the humidity was cycled to 90% RH. The humidity was cycled every 10 minutes for a duration of 100 minutes. The response time of the humidity

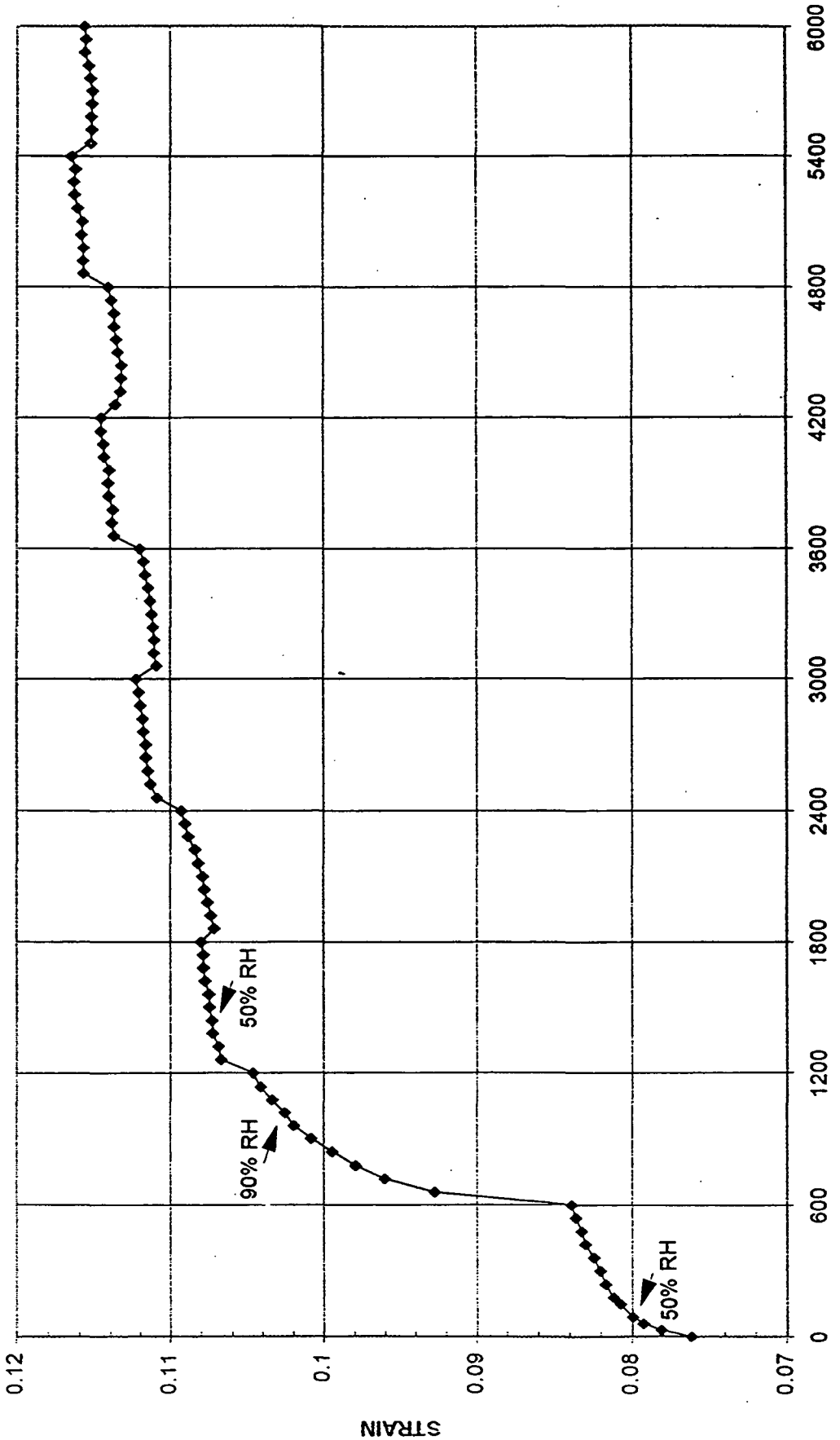

Figure 62: Average response of extracted fibers to cyclic humidity, 50 to 90% RH.

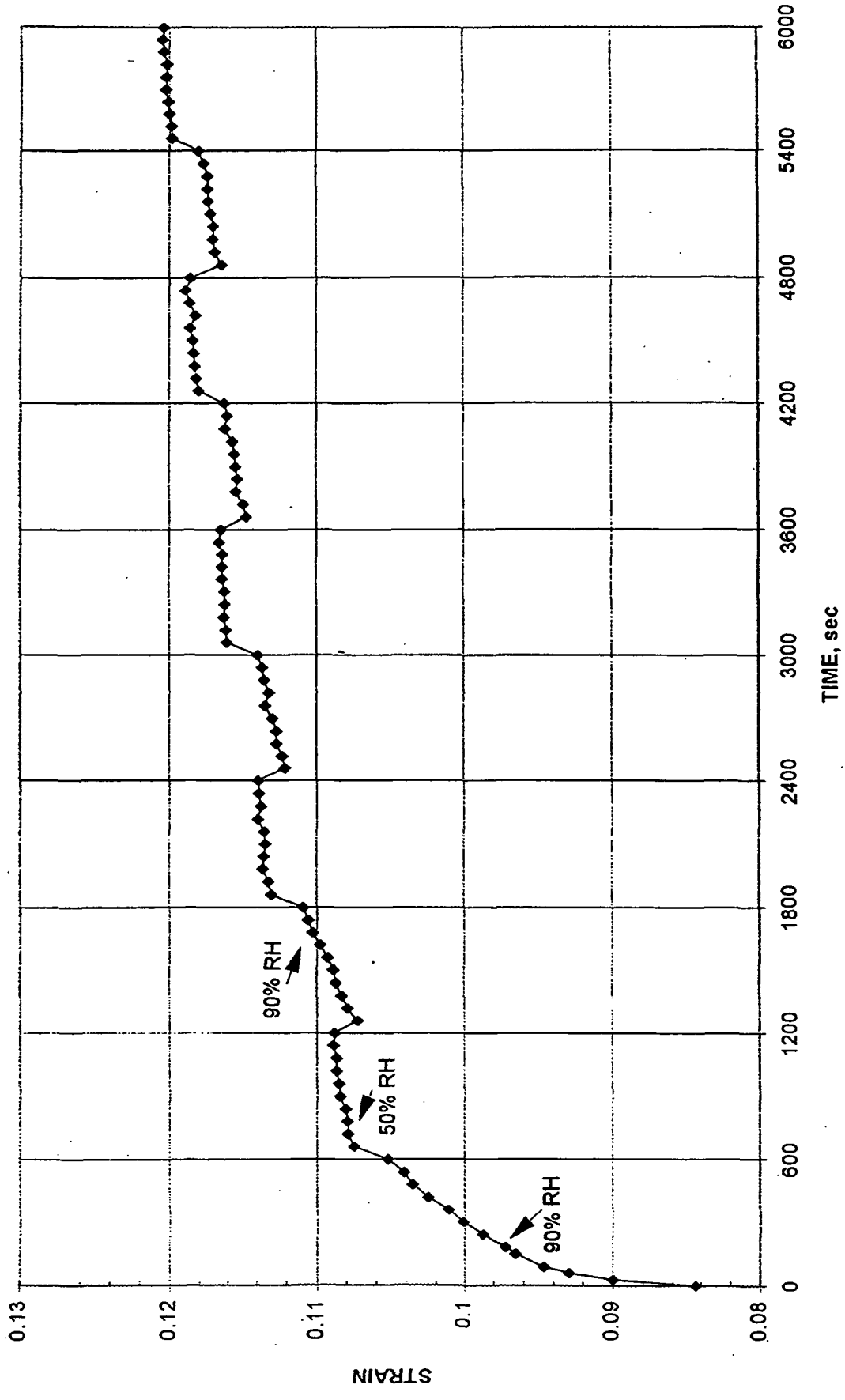

Figure 63: Average response of extracted fibers to cyclic humidity, 90 to 50% RH.

sensor was five seconds, and the fiber appears to have responded instantaneously. The first branch of the creep curve is similar to the 50% constant humidity case. At time zero, an instantaneous strain is present and the shape of the curve for the first 600 seconds is similar to the constant humidity case.

At 600 seconds, the humidity is changed to 90%. This second creep branch is very similar to the initial strain of a fiber conditioned at 90% RH. It looks as if the fiber was conditioned and loaded at 90% RH. The instantaneous elastic component is seen as a large jump in strain when the humidity was changed. This instantaneous component behaves as if the fiber were conditioned and loaded at 90% RH. The remainder of this branch resembles the constant 90% case. This behavior is reminiscent of a superposition of states where the total strain at 1,200 seconds is equal to the strain at 50% RH in the first creep branch plus the strain at 90% RH for the second creep branch.

The third branch is equivalent to creep at 50% RH, and the remaining branches are reminiscent of long time creep behavior at constant relative humidity. Each branch is fairly flat and linear in logarithmic time. It is interesting to note that the fiber shrinks in the axial direction when going from the 50% humidity state to the 90% humidity state. This may be caused by the large swelling component for the radial direction.

Single extracted holocellulose fibers were cycled between 90% and 50% relative humidity in Figure 63. The first branch is composed of the initial strain at time zero followed by creep which is similar to the first 600 seconds of the constant 90% humidity case.

The second cycle of the curve is at 50% RH, and a large jump in strain is not present when the humidity was changed. In this case, the second branch is reminiscent of a fiber creeping at 50% RH at 600 seconds.

There is a profound difference in the creep behavior of the single fibers tested that depends on how the fibers were conditioned. If conditioned and loaded at 50% humidity,

instantaneous strain behavior is present when the humidity is changed to 90%. However, if conditioned and loaded at 90% humidity, an instantaneous strain is not visible when the humidity is changed to 50%.

Similarly, single holocellulose fibers were conditioned at 50% RH and loaded to 20 grams in Figure 64. After 10 minutes, the humidity was cycled to 90% RH. The humidity was cycled every 10 minutes for a duration of 100 minutes. The first branch of the creep curve is similar to the constant 50% humidity case. Again at time zero, an instantaneous strain is present and the shape of the curve for the first 600 seconds is similar to the constant humidity case.

The second branch which is at 90% RH and time equal to 600 seconds is very similar to the initial strain of a fiber conditioned and loaded at 90% RH. The instantaneous component is seen as a jump in strain when the humidity was changed. This instantaneous component behaves as if the fiber were conditioned and loaded at 90%RH. The rest of this branch looks like the constant 90% case. The holocellulose behavior is reminiscent of a superposition of states where the total strain at 1200 seconds is equal to the strain at 50% RH in the first creep branch plus the strain at 90% RH for the second creep branch.

The third branch is equivalent to creep at 50% RH, and the remaining branches are reminiscent of long time creep behavior at constant relative humidity. Again, each branch is fairly flat and linear in log time. In both fiber types, the fiber contracts when going from the 50% humidity state to the 90% humidity state.

Figure 65 is holocellulose fiber data for cycling between 90% and 50% relative humidity. The first branch is composed of the initial strain at time zero followed by creep which is similar to the first 600 seconds of the constant 90% humidity case.

The second branch of the curve is at 50% RH and a large jump in strain is not present when the humidity was changed. In this case, the second branch is reminiscent of a fiber creeping at 50% RH at 600 seconds.

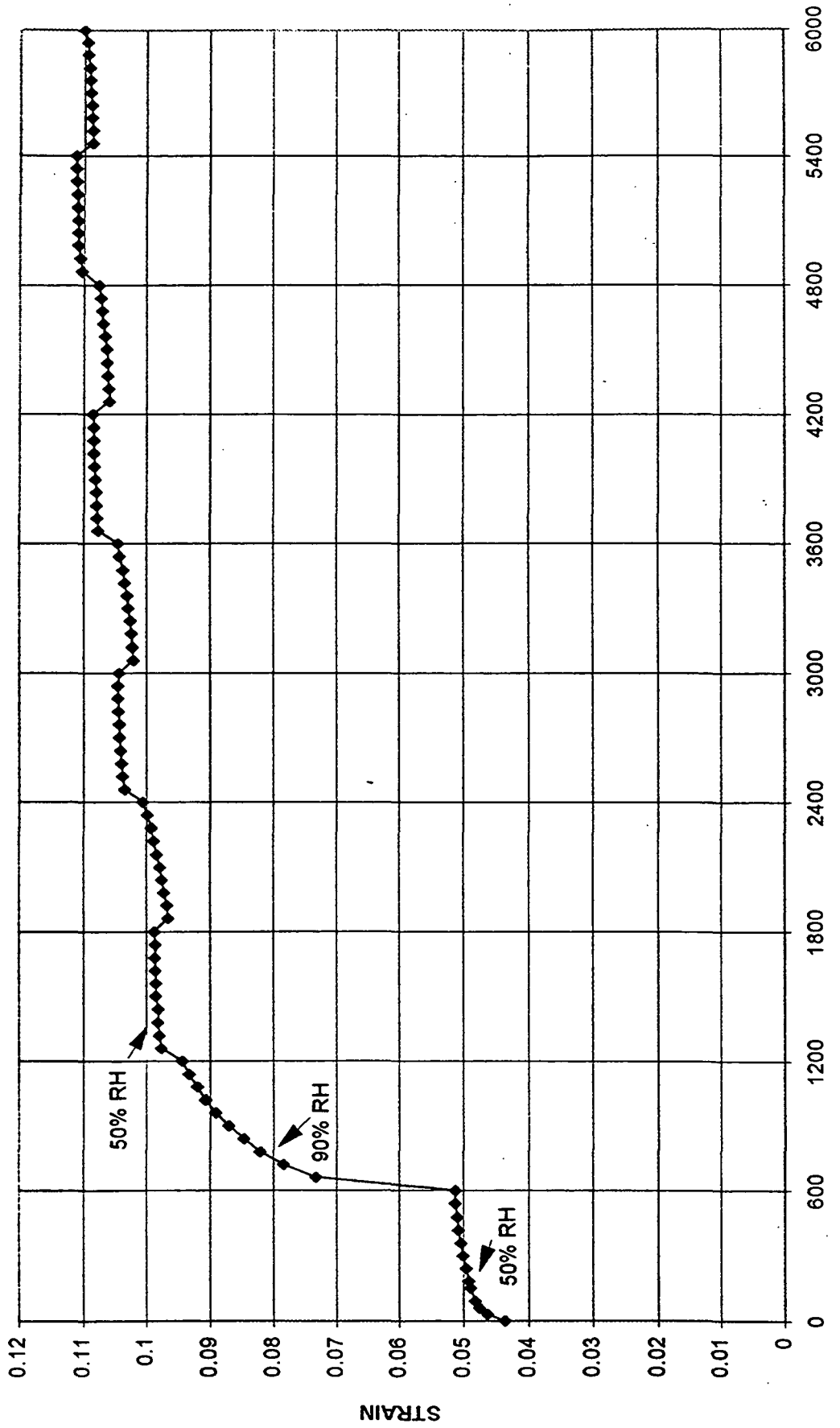

Figure 64: Average response of holocellulose fibers to cyclic humidity, 50 to 90% RH.

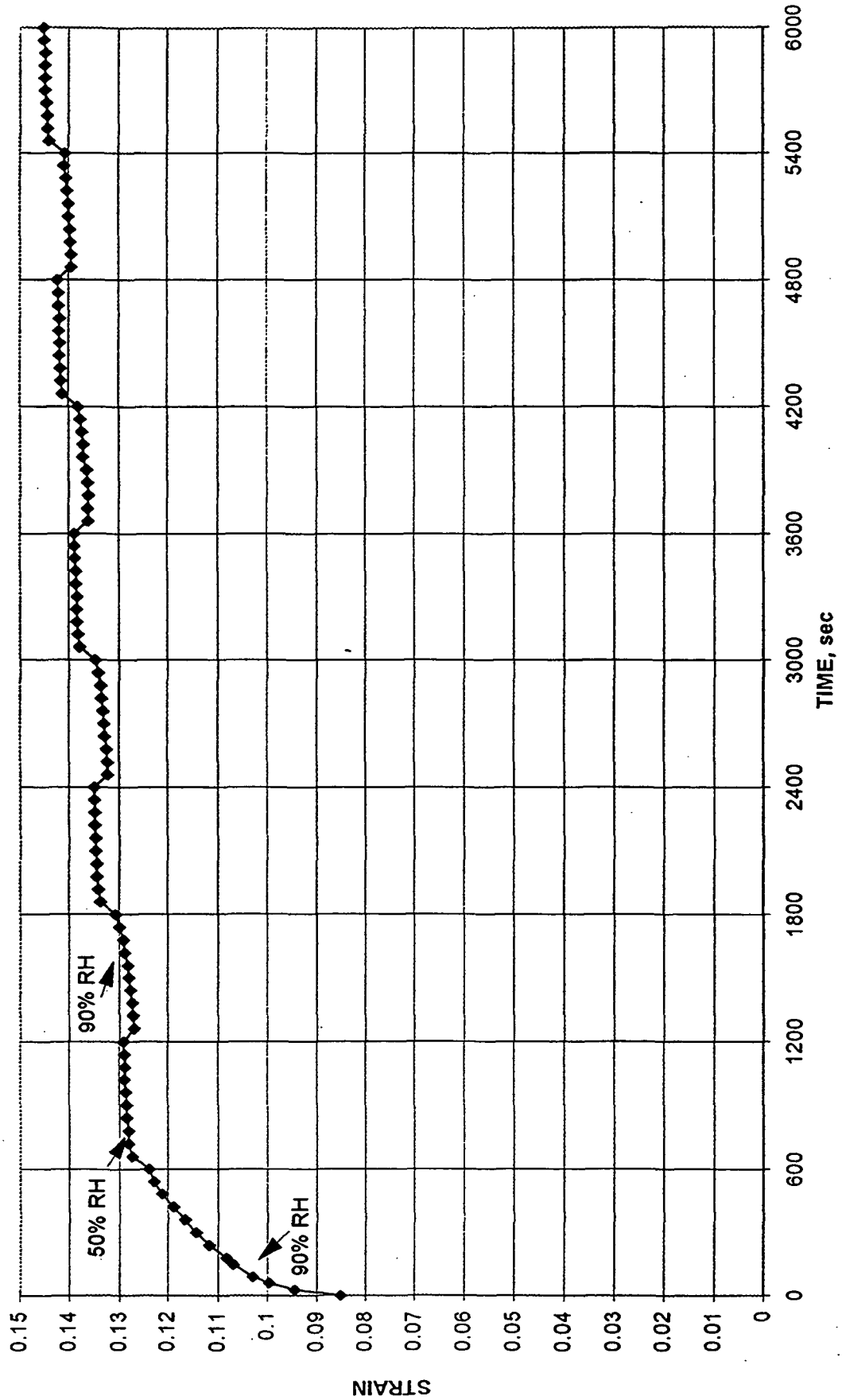

Figure 65: Average response of holocellulose fibers to cyclic humidity, 90 to 50% RH.

In both fiber types there is a profound difference in the creep behavior of the fiber that depends on how the fiber was conditioned. If conditioned and loaded at 50% humidity, instantaneous strain behavior is present when the humidity is changed to 90%. However, if conditioned and loaded at 90% humidity, an instantaneous strain is not present when the humidity is changed to 50%.

This data affords the opportunity to explore the definition of accelerated creep. In analyzing data, is the strain rate different under conditions of cyclic humidity? Plotted in Figure 66 is the constant extracted holocellulose 90% RH curve as well as the 90% RH state from each of the cyclic humidity curves, the 50–90% RH and the 90–50% RH data. The strain from the preceeding 50% RH state or states is subtracted from each 90% RH state represented in Figure 66. The constant humidity curve is an average curve of all the single fiber curves at 90% RH. This averaging process was used to form constant humidity creep responses for 50% RH as well as the 90% RH. These average creep responses are plotted as strain versus time in seconds. Strain is presented as a fraction of the initial fiber test span.

If a superposition principle can be applied to this data, then the time scale should be able to shift to form a smooth master creep curve. The time scale for each 90% RH state has been shifted by increments of 600 seconds in Figure 67. The resulting curves are relatively smooth. It appears that the superposition principle holds; therefore, the rate of strain in the corresponding cyclic state can be compared with the rate of strain in the constant humidity state. These curves have a little more noise or point-to-point variability than desired. The strain relaxation or non-recoverable strain have not been accounted for due to changes in humidity. The inclusion of these effects may improve the smoothness of the master curves.

The hypothesis that the cyclic humidity strain rate is not different than the constant humidity strain rate can be statistically tested. The log-time plot of the superimposed time scale is used to do a statistical analysis of the corresponding cyclic and constant humidity slopes. Even though the 90% curve is nonlinear in this basis, the analysis is done over short time

Figure 66: Comparison of extracted fiber creep at constant 90% RH and cyclic humidity.

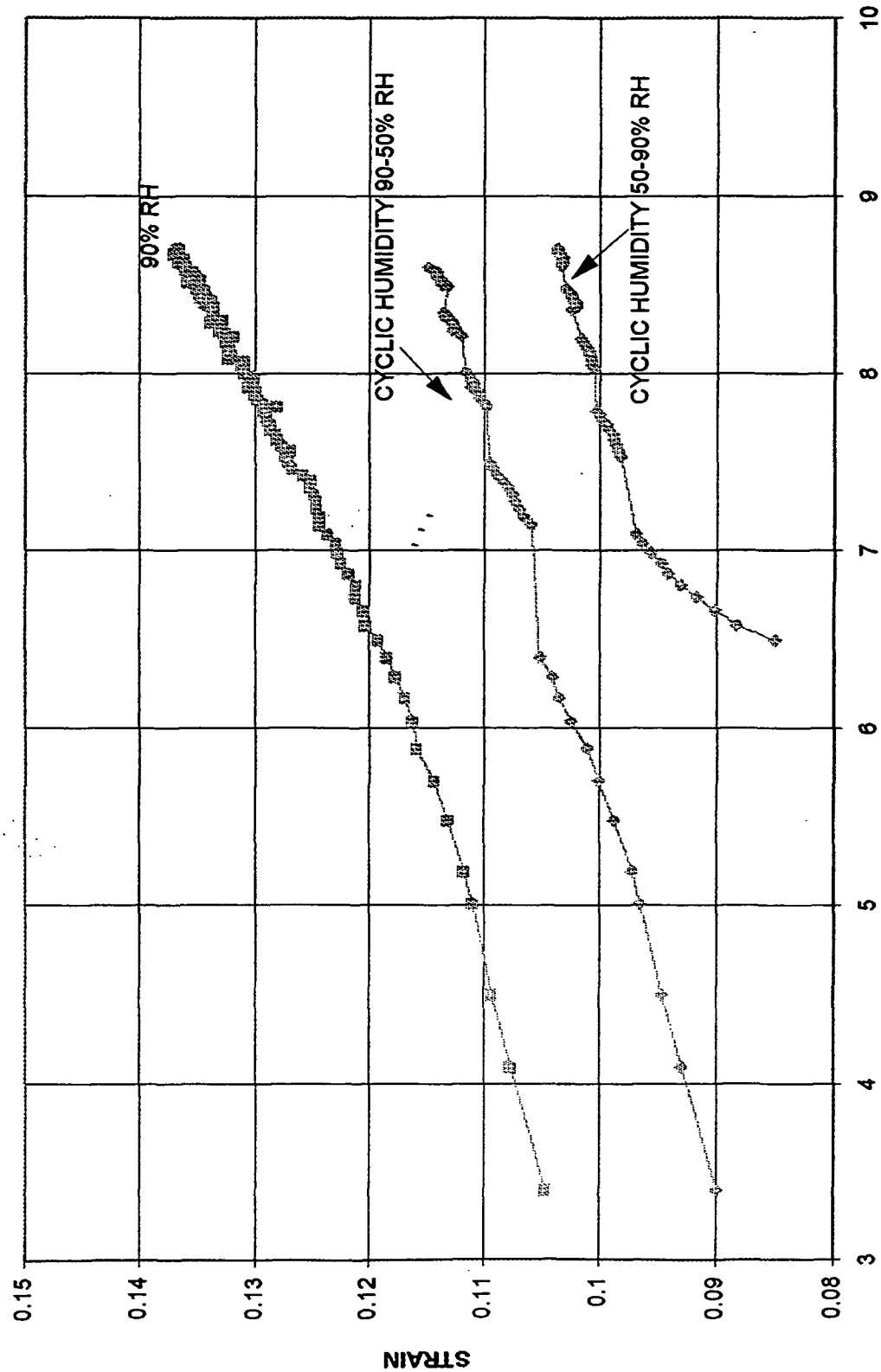

Figure 67: Extracted fiber time shifted curves for cyclic humidity data.

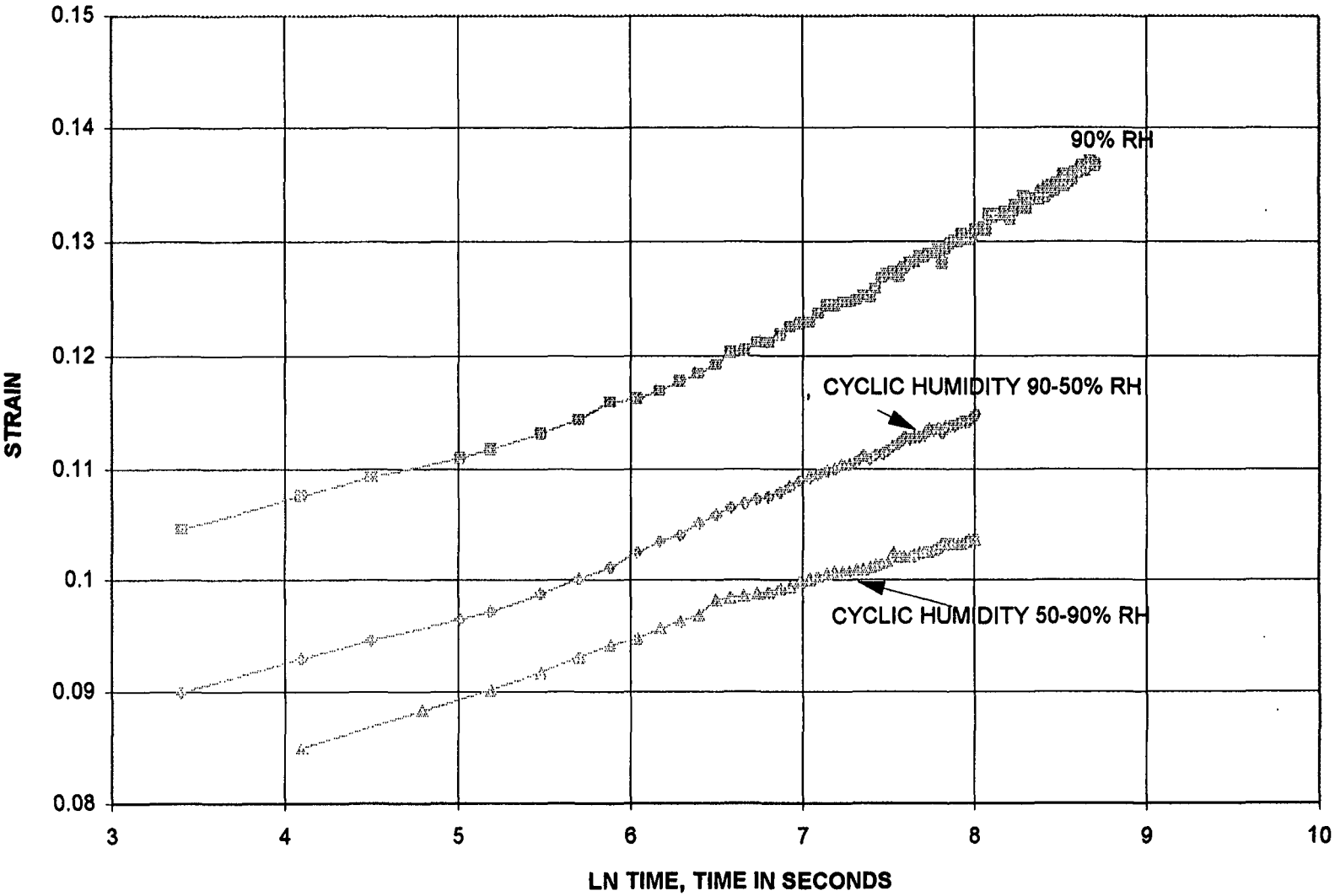

intervals of 10 minutes where the data is linear. The general equation[94] used to calculated the t-values for each cycle in Table 46 is as follows

$$[(Slope_{const.} - Slope_{cyclic})/((SE_{const.})^{1/2} + (SE_{cyclic}))^{1/2}] = t. \quad (52)$$

The slope values and the standard error values (SE) of the slopes are needed to calculate t for the corresponding constant and cyclic humidity data. The columns in Table 46 give the t values for the comparison of slopes in the different cycles. In 90% of the cases, the hypothesis is accepted at the 95% confidence level. Therefore, the strain rate defined as (de/d(lnt)) under cyclic humidity conditions at time, t, is not different than the strain rate at constant humidity conditions.

Table 46: Extracted holocellulose 90% state t-test; Ho, the cyclic humidity strain rate is not different than the constant humidity strain rate.

Cycle	t(50–90%)	Ho	t(90–50%)	Ho
1	-4.04	Reject	-1.64	Accept
2	7.31	Accept	2.17	Accept
3	3.55	Accept	1.94	Accept
4	5.42	Accept	2.71	Accept
5	3.45	Accept	1.69	Accept

Critical t = -1.86 Confidence level is 95%

Plotted in Figure 68 is the constant extracted holocellulose 50% RH curve as well as the 50% RH state from each of the cyclic humidity curves, the 50–90% RH, and the 90–50% RH data. The strain from the preceeding 90% RH state or states is subtracted from each 50% RH state represented in Figure 68. If a superposition principle can be applied to this data, then the time scale should be able to shift to form a smooth master creep curve for the 50% state.

The time scale for each 50% RH state has been shifted by increments of 600 seconds in Figure 69. The resulting curves are relatively smooth. It appears that the superposition principle holds; therefore, the rate of strain in the corresponding cyclic state was compared with the rate of strain in the constant humidity state.

Figure 68: Comparison of extracted fiber creep at constant 50% RH and cyclic humidity.

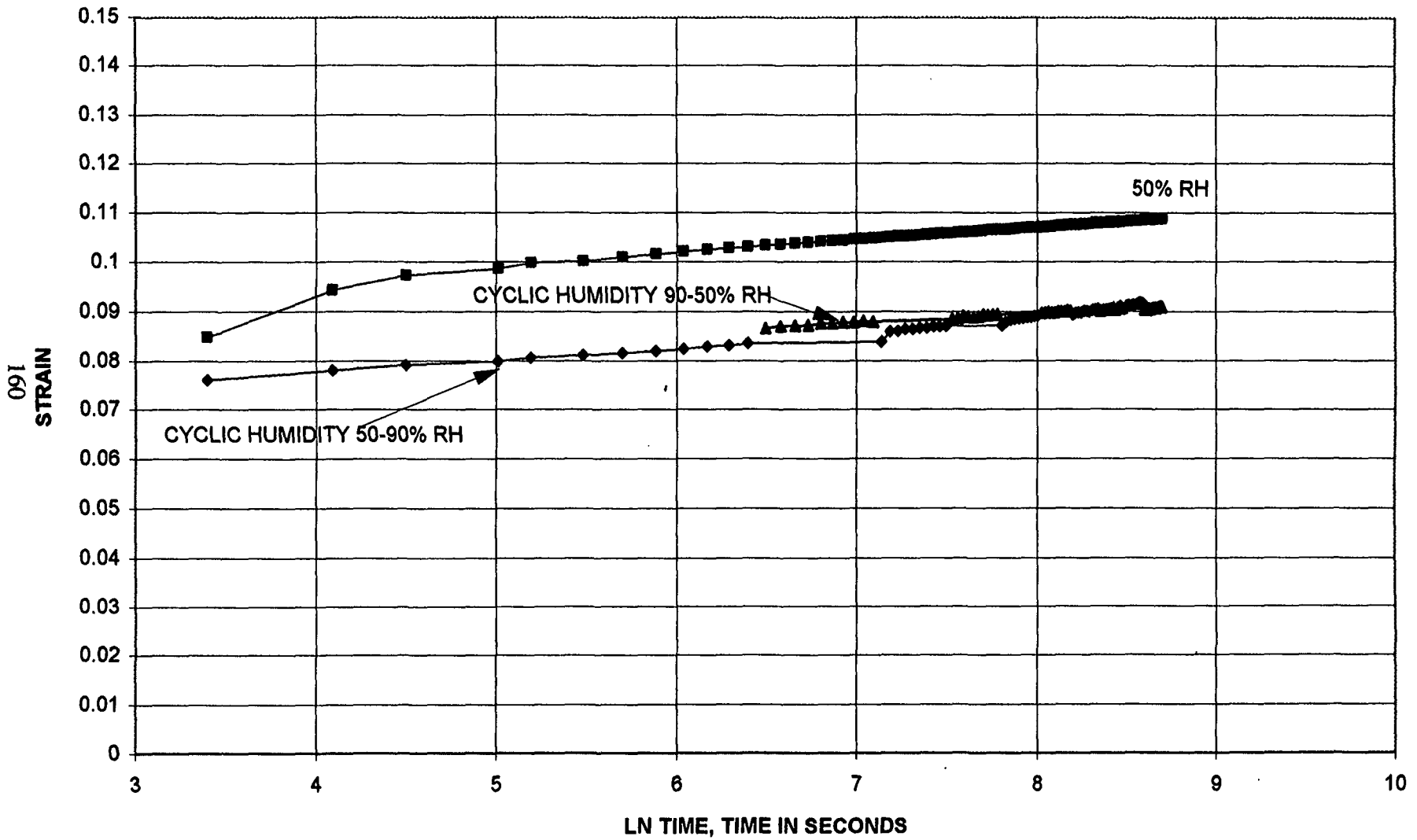

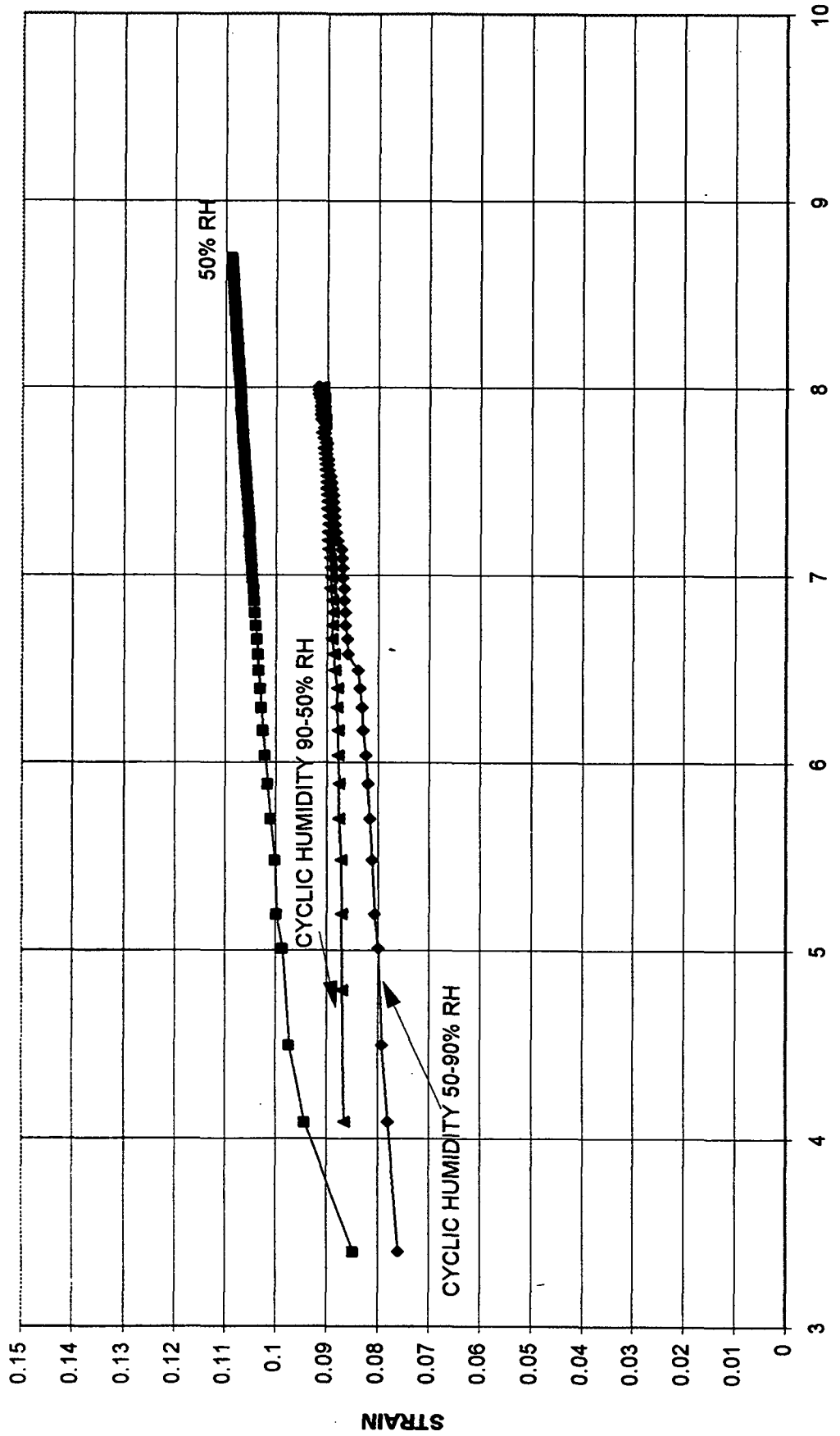

Figure 69: Extracted fiber time shifted curves for cyclic humidity data.

Table 47: Extracted holocellulose 50% state t-test; Ho, the cyclic humidity strain rate is not different than the constant humidity strain rate.

Cycle	t(50–90%)	Ho	t(90–50%)	Ho
1	8.53	Accept	20.59	Accept
2	7.05	Accept	3.83	Accept
3	-3.04	Reject	5.50	Accept
4	-2.54	Reject	-0.11	Accept
5	-3.21	Reject	-2.32	Reject

Critical t = -1.86 Confidence level is 95%

In Table 47, the hypothesis that the cyclic humidity strain rate is not different than the constant humidity strain rate can be statistically tested. The columns in Table 47 give the t values for the comparison of slopes in the different cycles for the 50–90% case and 90–50% case. Six of the cycles accept the null hypothesis and four reject it. Therefore, the hypothesis is not rejected at the 95% confidence level. The strain rate under cyclic humidity conditions at time, t, is not different than the strain rate at constant humidity conditions.

Similar analysis of the holocellulose 90% and 50% humidity states are presented. Plotted in Figure 70 is the constant holocellulose 90% RH curve as well as the 90% RH state from each of the cyclic humidity curves, the 50–90% RH, and the 90–50% RH data. Strain from the preceeding 50% RH state or states is subtracted from each 90% RH state represented in Figure 70. The time scale has been shifted in Figure 71. Corresponding plots for the holocellulose 50% humidity states are presented in Figures 72 and 73. It appears that the superposition principle holds for the holocellulose fiber regardless of the humidity state; therefore, the rate of strain in the corresponding cyclic state was compared with the rate of strain in the constant humidity state.

Table 48: Holocellulose 90% state t-test; Ho, the cyclic humidity strain rate is not different than the constant humidity strain rate.

Cycle	t(50–90%)	Ho	t(90–50%)	Ho
1	-18.68	Reject	-11.70	Reject
2	-1.88	Reject	-0.57	Accept
3	0.99	Accept	1.32	Accept
4	0.56	Accept	-0.81	Accept
5	2.34	Accept	1.29	Accept

Critical t = -1.86 Confidence level is 95%

Figure 70: Comparison of holocellulose fiber creep at constant 90% RH and cyclic humidity.

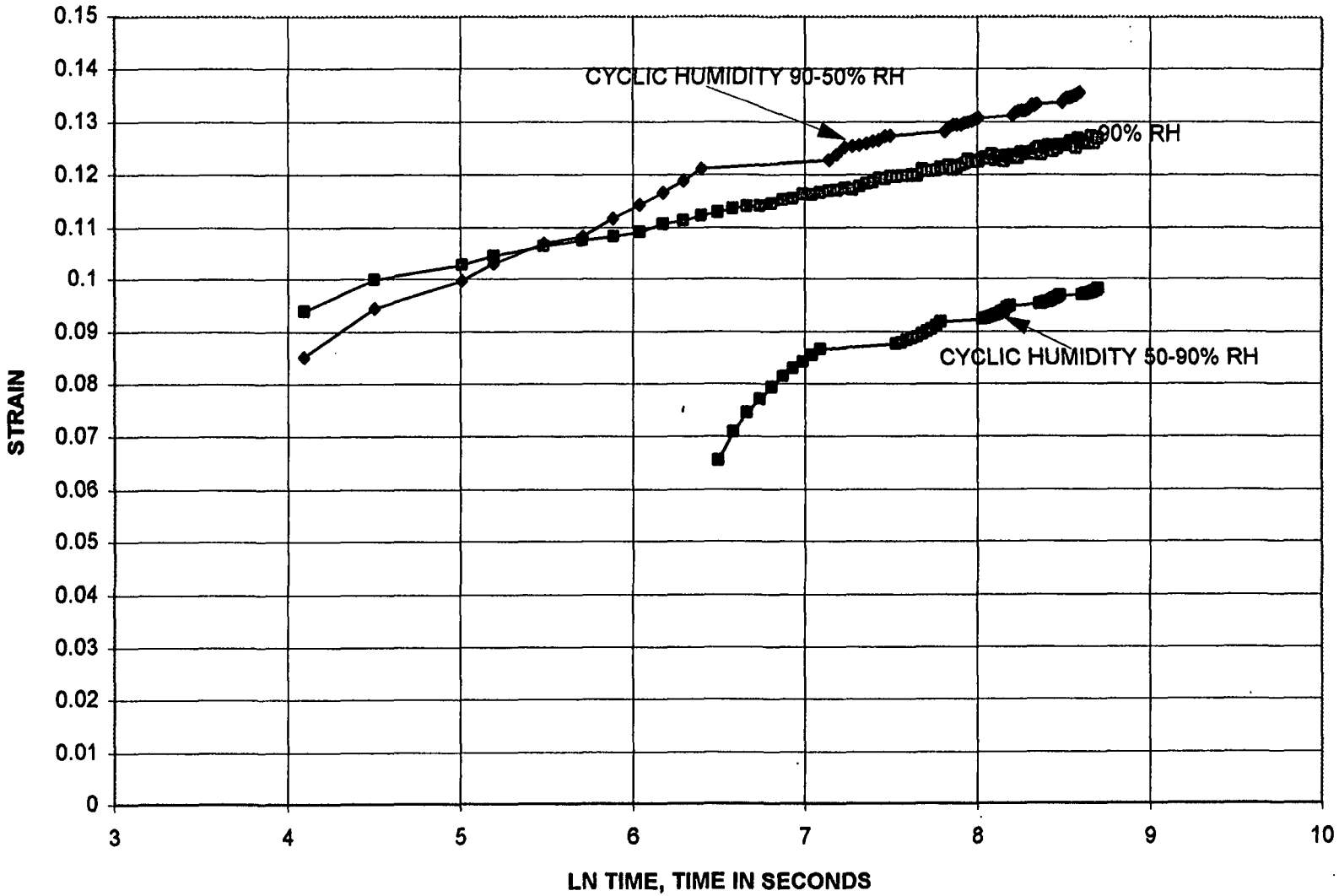

Figure 71: Holocellulose fiber time shifted curves for cyclic humidity data.

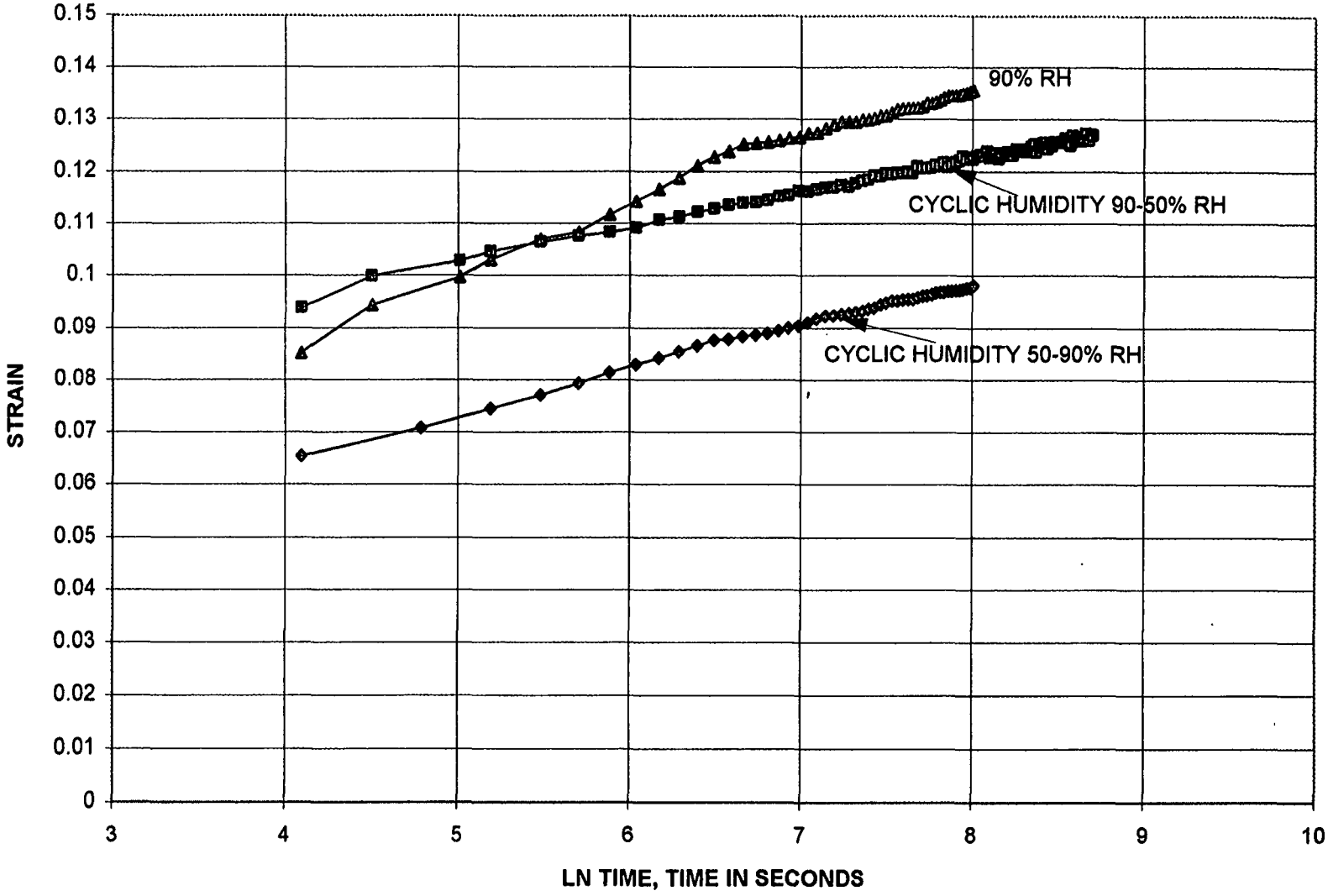

Figure 72: Comparison of holocellulose fiber creep at constant 50% RH and cyclic humidity.

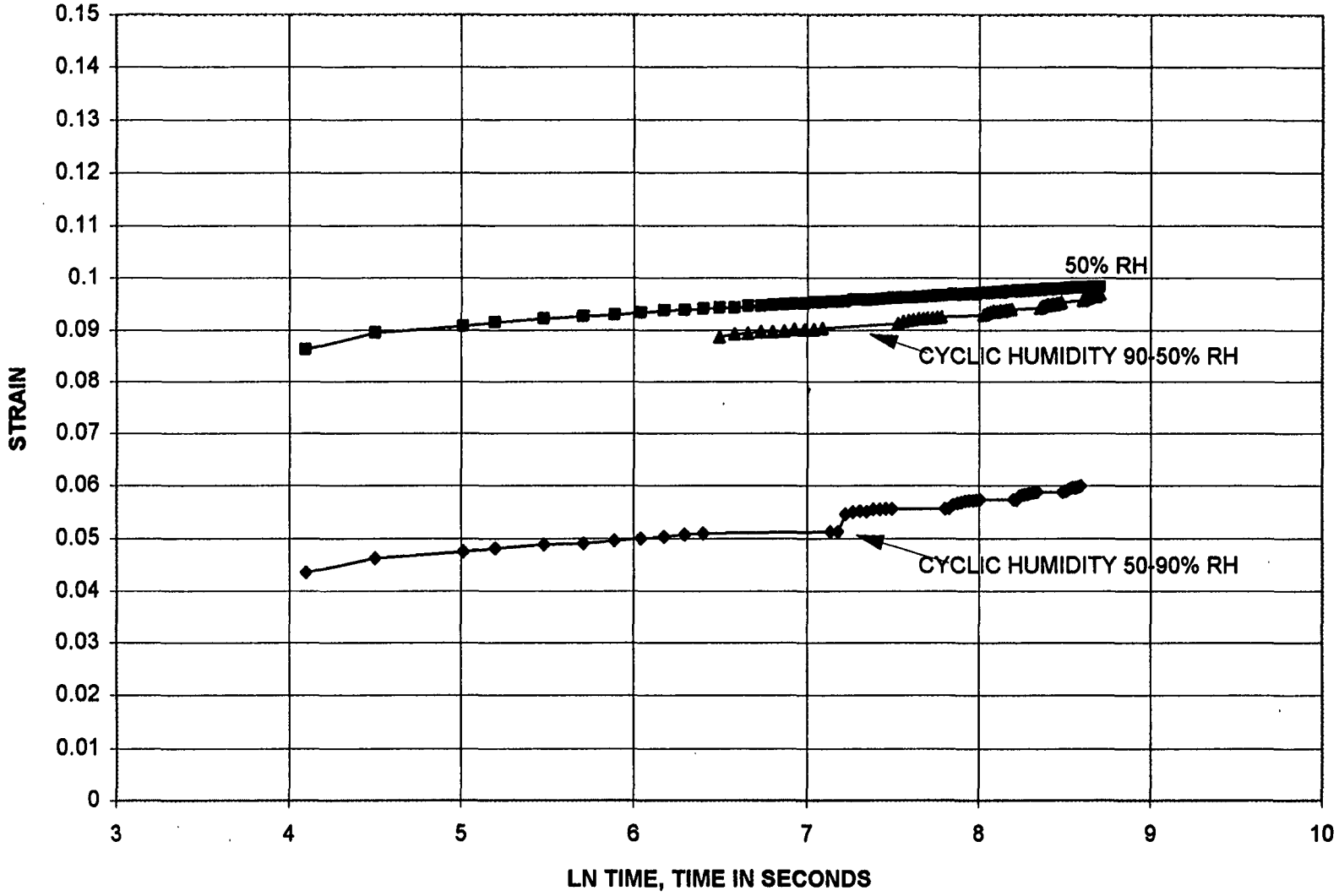

Figure 73: Holocellulose fiber time shifted curves for cyclic humidity data.

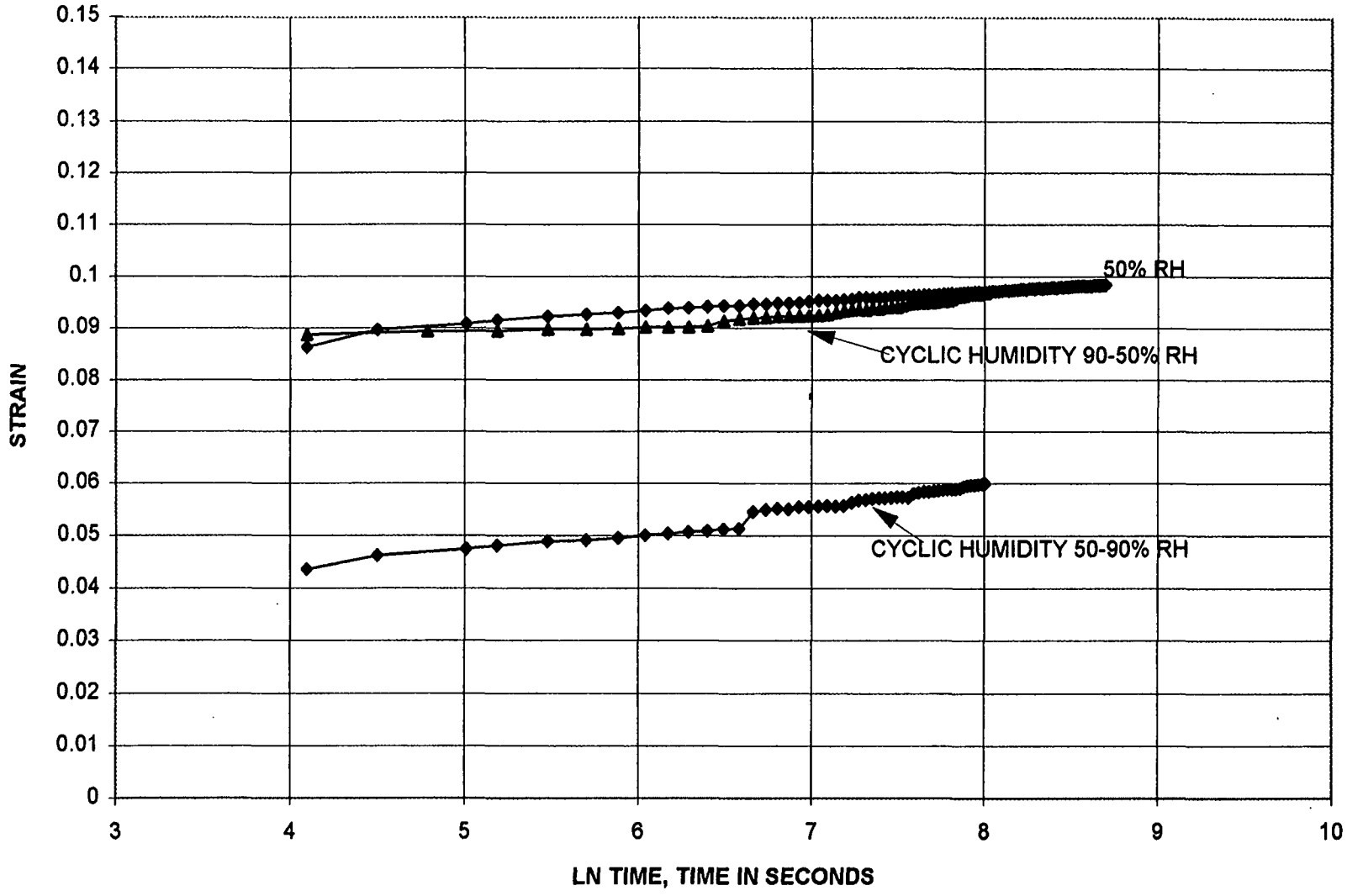

In Table 48 for the holocellulose fiber 90% state, the hypothesis that the cyclic humidity strain rate is not different than the constant humidity strain rate is not rejected at the 95% confidence level. Therefore, the strain rate under cyclic humidity conditions at time, t, is not greater than the strain rate at constant humidity conditions. Both fiber types did not reject the hypothesis at the 95% confidence level for the 90% RH state.

Table 49: Holocellulose 50% state t-test; Ho, the cyclic humidity strain rate is not different than the constant humidity strain rate.

Cycle	t(50–90%)	Ho	t(90–50%)	Ho
1	-1.89	Reject	18.84	Accept
2	-0.98	Accept	-1.39	Accept
3	-2.35	Reject	-2.94	Reject
4	-6.68	Reject	-3.68	Reject
5	-5.42	Reject	-4.54	Reject

Critical t = -1.86 Confidence level is 95%

The columns in Table 49 give the t values for the comparison of slopes in the different cycles for the 50% RH holocellulose case. In most cases, the hypothesis is rejected at the 95% confidence level. Therefore, the strain rate under cyclic humidity conditions at time, t, is not the same as the strain rate at constant humidity conditions.

Creep of single fibers under axial load was measured at two initial conditions. Fibers were conditioned at 50% RH, then loaded to 20 grams and cycled between 50% and 90% RH. The second set of conditions started with the fiber conditioned at 90% RH. The fiber attained moisture equilibrium within a few seconds after the change in humidity. When the relative humidity was changed from 50% to 90%, axial shrinkage of the fibers was observed. Cyclic creep results also show that creep strain is strongly influenced by the strain developed in the initial loading and the first humidity cycle. The strain rate, (de/d(lnt)), at any time under cyclic humidity conditions was equivalent to the strain rate under constant humidity conditions. The only exception to this conclusion was the 50% RH holocellulose fiber case.

Having answered the question, is the strain rate different under conditions of cyclic humidity? The second question considered was, is the total strain different under conditions of cyclic humidity? Figure 74 compares the extracted holocellulose constant humidity curves to the cyclic humidity curve which was conditioned at 50% humidity. The cyclic curve lies above the constant 90% humidity curve. This behavior is largely due to the jump in strain which occurred on the first cycle of the humidity. Similar behavior is seen in Figure 75 for the holocellulose constant humidity curves and the cyclic humidity curve which was conditioned at 50%.

If the fibers were conditioned at 90% RH and cycled from 90–50% RH, the behavior is very different as seen in Figures 76 and 77. The cyclic humidity curve lies almost on top of the 90% constant humidity curve. This result may be dominated by the fact that a large jump in strain in the first cycle when going from 90% to 50% humidity is not present. The extracted holocellulose fibers showed greater strain than the holocellulose fibers at a given time, t, regardless of conditioning at 50% RH or conditioning at 90% RH.

This result suggests that the behavior of fibers under cyclic conditions may be dominated by the instantaneous strain behavior at time zero; therefore, it is important for us to understand the origin of this strain. We know that fibers exhibit permanent set, therefore, it is important to determine how much of this instantaneous strain is permanent set and how much is recoverable. There is a large component of the total strain which cannot be accounted for in either classical theories of creep or permanent set according to the Hill creep recovery analysis section.

Scientists cannot expect to develop a theory for strain under cyclic humidity conditions until they understand the origin of this hidden component in the creep curves. In order to compare different fibers, it is necessary to know more about the strain at time equals zero and how much cyclic creep response is due to permanent set versus how much is due to this hidden component. A series of short creep and creep recovery experiments are needed. The duration of creep time should be reduced over several experiments to approach times close to time zero. The creep experiments should be followed by creep recovery experiments so the PSL and PSL

intercept can be determined. These creep experiments conducted at various load levels would elucidate additional information about the components of strain at time zero.

In conclusion, regardless of fiber type, the strain rate of single fibers, in axial load, is not different under conditions of constant 90% RH and cyclic humidity. The strain rate of single extracted holocellulose fibers, in axial load, is not different under conditions of constant 50% RH and cyclic humidity. However, holocellulose fibers had a different strain rate under conditions of constant 50% RH and cyclic humidity. Secondly, for both fiber types the total strain under conditions of cyclic humidity may be greater than under conditions of constant humidity. The phenomenon is very complex. The total strain depends on the initial humidity conditions as well as the instantaneous strain of the fiber upon initial loading.

Figure 74: A comparison of the average constant and cyclic humidity creep of extracted fibers.

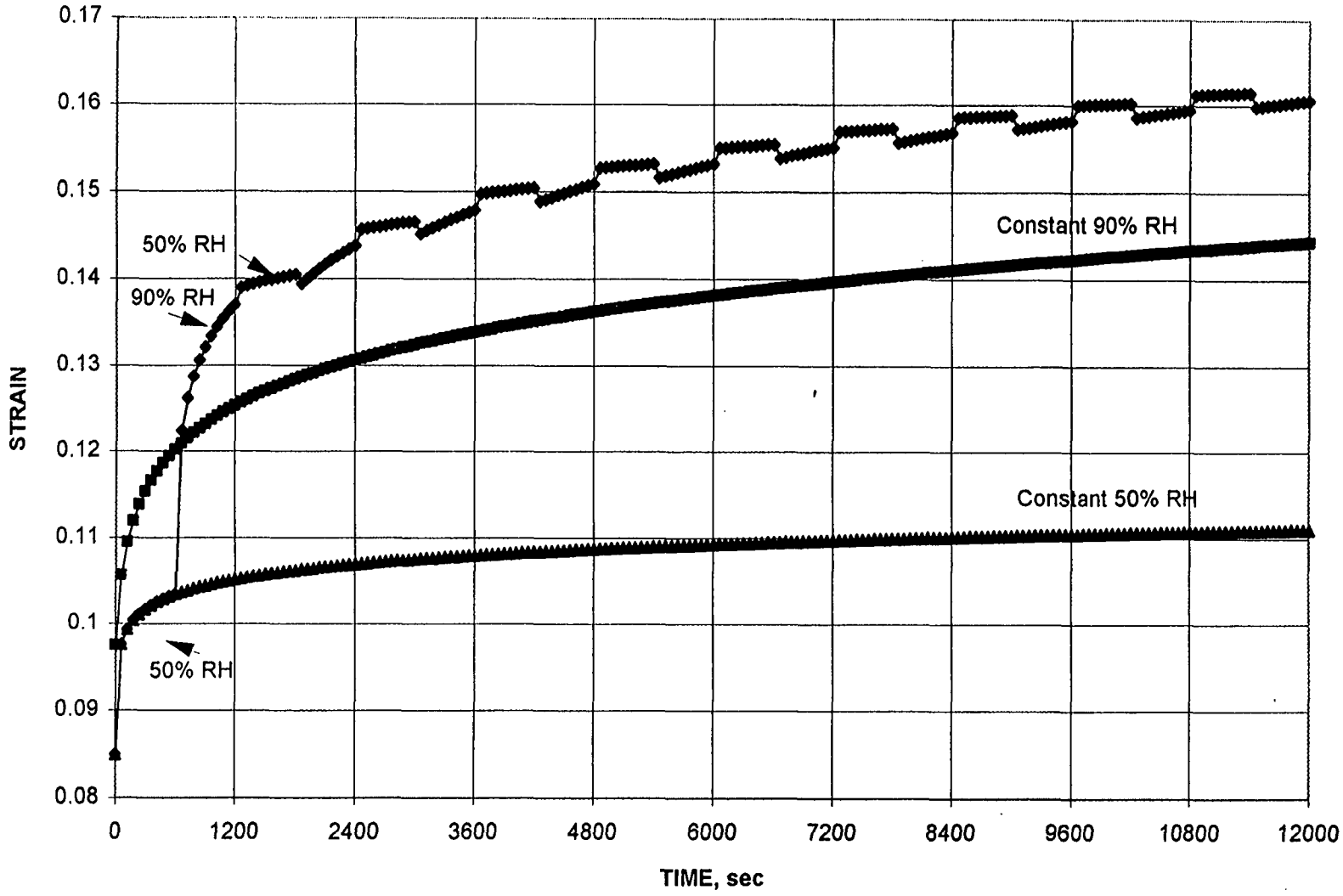

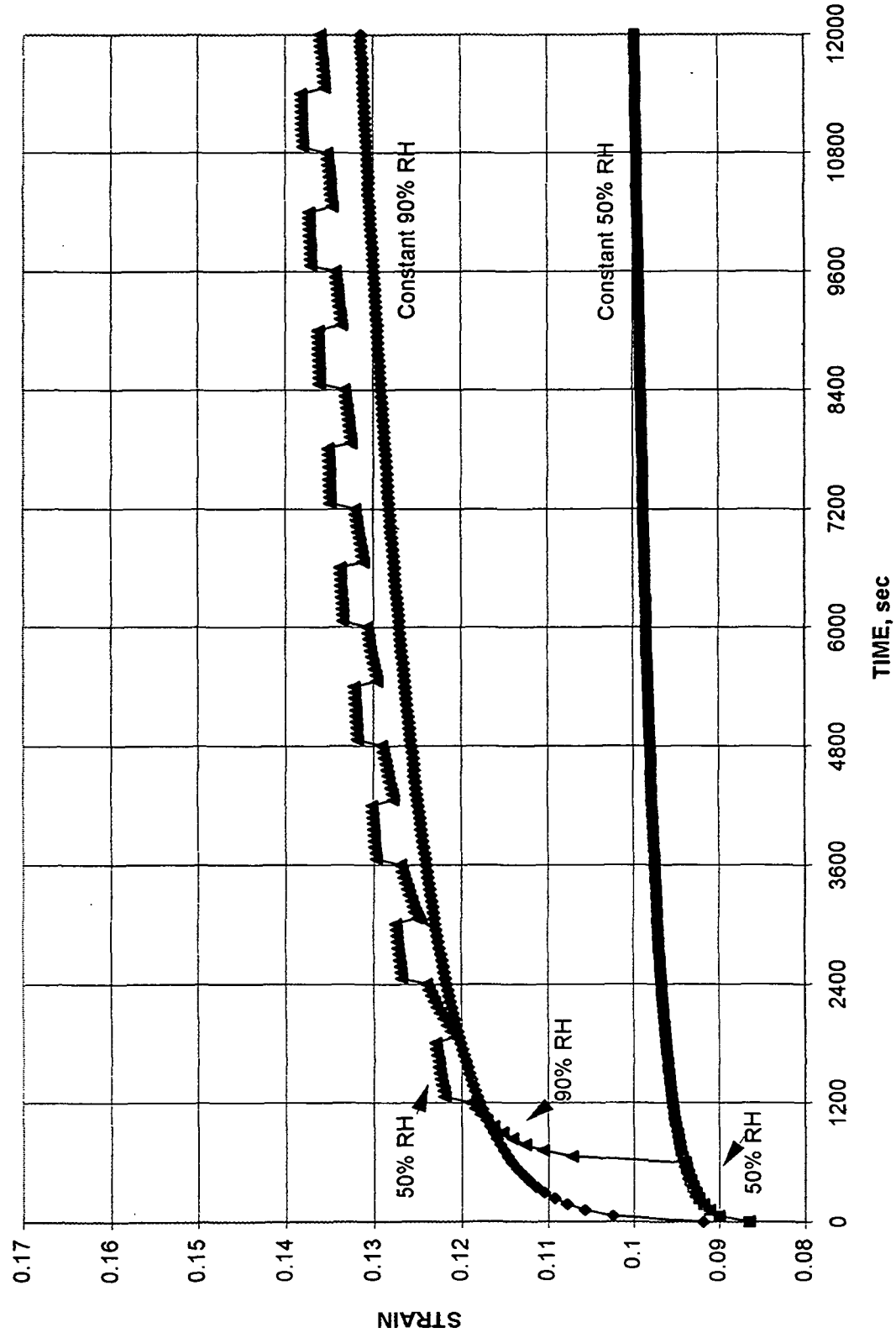

Figure 75: A comparison of the average constant and cyclic humidity creep of holocellulose fibers.

Figure 76: A comparison of the average constant and cyclic humidity creep of extracted fibers conditioned at 90% RH.

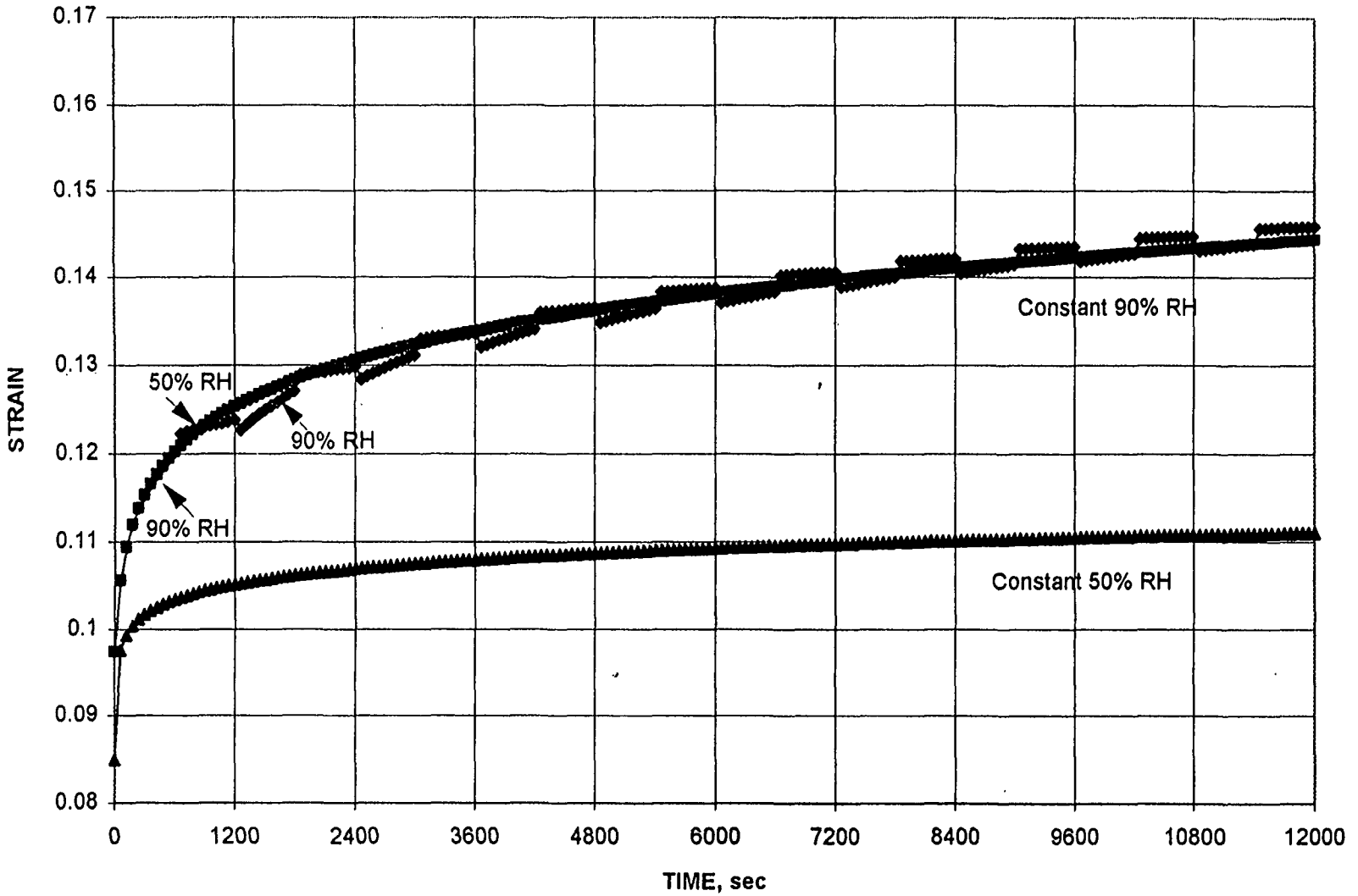

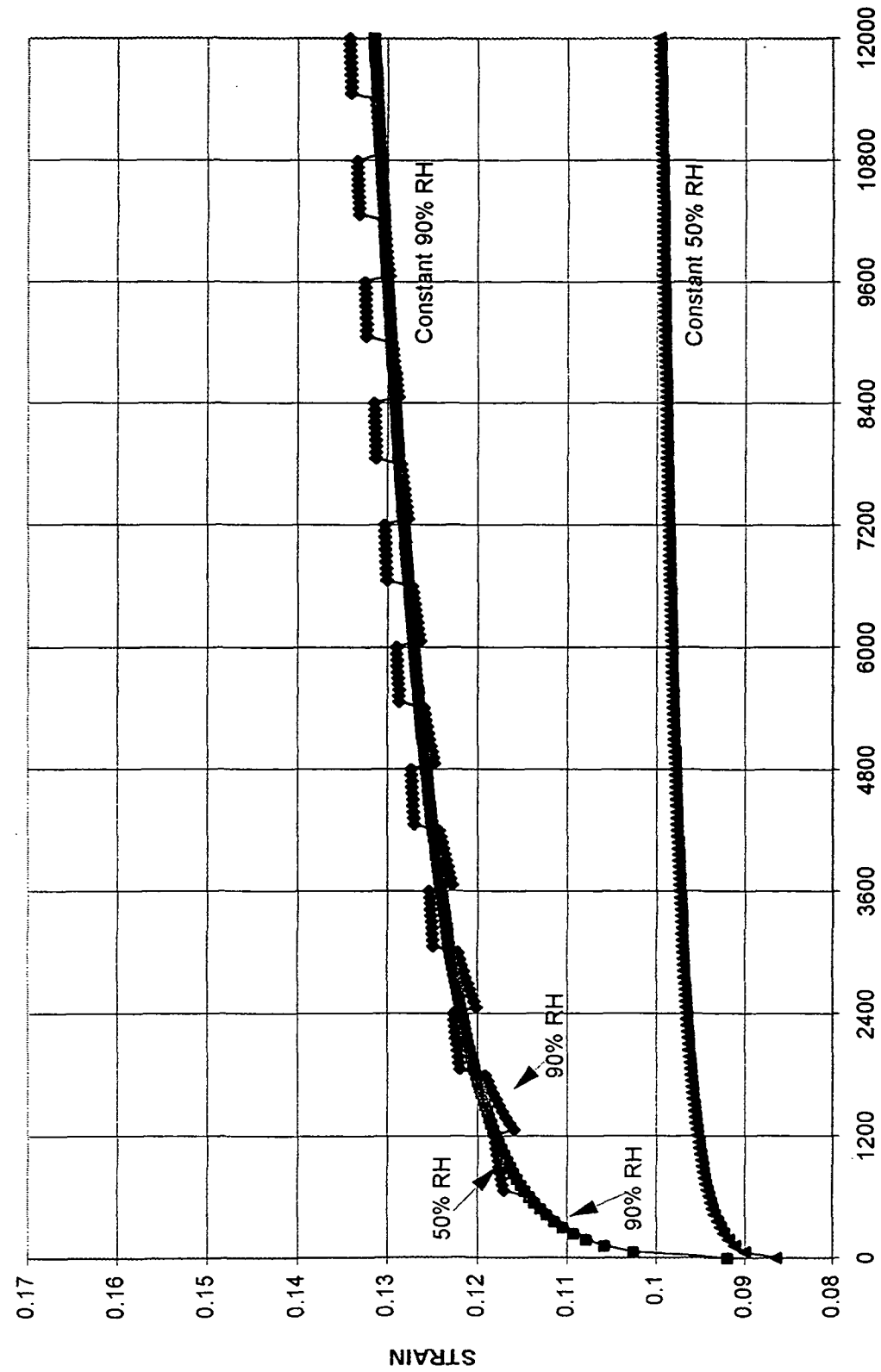

Figure 77: A comparison of the average constant and cyclic humidity creep of holocellulose fibers conditioned at 90% RH.

SUMMARY AND CONCLUSIONS

The objective of this thesis research was to determine, in a systematic manner, whether hemicelluloses influence tensile creep behavior of individual pulp fibers as a function of constant and cyclic humidity conditions. To achieve this objective, hemicelluloses were extracted from holocellulose loblolly pine fibers. These fibers were subjected to systematic axial tensile creep experiments under constant humidity conditions of 50 and 90% and cyclic humidity conditions of 50–90% RH and 90–50% RH. Fibers were also subjected to creep recovery experiments at 50 and 90% RH. The independent variables were hemicellulose content and relative humidity while the dependent variable was the creep phenomenon.

Differences between the two fiber types were found. However the differences were small compared to the differences between fibers. The first creep response of single fibers fits the Eyring model for polymers, but the permanent set of the fibers is a large component of the observed first creep strain. Only a small part of the permanent set can be explained by classical polymer theory that is linear in time and stress. Most of the permanent set occurs in the loading step and may be due to a reorganization of the cell wall material on a scale much larger than the unit cell.

The Eyring theory was used to evaluate the significance of hemicellulose content and relative humidity on the creep phenomenon in terms of constitutive parameters such as E1, E2, α, and χ. For single fiber creep, α was effectively reduced at 90% RH. Relative humidity had a significant effect on E2 for creep and creep recovery. The parameter, E2, decreased for creep and creep recovery experiments as humidity increased. Multiple regression analysis confirmed decreases in E2 with increasing humidity at the 93% and 99% confidence level. The parameter, α, was also affected by fiber type and decreases upon extraction for creep recovery of single fibers. Consequently, fiber type affects the creep phenomenon, but not significantly to warrant

modifying hemicelluloses as a possibility to decrease moisture sensitivity and reduce creep response.

Experiments in cyclic humidity conditions were designed to address two questions: (1) Is the strain rate under cyclic humidity conditions different than the strain rate under constant humidity conditions? (2) Is the total strain under cyclic humidity conditions larger than the total strain under constant humidity conditions? The creep of single fibers was measured under axial load and two initial conditions. Fibers were conditioned at 50% RH, then loaded to 20 grams and cycled between 50% and 90% RH. The second set of conditions started with the fiber conditioned at 90% RH. Single fibers attained moisture equilibrium within a few seconds after the change in humidity. The response of the fiber to cyclic humidity conditions was reminiscent of a superposition of states at constant humidity. The strain rate at any time under cyclic humidity conditions was equivalent to the strain rate under constant humidity conditions. The only exception to this conclusion was the 50% RH holocellulose fiber case. The total strain rate under cyclic humidity conditions will be higher than the lower constant humidity state. When the fiber is conditioned at 50% RH the total strain will exceed the strain of the 90% RH state after several cycles. This excess strain can be explained by the strain developed in the first creep at 50% RH. When the fiber is conditioned at 90% RH there is very little difference in strain between constant and cyclic humidity conditions. Axial shrinkage of the fibers was observed when the relative humidity was changed from 50% to 90%. This may be caused by the large swelling component for the radial direction.

Results show that creep strain is strongly influenced by the strain developed in the initial loading and first humidity cycle. Results also show that this strain is responsible for most of the permanent set of the fiber. These results point to a neglected area of research. We must measure and explain the instantaneous strain of single fibers before we can fully quantify their behavior under either constant or cyclic humidity conditions. Paper strained at a constant load and humidity is known to have a large component of permanent set. It is suspected that the total

strain of paper studied under cyclic humidity conditions is dominated by the strain developed in the first cycle. Until the origin of this component of the creep strain is subjected to theoretical interpretation it is unlikely that we can develop a predictive theory for the dimensional stability of paper products or the lifetime of corrugated containers.

RECOMMENDATIONS FOR FUTURE WORK

Future work should focus on determining the mechanism of the large strain observed at initial loading and formulating a theory for extension of the Eyring theory. Scientists cannot expect to develop a theory for strain under cyclic humidity conditions until they understand the origin of this hidden component in the creep curves. In order to compare different fibers, it is necessary to know more about the strain at time equals zero and how much cyclic creep response is due to permanent set versus how much is due to this hidden component.

A series of short creep and creep recovery experiments are needed. The duration of creep time should be reduced over several experiments to approach times close to time zero. The creep experiments should be followed by creep recovery experiments so the PSL and PSL intercept can be determined. These creep experiments conducted at various load levels would elucidate additional information about the components of strain at time zero. This information is necessary to modify the Eyring theory.

The Eyring theory does not account for orientation; therefore, one cannot predict the fibril angle. Further modification of the theory should include prediction of microfibril angle. Stress relaxation measurements should be made in order to better quantify the elastic constants of the fiber cell wall.

Axial shrinkage of the fibers was observed when the relative humidity was changed from 50% to 90%. This may be caused by swelling or structural changes within the fiber. A swelling mechanism can be evaluated by using a scanning electron microscope to measure the fiber width and length changes when cycling to various humidity levels. If the axial shrinkage of the fibers is due to structural changes or bond breakage, nuclear magnetic resonance, NMR, can be used to evaluate the mechanism.

We must measure and explain the instantaneous strain of single fibers before we can fully quantify their behavior under either constant or cyclic humidity conditions. Paper strained at a

constant load and humidity is known to have a large component of permanent set. It is suspected that the total strain of paper studied under cyclic humidity conditions is dominated by the strain developed in the first cycle. Until the origin of this component of the creep strain is subjected to theoretical interpretation it is unlikely that we can develop a predictive theory for the dimensional stability of paper products or the lifetime of corrugated containers. Creep of the fiber-to-fiber bond should be measured to further understand the contribution of fiber creep and fiber bonds to paper creep.

LITERATURE CITED

1. Grant, J. Non-woody Fibers: How They Are Used by the World's Pulp and Paper Industry. Paper Trade Journal. 35–38(January 30, 1967).

2. Laufenburg, T., and Ellis, R. Combined Board Performance Under Cyclic Humidity Conditions: Research Program of the Container and Kraft Paper Group of the American Paper Institute, 1990. Institute of Paper Science and Technology, Atlanta, GA.

3. Soremark, C., and Fellers, C. Mechano-sorptive Creep and Hygroexpansion of Corrugated Board in Bending. 1991 International Paper Physics Conference. 549-559.

4. Armstrong, L.D., and Christensen, G.N. Influence of Moisture Changes on Deformation of Wood Under Stress. Nature. 191:869–870(1961).

5. Brezinski, J.P. The Creep Properties of Paper. Tappi Journal. 39(2):116–128(1956).

6. Hill, R.L. The Creep Behavior of Individual Pulp Fibers Under Tensile Stress. Tappi Journal. 50(8):432–440(1967).

7. Browning, B.L. The Chemistry of Wood. Huntington, NY, Robert E. Krieger Publishing Company, 1975.

8. Heyn, A.N.J. Elementary Fibril and Supramolecular Structure of Cellulose in Softwood Fiber. Journal of Ultrastructure Research. 26:52–68(1969).

9. Hearle, J.W.S. A Fringed Fibril Theory of Structure in Crystalline Polymers. Journal of Polymer Science. 28(117):432–435(1958).

10. Hearle, J.W.S. Structure and Mechanical Properties of Fibers. Journal of Textile Institute Proceedings. 53(8):449–464(1962).

11. Heyn, A.N.J. Microcrystalline Structure of Cellulose in Cell Walls of Cotton, Ramie, and Jute Fibers as Revealed by Negative Staining of Sections. Journal of Cell Biology. 29(2):181–197(1966).

12. Preston, R.D. Cellular Ultrastructure of Woody Plants. Syracuse, NY, Syracuse University Press, 1965.

13. Muhlethaler, K. The Fine Structure of the Cellulose Microfibril. In Cellular Ultrastructure of Woody Plants. W.A. Cote, Jr., ed. Syracuse, NY, Syracuse University Press, 1965. 191–198.

14. Keissig, H. The X-ray Investigations of the Large Period of Cellulose. Das Papier 12:117–122(1958). On the Structure of Cellulose in Fibrous and Film Forming Precipitation Products. Das Papier. 22:261–268(1968).

15. Ruck, H. Studies on Intramicellular Reactions in the Mercerizing Process of Cellulose. Das Papier 16:703–712(1962).

16. Thompson, N.S. Discussion Session Sponsored by the Technical Association of the Pulp and Paper Industry. The Institute of Paper Chemistry, Appleton, WI. (May 12, 1969).

17. Holland, V.F., and Lindenmeyer, P.H. Morphology and Crystal Growth Rate of Polyethylene Crystalline Complexes. Journal of Polymer Science. 57:589–608(1962).

18. Tonnesen, B.A., and Ellefsen, O. Chain Folding a Possibility to be Considered in Connection with the Cellulose Molecule? Norsk Skogindustri. 14(7):266–269(1960).

19. Manley, R.S.J. The Molecular Morphology of Native Cellulose. Nature. 204:1154–1157(1964).

20. Dolmetsch, H. Cellulose—Its Process of Formation. Das Papier 17(12):710–721(1963).

21. Lindenmeyer, P.H. Crystallization and Molecular Folding. Science. 147:1256–1262(1965).

22. Stein, R.S. Structural Interpretations of Mechanical Properties of Polycrystalline Polymers. Society of Plastics Engineers Transactions. 4(3):178–186(1964).

23. Murphey, W.K. Cell-Wall Crystallinity as a Function of Tensile Strain. Forest Products Journal. 13(4):151–155(1963).

24. Jentzen, C.A. The Effect of Stress Applied During Drying on the Mechanical Properties of Individual Pulp Fibers. Doctoral Dissertation. Appleton, WI, The Institute of Paper Chemistry, 1964.

25. Bucher, H. Discontinuities in the Microscopic Structure of Wood Fibers. In Bolam's Fundamentals of Papermaking Fibers. Kenley, Surrey, England, Technical Section of the British Paper and Board Maker's Association, Inc., 1958.

26. Frey-Wyssling, A. A General Structure of Fibers. In Bolam's Fundamentals of Papermaking Fibers. Kenley, Surrey, England, Technical Section of the British Paper and Board Maker's Association, Inc., 1958.

27. Wardrop, A.B. Morphological Factors Involved in the Pulping and Beating of Wood Fibers. Svensk Papperstidning. 66(7):231–427(1963).

28. Emerton, H.W. The Outer Secondary Wall: It's Structure. In Bolam's Fundamentals of Papermaking Fibers. Kenley, Surrey, England, Technical Section of the British Paper and Board Maker's Association, Inc., 1958. 35.

29. Koch, P. Utilization of Southern Pine. Vol. 1. The Raw Material. Washington D.C., U.S. Dept. of Agricultural Forest Service, 1972. 55–424.

30. Jayme, G., and Hunger, G. Electron Microscope 2- and 3- Dimensional Classification of Fiber Bonding. In Bolam's Fundamentals of Papermaking Fibers. Kenley, Surrey, England, Technical Section of the British Paper and Board Maker's Association, Inc., 1958.

31. Meier, H. The Distribution of Polysaccharides in Wood Fibers. Journal of Polymer Science. 51:11–18(1961).

32. Meier, H. Chemical and Morphological Aspects of the Fine Structure of Wood. Pure Applied Chemistry. 5(1/2):37–52(1962).

33. Preston, R.D. The Sub-Microscopic Morphology of Cellulose. Polymer. 3:511–528(1962).

34. Ranby, B.G. The Fine Structure of Cellulose Fibrils. In Bolam's Fundamentals of Papermaking Fibers. Kenley, Surrey, England, Technical Section of the British Paper and Board Maker's Association, Inc., 1958.

35. Beyers, E.M. An Autoradiographic Study of the Hemicellulose Distribution in the Walls of *Pinus Resinosa* Tracheids. Doctoral Dissertation. Appleton, WI, The Institute of Paper Chemistry, 1989.

36. Hamilton, J., and Quimby, G. The Extractive Power of Lithium, Sodium, and Potassium Hydroxide Solutions for the Hemicelluloses Associated with Wood Cellulose and Holocellulose from Western Hemlock. Tappi Journal. 40(9):781–786(1957).

37. Leopold, B. Chemical Composition and Physical Properties of Wood Fibers. II: Alkali Extraction of Holocellulose Fibers from Loblolly Pine. Tappi Journal. 44(3):232–235(1961).

38. Jones, J.K.N., Wise, L.E., and Merler, E. The Hemicelluloses Present in Aspen Wood (*Populus tremuloides*). Part III: The Constitution of Pentosan and Hexan Fractions. Canadian Journal of Chemistry. 35(7):634–645(1957).

39. Meier, H. Studies on Hemicelluloses from Pine (*Pinus silvestris L.*). Acta Chemica Scandinavica. 12:1911–1918(1958).

40. Ward, K., and Murray, M. Alkaline Extraction of Spruce Pulps. Tappi Journal. 42(1):17–20(1959).

41. Morak, A.J., and Ward, K., Jr. Investigations of the Mannans and Xylans in Softwood: II. Tappi Journal. 4(1):12–22(1961).

42. Nelson, R. Fractionation of Hemicelluloses. Tappi Journal. 43(4):313–319(1960).

43. Spiegelberg, H.L. The Effect of Hemicelluloses on the Mechanical Properties of Individual Pulp Fibers. Doctoral Dissertation. Appleton, WI, The Institute of Paper Chemistry, 1966.

44. Timell, T. Wood Hemicelluloses. Syracuse, NY, The College of Forestry at Syracuse University, 1963.

45. Leaderman, H. Elastic and Creep Properties of Filamentous Materials and Other High Polymers. Washington, D.C., The Textile Foundation, 1943.

46. Alfrey, T. Jr. Mechanical Behavior of High Polymers. New York, Interscience Publishers, Inc., 1948.

47. Ferry, J.D. Viscoelastic Properties of Polymers. New York, John Wiley and Sons, Inc., 1961.

48. Halsey, G., White, H., and Eyring, H. Mechanical Properties of Textiles: I. Textile Research Journal. 15(9):295–311(1945).

49. Holland, H.D., Halsey, G., and Eyring, H. Mechanical Properties of Textiles: VI. A Study of Creep of Fibers. Textile Research Journal. 16(5):201–210(1946).

50. Meyer, K.H., and Lotmar, W. The Elasticity of Cellulose. The Structure of the Crystallized Components of Cellulose: IV. Helvetica Chimica Acta. 19(1):69–86(1936).

51. Meredith E. Mechanical Properties of Textile Fibers. New York, Interscience Publishers Inc., 1956.

52. Leopold, B., and McIntosh, D. Chemical Composition and Physical Properties of Wood Fibers: III. Tensile Strength of Individual Fibers from Alkali Extracted Loblolly Pine Holocellulose. Tappi Journal. 44(3):235–240(1961).

53. Wardrop, A.B. Cell Wall Organization and the Properties of the Xylem: I. Cell Wall Organization and the Variation of Breaking Load in Tension of the Xylem in Conifer Stems. Australian Journal of Scientific Research. 4(4):391–414(1951).

54. DeRuvo, A. Influence of Temperature and Humidity of the Elastic and Expansional Properties of Paper and the Constituent Fiber. Transactions of the BPBIF Symposium on the Fundamental Properties of Paper Related to Uses. (1973). Cambridge, BPBIF, 1976. 785–807.

55. Cousins, W.J. Young's Modulus of Hemicellulose as Related to Moisture Content. Wood Science and Technology. (12):161–167(1978).

56. Cousins, W.J. Elastic Modulus of Lignin as Related to Moisture Content. Wood and Science Technology. (10):9–17(1976).

57. Kersavage, P.C. Moisture Content Effect on Tensile Strength Properties of Individual Douglas-fir Latewood Tracheids. Wood and Fiber. 5(2):105–117(1973).

58. Hardacker, K.W. Effects of Loading Rate, Span, and Beating on Individual Wood Fiber Tensile Properties. The Physics and Chemistry of Wood Pulp Fibers. TAPPI PRESS. TAPPI STAP. (8):201–216(1970).

59. Steinberger, R.L. Creep in Cellulose Acetate Filaments. Textile Research Journal. 6:191–206(1936).

60. Pinte, C.J., and Henno, J. Mechanical Properties of Viscose and Acetate Rayon Subjected to Constant Loadings as a Function of Time. Bulletin de I' Institut Textile de France. 6:35(1947).

61. Byrd, V.L. Effects of Relative Humidity Changes During Creep on Handsheet Paper Properties. Tappi Journal. 55(2):247–252(1972).

62. Schniewond, A.P. Creep-Rupture Life of Douglas-fir Under Cyclic Environmental Conditions. Wood Science and Technology. 1(4):278–288(1967).

63. Salmen, L. Responses of Paper Properties to Changes in Moisture Content and Temperature. Proceedings of the Products of Papermaking Conference, Vol. 1. PIRA, :369-430(1993).

64. Gunderson, D.E., and Considine, J.M. Measuring the Mechanical Behavior of Paperboard in a Changing Humidity Environment. Proceedings of the TAPPI

International Process Materials and Quality Evaluation Conference. Atlanta, GA, TAPPI PRESS, 1986. 246–251.

65. Schaffer, E.L. Modeling the Creep of Wood in a Changing Moisture Environment. Wood and Fiber. 3:232–235(1972).

66. Haslach, H.W. Jr., Pecht, M.G., and Wu, X. Variable Humidity and Load Interaction in Tensile Creep of Paper. Proceeding of the International Paper Physics Conference. Kona, Hawaii, Tappi Press, Atlanta, GA, :219–224(1991).

67. Manson, J.A., and Sperling, L.H. Polymer Blends and Composites. New York, Plenum Press, (1976).

68. Levenspiel, O. Chemical Reaction Engineering. New York, John Wiley, and Sons, (1972).

69. Nielsen, L.E., and Landel, R.F. Mechanical Properties of Polymers and Composites. New York, Marcel Dekker, Inc., (1994).

70. SAS Institute Inc. SAS/STAT™ . User's Guide, Release 6.03 Edition. Cary, NC, SAS Institute Inc., (1988).

71. Burleigh, E.G., and Wakeham, H. Stress Relaxation of Cotton and Rayon Cords at Constant Length. Textile Research Journal. 17:245–255(1947).

72. Andersen, F. Studies on the Mechanical Properties of Cellulose Fibers in Relation to the Internal Structure, Transactions of the Danish Academy of Technical Sciences. The Danish Institute for Textile Research. 3(1950).

73. Mark, R.E. Cell Wall Mechanics of Tracheids. New Haven, Yale University Press, (1967).

74. Page, D.H., and El-Hosseiny, F. Mechanical Properties of Single Wood Pulp Fibers. Part VI. Fibril Angle and the Shape of the Stress-Strain Curve. Journal of Pulp and Paper Science. 9:99–100(1983).

75. Page, D.H., El-Hosseiny, F., and Winkler, K. Behavior of Single Wood Fibers Under Axial Tensile Strain. Nature. 229:252–253(1971).

76. Wise, L.E., Murphy, M., and D'Addieco, A.A. Chlorite Holocellulose, Its Fractionation and Bearing on Summative Wood Analysis and on Studies on the Hemicelluloses. Paper Trade Journal. 122(2):35–43(1946).

77. Thompson, N.S., and Kaustinen, O. Some Chemical and Physical Properties of Pulps Prepared by Mild Oxidative Action. Tappi Journal. 47(3):157–162(1964).

78. TAPPI Test Methods. Vol. 1. TAPPI Method T249 pm-75. TAPPI, Atlanta, GA, TAPPI PRESS, 1989.

79. Annergren, G., and Rydholm, S. On the Behavior of Hemicelluloses During Sulfite Pulping. Svensk Papperstidning. 62:737–746(1959).

80. TAPPI Test Methods. Vol. 1. TAPPI Method T230 om-89. TAPPI, Atlanta, GA, TAPPI PRESS, 1989.

81. Dimmel, D.R. Personal Communication, 1995. The Institute of Paper Science and Technology, Atlanta, GA.

82. Gentile, V.M. Effects of Physical Structure on the Alkaline Degradation of Hydrocellulose. Doctoral Dissertation. Appleton, WI, The Institute of Paper Chemistry, 1986.

83. OPTIMAS Technical Reference. Vol. 2. 6th ed. Seattle, WA, Optimas Corporation, 1994.

84. Hickey, K.L. Distribution of Strain Between Earlywood and Latewood in Cyclic Compression of Loblolly Pine. Masters Dissertation. Atlanta, GA, The Institute of Paper Science and Technology, 1992.

85. Rueckert, C.B. Evaluation of Strain in Earlywood and Latewood of Loblolly Pine in Cyclic Compression. A490 Progress Report 2. Atlanta, GA, The Institute of Paper Science and Technology. (February 23, 1994).

86. TAPPI Test Methods. Vol. 1. TAPPI Method T210 cm-85. TAPPI, Atlanta, GA, TAPPI PRESS, 1989.

87. Barkas, W.W., Hearmon, R.F.S., and Rance, H.F. Mechanical Properties of Wood and Paper. Amsterdam, North-Holland Publishing Company, 1953.

88. Hardacker, K. Institute of Paper Chemistry Project 3526 Status Report. Institute of Paper Chemistry, Appleton, WI, 1986.

89. Esser, J.R. The Dependence of Strain to Failure on Process Variables: Determining Relative Contributions of Fibers and Bonds. Masters Dissertation. Atlanta, GA, The Institute of Paper Science and Technology, 1994.

90. Brown, K.C., Mann, J.C., and Pierce, F.T. The Influence of Humidity on the Elastic Properties of Cotton. Part V—The Tensile Behavior. The Journal of the Textile Institute. 21:186T–204T(1930).

91. Kersavage, P.C. Moisture Content Effect on Tensile Properties of Individual Douglas-Fir Latewood Tracheids. Wood and Fiber. 5(2):105–117(1973).

92. Meredith, R. The Torsional Rigidity of Textile Fibers. The Journal of the Textile Institute. 45(7):T489–T 503(1954).

93. Ralston, M.L., and Jennrich, R.I. DUD: A Derivative-Free Algorithm for Nonlinear Least Squares. Technometrics. 20:7–14(1978).

94. Ostle, B. Statistics Research. 2nd ed. Amsterdam, The Iowa State Press, 1964.

95. Brownlee, K.A. Industrial Experimentation. Brooklyn, NY, Chemical Publishing Co., Inc., 1949.

96. TAPPI Test Methods. Vol. 1. TAPPI Method T204 om-88. TAPPI, Atlanta, GA, TAPPI PRESS, 1989.

97. TAPPI Test Methods. Vol. 1. TAPPI Method T22 om-88. TAPPI, Atlanta, GA, TAPPI PRESS, 1989.

98. Stratton, R.A. Characterization of Fiber-Fiber Bond Strength from Paper Mechanical Properties. Proceedings of the International Paper Physics Conference. TAPPI, Atlanta, GA, TAPPI PRESS, 1991. 561–577.

99. Kingsland, A. Personal Communication, 1994. The Institute of Paper Science and Technology, Atlanta, GA.

100. Preston, R.D. The Physical Biology of Plant Cell Walls. 1st ed. London, UK, Chapman and Hall, 1974. 280–330.

APPENDIX 1: FIBER PREPARATION

WOOD ACQUISITION AND HANDLING

Two 28-cm diameter, 152-cm long loblolly pine tree sections were obtained from the Union Camp Corporation Woodlands Division, Savannah, Georgia. The sections were peeled and wrapped in plastic and paper immediately after cutting. They arrived in good condition with no indication of drying and no evidence of biological deterioration.

The logs were cut with a band saw into one-inch pieces (measured along the cylindrical axis). The one-inch thick discs were further sawed into pie-shaped sections. These pie-shaped sections were then cut using a guillotine cutter to remove the 18th summerwood growth ring.

The 18th growth ring of the 25-year old tree was selected for testing because it was well beyond the juvenile wood stage. Only summerwood fibers were desired so the guillotine cutter was used to cut the summerwood chips out of the sections. This worked well provided that the pie-shaped sections were tangentially narrow, so that the arcs of the growth rings were nearly linear. All sections not destined for immediate use were preserved with 1 ml of 0.3% formaldehyde solution and stored in plastic bags at 40°F. After chips were formed, (Figure 1A) any unwanted wood was cut off with a razor blade, including transition wood between growth rings.

The chips were extracted[96] using a Soxhlet extractor with a 1:1 mixture of chloroform-ethanol. The chips were placed for 24 hours in each of the following solvents: 100% methanol, 75% methanol, 50% methanol, 25% methanol, and distilled water. The chips contained 2.56% extractives and 58.73% water.

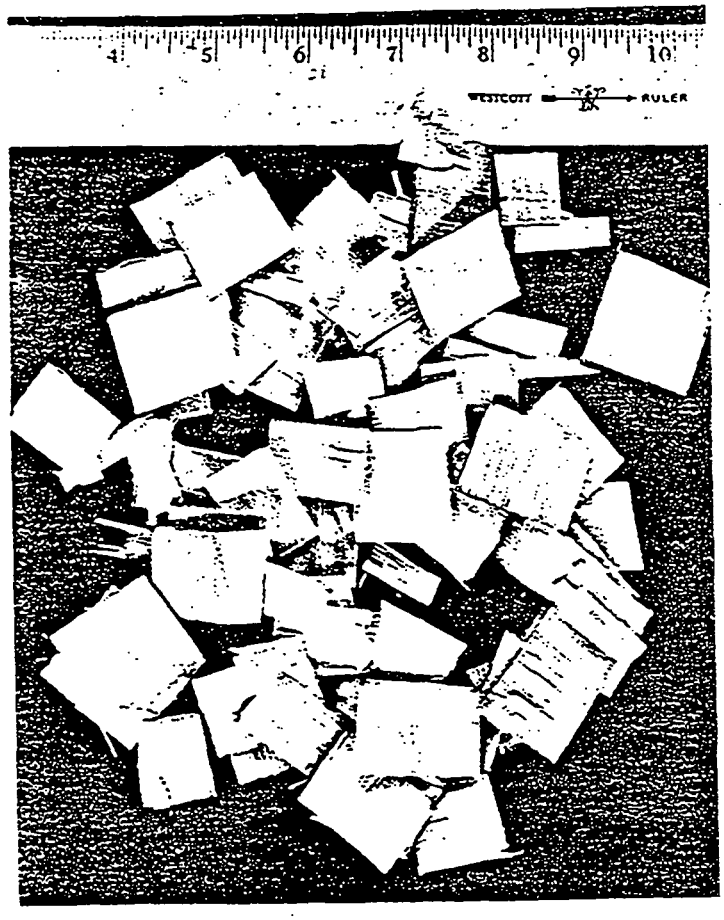

Figure 1A: Summerwood loblolly pine chips.

Holopulping Procedure

The process used to convert wood chips to holocellulose chips uses a mixture of sodium chlorite and acetic acid similar to that of Wise[76] and Thompson and Kaustinen.[77] This mixture produces chlorine dioxide which is required for the delignification process.

A buffered chlorite solution was prepared by adding 60 gm of sodium chlorite and 40 gm of sodium acetate to a 1-liter volumetric flask and filling the flask with distilled water to the mark. Fifty o.d. gm of summerwood chips were placed in a 500-ml Erlenmeyer filter flask. Three hundred ml of buffered chlorite solution and 20 ml of glacial acetic acid were added to the filter flask. The flask was sealed with a stopper and attached to a vacuum line through a three-way stopcock. A vacuum was drawn on the reaction mixture for one hour to remove entrapped air and to assist penetration of the liquor. The reaction, as indicated by evolution of chlorine dioxide, a yellow-green gas, began about one-half hour after the vacuum was released. The filter flask was placed in a dark fume hood. The sodium acetate and acetic acid formed a buffer solution that held the solution pH around 4 for the duration of the chlorite procedure. Upon cessation of the evolution of chlorine dioxide, additional chlorite was used (300 ml of buffered chlorite and 20 ml of glacial acetic acid).

After five chlorite treatments, the solution was filtered using a Buchner funnel in a fume hood. Residual chlorine dioxide was neutralized with sodium sulfite. The solution was disposed of in the acid bleach waste container. The chips were washed with distilled water and transferred back to the Erlenmeyer flask. The chips were soaked in distilled water overnight to allow residual chemical to diffuse out of the chips. The chips were washed and filtered once more. At this time the chips appeared yellow to white, and the fibers on the surface were loose. The chips had hard cores that had not been effectively delignified by the chlorite procedure. Samples tested contained 4.13% Klason lignins. The chips were returned to the Erlenmeyer flask for two additional chlorite treatments. As delignification reached completion, the wood chips became spongy.

Upon completion of the procedure, holopulped samples tested using T22om-88[97] contained 0.178% ± 0.013% Klason lignin. Half the holopulped sample was stored at 40°F for single fiber testing. The remaining holopulped sample was extracted using aqueous alkaline. The extraction procedure (Table 1A) is designed to provide a gradual removal of the various polysaccharides.

Table 1A: Successive extraction of holocellulose fibers.

Extraction Step	
1. Original holocellulose	
2. Hot water	90°C; two 2-hour treatments
3. 0.1N KOH	
4. 0.4N KOH	
5. 1.5N KOH	
6. 1.5N KOH + 0.75M H_3BO_3	
7. 3.0N KOH + 0.75M H_3BO_3	
8. 6.0N KOH + 0.75M H_3BO_3	
9. 6.0N NaOH	

Different polysaccharides are removed during three distinct stages of the extraction sequence. A summary of the extracted fiber stages is listed in Table 2A. In the first stage, which comprises extraction with 90°C water and 0.1N KOH, the galactan is removed preferentially. This is easily understood, since most of the galactan-containing polysaccharides are known to be located in the outside cell wall layers.[36-43]

In the second stage, which comprises extractions with 0.4N and 1.5N KOH, almost all of the xylan based polysaccharides are removed (except <0.1%). In the third stage, which comprises extraction with KOH of increasing concentration, in the presence of borate, the glucomannan is removed preferentially.

Table 2A: Extracted fiber stages.

Fiber Stage	Stage 1	Stage 2	Stage 3
Components Present	Cellulose xylan glucomannan	Cellulose glucomannan	Cellulose
Components Removed	galactan	xylan	glucomannan

Unless otherwise stated, all extractions were carried out at room temperature and consisted of one treatment for two hours, followed by a second identical treatment with fresh reagent for another two hours.

Before placing the pulp in each of the caustic solutions, nitrogen was bubbled through the solution for one-half hour to purge any oxygen. This nitrogen purge continued throughout the extraction to prevent surface absorption of oxygen. A perforated paraffin covering placed over the reaction beaker prevented air from sweeping the surface of the liquid. This exclusion of air minimized any degradative effects of the caustic on the cellulose.

After each extraction, the pulp was washed with distilled water and 1% aqueous acetic acid until a neutral pH was reached. The suspension was washed again with distilled water. The slurry was removed, labeled, and stored at 40°F after the hemicellulose extraction stages were completed.

Carbohydrate compositions for the original holocellulose fibers, extracted hemicellulose fibers through step 8 as described in Table 1A, and the extracted hemicellulose fibers through step 9 as described in Table 1A were carried out in duplicate by capillary-column gas chromatography using a modified TAPPI T249 pm procedure[78] (Table 3A).

Table 3A: Carbohydrate composition.

	Sugar, % o.d. sample weight				
Sample	Arabinan	Xylan	Mannan	Galactan	Glucan
Holopulp	0.6	5.6	16.8	0.5	76.3
Extracted through Step 8	<0.1	<0.1	5.7	<0.1	94.2
Extracted through Step 9	<0.1	<0.1	3.8	<0.1	96.2

Alkaline Degradation of Pulp Samples

In order to obtain information on the extent of degradation of the cellulose caused by the alkali extraction procedure, viscosities[80] were determined for samples after various extraction steps and compared to the viscosity of the unextracted holocellulose (Table 4A). Since there was a significant viscosity change due to the extraction procedure used, it was concluded that the cellulose may have been degraded (Table 5A).

Table 4A: Viscosities.

Sample	Viscosity (cP)	Std. dev.	Number of observations
Unextracted holocellulose	19.3	0.2	5
Extracted with 1.5N KOH	23.7	0.2	4
Extracted with KOH + H_3BO_3	25.8	0.3	4
Extracted with 6.0N NaOH	18.1	0.5	4

Table 5A: Analysis of variance for viscosities.

Effect of extraction on viscosity:

Source	DF	Sum of Squares	Mean Square	F-Ratio
A(Extraction)	3	163.6164	54.5388	553.90**
Error	13	1.2800	0.09846	
Total	16	164.8964		

Term	Count	Mean	Standard Error
All	17	21.61471	
A(Extraction)			
(None) Holocellulose	5	19.338	0.1403
Extracted with 1.5N KOH	4	23.730	0.1568
Extracted with KOH + H_3BO_3	4	25.832	0.1568
Extracted with 6.0N NaOH	4	18.127	0.1568

**Significant at 99% confidence level.

Fiber Characterization

Since wood was selectively hand-chipped, it was desirable to know the percentage of summerwood versus springwood in the fiber sample. Differentiation between springwood and summerwood is based on the cell wall thickness and width of fibers. When stained with "C" stain the springwood fibers have a lighter color. The light microscope was used at magnifications of 40x and 100x, with agreement between the two techniques. At 40x magnification the color differences are more pronounced, but the higher magnification enhances the cell wall. A total fiber count of 1,151 was recorded, with 80.9% being summerwood, 19.1% being springwood.

The width and lumen diameter of 100 holocellulose and 100 extracted holocellulose fibers were measured using 400x magnification on a Zeiss Axioskop with the aid of OPTIMAS image analysis software.[83] Congo Red was used to increase fiber visibility. Computer output included fiber perimeter values, which were calculated as two times fiber width plus four times cell wall thickness. The data from both samples are listed in Tables 6A and 7A.

The net cross-sectional area of each fiber sample was calculated[98] using the following relationship:

$$\text{(Gross Area) - (Lumen Area) = Net Cross-Sectional Area} \qquad (1A)$$

$$W^2\pi/4 - L^2\pi/4 = \text{Net Cross-Sectional Area} \qquad (2A)$$

Using the above relationship, the cross-sectional area for the holocellulose fiber sample is 537 μm^2 and the cross-sectional area for the extracted holocellulose fiber sample is 633 μm^2. When applying a 20-gm tensile load to the single fibers, the engineering stress was calculated to be 36.8×10^8 dynes/cm^2, for a holocellulose fiber and 31.2×10^8 dynes/cm^2 for an extracted holocellulose fiber.

Microfibril Angle

The average microfibril angle of several pulp samples was measured at the Pulp and Paper Research Institute of Canada using Page's technique.[99] Fibers were mercury impregnated and viewed

through a polarizing microscope with vertical illumination.[100] A rotating stage calibrated in degrees allowed the angle between the longitudinal axis of the fiber and the microfibrils to be reported.

Table 8A: Microfibril angle in degrees.

Sample	Microfibril Angle(Std. Dev.)
Unextracted holocellulose	32.0 ± 6.03
Extracted with KOH + H_3BO_3 (through step 8)	29.2 ± 6.22
Extracted with 6.0N NaOH (through step 9)	26.3 ± 5.46

Table 6A: Holocellulose fiber width (FW), lumen width (LW), and wall thickness (CW1, CW2).

	FW	LW	CW1	CW2		FW	LW	CW1	CW2
1	28.55	11.71	8.21	8.64	51	27.57	14.06	8.21	5.30
2	31.15	12.88	7.02	11.25	52	26.25	9.37	7.03	9.84
3	25.98	10.54	9.36	6.09	53	25.69	12.88	5.86	6.95
4	22.23	8.20	5.86	8.17	54	26.79	15.25	5.87	5.67
5	36.22	17.58	9.38	9.25	55	23.74	10.56	4.69	8.49
6	31.17	12.92	7.04	11.21	56	30.47	17.58	7.03	5.86
7	21.14	12.92	3.52	4.70	57	31.64	19.94	5.86	5.83
8	33.93	17.55	7.02	9.36	58	25.94	7.04	9.37	9.53
9	26.22	9.40	8.22	8.60	59	25.34	11.71	8.20	5.43
10	32.82	14.07	9.37	9.38	60	19.46	10.52	4.68	4.25
11	29.77	11.71	8.20	9.86	61	30.54	10.58	10.56	9.41
12	31.66	10.56	10.55	10.55	62	25.47	12.90	7.04	5.53
13	32.84	18.78	7.03	7.03	63	31.19	10.54	10.53	10.12
14	21.07	8.20	7.03	5.85	64	38.66	19.95	10.56	8.15
15	35.80	12.89	12.89	10.01	65	36.35	15.22	12.88	8.24
16	34.76	14.06	11.72	8.99	66	29.56	8.20	11.71	9.65
17	32.36	14.07	10.56	7.73	67	33.99	17.58	7.03	9.38
18	38.06	11.71	11.71	14.63	68	36.17	11.75	12.92	11.51
19	33.36	18.77	5.86	8.73	69	30.45	7.03	11.71	11.71
20	35.12	23.42	7.02	4.69	70	33.97	14.06	14.06	5.85
21	28.94	15.23	5.87	7.84	71	35.14	22.26	7.03	5.86
22	30.71	10.54	9.37	10.80	72	22.58	8.19	5.86	8.53
23	37.45	8.20	14.04	15.20	73	24.64	15.25	4.69	4.69
24	24.57	5.87	8.21	10.49	74	26.15	7.01	11.71	7.42
25	36.31	9.38	11.73	15.20	75	25.81	8.18	9.37	8.26
26	29.36	8.23	9.39	11.75	76	31.52	11.74	8.22	11.55
27	16.58	5.86	5.87	4.85	77	26.01	12.92	7.05	6.04
28	32.87	15.26	10.57	7.04	78	28.16	11.73	4.70	11.74
29	27.07	15.22	5.86	5.99	79	25.19	12.88	4.68	7.62
30	19.74	10.53	4.69	4.52	80	29.31	11.72	10.55	7.03
31	21.11	9.37	5.87	5.87	81	25.00	12.89	5.86	6.26
32	37.09	17.55	9.37	10.17	82	29.86	16.42	5.85	7.59
33	21.97	11.71	4.68	5.57	83	37.33	18.76	9.38	9.19
34	25.80	16.41	4.69	4.70	84	11.69	4.67	3.52	3.51
35	26.96	14.06	5.86	7.04	85	23.43	9.36	5.86	8.20
36	31.95	11.75	9.39	10.80	86	30.52	17.58	8.20	4.74
37	29.06	10.57	9.39	9.09	87	26.42	12.93	7.05	6.43
38	18.54	7.05	5.87	5.62	88	37.89	24.62	7.04	6.24
39	24.50	12.87	5.86	5.77	89	29.84	9.40	10.55	9.89
40	37.20	17.57	9.37	10.27	90	36.37	21.11	8.21	7.04
41	28.27	12.89	8.21	7.17	91	26.17	8.21	8.20	9.76
42	19.40	4.68	8.19	6.53	92	28.21	18.76	4.69	4.76
43	29.02	5.87	14.08	9.07	93	31.45	19.93	5.86	5.66
44	30.53	17.62	7.05	5.87	94	31.30	16.40	7.04	7.86
45	24.47	12.88	8.20	3.40	95	32.15	22.26	5.86	4.03
46	35.14	14.07	11.72	9.34	96	39.24	18.75	11.72	8.77
47	38.66	23.43	8.20	7.03	97	33.94	15.27	10.58	8.09
48	21.28	5.86	7.04	8.39	98	25.25	10.54	7.03	7.68
49	29.75	8.20	11.71	9.84	99	40.89	24.65	7.04	9.20
50	27.23	12.89	7.03	7.31	100	32.79	16.39	8.20	8.20

Arithmetic average fiber width (W)	=	29.29	microns
Arithmetic average lumen diameter (L)	=	13.21	microns
Arithmetic average fiber wall thickness	=	8.04	microns
Runkel ratio (W-L)/Average lumen width	=	1.22	microns
Perimeter (2xW) + (4x(W-L)/2)	=	90.75	microns
Standard Deviation (fiber width)	=	5.59	
Standard Deviation (lumen width)	=	4.62	
Standard Deviation (wall thickness)	=	2.49	

Table 7A: Extracted holocellulose fiber width (FW), lumen diameter (LW), and wall thickness (CW1, CW2).

	FW	LW	CW1	CW2		FW	LW	CW1	CW2
1	35.05	9.38	10.56	15.11	51	33.97	11.72	10.54	11.71
2	35.31	7.02	14.07	14.22	52	30.86	10.55	10.56	9.75
3	22.49	4.69	8.20	9.60	53	30.91	8.19	11.71	11.01
4	24.61	10.54	5.87	8.21	54	40.97	15.22	12.87	12.88
5	35.21	5.87	14.08	15.26	55	36.42	14.07	10.55	11.79
6	36.63	7.03	17.59	12.00	56	29.43	9.38	10.55	9.50
7	28.64	7.05	11.74	9.85	57	34.53	14.07	9.38	11.08
8	33.82	10.58	11.75	11.49	58	30.62	11.72	10.55	8.35
9	26.01	10.58	8.22	7.21	59	30.24	12.88	9.37	7.99
10	29.52	12.88	10.54	6.09	60	25.14	10.53	8.20	6.41
11	30.12	9.39	8.23	12.50	61	25.07	14.08	4.70	6.29
12	30.33	8.22	9.39	12.72	62	32.81	11.72	10.90	10.20
13	28.38	10.54	7.04	10.79	63	28.46	9.37	8.20	10.90
14	29.94	11.71	8.19	10.04	64	26.95	12.91	8.23	5.81
15	26.46	11.74	7.05	7.67	65	25.84	8.23	8.22	9.40
16	31.80	7.01	11.71	13.08	66	46.81	21.06	10.54	15.21
17	30.12	5.87	10.57	13.68	67	38.01	14.05	10.55	13.40
18	20.09	5.87	7.05	7.18	68	35.32	12.89	8.21	14.22
19	17.89	7.04	3.53	7.32	69	37.53	11.74	11.73	14.06
20	15.84	5.84	4.69	5.31	70	34.47	8.20	14.04	12.23
21	31.53	5.88	11.73	13.92	71	24.05	10.55	7.04	6.46
22	36.22	9.39	12.90	13.93	72	36.71	17.62	9.40	9.69
23	32.99	11.74	11.74	9.50	73	39.83	15.24	11.71	12.88
24	29.56	8.20	8.20	13.17	74	27.54	9.37	8.20	9.98
25	18.31	9.38	5.86	3.07	75	30.87	12.89	9.38	8.59
26	27.31	11.73	8.21	7.37	76	30.77	11.74	11.74	7.30
27	22.91	7.03	9.37	6.51	77	28.21	10.54	6.19	11.48
28	28.18	15.26	5.86	7.06	78	23.40	9.37	4.68	9.35
29	31.11	15.26	7.04	8.81	79	28.35	8.22	9.38	10.75
30	32.74	15.23	8.21	9.30	80	28.03	8.21	9.39	10.43
31	30.46	14.08	8.21	8.18	81	33.11	12.90	9.39	10.81
32	22.62	8.20	7.03	7.40	82	31.40	15.22	7.03	9.15
33	22.65	8.21	7.03	7.41	83	32.98	11.72	10.55	10.71
34	34.45	18.75	9.37	6.33	84	32.63	10.55	10.55	11.54
35	32.79	11.71	11.71	9.37	85	32.87	15.26	12.91	4.69
36	28.82	10.54	9.37	8.92	86	33.22	12.89	10.56	9.77
37	31.50	11.73	10.56	9.21	87	34.67	12.90	10.55	11.22
38	26.06	8.22	9.39	8.45	88	30.38	14.09	7.04	9.25
39	28.15	8.21	9.38	10.56	89	28.10	12.87	5.86	9.37
40	27.56	7.05	8.22	12.29	90	25.39	14.06	5.86	5.47
41	26.10	4.69	10.57	10.84	91	25.77	14.06	7.03	4.68
42	32.98	12.89	8.21	11.88	92	41.49	15.26	12.91	13.32
43	32.57	15.26	3.53	13.79	93	44.00	22.28	11.74	9.98
44	28.10	8.19	8.20	11.71	94	30.45	14.05	5.86	10.54
45	27.17	11.70	7.03	8.44	95	25.84	12.89	5.87	7.09
46	41.01	17.58	10.55	12.89	96	33.26	16.38	8.20	8.69
47	31.07	11.71	9.38	9.97	97	35.89	19.91	7.03	8.94
48	37.13	17.55	8.19	11.38	98	31.20	9.37	9.38	12.45
49	32.08	16.40	9.38	6.30	99	40.13	16.38	11.70	12.05
50	30.73	15.23	8.21	7.29	100	27.18	11.72	6.19	9.27

Arithmetic average fiber width (W)	=	30.67	microns
Arithmetic average lumen diameter (L)	=	11.61	microns
Arithmetic average fiber wall thickness	=	9.53	microns
Runkel ratio (W-L)/Average lumen width	=	1.64	microns
Perimeter (2xW) + (4x(W-L)/2)	=	99.48	microns
Standard Deviation (fiber width)	=	5.38	
Standard Deviation (lumen width)	=	3.61	
Standard Deviation (wall thickness)	=	2.57	

APPENDIX 2: APPARATUS

LOAD MEASUREMENT

The Scientec, Inc. model 202–001 electronic balance cell combines substantial load range and good sensitivity. The full scale load is 50 grams in tension or compression with sensitivity of 1 mg. The weighing speed is 0.08 seconds. The cell is cylindrical in shape and suspended from a mounting plate by four spring tempered, phosphorous bronze, flexure strips, which allow easy motion along the load axis but rigid constraint in all other directions. The ± 5 volt DC scale output of the load measuring system is applied directly to a personal computer and board.

Calibration is accomplished by hanging weights from the end of a thread attached to the active clamp and passing over a ball-bearing pulley supported by the right hand clamp structure. Using this method, an average weight/voltage value of 21.39 gms/volt was determined. Collected data is reported in Table 9A. The linear fit, $y = a + b(x)$, where $a = 1.712 \times 10^{-5}$, $b = 4.675 \times 10^{-2}$, has a correlation coefficient of $R^2 = 1.000$.

Table 9A: Load cell calibration.

x (grams)	y (volts)
2	0.0935
5	0.2338
10	0.4675
20	0.9350
50	2.3375

A relationship between voltage output and the Fiber Load Elongation Apparatus II (FLERII) load dial setting was determined by placing a paper clip into the FLERII and following the single fiber axial tensile test method described in a following section. The relationship for the voltage output and the dial setting was 0.91 volts/dial setting. The single fiber axial tensile tests will be run using a 20-gram load which corresponds to a FLERII dial setting of 6.03.

DEFORMATION MEASURMENT

When a fiber is loaded, it undergoes a dimensional change. This change is measured directly and without interfering with the load measurement by using an Accumeasure System 1000 capacitance transducer directly at the active clamp. The ASP-20 sensor has a 0.5-mm full scale range and a 0.5-μm sensitivity. A model AS1021PA amplifier (serial number 830676) is used in conjunction with the sensor and is mounted in an electronics rack. Its 0–10-volt output is applied to a personal computer and board.

Displacement sensor calibration is accomplished by placing the sensor in the calibration jig and displacing a screw micrometer head a specified distance. The voltage output from the sensor is recorded at each distance interval. The calibration data is reported in Table 10A.

Table 10A: ASP1021PA Calibration.

Point Number	x(mils)	y(volts)	y1(volts)	y1-y(volts)
1	2.0000	0.9970	0.9997	-0.0027
2	4.0000	2.0020	1.9993	0.0027
3	6.0000	3.0000	2.9990	0.0010
4	8.0000	3.9980	3.9987	-0.0007
5	10.0000	5.0000	4.9984	0.0016
6	12.0000	5.9990	5.9980	0.0010
7	14.0000	6.9950	6.9977	-0.0027
8	16.0000	7.9960	7.9974	-0.0014
9	18.0000	8.9960	8.9971	-0.0011
10	20.0000	9.9990	9.9967	0.0023

The linear fit, $y1 = a + b(x)$, where $a = 0.00000000$, $b = 0.49983636$, has a correlation coefficient of $R^2 = 0.99999958$. The percent error versus the displacement distance of the micrometer head from the sensor is plotted in Figure 2A. The conversion factor relating the voltage output to the test specimen displacement is 5.08166×10^{-2} mm/volt.

Figure 2A: Percent error versus gap.

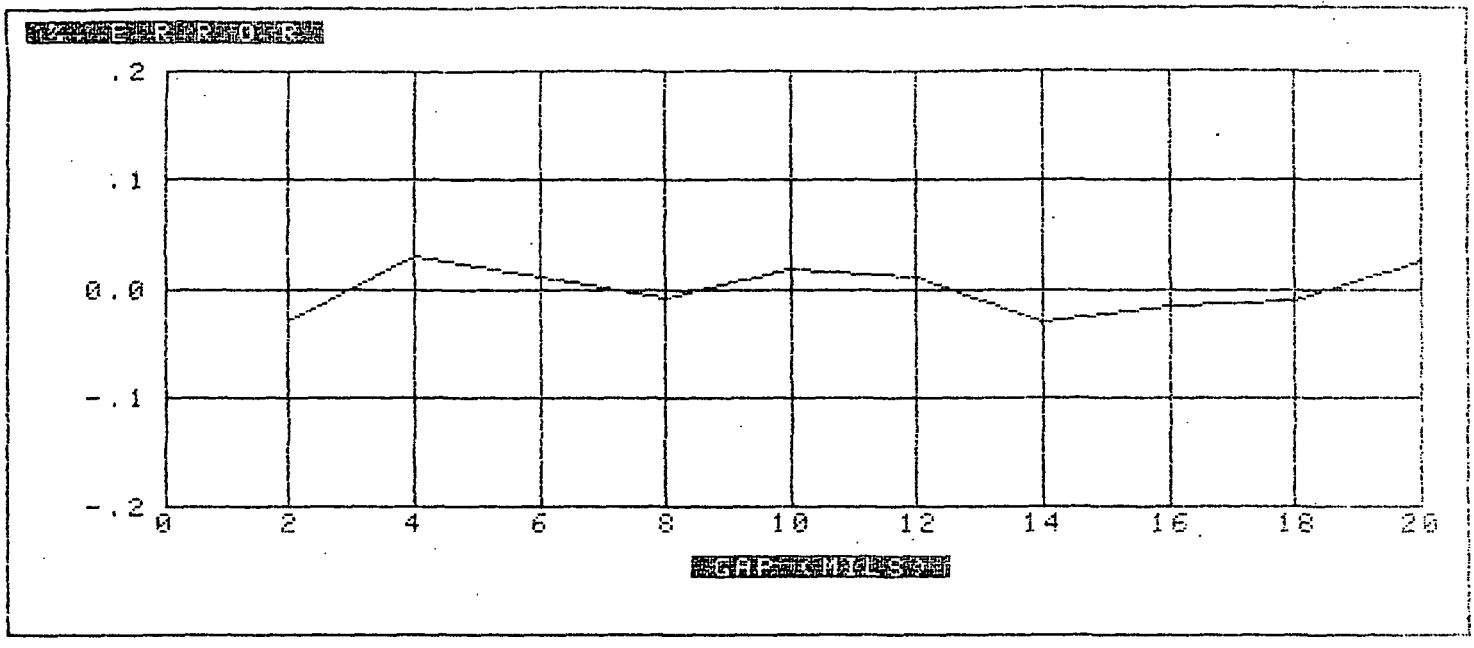

LOAD APPLICATION

Load is applied by moving the electronic balance cell along the load axis with a differential screw. An Electro-Craft E352-MG motor-generator turns the screw and is mounted on a PIC PB2-20 precision ball slide to translate the screw. It is necessary to replace brushes in the motor after 3,000 hours of working time. The motor is driven in servo mode through an Electro-Craft series E-352-b controller, which moves the motor to null the difference between a reference voltage and a feedback voltage.

The reference voltage is a reference ramp, generated as described in the next section. The feedback voltage is the load output signal, so the apparatus is operated in a constant rate of loading. If the ramp is halted, the constant load is maintained with respect to time.

Ramp Generator

Control of fiber loading is centered in the linear ramp generator, which produces the reference voltage for servo-motor control. A relationship between the loading rate and the FLERII dial setting was determined by placing a paper clip into the FLERII and recording the data listed in Table 11A.

Table 11A: Loading rate dial setting.

Dial Setting	Loading Rate(gm/sec)	Loading Rate(gm/sec dial unit)
100	5.9740	0.05974
200	11.2750	0.05638
300	17.7704	0.05907
600	35.1392	0.05857
900	51.3414	0.05705

The average loading rate for each unit dial setting is 0.05816 ± 0.00141 gm/sec. The single fiber axial tensile tests are run using a loading rate of 1.0 gm/sec which corresponds to a dial setting of 17.2.

ADJUSTMENT OF MOISTURE CONTENT

The apparatus is located in a 50%-RH, 73°F-room. For various relative humidities, provision has been made to surround the specimen with air-conditioned to various moisture levels. This is accomplished by mixing dry house air (at 10 psig) with filtered house air (at 23 psig) which has been saturated with moisture by passing it as a stream of fine bubbles through a five-foot water column. A Vaisala model HMP 35 probe and HMI 32 indicator unit give readings of the temperature and relative humidity of the mixed gas. The probe response time is five seconds. The temperature measurement range is -40 to +60°C (-40 to +140°F). The temperature dependence is ±0.04% RH/°C. The humidity range is about 3 to 100% RH. The accuracy of the probe against field references is ±2% RH (0–90% RH) and ±3% RH (90–100% RH). The gas inlet tube is positioned directly across from the relative humidity sensor. The Vaisala HMP35 probe is calibrated using saturated solutions of potassium acetate (22.9% RH), potassium chromate (86.5% RH), and ammonium monophosphate (92.9% RH) in a hydroexpansivity cabinet.

The water column was designed to facilitate cleaning of the column and the screen at the bottom of the column. Settling of biological sediment on the inside of the tank and in the screen pores can decrease the ability to attain 90% RH. The design allows access to the full diameter of the tank at the top and bottom. The screen is removable and can be pressure-washed to remove any blockages in the pores.

The relative humidity chamber inside the FLERII (Figure 3A) completely encloses the fiber test specimen and allows for shorter cycling times during testing. The relative humidity sensor is directly across form the relative humidity sensor. The air chamber has a removable front cover which allows the insertion of the fiber into the fiber holders. The front cover is perforated to allow continued fresh air flow into the chamber.

Figure 3A: Relative humidity chamber.

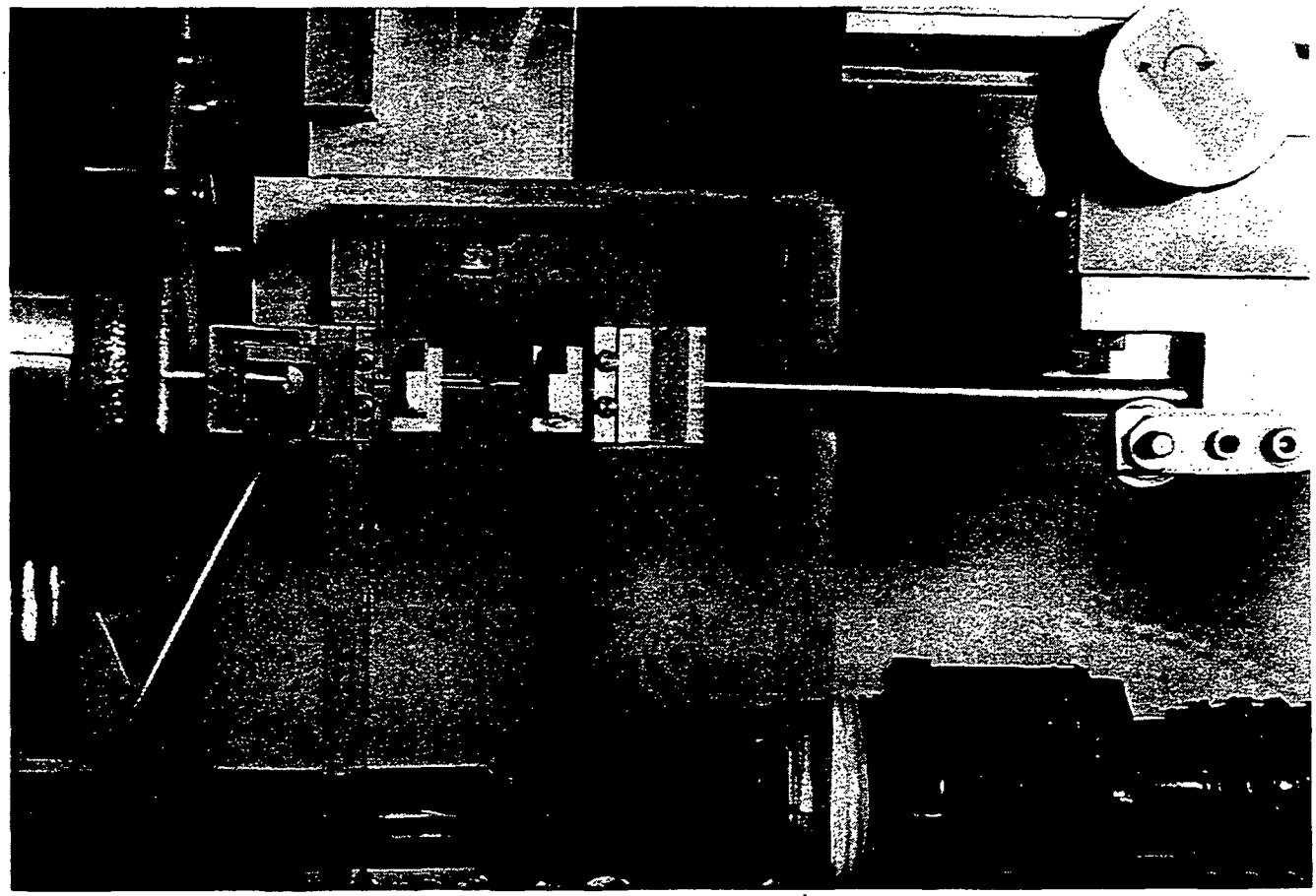

FIBER HOLDER DESIGN

The fiber holder and pins design is illustrated in Figure 4A. There are 16 machine-matched fiber holder and pin sets. The pins holding the fibers are placed into machined slots with specified tolerances.

The left-hand part containing the machined slot for the fiber pin is permanently epoxied using EPOXI-PATCH 907 BLUE and screwed into the active clamp. The active clamp is attached to the axially mounted sensing member of the electronic balance cell. This is the clamp through which the load is applied to the fiber. The left-hand part design is illustrated in Figure 5A. A similar right-hand counterpart containing a machined slot for a right-hand fiber pin is permanently epoxied and screwed into the right clamp attached to the adjustable FLERII arm. The right-hand part design is illustrated as Figure 6A. Visible slop between the pin and the machined right-hand part and the pin and the machined left-hand part can be partially removed manually with the FLERII fine adjustment knob. Additional slop in the system can be compensated for by the computer record of load and displacement.

Figure 4A: Fiber Holder/Pins

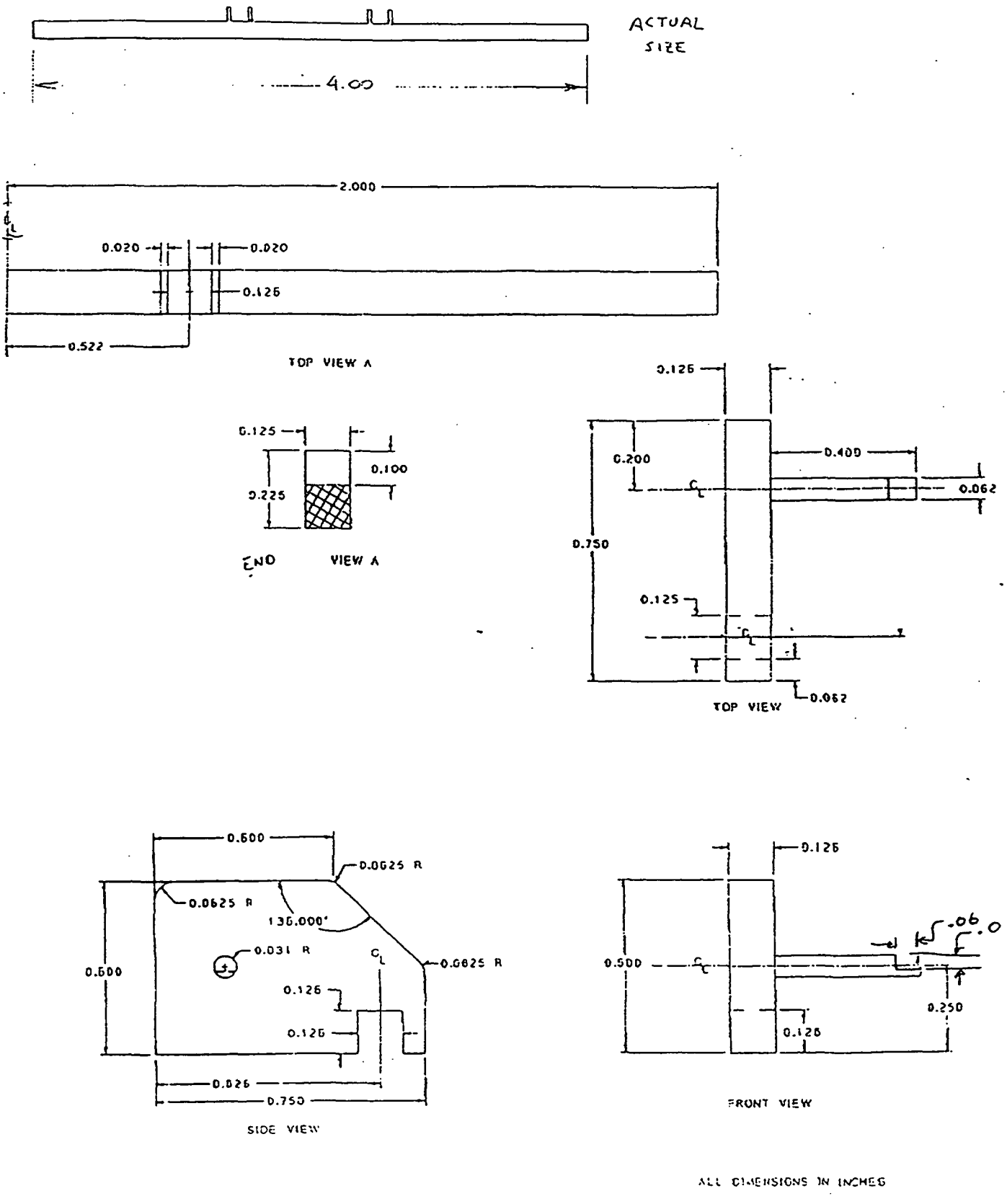

Figure 5A: Left-Hand (Load Cell) Pin Holder

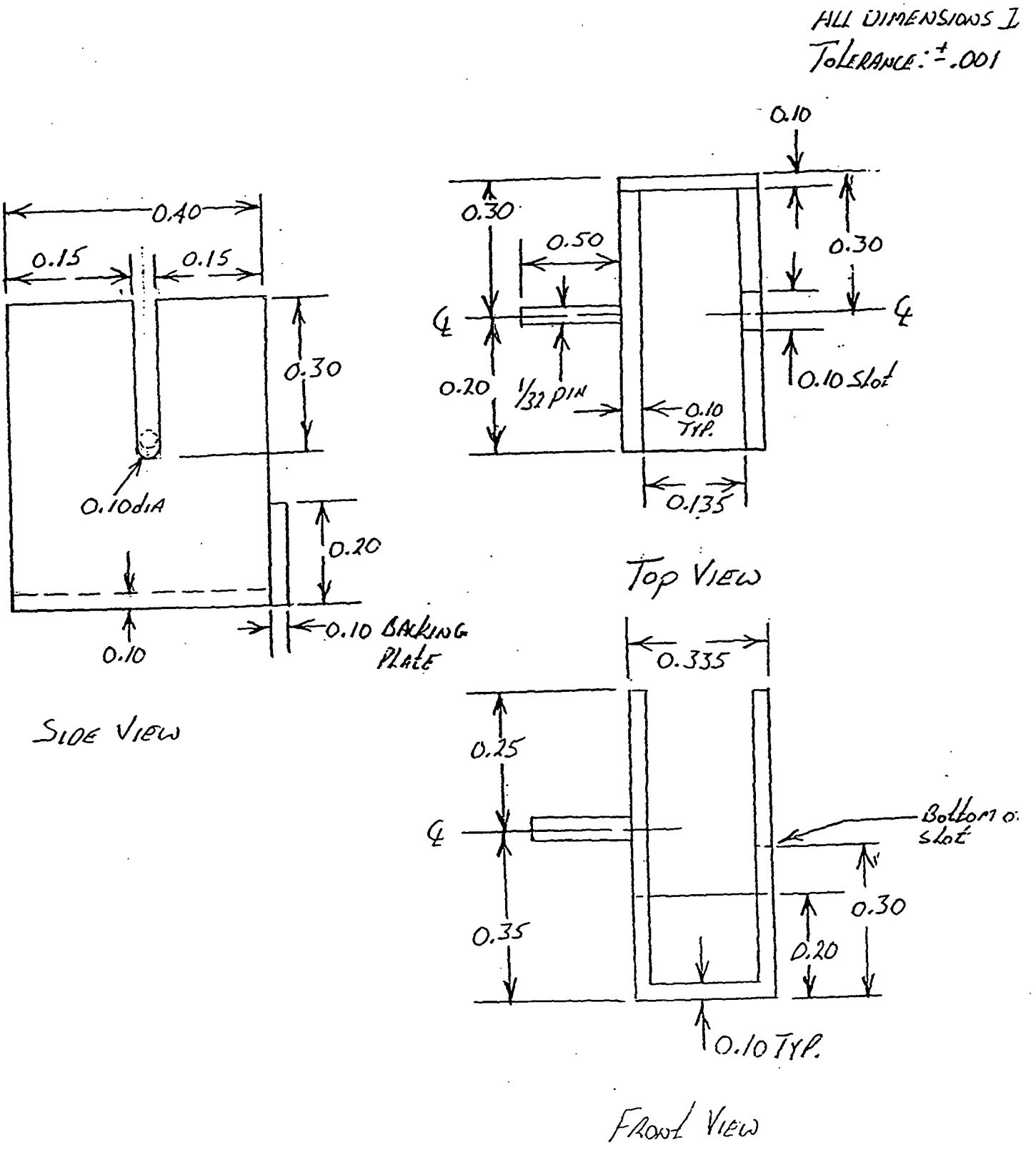

Figure 6A: Right-Hand (Adjustable Arm) Pin Holder

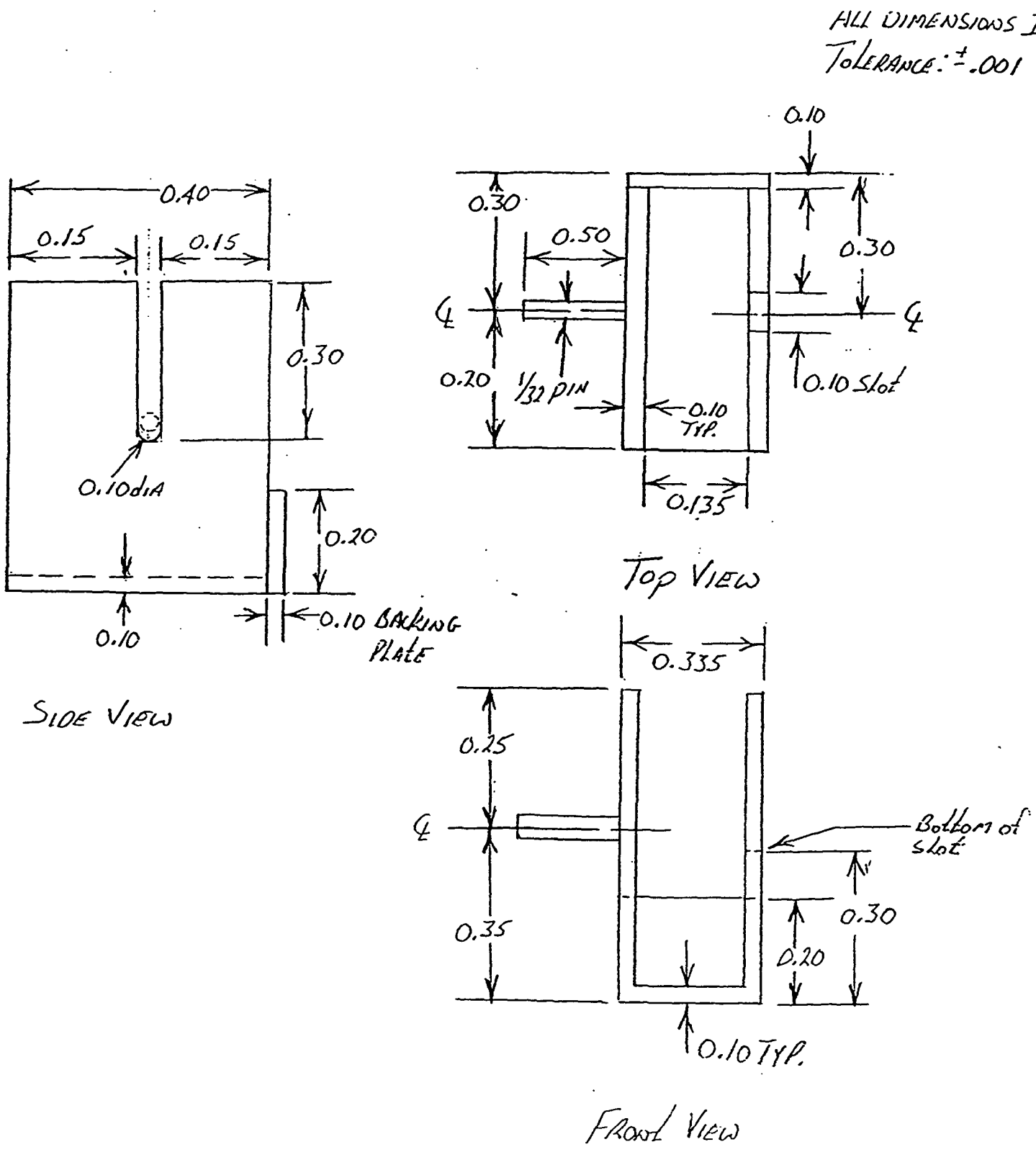

FIBER MOUNTING

A minute amount of fibers was placed on a black glass plate. A single drop of water was added to the fibers to make a very dilute slurry. With the aid of a low magnification stereoscope, single fibers were pulled at one end from the slurry with a dissecting probe. Using the probe, the ends of the single fiber were tacked to the glass plate to prevent the fiber from shrinking and curling while drying.

An epoxy resin, EPOXI-PATCH 907 BLUE, was used to mount single fibers on a set of pins. The epoxy, formerly called EPON 907 as used by Speigelberg,[43] was purchased from the Dexter Adhesives and Structural Materials Division of the Dexter Corporation. The epoxy was mixed using a 10:6 ratio by weight of resin to hardener component. Using a dissecting probe, epoxy was placed on the flat portion of each pin in the fiber holder set. Care was taken not to overload the pins with epoxy. Using excessive amounts of epoxy would have caused the epoxy to creep from the pins onto the fiber. Wicking of the epoxy into the fiber was not noted by Speigelberg[43] or Hill.[6] The fiber holder set was then placed under the stereoscope. Using a clean probe, a single dried fiber was lifted from the glass plate by one end of the fiber. The fiber end on the probe was depressed into one of the epoxied pins, followed by the other end in the corresponding pin so the axial alignment could be adjusted. The glue line was brought to a well defined edge. After each fiber was affixed in a fiber holder set, the fibers were checked under higher magnification for any curl or twisting which would cause the fiber to be rejected. A matched fiber holder set containing an epoxied fiber is shown in Figure 7A. Mounted fibers were dried in 73°F and 50% RH laboratory for at least 24 hours prior to testing.

Before loading each sample, the distance between the left-hand (load cell) pin holder and the right-hand (adjustable arm) pin holder is adjusted using an empty fiber holder and pin set. Then the single fiber axial tensile test procedure is followed using a fiber sample. Before straining, fibers were rechecked for straightness, parallelism to the strain direction and damage during mounting; the span length could be accurately measured.

Single Fiber Axial Tensile Test

1. Turn power on.

2. Simultaneously slide fiber holder and pin set sample into the left-hand (load cell) and the right-hand (adjustable arm) pin holder.

    a. Release or allow the fiber holder (bar) to fall out of the pin set.

    b. Remove the fiber holder (bar) from the FLERII relative humidity chamber since it will rust in humid environments (Figure 3A).

    c. Adjust coarse and fine knobs of adjustable arm to zero out load.

3. Set zero position of load cell.

    a. Switch OFFSET out.

    b. Turn differential screw by hand until elongation meter reads about 15.

    c. Flip OFFSET switch in and adjust offset control so that elongation output meter (on same panel as RH meter) reads zero. Lock control. (Both load and elongation indictor meters should return to zero.)

    d. Apply 0.1 gram to the test fiber.

    e. Measure length of test fiber using a stereoscope.

4. Flip servo on.

5. Rezero with offset in.

6. Prepare for test.

    a. Preset ramp generator controls as desired.

    b. Set FEEDBACK switch to LOAD.

    c. Lock adjustable arm in place.

    d. Start designated LABTECH CONTROL program.

7. Test.

    a. Push SET.

    b. Push PULL.

    c. Push RUN.

8. Flip servo switch off immediately following test.

Figure 7A: Fiber holder set.

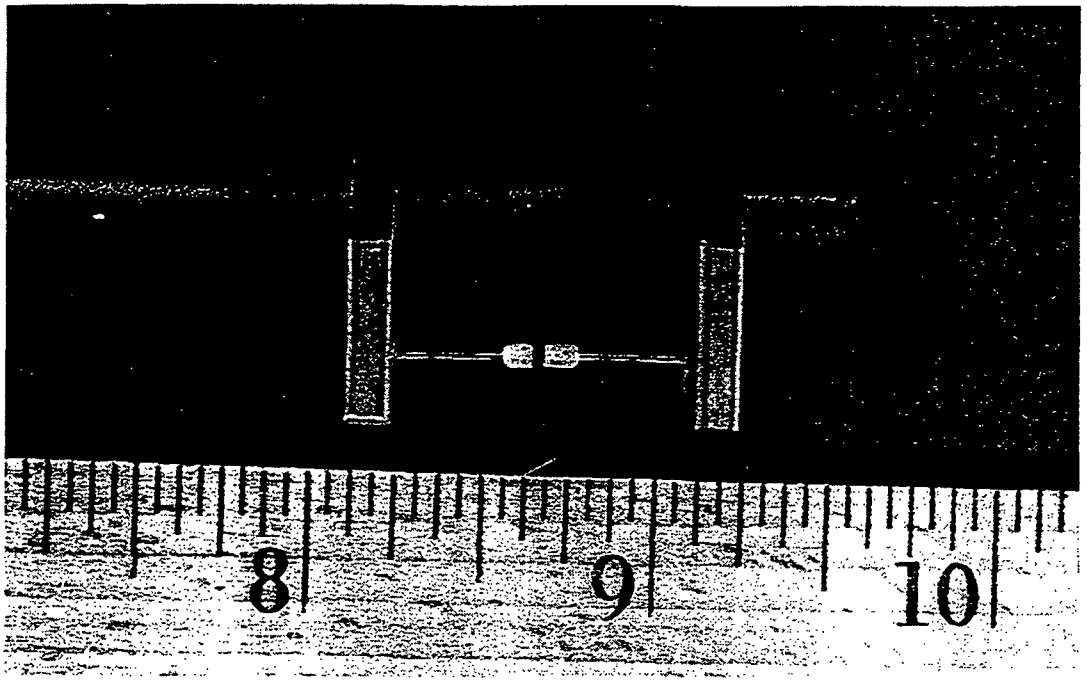

Visual Observation

An AO Stereostar/Zoom microscope (562"C," with 25X eyepieces) and a Starlite illuminator have been mounted so that the fiber length may measured after mounting. The magnification range is 17.5X to 105X with an adequately long working distance of four inches.

Programming for Testing

Version 3.1.0 of the software LABTECH CONTROL was used to write basically four types of testing programs: constant humidity creep and constant humidity moisture pickup, cyclic humidity creep, creep recovery, and various loadings and unloadings. The software was obtained from LABTECH in Wilmington, Massachussetts. All fibers were loaded at 1 gram/sec to a maximum load of 20 grams. Data in the form of stress, strain, time, and relative humidity were recorded every 0.2 second for the first 3 minutes. After loading, rate of data collection is specified to accommodate each testing program need. All programs are included as Figures 8A-10A.

Figure 8A: Programming for constant humidity creep and constant humidity moisture pickup measurements.

Programming for Constant Humidity Creep and Constant Humidity Moisture Pickup Measurements
LABTECH CONTROL Global Setup Checking MODE: Normal

Bl.	Block	Intfc	Block	Block	Scale	Offset	Iter	S	Stage Information	File	Sc	Wd No.	Name	Dev Ch	Function	Info.	Factor
	t	Duration	Rate	Start	Tr.	Trigger	Name	#	#					g	(sec)	(Hz)	State	Ch.	Level	(first)	
1	Setpoint			Replay	wf1.prn	100.000	0.000	1	1	0.000	1.000	Keypress	1	0.000							
	2	1.72E+05	1.67E-03	Normal	1	0.000															
2	DUMMY OUTPUT	1	1	Analog Out	PID(10)	1.000	0.000	1	1	0.000	1.000	Keypress	1	0.000							
	2	0.500	3.000	Normal	1	0.000															
3	Constant			1	0.000	120.000	0.000	1	1	0.000	1.000	Keypress	1	0.000					2	1.72E+05	
	1.66E-03	Normal	1	0.000																	
4	Dry air setpoin			(3)-(1)	0.000	1.000	0.000	1	1	0.000	1.000	Keypress	1	0.000					2	1.72E+05	
	1.000	Normal	1	0.000																	
5	LOAD, GRAMS	1	2	Analog In	0..5 V	21.390	0.000	2	1	180.000	5.000	Keypress	1	0.000	c:\ltc\data*	1	1				
	2	8.64E+04	1.67E-02	Normal	1	0.000															
6	DISPLACEMENT, m	1	3	Analog In	0..10 V	5.08E-02	0.000	2	1	180.000	5.000	Keypress	1	0.000	c:\ltc\data*	1	3				
	2	8.64E+04	1.67E-02	Normal	1	0.000															
7	Time[Ld/Dis]			Time	Elapsed			2	1	180.000	5.000	Keypress	1	0.000	c:\ltc\data*						
	2	8.64E+04	1.67E-02	Normal	1	0.000															
8	% RH	1	1	Analog In	0..1 V	99.100	0.000	2	1	180.000	5.000	Keypress	1	0.000	c:\ltc\data*						
	2	8.64E+04	1.67E-02	Normal	1	0.000															
9	Dry air Output	1	1	Analog Out	PID(4)	2.00E-02	2.600	2	1	0.000	1.000	Keypress	1	0.000							
	2	8.64E+04	1.000	Normal	1	0.000															
10	% RH	1	1	Analog In	0..1 V	99.100	0.000	2	1	0.000	1.000	Keypress	1	0.000		1	2				
	2	8.64E+04	1.000	Normal	1	0.000															
11	WET AIR OUTPUT	1	0	Analog Out	PID(10)	2.00E-02	3.000	2	1	0.000	1.000	Keypress	1	0.000							
	2	8.64E+04	1.000	Normal	1	0.000															
12	Load setpt			Replay	wf1.prn	1.000	0.000	1	1	19.000	1.000	Keypress	1	0.000							
13	LOAD, GRAMS	1	2	Analog In	0..5 V	21.390	0.000	2	1	0.000	1.000	Keypress	1	0.000		1	4				
	2	8.64E+04	20.000	Normal	1	0.000															
14	MOTOR DRIVE	0	0	Analog Out	PID(13)	4.68E-02	0.000	2	1	1.000	20.000	Keypress	1	0.000							
	2	8.64E+04	20.000	Normal	1	0.000															
15	MOTOR CURRENT	1	0	Analog In	0..5 V	1.000	0.000	2	1	0.000	1.000	Keypress	1	0.000							
	2	8.64E+04	5.000	Normal	1	0.000															

Setup OK

Interface Devices:
0: PCL-818/780
1: PCL-818/780

Figure 9A: Programming for cyclic humidity creep.

Programming for Cyclic Humidity Creep Measurements
LABTECH CONTROL Global Setup Checking MODE: Normal

Bl.	Block	Intfc	Block	Block	Scale	Offset	Iter	S	Stage Information	File	Sc	Wd No.	Name	Dev Ch	Function	Info.	Factor
		t	Duration	Rate	Start	Tr.	Trigger	Name	#	#				g	(sec)	(Hz)	State	Ch.	Level	(first)	
1	Setpoint			Replay	wf1.prn	100.000	0.000	1	1	0.000	1.000	Keypress	1	0.000							
	2	1.72E+05	1.67E-03	Normal	1	0.000															
2	DUMMY OUTPUT	1	1	Analog Out	PID(10)	1.000	0.000	1	1	0.000	1.000	Keypress	1	0.000							2
	0.500	3.000	Normal	1	0.000																
3	Constant			1	0.000	120.000	0.000	1	1	0.000	1.000	Keypress	1	0.000						2	1.72E+05
	1.66E-03	Normal	1	0.000																	
4	Dry air setpoin			(3)-(1)	0.000	1.000	0.000	1	1	0.000	1.000	Keypress	1	0.000						2	1.72E+05
	1.000	Normal	1	0.000																	
5	LOAD, GRAMS	1	2	Analog In	0..5 V	21.390	0.000	2	1	180.000	5.000	Keypress	1	0.000	c:\ltc\data*	1	1				
	2	8.64E+04	1.67E-02	Normal	1	0.000															
6	DISPLACEMENT, m	1	3	Analog In	0..10 V	5.08E-02	0.000	2	1	180.000	5.000	Keypress	1	0.000	c:\ltc\data*	1	3				
	2	8.64E+04	1.67E-02	Normal	1	0.000															
7	Time[Ld/Dis]			Time	Elapsed			2	1	180.000	5.000	Keypress	1	0.000	c:\ltc\data*						
	2	8.64E+04	1.67E-02	Normal	1	0.000															
8	% RH	1	1	Analog In	0..1 V	99.100	0.000	2	1	180.000	5.000	Keypress	1	0.000	c:\ltc\data*						
	2	8.64E+04	1.67E-02	Normal	1	0.000															
9	Dry air Output	1	1	Analog Out	PID(4)	2.00E-02	2.600	2	1	0.000	1.000	Keypress	1	0.000							
	2	8.64E+04	1.000	Normal	1	0.000															
10	% RH	1	1	Analog In	0..1 V	99.100	0.000	2	1	0.000	1.000	Keypress	1	0.000		1	2				
	2	8.64E+04	1.000	Normal	1	0.000															
11	WET AIR OUTPUT	1	0	Analog Out	PID(10)	2.00E-02	3.000	2	1	0.000	1.000	Keypress	1	0.000							
	2	8.64E+04	1.000	Normal	1	0.000															
12	Load setpt			Replay	wf1.prn	1.000	0.000	1	1	19.000	1.000	Keypress	1	0.000							
13	LOAD, GRAMS	1	2	Analog In	0..5 V	21.390	0.000	2	1	0.000	1.000	Keypress	1	0.000		1	4				
	2	8.64E+04	20.000	Normal	1	0.000															
14	MOTOR DRIVE	0	0	Analog Out	PID(13)	4.68E-02	0.000	2	1	1.000	20.000	Keypress	1	0.000							
	2	8.64E+04	20.000	Normal	1	0.000															
15	MOTOR CURRENT	1	0	Analog In	0..5 V	1.000	0.000	2	1	0.000	1.000	Keypress	1	0.000							
	2	8.64E+04	5.000	Normal	1	0.000															

Setup OK

Interface Devices:
0: PCL-818/780
1: PCL-818/780

Figure 10A: Programming for creep recovery measurements.

Programming for Creep Recovery Measurements
LABTECH CONTROL Global Setup Checking MODE: Normal

Bl.	Block	Intfc	Block	Block	Scale	Offset	Iter	S	Stage Information		File	Sc	Wd No.	Name	Dev Ch	Function	Info.	Factor
		t	Duration	Rate	Start	Tr.	Trigger	Name	#	#				g	(sec)	(Hz)	State	Ch.	Level		(first)		
1	RH Setpoint			Keyboard					1	1	0.000	1.000	Keypress	1	0.000							2	1.72E+05	0.500
	Normal	1	0.000																					
2	DUMMY OUTPUT	1	1	Analog Out	PID(8)	1.000	0.000		1	1	0.000	1.000	Keypress	1	0.000							2		
	0.100	10.000	Normal	1	0.000																			
3	Constant			1	0.000	120.000	0.000		1	1	0.000	1.000	Keypress	1	0.000							2	1.72E+05	
	1.66E-03	Normal	1	0.000																				
4	Dry air setpoin			(3)-(1)	0.000	1.000	0.000		1	1	0.000	1.000	Keypress	1	0.000							2	1.72E+05	
	1.000	Normal	1	0.000																				
5	DISPLACEMENT, m	1	3	Analog In	0..10 V	5.08E-02	0.000		2	1	180.000	5.000	Keypress	1	0.000	c:\ltc\data*	1	3						
		2	8.64E+04	1.67E-02	Normal	1	0.000																	
6	Time[Ld/Dis]			Time	Elapsed				2	1	180.000	5.000	Keypress	1	0.000	c:\ltc\data*								
	2	8.64E+04	1.67E-02	Normal	1	0.000																		
7	Dry air Output	1	1	Analog Out	PID(4)	2.00E-02	2.600		2	1	0.000	1.000	Keypress	1	0.000									
	2	8.64E+04	1.000	Normal	1	0.000																		
8	% RH	1	1	Analog In	0..1 V	99.100	0.000		2	1	180.000	5.000	Keypress	1	0.000		1	2						
	2	8.64E+04	1.000	Normal	1	0.000																		
9	WET AIR OUTPUT	1	0	Analog Out	PID(8)	2.00E-02	3.000		2	1	0.000	1.000	Keypress	1	0.000									
	2	8.64E+04	1.000	Normal	1	0.000																		
10	LOAD SETPOINT			Replay	wf2.prn	1.000	0.000		1	1	0.000	1.000	Keypress	1	0.000									
	2	1200.000	8.33E-04	Normal	1	0.000																		
11	LOAD, GRAMS	1	2	Analog In	0..5 V	21.390	0.000		2	1	0.000	1.000	Keypress	1	0.000		1	1						
	2	8.64E+04	20.000	Normal	1	0.000																		
12	RAMP SETPOINT			Replay	wf1.prn	1.000	0.000		20	1	19.000	1.000	Keypress	1	0.000							2		
	1.000	1.000	Off Lev.	11	18.000									3	19.000	1.000	On Edge	10	2.000					
13	MOTOR DRIVE	0	0	Analog Out	PID(11)	4.68E-02	0.000		20	1	5.000	20.000	Keypress	1	0.000									
	2	8.64E+04	20.000	Off Edge	10	2.000								3	0.000	20.000	On Level	11	19.000					
14	MOTOR RAMP	0	0	Analog Out	PID(11)	4.68E-02	0.000		20	1	1.000	5.000	Keypress	1	0.000							2		
	25.000	5.000	Off Lev.	11	19.500									3	20.000	5.000	On Edge	12	2.000					
15	LOAD			(11)	0.000	1.000	0.000		2	1	180.000	5.000	Keypress	1	0.000	c:\ltc\data*								
	2	8.64E+04	1.67E-02	Normal	1	0.000																		
16	%RH			(8)	0.000	1.000	0.000		2	1	180.000	5.000	Keypress	1	0.000	c:\ltc\data*								
	2	8.64E+04	1.67E-02	Normal	1	0.000																		

Setup OK
Interface Devices:
0: PCL-818/780
1: PCL-818/780

TENSILE STRENGTH MEASUREMENTS

The holocellulose fibers failed at an average load of 35.1 ± 9.0 grams. The extracted holocellulose fibers failed at an average load of 32.8 ± 7.7 grams.

Figure 11A: Load-to-failure data for five single holocellulose fibers.

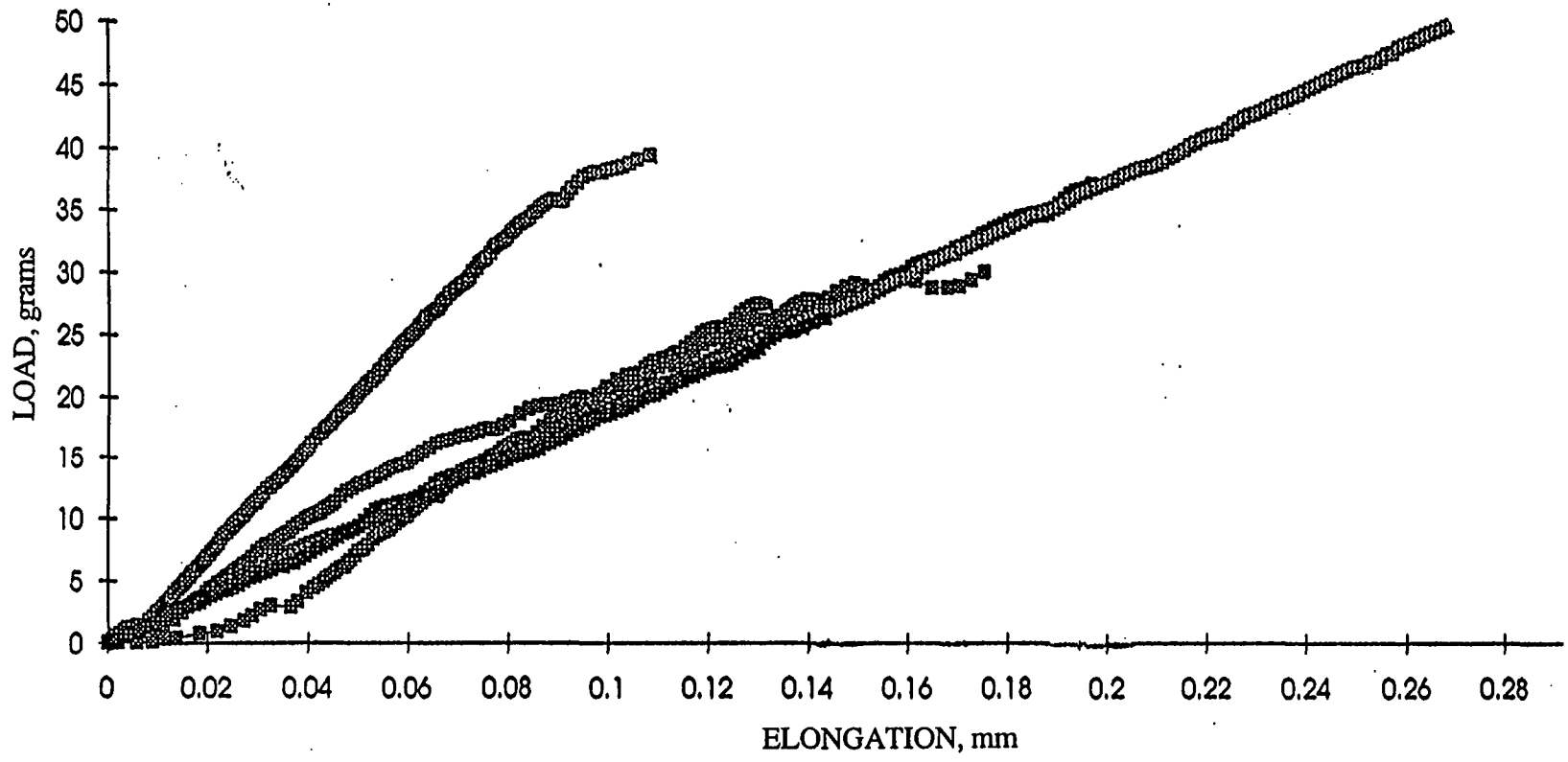

Figure 12A: Load-to-failure data for seven single extracted holocellulose fibers.

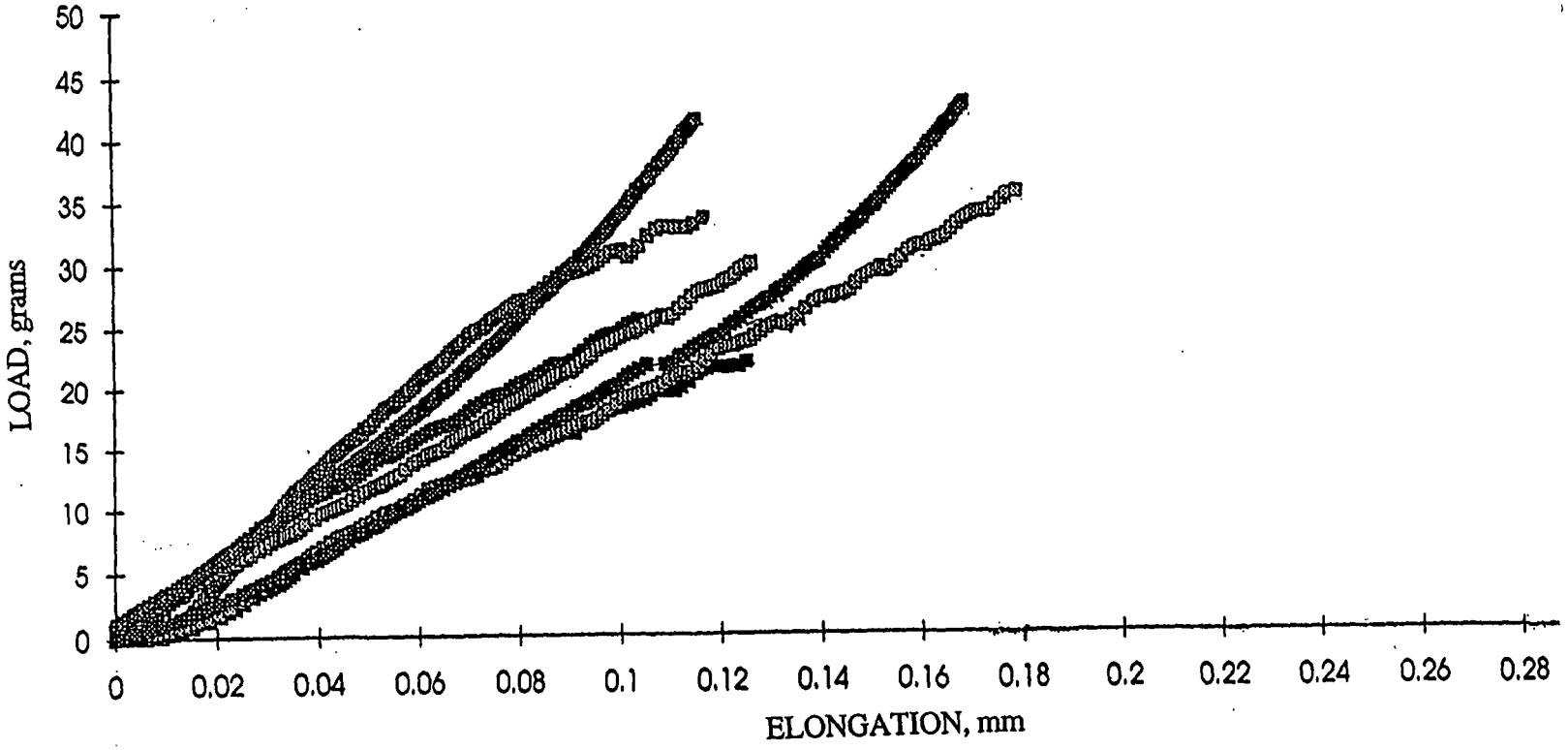

APPENDIX 3: HUMIDITY

THERMOGRAVIMETRIC ANALYSIS RELATIVE HUMIDITY CHAMBER

Thermogravimetry (TG) provides a quantitative measurement of any weight changes associated with thermally induced transitions. For example, TG can record directly the loss in weight as a function of temperature or time (when operating under isothermal conditions, 72°F) for transitions that involve hydration from 50 to 90% RH. The usual temperature range for the equipment is from ambient to 1200°C.

The thermogravimetric analysis equipment has a symmetrical high-sensitivity beam microbalance. The balance is positioned in a sealed casing which enables nitrogen to protectively sweep humidified air from the beam. The beam is articulated on a torsional ribbon. Sample and counter weight are symetrically hung in a basket and an open crucible. The basket goes down without rubbing into the relative humidity chamber. Extracting the basket and fiber sample from the relative humidity chamber is done by removing the front cover of the chamber. Automatic electromagnetic rebalancing compensates for the variations in weight of the sample and delivers a linear electric signal which represents the exchanges in mass between the sample and the hydration phase. Initial balancing is made easier by electromagnetic taring. Additional thermogravimetric analysis specifications are listed in Table 12A.

Table 12A: Thermogravimetric Analysis Specifications.

Maximum load, by suspension	3g
Usual loading	0 to 500 mg
Dynamic range:	
10 ranges (25 cm, full scale) + 0.1 to + 100 mg	(extension: x2)
Maximum sensitivity	4 µg/cm
Minimum detectable weight change	1 µg
Balance accuracy	better than 0.1%
Electronic taring	±200 mg
Digital resolution	± 20.000 points

The thermogravimetric analysis equipment is connected on line with a data-processing unit. Digital conversion, display, and transmission functions are provided by a collection of digital displaying voltmeters. The computer stores and processes the digital signals. Data can be sent directly to a plotter.

Samples of single separated fibers weighing approximately 5 mg are placed in a 160-mesh, 316-stainless steel wire cloth basket (Figure 13A) that is attached to an automatic recording balance and surrounded by a constant relative humidity environment created by a double-walled chamber (Figures 14A and 15A). It is necessary for the basket to be porous enough that the fibers can be conditioned to various relative humidities but not so porous that the single fibers are lost through the openings. The combined weight of the porous basket and sample is approximately 380 mg. The basket is held together by a wire loop which is also used to suspend the basket from the balance.

The relative humidity sensor used in the creep response experiments is used in the new relative humidity chamber to monitor temperature and relative humidity. The water tank and a dry air line used to generated various relative humidities in the creep response experiments is connected to the double-walled relative humidity chamber and controlled using optimized FLER relative humidity programs.

The newly designed chamber allows determination of the moisture pickup of single fibers at 50 and 90% RH. At 50% RH the holocellulose fibers contain 10.35%, moisture whereas the extracted holocellulose fibers contain 8.73%. The basket without a fiber sample is cycled from 50–90% RH every six hours in the thermogravimetric analysis relative humidity chamber. The plot of moisture regain vs. time is included as Figure 16A. The basket has an average moisture change of 25.34 micrograms for a change in relative humidity. The moisture regain vs. time for holocellulose and extracted holocellulose fibers is also plotted as Figures 17A-20A. The moisture regain information is highlighted in Table 13A. The average moisture content of the two fiber samples is calculated. The moisture content of the holocellulose fiber is higher than the extracted holocellulose fiber at 90% RH. The moisture changes and the moisture contents are significantly different at the 99% confidence level (Tables 14A and 15A).

Table 13A: Moisture Regain.

	Moisture Change from 50–90% (micogram)	Moisture Change from 90–50% (microgram)
Holocellulose	269.57	307.16
	290.16	293.26
		259.61
Extracted Holocellulose	226.14	259.86
	251.86	265.36
	253.06	261.06
		274.06
	%Moisture Content from 50–90%	%Moisture Content from 90–50%
Holocellulose	5.95	6.78
	6.41	7.30
	6.46	
Average	6.28	7.04
Extracted Holocellulose	5.25	6.03
	5.85	5.95
	5.47	5.64
		5.92
Average	5.52	5.89

Table 14A: Analysis of variance for moisture change.

Effect of moisture change fiber samples.

Source	DF	Sum of Squares	Mean Square	F-Ratio
A(Fiber samples)	3	3958.859	1319.620	9.03**
Error	8	1168.765	146.095	
Total	11	5127.624		

Term	Count	Mean	Standard Error
All	12	267.5967	
A(Fiber samples)			
Holocellulose cycled 50–90%RH	3	273.1113	6.9784
Extracted cycled 50–90%RH	3	243.6867	6.9784
Holocellulose cycled 90–50%RH	2	300.2100	8.5468
Extracted cycled 90–50%RH	4	265.0850	6.0435

**Significant at 99% confidence level.

Table 15A: Analysis of variance for moisture content.

Effect of moisture change fiber samples.

Source	DF	Sum of Squares	Mean Square	F-Ratio
A(Fiber samples)	3	3.0368	1.0122	14.36**
Error	8	0.5640	0.0705	
Total	11	3.6008		

Term	Count	Mean	Standard Error
All	12	6.0841	
A(Fiber samples)			
Holocellulose cycled 50–90%RH	3	6.2733	0.1533
Extracted cycled 50–90%RH	3	5.5233	0.1533
Holocellulose cycled 90–50%RH	2	7.04	0.1877
Extracted cycled 90–50%RH	4	5.885	0.1327

**Significant at 99% confidence level.

The newly designed chamber allows determination of the time necessary for single fibers at 50 and 90% RH to come to equilibrium. The basket without a fiber sample is cycled from 50–90% RH every six hours in the thermogravimetric analysis relative humidity chamber. The plot of moisture regain vs. time is included as Figure 16A. The first 75 minutes at 50% RH indicates the balance coming to equilibrium. The moisture regain vs. time for holocellulose and extracted holocellulose fibers is also plotted as Figures 17A–20A. The holocellulose and extracted holocellulose fibers essentially come to equilibrium at 50 and 90% RH instantaneously. Since the single fiber samples come to equilibrium instantaneously, a cycle time of 10 minutes is used to change relative humidity conditions in the FLER relative humidity chamber. Figure 21A depicts the 10-minute relative humidity cycling sequence of 50–90% for a single fiber tested in the FLER relative humidity chamber. The air flow rate for 50% and 90% RH is 5.3 and 4.2 l/min.

Figure 13A: Single fibers in wire mesh basket.

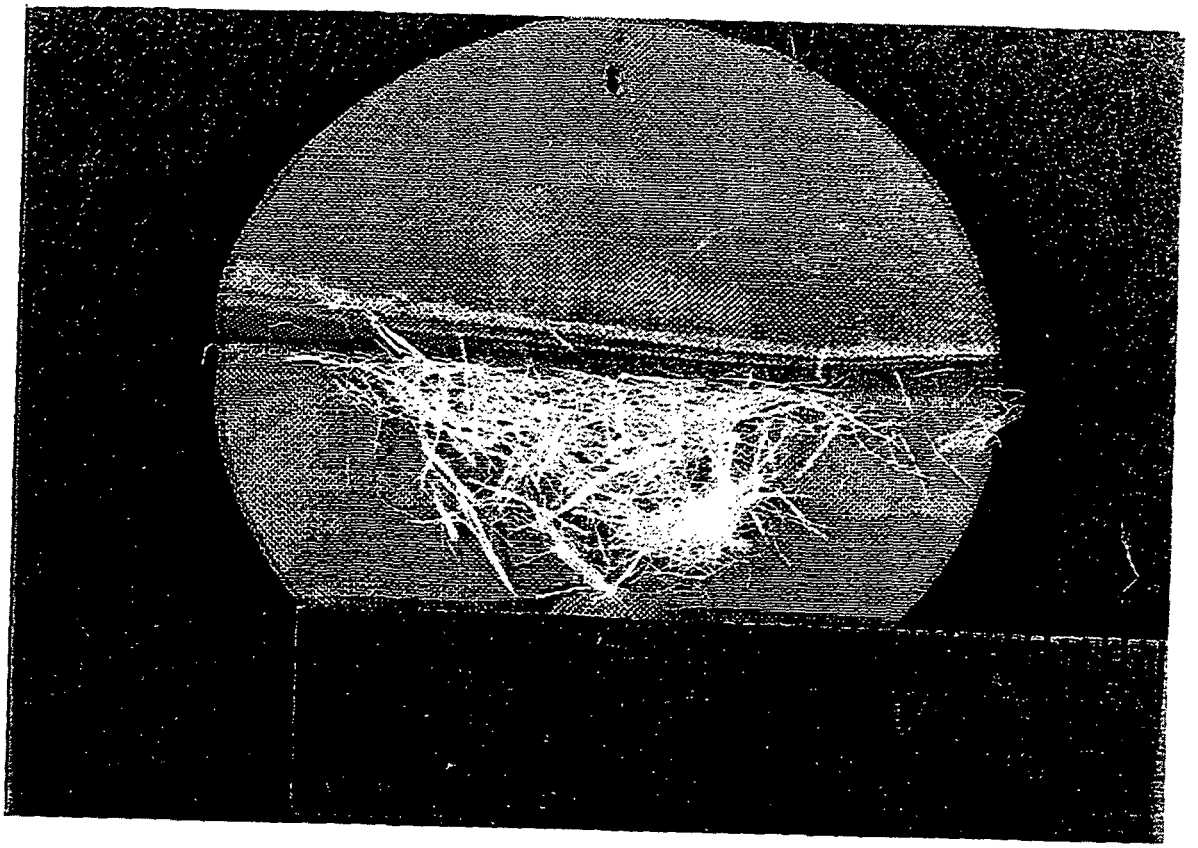

Figure 14A: Double-walled relative humidity chamber.

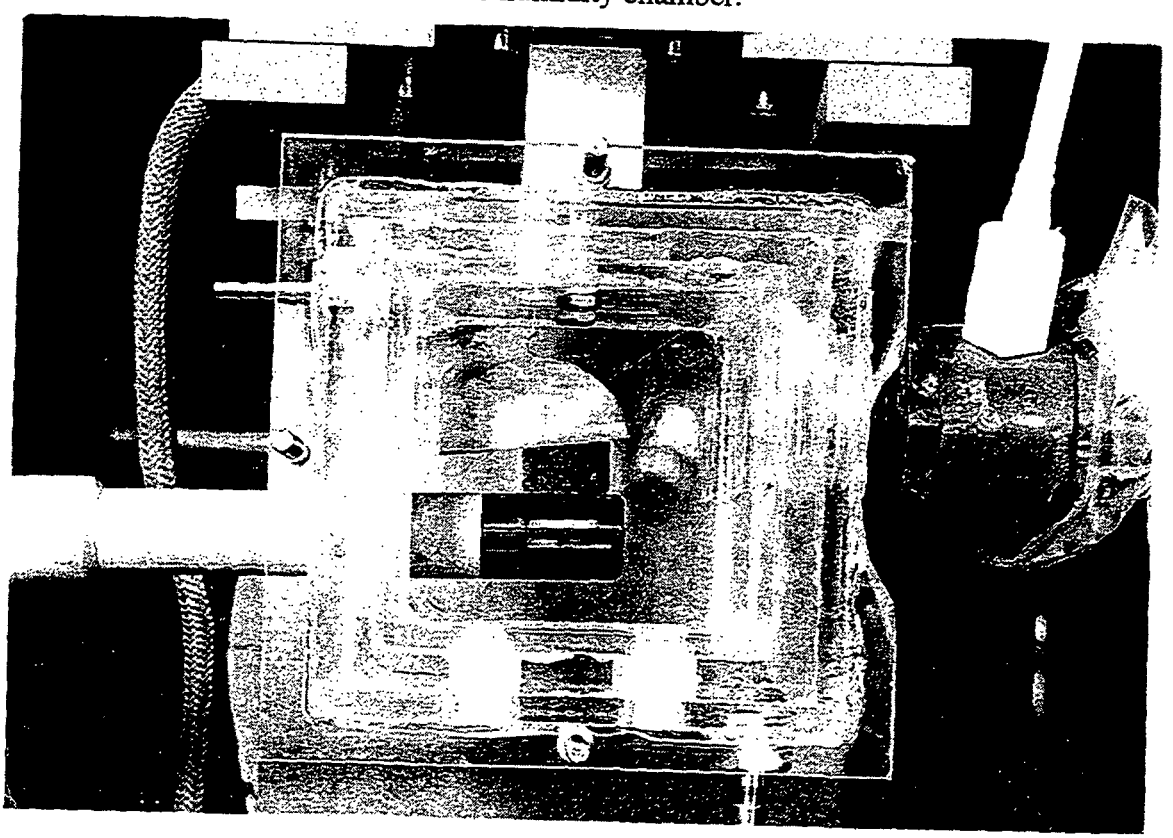

Figure 15A: Double-walled relative humidity chamber.

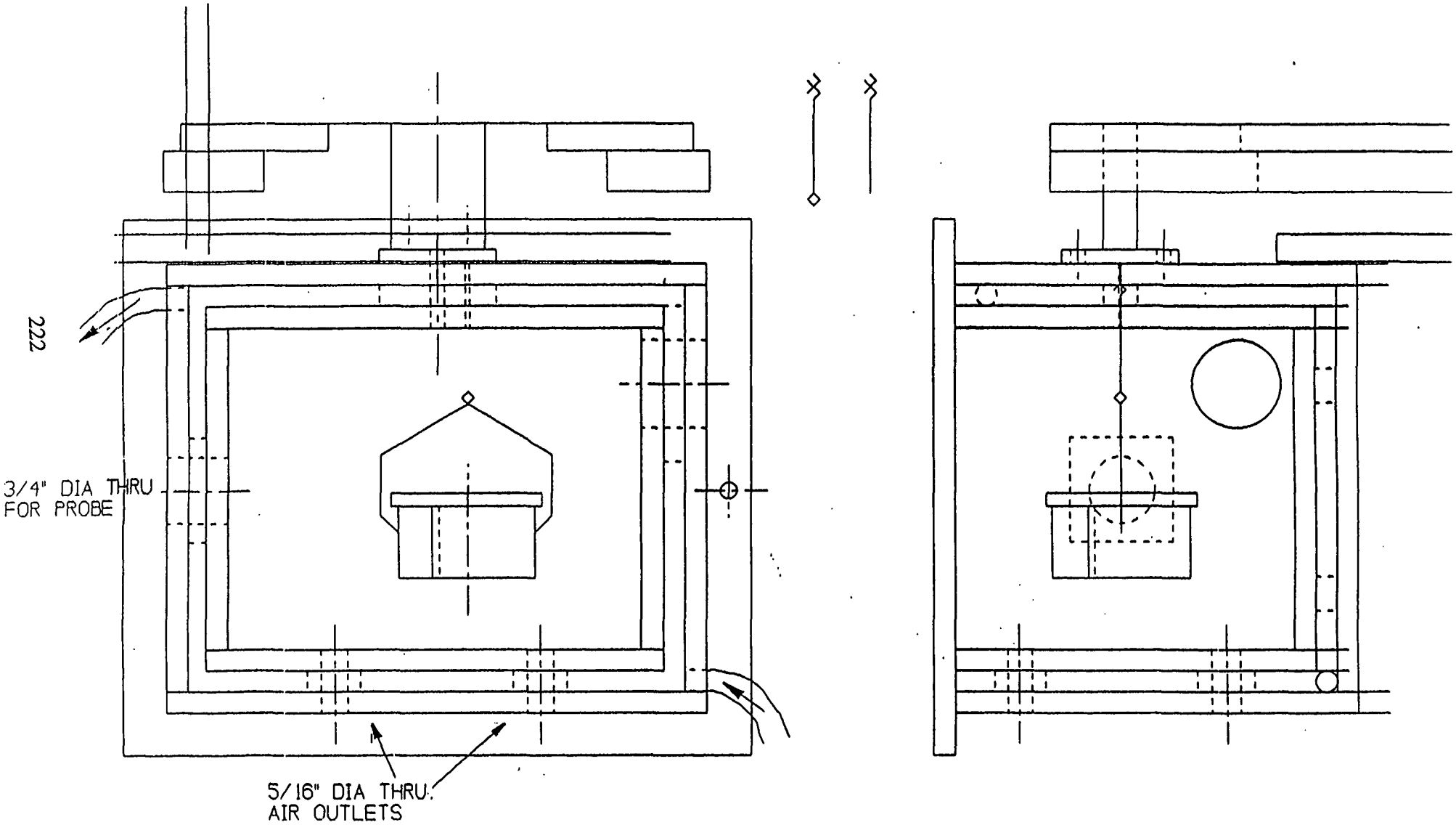

Figure 16A: The weight of the empty basket for changes in relative humidity.

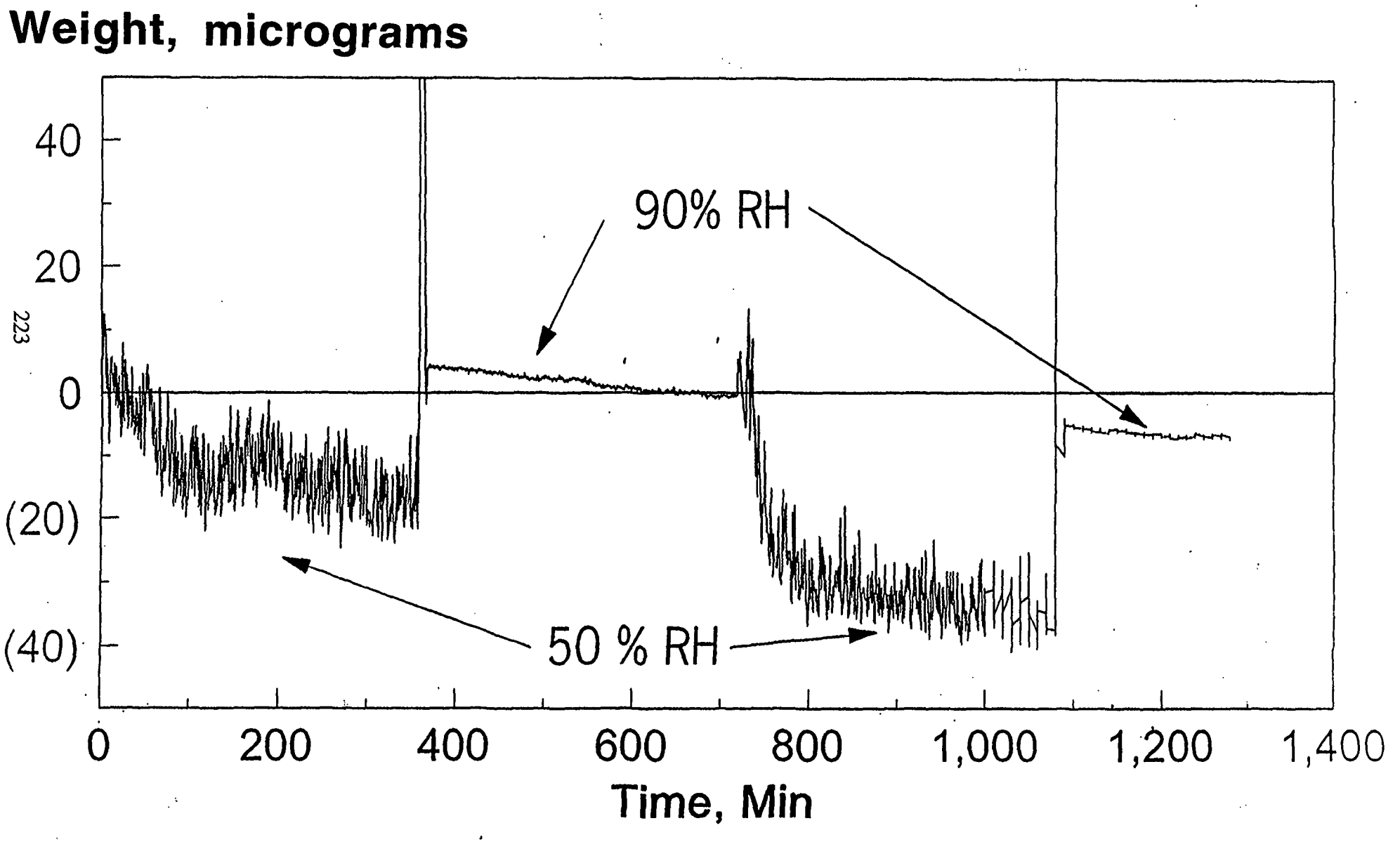

Figure 17A: Moisture regain for holocellulose.

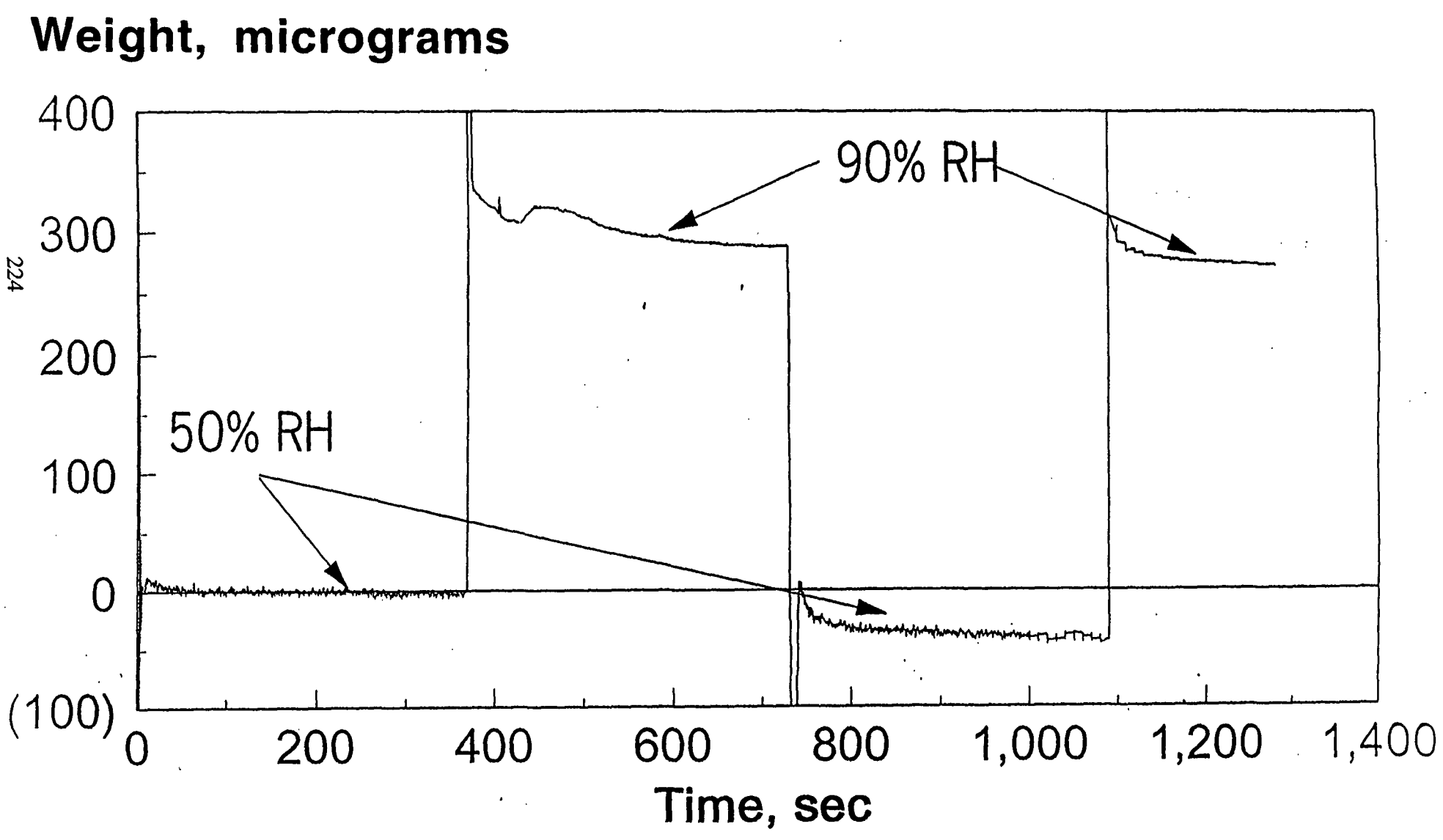

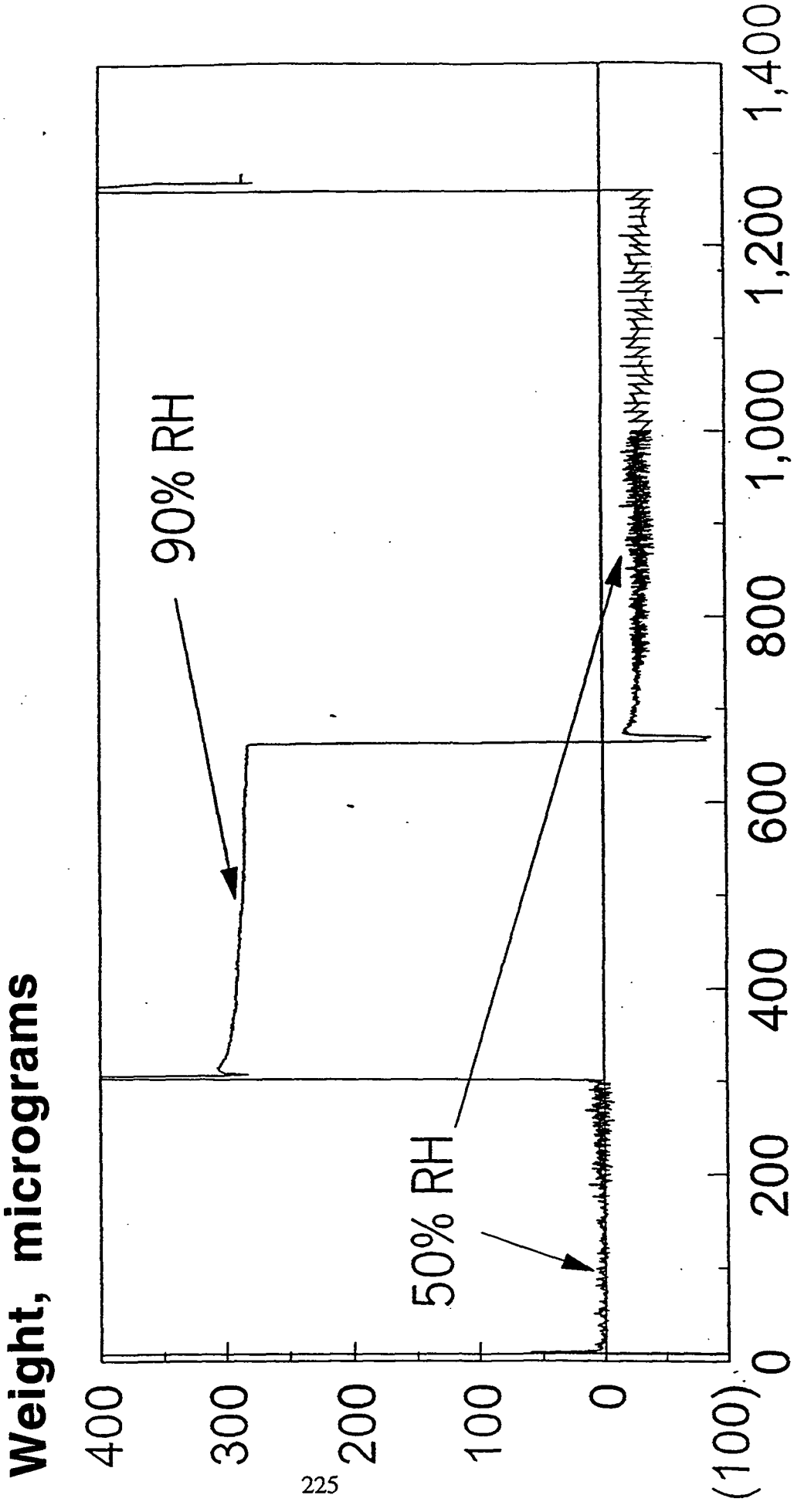

Figure 18A: Moisture regain for holocellulose.

Figure 19A: Moisture regain for extracted holocellulose.

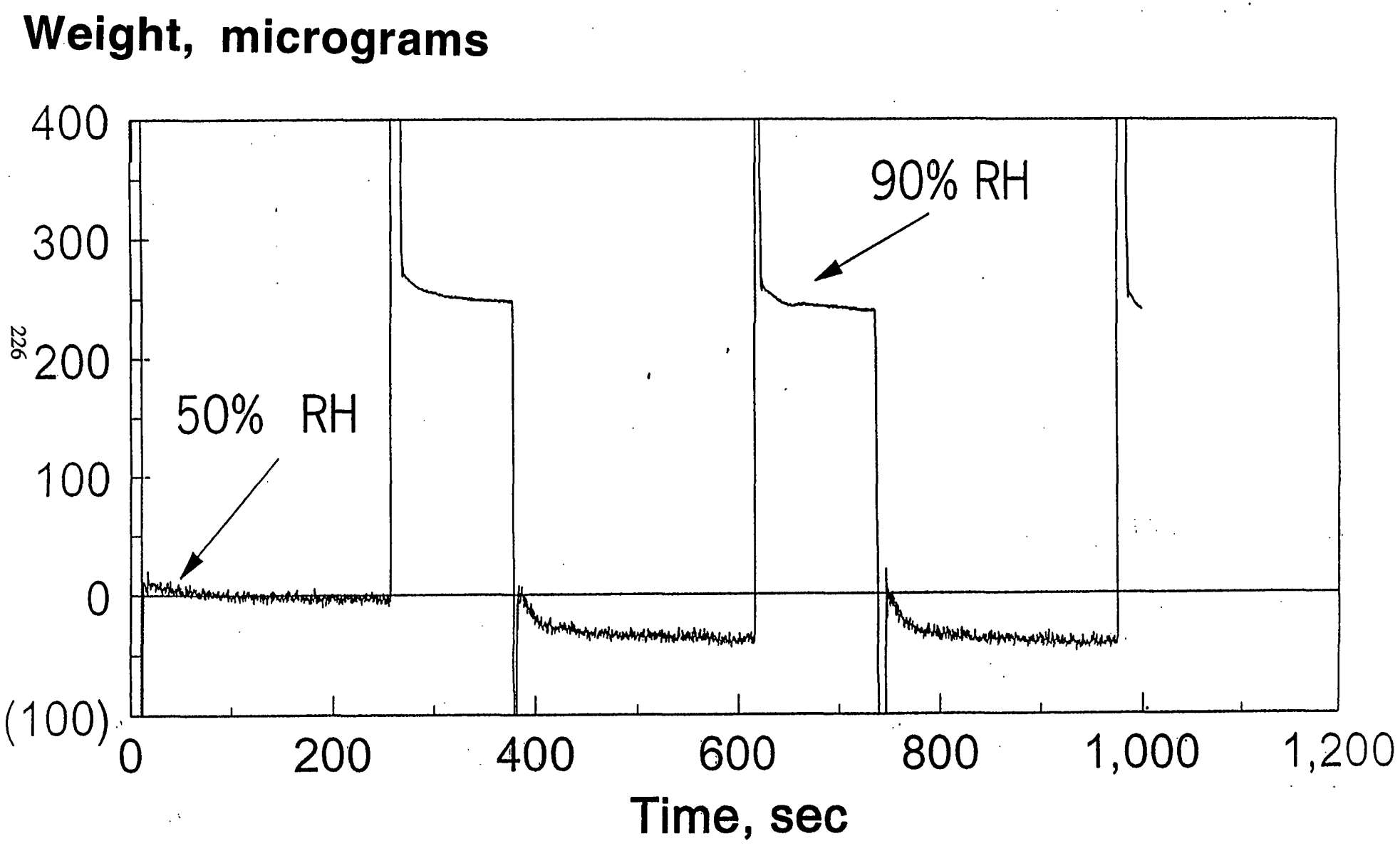

Figure 20A: Moisture regain for extracted holocellulose.

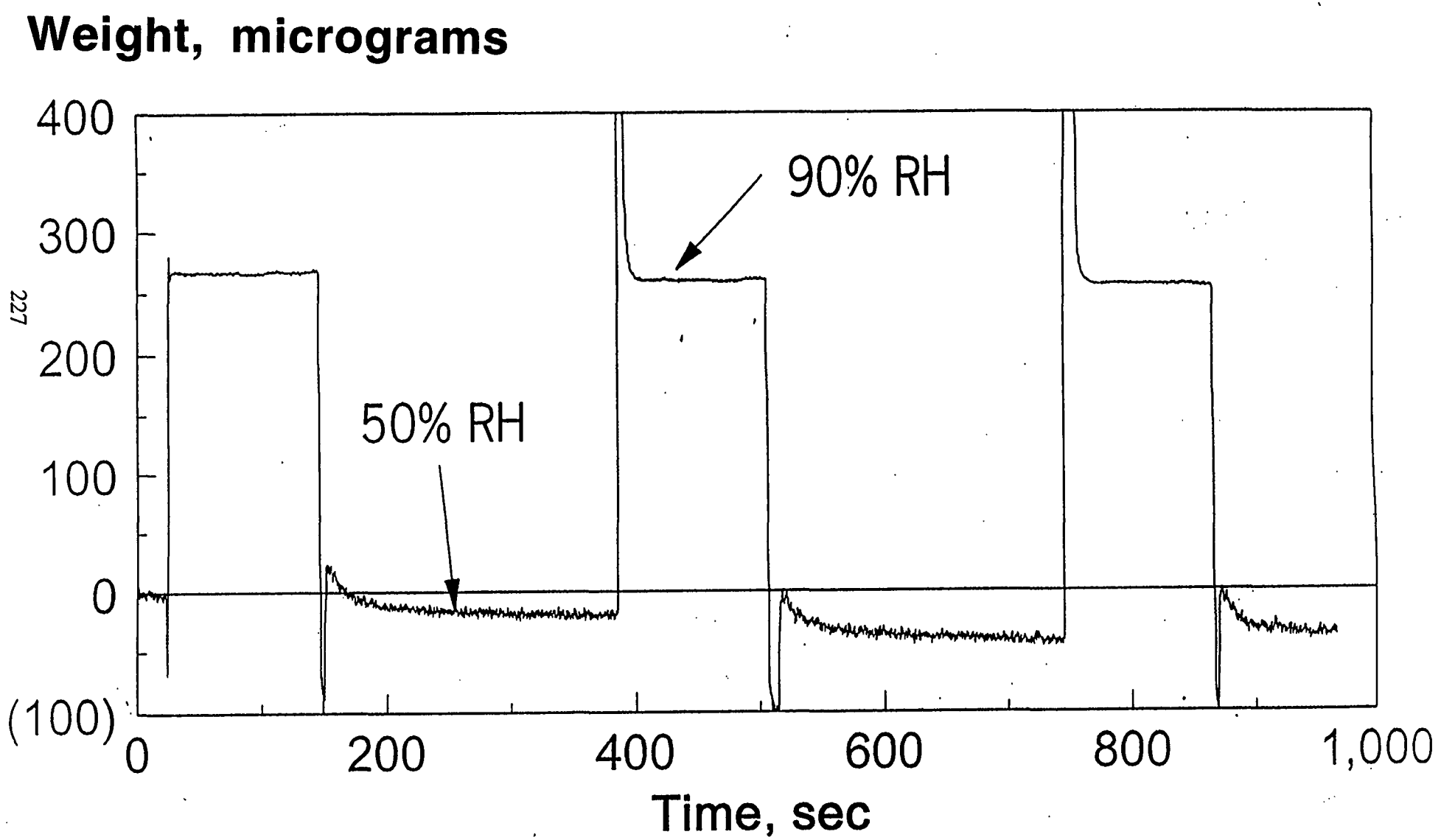

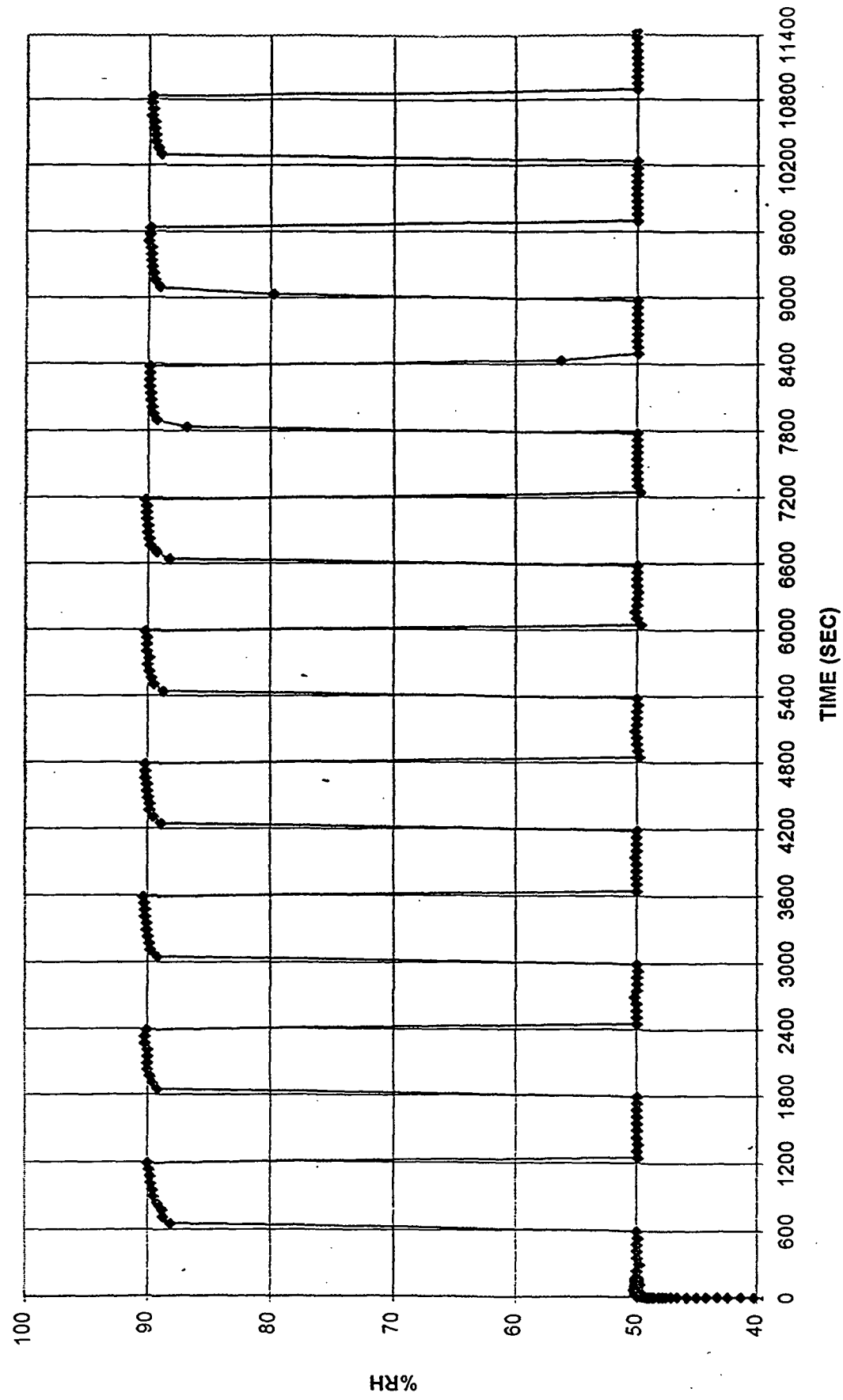

Figure 21A: Relative humidity cycling sequence.

APPENDIX 4: FIBER DATA

Table 16A: Initial fiber test spans for single fiber creep.

Fiber Type	Relative Humidity, %	Fiber Number	Initial Test Span, mm
Holocellulose	50	1	1.05
		2	0.825
		3	1.05
		4	0.75
		5	0.75
		6	0.975
		7	0.90
		8	0.75
		9	0.825
		10	0.90

Fiber Type	Relative Humidity, %	Fiber Number	Initial Test Span, mm
Holocellulose	90	1	0.825
		2	1.05
		3	0.75
		4	0.75
		5	0.75
		6	0.975
		7	0.825

Fiber Type	Relative Humidity, %	Fiber Number	Initial Test Span, mm
Extracted	50	1	0.75
		2	0.90
		3	1.05
		4	0.75
		5	0.825
		6	1.05
		7	0.90
		8	0.90
		9	0.975
		10	0.75
		11	0.75
		12	1.05

Fiber Type	Relative Humidity, %	Fiber Number	Initial Test Span, mm
Extracted	90	1	1.05
		2	0.90
		3	0.90
		4	0.90
		5	0.825
		6	0.75
		7	1.05
		8	0.75
		9	0.75
		10	0.825
		11	0.90

Table 17A: Initial fiber test spans for single fiber creep and creep recovery.

Fiber Type	Relative Humidity, %	Fiber Number	Initial Test Span, mm
Holocellulose	50	1	0.825
		2	0.825
		3	0.90
		4	0.75
		5	0.975
Fiber Type	Relative Humidity, %	Fiber Number	Initial Test Span, mm
Holocellulose	90	1	0.825
		2	0.975
		3	0.75
		4	1.05
		5	1.05
Fiber Type	Relative Humidity, %	Fiber Number	Initial Test Span, mm
Extracted	50	1	1.05
		2	0.75
		3	0.825
		4	0.825
		5	1.05
Fiber Type	Relative Humidity, %	Fiber Number	Initial Test Span, mm
Extracted	90	1	0.90
		2	0.975
		3	1.05
		4	0.90
		5	0.90

Table 18A: Initial fiber test spans for single fiber cyclic creep.

Fiber Type	Relative Humidity, %	Fiber Number	Initial Test Span, mm
Holocellulose	50–90	1	0.75
		2	0.90
		3	0.90
		4	0.90
		5	0.75
		6	0.90
		7	0.90
		8	0.90
		9	0.825
		10	0.90
		11	0.90
		12	0.825
		13	0.75
		14	0.75

Fiber Type	Relative Humidity, %	Fiber Number	Initial Test Span, mm
Holocellulose	90–50	1	0.825
		2	0.90
		3	0.90
		4	0.825
		5	0.75
		6	0.975
		7	1.05
		8	0.75
		9	0.90
		10	0.75

Fiber Type	Relative Humidity, %	Fiber Number	Initial Test Span, mm
Extracted	50–90	1	0.75
		2	1.05
		3	0.75
		4	0.90
		5	1.05
		6	0.75
		7	0.90
		8	0.90
		9	0.75
		10	0.75

Fiber Type	Relative Humidity, %	Fiber Number	Initial Test Span, mm
Extracted	90–50	1	0.75
		2	0.75
		3	0.75
		4	1.05
		5	0.90
		6	0.75
		7	1.05
		8	0.90
		9	0.825
		10	0.90

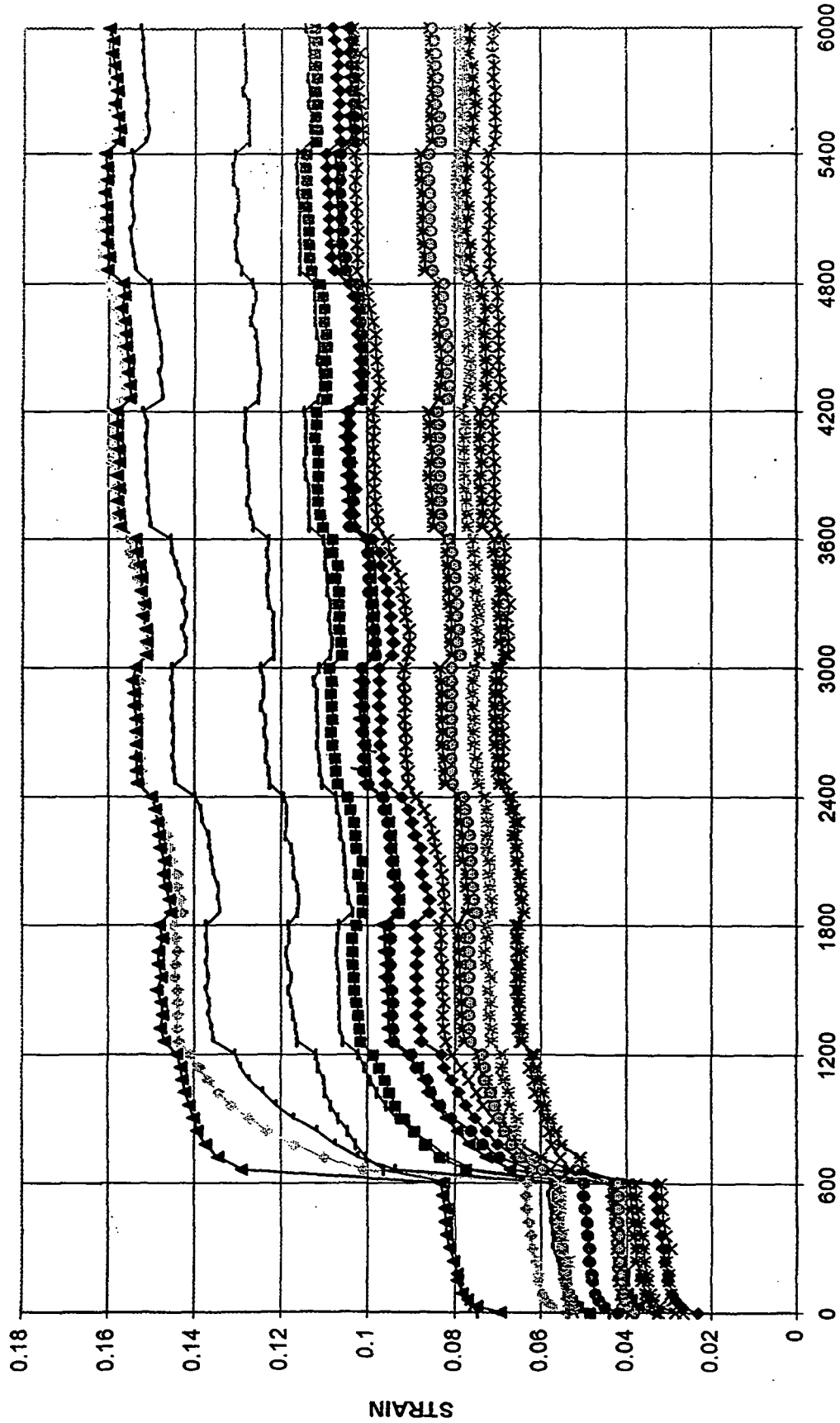

Figure 22A: Single holocellulose fiber creep 50-90% RH.

Figure 23A: Single holocellulose fiber creep 90-50% RH.

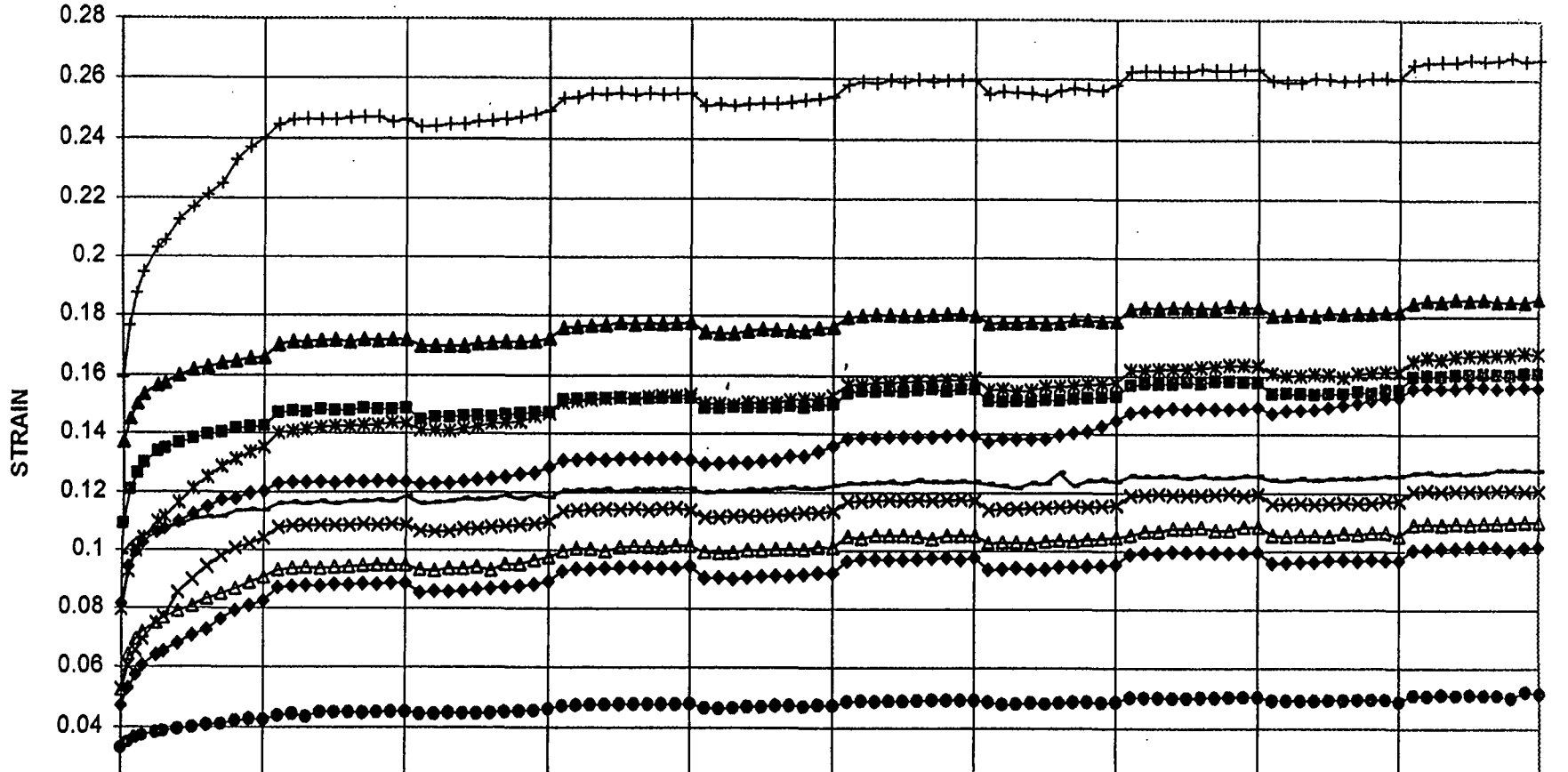

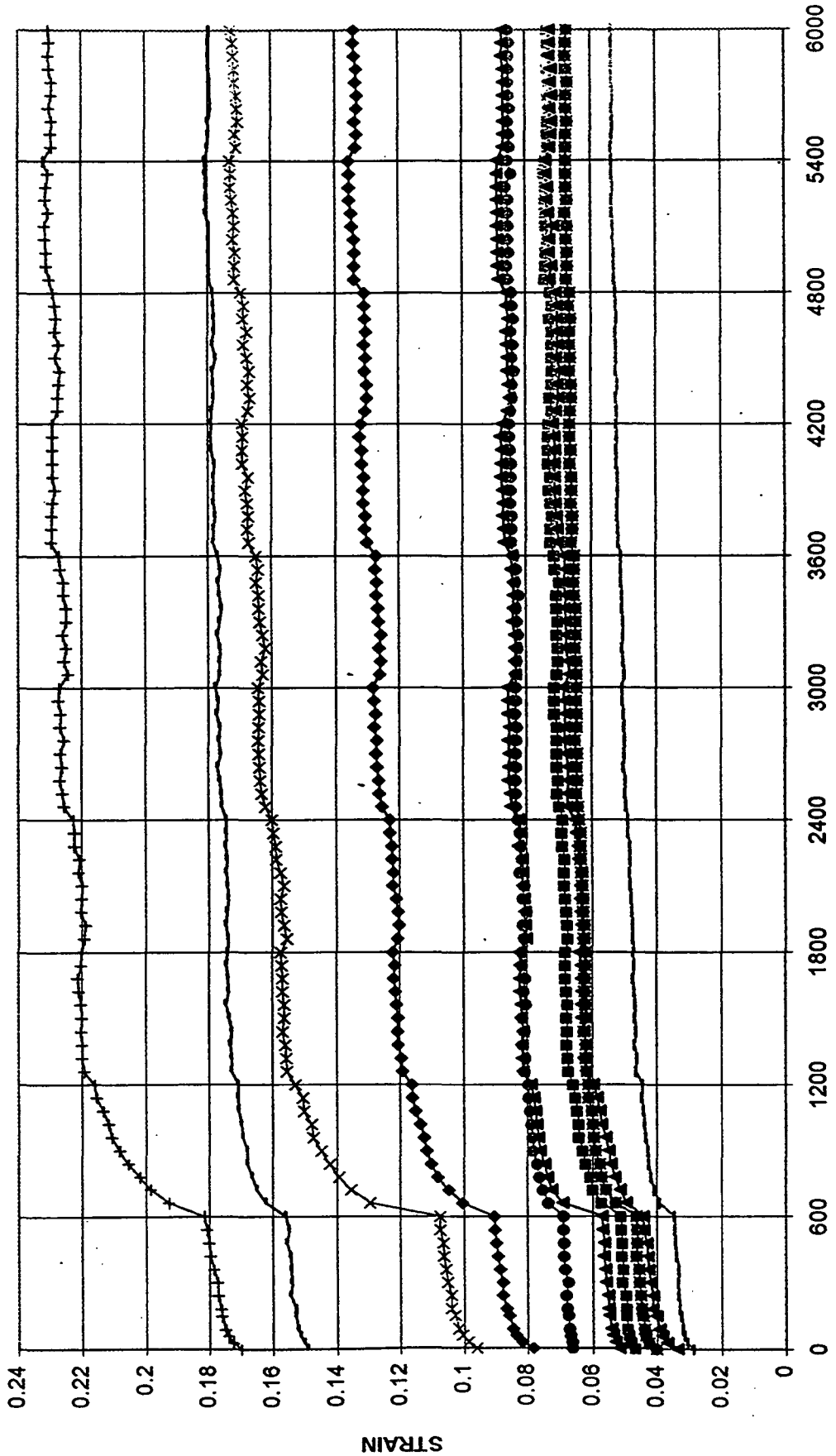

Figure 24A: Single extracted holocellulose fiber creep 50-90% RH.

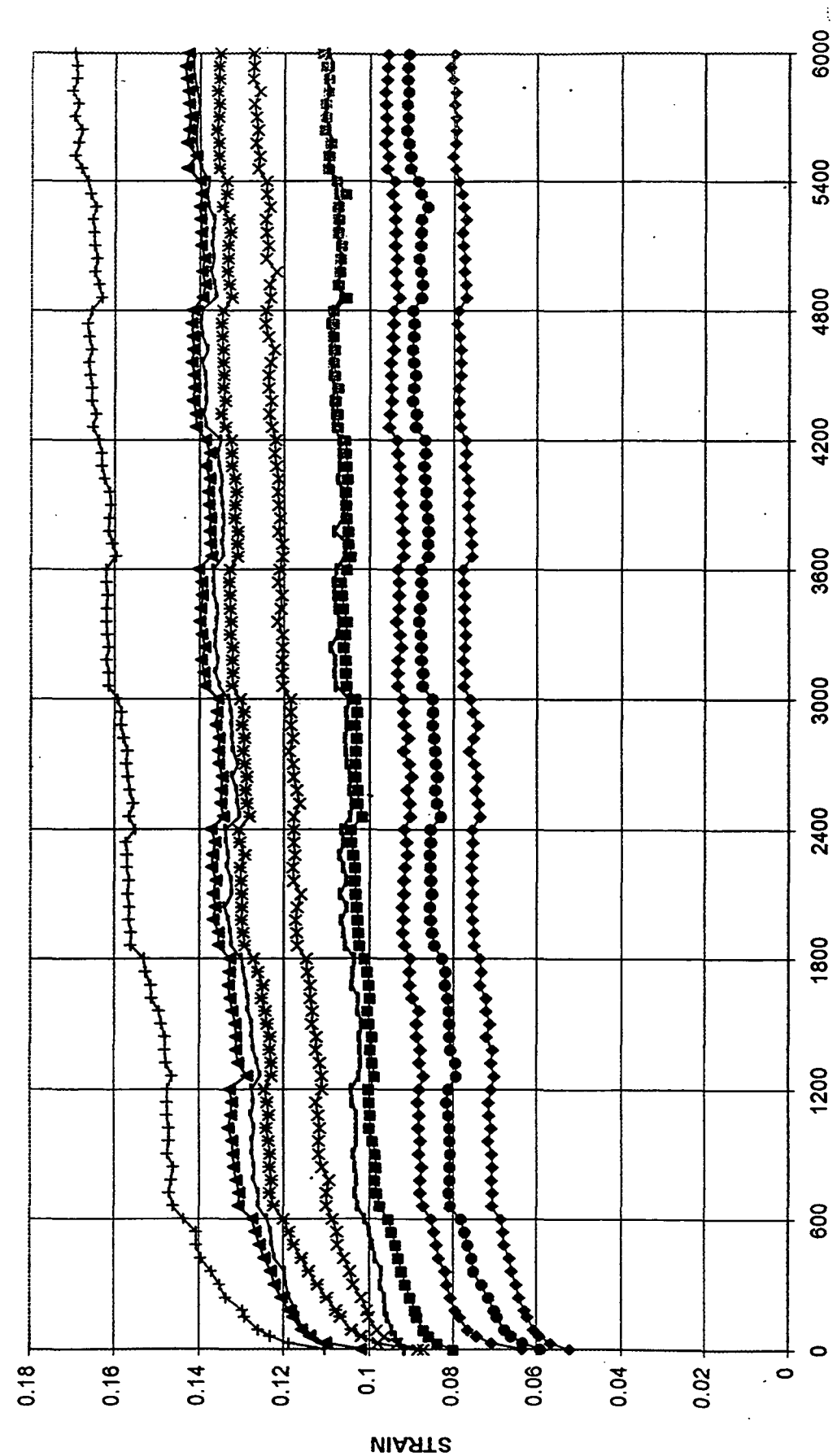

Figure 25A: Single extracted holocellulose fiber creep 90-50% RH.

APPENDIX 5: SAS PROGRAMMING

GENERAL SAS PROGRAM

For fitting single creep curve or single creep recovery curve.

```
PROC NLIN DATA=kelly.call best=10 SAVE CONVERGE=1E-06 EFORMAT;
PARMS  E1=1831E+8 E2=789E+8 x=1.5e-09 a=3.5e-9  ;
BOUNDS E1>0,E2>0,x>0,a>0    ;
T=TIME;R=1-(E2/(E1+E2));R1=(E2/(E1+E2)**2)-(1/(E1+E2));
ARG= .5*A*R*F;
R2=E2**2/((E1+E2)**2);
COTH=1/TANH(ARG);
CSCH=1/SINH(ARG);
SECH=1/COSH(ARG);
AP=A*X*E2*R;
BP=LOG(COTH);
G=.5*(AP*T+BP);
COTHG=1/TANH(G);
CSCHG=1/SINH(G);
SECHG=1/COSH(G);
DGDA=.5*(E2*R*T*X-.5*R*F*CSCH*SECH);
DGDX=.5*A*E2*R*T;
DGDE1=.5*((A*R2*T*X)-((.5*A*E2*F*CSCH*SECH)/((E1+E2)**2)));
DGDE2=.5*(A*E2*R1*T*X+A*R*T*X-.5*A*R1*F*CSCH*SECH);
DER.A=LOG(COTHG)/(A**2*E2)+((CSCHG*SECHG*DGDA)/(A*E2));
DER.X=(CSCHG*SECHG*DGDX)/(A*E2);
DER.E1=(CSCHG*SECHG*DGDE1)/(A*E2);
DER.E2=(-F/(E2**2))+LOG(COTHG)/(A*(E2**2))+((CSCHG*SECHG*DGDE2)/(A*E2));
MODEL e = F/E2-(1/(A*E2))*LOG(COTHG);
OUTPUT OUT=KELLY.TOTAL P=PRED R=RES L95M=L195M U95M=U95M STDP=STDP STDR=STDR;
RUN;
```

SAS FITTINGS

Table 19A: Fitted Eyring parameters for single fiber creep.

Units: Alpha (cm^2/dynes), Chi (sec^{-1}), Moduli (dynes/cm^2)

Holocellulose, 50% RH

Fiber	E1	E2	Alpha, α	Chi, χ
1	1.08×10^{10}	2.36×10^{10}	1.83×10^{-8}	4.05×10^{-13}
2	1.50×10^{10}	2.20×10^{10}	1.26×10^{-8}	8.37×10^{-12}
3	1.20×10^{10}	3.58×10^{10}	9.83×10^{-9}	9.99×10^{-9}
4	4.94×10^{9}	1.99×10^{10}	2.63×10^{-8}	1.03×10^{-10}
5	1.23×10^{10}	2.86×10^{10}	2.58×10^{-8}	1.95×10^{-14}
6	7.73×10^{9}	2.11×10^{10}	3.02×10^{-8}	1.01×10^{-15}
7	1.00×10^{10}	5.30×10^{10}	5.86×10^{-8}	1.24×10^{-15}
8	9.92×10^{10}	6.05×10^{10}	9.14×10^{-9}	4.63×10^{-13}
9	1.86×10^{10}	7.52×10^{10}	1.84×10^{-8}	8.99×10^{-10}
10	1.02×10^{10}	2.79×10^{10}	2.48×10^{-8}	3.27×10^{-14}

Holocellulose, 90% RH

Fiber	E1	E2	Alpha, α	Chi, χ
1	3.00×10^{10}	1.90×10^{10}	4.24×10^{-9}	3.00×10^{-8}
2	2.47×10^{10}	4.30×10^{10}	6.11×10^{-9}	9.90×10^{-8}
3	1.00×10^{10}	1.68×10^{10}	8.20×10^{-9}	4.50×10^{-8}
4	6.50×10^{9}	1.34×10^{10}	1.57×10^{-8}	5.34×10^{-12}
5	2.80×10^{10}	2.07×10^{10}	8.07×10^{-9}	5.14×10^{-11}
6	1.61×10^{10}	2.23×10^{10}	9.79×10^{-9}	2.92×10^{-10}
7	3.17×10^{10}	5.04×10^{10}	7.67×10^{-9}	1.65×10^{-8}

Units: Alpha (cm^2/dynes), Chi (sec^{-1}), Moduli (dynes/cm^2)

Extracted Holocellulose, 50% RH

Fiber	E1	E2	Alpha, α	Chi, χ
1	1.12×10^{10}	1.66×10^{10}	1.67×10^{-8}	2.07×10^{-11}
2	2.19×10^{10}	2.71×10^{10}	8.98×10^{-9}	3.97×10^{-6}
3	2.03×10^{10}	3.54×10^{10}	9.51×10^{-9}	2.27×10^{-6}
4	2.09×10^{10}	3.41×10^{10}	9.23×10^{-9}	4.37×10^{-8}
5	1.81×10^{10}	4.49×10^{10}	1.40×10^{-8}	4.56×10^{-8}
6	9.55×10^{10}	7.77×10^{10}	7.74×10^{-9}	5.83×10^{-9}
7	1.18×10^{10}	1.86×10^{10}	2.23×10^{-8}	1.11×10^{-12}
8	6.47×10^{9}	3.31×10^{10}	3.54×10^{-8}	1.71×10^{-10}
9	2.87×10^{9}	1.33×10^{10}	3.33×10^{-8}	2.42×10^{-10}
10	5.77×10^{9}	1.64×10^{10}	2.84×10^{-8}	6.79×10^{-13}
11	9.78×10^{9}	2.78×10^{10}	3.53×10^{-8}	4.06×10^{-15}
12	1.54×10^{10}	2.97×10^{10}	6.72×10^{-9}	6.50×10^{-6}

Extracted Holocellulose, 90% RH

Fiber	E1	E2	Alpha, α	Chi, χ
1	2.00×10^{10}	1.54×10^{10}	5.07×10^{-9}	4.99×10^{-8}
2	7.27×10^{9}	5.14×10^{9}	1.67×10^{-8}	1.37×10^{-17}
3	1.36×10^{10}	6.78×10^{9}	5.98×10^{-9}	1.00×10^{-9}
4	1.13×10^{10}	1.57×10^{10}	8.88×10^{-9}	9.81×10^{-9}
5	2.00×10^{10}	2.32×10^{10}	7.00×10^{-9}	8.10×10^{-8}
6	2.30×10^{10}	4.03×10^{10}	1.03×10^{-8}	1.56×10^{-8}
7	2.04×10^{10}	1.96×10^{10}	1.01×10^{-8}	8.66×10^{-11}
8	1.85×10^{10}	2.89×10^{10}	1.56×10^{-8}	6.53×10^{-13}
9	5.37×10^{10}	4.20×10^{10}	3.72×10^{-9}	1.00×10^{-7}
10	1.01×10^{10}	1.02×10^{10}	1.03×10^{-8}	1.70×10^{-10}
11	1.85×10^{10}	3.70×10^{10}	8.67×10^{-9}	2.78×10^{-8}

Table 20A: Fitted Eyring parameters for single fiber creep recovery.

Units: Alpha (cm^2/dynes), Chi (sec^{-1}), Moduli (dynes/cm^2)

Holocellulose, 50% RH

Fiber	E1	E2	Alpha, α	Chi, χ
1	1.63×10^{11}	1.98×10^{11}	6.54×10^{-9}	1.05×10^{-8}
2	1.00×10^{9}	6.61×10^{10}	6.80×10^{-13}	4.69×10^{-7}
3	8.99×10^{10}	8.21×10^{10}	8.32×10^{-9}	1.99×10^{-7}
4	1.42×10^{11}	9.21×10^{10}	6.06×10^{-9}	1.39×10^{-7}
5	2.00×10^{11}	1.29×10^{11}	7.36×10^{-9}	1.31×10^{-7}

Holocellulose, 90% RH

Fiber	E1	E2	Alpha, α	Chi, χ
1	2.50×10^{11}	6.85×10^{10}	8.50×10^{-9}	2.01×10^{-7}
2	1.00×10^{11}	4.79×10^{10}	7.11×10^{-9}	1.85×10^{-7}
3	1.00×10^{11}	5.46×10^{10}	7.71×10^{-9}	1.84×10^{-7}
4	1.09×10^{11}	7.63×10^{10}	6.84×10^{-9}	2.06×10^{-7}
5	2.08×10^{11}	4.64×10^{10}	4.11×10^{-9}	5.97×10^{-6}

Extracted Holocellulose, 50% RH

Fiber	E1	E2	Alpha, α	Chi, χ
1	5.00×10^{10}	7.67×10^{10}	6.38×10^{-9}	2.38×10^{-7}
2	9.27×10^{10}	4.99×10^{10}	7.75×10^{-9}	6.42×10^{-8}
3	1.50×10^{11}	1.11×10^{11}	7.75×10^{-9}	6.44×10^{-8}
4	2.31×10^{11}	1.83×10^{11}	6.82×10^{-9}	6.87×10^{-8}
5	1.84×10^{11}	1.50×10^{11}	9.95×10^{-9}	1.35×10^{-7}

Extracted Holocellulose, 90% RH

Fiber	E1	E2	Alpha, α	Chi, χ
1	8.67×10^{10}	3.38×10^{10}	7.09×10^{-9}	1.99×10^{-7}
2	1.01×10^{11}	4.26×10^{10}	8.66×10^{-9}	1.98×10^{-7}
3	8.14×10^{10}	7.66×10^{10}	8.16×10^{-9}	6.89×10^{-7}
4	8.28×10^{10}	7.25×10^{10}	2.02×10^{-8}	1.00×10^{-12}
5	1.03×10^{11}	9.09×10^{10}	7.09×10^{-9}	2.00×10^{-7}